Synthesis and Characterization of Copolymers: Tuning Material Properties of Polythiophenes and Epoxy-Thiol Polymer Networks, and Application of Low-Field NMR Spectroscopy to Multicomponent Polymer Systems

By: Michael J. Minkler, Jr.

A Dissertation

Submitted to the Graduate Faculty of Auburn University

In partial fulfillment of the

Requirements for the Degree of

Doctor of Philosophy

Auburn, Alabama

August 8th, 2020

Keywords: polythiophene, conductive polymers, microstructure,

statistical copolymers, low-field NMR spectroscopy

Approved by

Bryan Beckingham, Chair, Assistant Professor of Chemical Engineering

Xinyu Zhang, Associate Professor of Chemical Engineering

Virginia Davis, Alumni Professor of Chemical Engineering

Russell Mailen, Assistant Professor of Aerospace Engineering

Edward Davis, Assistant Professor of Mechanical Engineering

Abstract

Society's demands for more products and more energy places great strain on the industries responsible for producing them. Polymers present the opportunity to replace many of the "traditional" materials and open the door for advancement of technologies in ways previously unattainable. Polymers present many advantages over other materials as their inherent material properties are often easily altered, or tuned, via subtle yet distinct differences in their microstructures. Alteration of polymer microstructures and their effect on the resulting material properties is an ongoing investigation undertaken by many research groups. Timely and accurate characterization of these materials is critical to keep up with the hastening pace of the evolution of polymer science. This dissertation seeks to add to this discussion by providing insight into polythiophene copolymer microstructure-property relationships, reaction kinetics of an epoxy/thiol based crosslinked copolymer system, and application of low-field ^{1}H NMR spectroscopy to compositional analysis of multicomponent polymer systems.

As the demand for energy increases, the need for more efficient methods of energy generation is growing. Conductive polymers such as polythiophene and its derivatives present the opportunity to realize devices with tunable properties to aid in the recovery of the waste heat, which accounts for a large amount of the energy expended during energy generation. Poly(3-alkylthiophene)s have been widely studied for these application due to their well-controlled synthesis, typically enhanced solubility, and favorable optoelectronic and solid-state properties. Poly(3-hexylthiophene) is the most studied and utilized poly(alkylthiophene), however, other thiophene derivatives present alternative advantages such as enhanced charge transport, chemical stability, and a wide variety of functionalities. It is often desirable for a material to have a combination of these properties. Small

changes to polythiophene microstructure, either by 3-position substitution or by copolymerization of thiophene derivatives, yields polymers with tunable properties and favorable combinations of homopolymer properties to enhance resulting device performance. This dissertation explores topics pertinent to polythiophene copolymer chemistries such as the tuning material properties via statistical copolymerization of 3-hexylthiophene with unsubstituted thiophene or 3-methoxy thiophene, and compositional drift of thiophene comonomers synthesized via Grignard metathesis.

In addition, this dissertation explores the application of low-field ^{1}H NMR spectroscopy to the compositional analysis of a variety of polyolefins. Nuclear magnetic resonance (NMR) spectroscopy is arguably one of the most widely used characterization techniques as it is capable of characterizing many critical aspects of polymer materials. Traditional, or high-field, spectrometers (spectrometers rated at >300 MHz) are the most widely used version of these instruments in contemporary macromolecular science as they produce high-quality data and are capable of detecting subtle but distinct differences in polymer architecture. However, high-field spectrometers have several critical requirements for operation including cryogenic fluids, specially-trained personnel, and large amounts of laboratory footage. Recently, low-field NMR spectrometers have started to take a foothold in the industry as a viable replacement for their high-field counterparts. The main drawback of low-field NMR spectrometers as compared to high-field instruments is the broader peaks often associated with the weaker magnetic fields. This problem is further exacerbated by the repeat units within polymer backbones as repetitive signals coalesce and widen the observed spectral peak further. To combat this issue, many experimental parameters can be tuned such as sample concentration and molecular weight. In addition, many instrumental parameters, such as the number of scans and relaxation delay, can be adjusted to more closely emulate a high-field experiment. Low-field NMR spectroscopy is utilized to accurately determine

the microstructure and composition of mixed microstructure polyisoprenes, symmetric triblock copolymers, and polymer blends through a plethora of combinations of experimental and instrumental parameters to within 1-2% of a high-field NMR spectrometer (400 MHz). The ability of the low-field NMR spectrometer to accurately determine polyolefin microstructures and compositions will prove invaluable to both industry and academia as it will hasten research and analytical rates and also reduce the overall costs.

The last subject discussed in this dissertation is the cure kinetics of an epoxy/thiol based crosslinked copolymer system intended to address environmental concerns with leakage of fracking wellbores. Hydrocarbons, brine, and other injected chemical components have the potential to leak from both operating and abandoned wells into the surrounding environment, contaminating resources such as groundwater supplies and ecosystems impacting human health. Mitigating the impact of leakage thereby requires solutions to extend wellbore lifetime and seal leakage pathways in these systems. Traditional strategies for intervening to end leakage in fractured wellbore systems rely on injection of solid particle slurries (> 100 microns) into the concrete to seal the fracture. But penetration into small cracks require commercially available ultra-fine (< 10 micron particles) cement technologies, that are significantly more expensive and have short set times, complicating injection operations. Two polymer systems were explored that address the potential hazard by sealing leakage pathways in fractured wellbore systems. As expected, the reaction rate of our system is highly dependent on curing temperature as are the resulting physical properties. A firm understanding of the relationships between system chemistry, cure kinetics and material properties will allow for tailoring the design of the polymer sealant to particular subsurface wellbore conditions.

Table of Contents

Table of Figures

Table of Tables

Table of Schemes

List of Abbreviations

10P [10 mole % PEOD in PEOD/DGEBA crosslinked network]

3BT [3-bromothiophene]

3EHT [3-(2'-ethylhexyl)thiophene]

3HT [3-hexylthiophene]

40P [40 mole % PEOD in PEOD/DGEBA crosslinked network]

4SH [Pentaerythritol tetra(3-mercaptopropionate)]

60P [60 mole % PEOD in PEOD/DGEBA crosslinked network]

90P [90 mole % PEOD in PEOD/DGEBA crosslinked network]

AT [acquisition time]

ATR [attenuated total reflectance]

CB [chlorobenzene]

CDCl3 [deuterated chloroform]

CHCl3 [chloroform]

CV [cyclic voltammerty]

DB3EHT [2,5-dibromo-3-(2'-ethylhexylthiophene)]

DB3HT [2,5-dibromo-3-hexylthiophene]

DBT [2,5-dibromothiophene]

DBTDL [dibutylin dilaurate]

DCH [hexamethylene diisocyanate]

DFT [density functional theory]

DGEBA [bisphenol a diglycidyl ether]

DMA [dynamic mechanical analysis]

DMAP [4-(dimethylamino)pyridine]

DSC [differential scanning calorimetry]

ET [experimental time]

FPT [freeze-pump-thaw]

GDP [gross domestic production]

GPC [gel-permeation chromatography]

GRIM [Grignard metathesis]

HH [head-head coupling]

HOMO [highest-occupied molecular orbital]

HT [head-tail coupling]

LFNMR [low-field nuclear magnetic resonance spectroscopy]

LUMO [lowest-unoccupied molecular orbital]

MeOH [methanol]

MoT [3-methoxythiophene]

MW [molecular weight]

n [number of scans]

NBS [N-bromosuccinimide]

NidpppCl2 [1,3-bis(diphenylphosphino)propane nickel(II) chloride]

NMR [nuclear magnetic resonance spectroscopy]

NP [number of points]

P3AT [poly(3-alkylthiophene)]

P3BT [poly(3-butylthiophene)]

P3EHT [poly(3-(2'-ethylhexyl)thiophene]

P3HT [poly(3-hexylthiophene]

P3OT [poly(3-octylthiophene)]

PEOD [poly(ethylene oxide) diglycidyl ether]

PI [polyisoprene]

PICH [polyisoprene synthesized in neat cyclohexane]

PICT [polyisoprene synthesized in cyclohexane/triethylamine blend]

PMMA [poly(methyl methacrylate)]

PMoT [poly(3-methoxythiophene]

PPD [p-phenylenediamine]

PS [polystyrene]

PTMG [poly(tetramethylene ether) glycol]

R [spectral resolution]

RAF [Rigid Amorphous Fraction]

RD [relaxation delay]

SBS [styrene-butadiene-styrene triblock copolymer]

SIS [styrene-isoprene-styrene triblock copolymer]

SNR [signal-to-noise ratio]

SW [spectral width]

TEA [triethylamine]

TEG [thermoelectric generator]

THF [tetrathydrofuran]

TMS [tetramethylsilane]

TPB [tripheynl bismuth]

Triol [2-ethyl-2-(hydroxymethyl)-1,3-propane diol]

TT [tail-tail coupling]

WAXS [wide angle X-ray scattering]

WWII [World War 2]

XRD [X-ray diffraction]

Acknowledgements

It is with great pride and relief that I am finally able to write this portion of my dissertation. I have had the opportunity during grad school to grow in ways that I never dreamed were possible and the journey has been long but also short. I have also gotten exactly what I was seeking following my Baccalaureate degree, a higher level of exposure to fundamental science and a greater capability to ask the right questions. I have been busy during graduate school and have had the opportunity to learn and grow with many great fellow scientists. I would be remiss if I did not start with my advisor, Bryan Beckingham. I do not believe there to be another person who could've better served as my advisor. I knew from the second you mentioned chemistry (more specifically polymer chemistry) in your presentation to us during the graduate student-professor introductions that I would enjoy working with and learning from you. If I had to point out the three biggest things I have learned from you, they would be as follows: a balanced researcher equals a good researcher, the question is often more important than the answer, and polymers are the future (but we can't tell non-polymer people that ☺). As the first graduating Ph.D. from our lab, I sincerely thank you for your effort and guidance as I know it has been an adventure and I look forward to potentially working with you in the future.

Next, I would like to thank my lab mates (both current and former); Bree, Sneha, Luca, Vinita, and Bradley. Bree, I think you deserve special recognition as you have had the greatest exposure over the last ~5 years to all of my relentless puns and dad-jokes but still choose to interact with me. But seriously, you have been a loyal friend through many hardships I've faced during grad school and I will never forget that. Sneha, I will cherish the times we spent in front of the Pulsar trying to figure it out when we knew basically nothing (it paid off… yay!) and the times we went on rides on the Harley! I will miss the almost daily analysis of my psyche by Luca who I am convinced will one day hold a Ph.D. in psychology. I do not believe there is another person on Auburn's campus (outside of myself) who is as happy to interact with my dogs as Vinita is; I hope that you one day get another dog of your own! And finally, Bradley, whilst new to our group you have definitely already made an impression, I'll leave Auburn happy knowing that someone might carry the torch of puns and dad jokes for me. To all of my undergraduate mentees (Avery, Jihyuk, Tucker, Claudia [Mengyang], Zack [Xinyu], Lily, Barbara, Sam, Jacob, and Alisa), I also owe you a great deal of gratitude as you all provided new ways for me to grow as a researcher and person, most of the time in unexpected ways. I cherish every interaction we had, and I hope that you all continue to be the amazing folk that you are and that you find success in everything you do. I am fortunate to have been part of such an awesome research group and will look forward to the day that our paths cross again.

My journey here at Auburn was also guided and touched by many other amazing people outside of my research group. If I had to thank each and every one of them, I think it would probably double the length of this dissertation but single spaced; I will mention a few however. I should start with all of my committee members for your guidance in both my personal and professional growth: Dr. Xinyu Zhang, Dr. Virginia Davis, Dr. Russell Mailen, and Dr. Edward Davis. I greatly appreciate interacting with each of you and have gained new perspectives on both my own work and on others' work as a result. I do feel the need to put it in writing here though for Dr. Virginia

Davis, that Green Day is in fact considered a punk rock band. Next I would like to thank my collaborators from Dr. Andrew Adamczyk's research group (Dr. Adamczyk himself, Katie Lawson, and Ashraf Ali) for providing their expertise on the computation methods detailed in Chapter 7 as I feel that the DFT experiments added an extra level of security and assurance to my experimental work. I would also like to thank Dr. Rong Zhao for all of the electrochemical characterization assistance she provided and the innumerous lunchtime conversations we had discussing how I could possibly survive off of PB&J for so long. I would like to also thank my collaborators from my work with the epoxy/thiol-based cure kinetics work Dr. Maria Auad, Dr. Anton Schindler, Dr. Lauren Beckingham and Nima Alizadeh. Your input and support on this work only enhanced the quality of the research I got to perform and communicate.

I would like to now thank my friends and family for their undying support during my education here. Specifically, I have to thank my friends Vlad and Ana Saveljevs for awakening both the athlete and entrepreneur within me. I have found two new hobbies as a result of our friendship and I foresee that my future will involve weight lifting, materials science, motorcycles, and a business of my own. I have made so many friends whilst here doing a variety of activities and as such, I feel it better to mention the activities because I could go on and on about all of the amazing people that were my counterparts. So to my fellow Spartans, ultimate Frisbee-ers, Fodder for Mind participants, and Tiger Cage Teammates I thank you for making this graduate school experience a complete one.

To my mom and dad, I thank you for the example you set for me growing up. While both of you work in very different fields, I learned the same lesson from both of you. That is, that nothing is ever too hard to accomplish, it's always about how bad you want it. And as such, I will carry that philosophy with me the rest of my life and always relentlessly pursue my dreams and passions. To my brother and sister, I am proud that both of you have found career paths that you love and can enjoy. Though I have been far away, I still feel close to my family and hope to always be able to provide support in the way that I have been supported whilst experiencing my growth here at Auburn. I want to also make mention of the loss I have felt as a result of my grandpa, Jim, passing away in 2016 during my first full summer here. His outlook on the world of "never know a stranger" is a large part of my personality and I will never hesitate to meet new people as a result. My endless rambling is definitely a result of being close to him, he always loved to tell limericks (a kind of lost art these days) and so I wrote an amateur one to dedicate this dissertation to his memory.

"B.S. to Ph.D"

A Missouri boy graduated from Mizzou,
Then moved to Auburn for degree number two,
He grew and he learned,
From the experience he yearned,
And now he'll be an Auburn grad too.

I am looking forward to the future and hope this dissertation provides clear evidence for my viability as an effective researcher and my ability to pivot/ adapt to unknown challenges. If any questions arise after reading this document, please don't hesitate to reach out! Tschuss!

Chapter 1 - Introduction

It is nearly impossible to look around in modern times and find a facet of our daily lives in which polymers do not affect us. For instance, polymers can be found in the seat cushion you may currently be sitting on, the rubber on the bottom of your shoes, the clothes that you are wearing, and in the systems by which you received this document. Polymers are so integrated into our daily lives that it would be impossible to maintain our current way of life without them. There are as wide a variety of polymers as there are applications for them. Polymers can have structures that contain many types of atoms such as fluorine, chlorine, or sulfur; although they are largely carbon-based. They can have many conformations such as linear or branched chains. And finally, their bonds may vary from a simple single-bonded structure to alternating (conjugated) double bonds. The combination of all of these chemical features makes up what is known as the polymer microstructure. The microstructure of polymers plays a critical role in the resulting material properties. Fortunately, polymer microstructures are, in general, amendable to alterations or tuning and thus may be manipulated and designed for many specialized applications.

What classifies a molecule as a polymer? Polymers are long chains of repeating smaller units (called mers) that are covalently bonded. Copolymers have one or more type of repeat units and this can lead to random, block, or statistical mer distributions along the polymer chain. By changing the mer units in a polymer chain the overall material properties change greatly. These changes can be quantified by various methods of characterization. Examples of property changes include the chemical environment (probed with nuclear magnetic resonance spectrum shift), physical properties as evident by various signature temperatures, crystallinity, glass transition temperatures, degradation temperatures, etc. and their optical properties such as absorption behavior, optoelectronic band gaps, and UV-oxidative stability. The relationships between

microstructure and overall material properties are the focus of this research. More specifically, the impact of varied chemical structure and composition in polythiophene copolymers on optoelectronic and solid-state properties is of primary focus. By statistical copolymerization of two or more chemically different thiophene monomers, namely unsubstituted thiophene and 3-substituted thiophenes, a range of copolymers with varied composition are synthesized. This route presents an ideal platform to investigate microstructure-property relationships as alteration to the polymer synthesis method needed is merely a variation of the relative amounts of monomers and the monomers themselves. Additionally, this work investigates and benchmarks the utility of new, digitalized low-field ^{1}H NMR spectrometers for the characterization of copolymer and polymer blend systems, which is of critical importance for understanding structure-property relationships in these systems.

1.1- Motivation

1.1.1- Polythiophene Copolymers

With the ever-increasing population of the world, the demand placed on the energy generation sectors continues to grow. This demand places strain on an already over-burdened section of society. Much of this strain results from the largely inefficient technology and equipment that are used in the generation of electricity. Many generators are only 30-40% efficient at best, not taking into account the loss of efficiency over time from the usage of non-ideal operating conditions.[1,2] The current demand for electrical energy in the United States is approximately 4.08 trillion kWh of electricity annually. Taking into consideration the amount of electricity demanded and the efficiency of the equipment used to generate it, it is apparent how much energy is wasted; 2.98 trillion kWh and 1.92 trillion kWh for the 30% and 40% efficiencies respectively. If we take the optimum case (40% efficient electricity generating equipment) and implement energy recovery technology assuming only a 1% recovery of the wasted energy, an approximate 19.2 billion kWh

can be recovered; 1% recovery is purposefully an underestimate and is only a 0.6% increase of efficiency of the overall equipment efficiency. To put that energy number in more relatable terms, that translates to an approximate savings of $600 billion on the operational side of the industry.[3]

The technologies currently utilized in this field are often unable to be deployed effectively, expensive to manufacture, and/or do not possess the desired material properties.[4] Two such methods for waste energy recovery are heat exchangers and thermoelectric generators (a solid-state heat exchanger). Traditional waste-heat recovery heat exchangers are costly to maintain, require significant space, and are often inefficient.[5] Thermoelectric generators are a unique method for waste-heat recovery in that they convert low-grade waste heat directly to electricity via the Seebeck Effect (aka Peltier Effect). Many current thermoelectric generators are comprised of small molecules such as constantan and alumel, which are not able to be effectively deployed into the field and have limited tunability with regards to properties and thermoelectric transductance. The Seebeck Effect occurs when two conductive materials are joined at each end and one side is heated while the other remains cool, Thomas Seebeck discovered this phenomenon in the early 1800s.[6] A schematic of a thermoelectric generator can be found in **Figure 1.1**. As one junction is subjected to heat, electrons flow from the hot side to the cool side generating an electric current. The materials used in thermoelectric generators prevent them from being used effectively as waste-heat recovery systems since they are not easily deployable or retrofitted into the structure of power plants. The difficulty of creating and deploying these devices can be overcome with polymers. Polymers can, generally speaking, create devices that are tunable, flexible, and durable enough to handle a wide variety of applications.

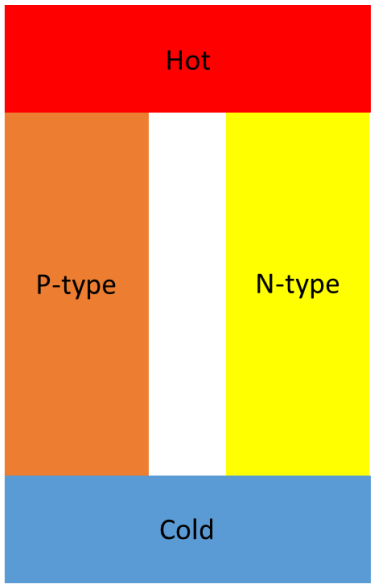

Figure 1.1 Schematic of a thermoelectric generator.

Polythiophenes have attracted much attention due to their well-controlled synthesis, favorable optoelectronic properties, and thermal stability.[7–18] Polythiophenes are commonly used in thin-film transistors, chemical sensors, thermoelectric generators, and bulk-heterojunction solar panels.[7–18] Substitution of various active groups onto the three position of the cyclic thiophene ring provides a direct way to tune the properties of polythiophenes. While it is known that polymer microstructure affects the solid-state properties of polythiophenes, a more complete understanding would allow for "tunable" organic electronic devices with a wider range of properties. Since these conductive polymers generally serves as the active portion of devices in which they are integrated, their material properties are inherently correlated with device performance.

Here, by systematically varying substituent groups on the cyclic thiophene rings changes in microstructure will be induced and the effect on the solid-state and solution properties investigated. While fabrication and performance benchmarking of polythiophene-based devices are outside the scope of this dissertation, tuning and characterization of relevant material properties of

polythiophene-copolymers are explored and discussed. In particular, relative polymer molecular weights are extracted via gel-permeation chromatography, copolymer compositions are extracted via ^{1}H nuclear magnetic resonance spectroscopy, melting temperature and relative crystallinity are investigated via differential scanning calorimetry, optoelectronic band gap and UV-light absorption behavior are investigated via UV-Vis spectrophotometry, and highest-occupied molecular orbital energy levels are investigated via cyclic voltammetry.

1.1.2- Benchmarking of a Low-Field ^{1}H NMR Spectrometer

Many modern manufacturers of analytical instruments have begun to produce instruments that are both more accessible and provide data that approaches the quality of their more expensive counterparts. The most relevant example of this phenomena to this work is the benchtop NMR spectrometer (60 MHz Oxford Instruments Pulsar[20]) located in the Beckingham Polymer Research Lab at Auburn University. The spectrometer is used almost daily for routine analyses and generally expedites the rate at which many projects can move forward. Most commonly, molecular composition are investigated in order to evaluate structure-property relationships and NMR spectroscopy is a generally accepted route for detection of chemical species and quantification of their relative compositions within a sample. Low-field NMR spectroscopy was used in this dissertation to assist in accurate and time-efficient synthesis and characterization of thiophene monomers. Low-field NMR spectroscopy as discussed in this dissertation refers directly to the 60 MHz Oxford Instruments Pulsar NMR spectrometer. This instrument is similar to early model NMR spectrometers with regard to magnetic field strength but due to advances in modern computer science is capable of producing results similar to that of contemporary high-field instruments. In this dissertation, low-field NMR spectroscopy is used to analyze a series of monomers, polymers, and polymer blends and the resulting spectra are compared against high-

field results. This work is critical as there is limited literary evidence of low-field NMR spectroscopy as it applies to polymeric systems and much suspicion abounds within the field as to its use. I hope that through this document (and the relevant publications), more of the research community (industrial and academic alike) will recognize the value and utility of low-field NMR spectroscopy for polymer systems.

This dissertation is organizd as follows. In Chapter 2 the necessary background information to introduce this work is presented and discussed. Chapter 3 provides general background materials on the experimental and characterization methods. Chapters 4-9 are adaptations of published manuscripts. Chapter 4 discusses the various experimental and instrumental parameters relevant to low-field NMR spectroscopy and their impact on data quality. Chapter 5 further explores the application of low-field spectroscopy to a wider variety of polymer/copolymer systems. Chapter 6 discusses the statistical copolymerization of 3-hexylthiophene and unsubstituted thiophene and their resulting properties. Chapter 7 discusses the properties and synthesis of poly(3-hexylthiophene-*co*-3-methoxythiophene). Chapter 8 investigates the evolution of GRIM-synthesis copolymer compositional evolution. Chapter 9 details a special topic in which components of a thiol-epoxy crosslinked network are varied to tune reaction cure kinetics and pertinent mechanical properties. Lastly, Chapter 10 discusses potential projects to build upon the work discussed in this dissertation.

1.2- References

(1) What is U.S. Electricity Generation by Energy Source? - FAQ - U.S. Energy Information Administration (EIA) https://www.eia.gov/tools/faqs/faq.php?id=427&t=3 (accessed Nov 2, 2017).

(2) World's Most Powerful Thermoelectric Generator > ENGINEERING.com https://www.engineering.com/ElectronicsDesign/ElectronicsDesignArticles/ArticleID/8689/Worlds-Most-Powerful-Thermoelectric-Generator.aspx (accessed Nov 2, 2017).

(3) SAS Output https://www.eia.gov/electricity/annual/html/epa_08_04.html (accessed Nov 2, 2017).

(4) We, J. H.; Kim, S. J.; Cho, B. J. Hybrid Composite of Screen-Printed Inorganic Thermoelectric Film and Organic Conducting Polymer for Flexible Thermoelectric Power Generator. *Energy* **2014**, *73* (Supplement C), 506–512. https://doi.org/10.1016/j.energy.2014.06.047.

(5) Turton, R.; Bailie, R.; Whiting, W.; Shaeiwitz, J. *Analysis, Synthesis, and Design of Chemical Processes*, Third Edition.

(6) Mani, P.; Nakpathomkun, N.; Hoffmann, E. A.; Linke, H. A Nanoscale Standard for the Seebeck Coefficient. *Nano Lett.* **2011**, *11* (11), 4679–4681. https://doi.org/10.1021/nl202258f.

(7) McCullough, R. D. The Chemistry of Conducting Polythiophenes. *Advanced Materials* **1998**, *10* (2), 93–116. https://doi.org/10.1002/(SICI)1521-4095(199801)10:2<93::AID-ADMA93>3.0.CO;2-F.

(8) McCullough, R. D.; Lowe, R. D.; Jayaraman, M.; Anderson, D. L. Design, Synthesis, and Control of Conducting Polymer Architectures: Structurally Homogeneous Poly(3-Alkylthiophenes). *J. Org. Chem.* **1993**, *58* (4), 904–912. https://doi.org/10.1021/jo00056a024.

(9) Balko, J.; Lohwasser, R. H.; Sommer, M.; Thelakkat, M.; Thurn-Albrecht, T. Determination of the Crystallinity of Semicrystalline Poly(3-Hexylthiophene) by Means of Wide-Angle X-Ray Scattering. *Macromolecules* **2013**, *46* (24), 9642–9651. https://doi.org/10.1021/ma401946w.

(10) Barbarella, G.; Bongini, A.; Zambianchi, M. Regiochemistry and Conformation of Poly(3-Hexylthiophene) via the Synthesis and the Spectroscopic Characterization of the Model Configurational Triads. *Macromolecules* **1994**, *27* (11), 3039–3045. https://doi.org/10.1021/ma00089a022.

(11) Boudouris, B. W.; Ho, V.; Jimison, L. H.; Toney, M. F.; Salleo, A.; Segalman, R. A. Real-Time Observation of Poly(3-Alkylthiophene) Crystallization and Correlation with Transient Optoelectronic Properties. *Macromolecules* **2011**, *44* (17), 6653–6658. https://doi.org/10.1021/ma201316a.

(12) Beckingham, B. S.; Ho, V.; Segalman, R. A. Melting Behavior of Poly(3-(2′-Ethyl)Hexylthiophene). *Macromolecules* **2014**, *47* (23), 8305–8310. https://doi.org/10.1021/ma501915v.

(13) Minkler, M. J.; Beckingham, B. S. Statistical Copolymers of 3-Hexylthiophene and Thiophene: Impact of Thiophene Content on Optoelectronic and Thermal Properties. *Materials Today Communications* **2019**, 100547. https://doi.org/10.1016/j.mtcomm.2019.100547.

(14) Son, S. Y.; Kim, J.-H.; Song, E.; Choi, K.; Lee, J.; Cho, K.; Kim, T.-S.; Park, T. Exploiting π–π Stacking for Stretchable Semiconducting Polymers. *Macromolecules* **2018**, *51* (7), 2572–2579. https://doi.org/10.1021/acs.macromol.8b00093.
(15) Chao, P.-Y.; Wu, H.-C.; Lu, C.; Hong, C.-W.; Chen, W.-C. Biaxially Extended Conjugated Polymers with Thieno[3,2-b]Thiophene Building Block for High Performance Field-Effect Transistor Applications. *Macromolecules* **2015**, *48* (16), 5596–5604. https://doi.org/10.1021/acs.macromol.5b01243.
(16) Hu, X.; Lawrence, J. A.; Mullahoo, J.; Smith, Z. C.; Wilson, D. J.; Mace, C. R.; Thomas, S. W. Directly Photopatternable Polythiophene as Dual-Tone Photoresist. *Macromolecules* **2017**, *50* (18), 7258–7267. https://doi.org/10.1021/acs.macromol.7b01208.
(17) Duong, D. T.; Toney, M. F.; Salleo, A. Role of Confinement and Aggregation in Charge Transport in Semicrystalline Polythiophene Thin Films. *Phys. Rev. B* **2012**, *86* (20), 205205. https://doi.org/10.1103/PhysRevB.86.205205.
(18) Davidson, E. C.; Beckingham, B. S.; Ho, V.; Segalman, R. A. Confined Crystallization in Lamellae Forming Poly(3-(2′-Ethyl)Hexylthiophene) (P3EHT) Block Copolymers. *Journal of Polymer Science Part B: Polymer Physics* **2016**, *54* (2), 205–215. https://doi.org/10.1002/polb.23904.
(19) Ho, V.; Beckingham, B. S.; Ng, H. H.; Segalman, R. A. Control of Thermal and Optoelectronic Properties in Conjugated Poly(3-Alkylthiophenes). *MRS Communications* **2014**, *4* (2), 45–50. https://doi.org/10.1557/mrc.2014.9.
(20) Chakrapani, S. B.; Minkler, M. J.; Beckingham, B. S. Low-Field 1H-NMR Spectroscopy for Compositional Analysis of Multicomponent Polymer Systems. *Analyst* **2019**, *144* (5), 1679–1686. https://doi.org/10.1039/C8AN01810C.

Chapter 2 - Background

Prior to World War II (WWII), the world was highly dependent on natural rubber from the rubber tree farms located in southeastern Asia. Around 95% of the world's rubber supply was sourced from there and as a result there was little motivation to increase the synthetic rubber production capabilities. During WWII, the United States remained somewhat uninvolved for much of the war; mainly participating for much of the war as a supplier to the Allies in Europe.1 However, in 1941 the United States placed a trade embargo on Japan to inhibit its ability to continue invading Ally-controlled colonies in southeastern Asia. Japan responded by declaring war on the Allies (now officially including the U.S. following the attack on Pearl Harbor) and by cutting off much of the aforementioned natural rubber supply. Following this ill-planned move by the Japanese, the United States, under President Franklin D. Roosevelt, established the War Production Board (WPB) which served to allocate U.S. resources and funding to directly benefit the wartime efforts of the Allied Forces.1 The WPB almost immediately sought to address the dwindling rubber supplies through the use of creative propaganda to bolster recycling efforts of rubber and funding the upscaling of synthetic polymer production. The U.S.'s, and probably the world's, first successful large-scale recycling program was birthed to recoup large amounts of the rubber used in consumer products; examples of the propaganda poster are shown in **Figure 2.1**. This resulted in about 900,000 lbs of rubber being recycled in the summer of 1942 alone![1–3]

The unintended effect of the Japanese' mishandling of the Pacific Theater, yielded economies in the Allied Forces that could not only produce synthetic rubbers but produce it in much larger quantities than ever before.[3–5] The U.S.'s production of rubber skyrocketed from a measly 60,000 lbs/year to nearly a million pounds per year. These synthetic polymer materials were generally higher-performing and could be used in a broader range of applications as compared to the natural

rubber that is chemically similar to polyisoprene.[6] This invigoration of synthetic materials' production led to better outfitting of the Allied Forces and aided in the recovery of the global economy from the Great Depression; this is evident through comparison of the two sides' GDPs throughout WWII, shown in **Figure 2.2**.[7]

Synthetic materials did more than just outfit the infantry and hold the frontlines, they enabled the realization of many new technologies for both war and civilian applications. Incidentally, the birth of synthetic polymers led to the production of atomic bombs as they required light-weight, high-temperature stable valve fittings and covers to realize this technology; this was provided by poly(tetrafluoroethylene) (PTFE).[8] This class of weapons of mass destruction might not have been realized in the same timely fashion had it not been for the lack of access to the natural rubber supply. Following the deployment of the atomic bombs (Fat Man and Little Boy) Japan surrendered and the second Great War was over, but the factories and production capabilities of wartime remained. Following dissolution of the WPB, the companies formerly supported by the Board during the war saw the potential profits and switched to producing consumer products. Production climbed all the way to ~two million tons of rubber/year by 1950 and has continued to climb to a staggering 448 million tons/year in 2015; now a ~$96 billion industry.[9] The effects the reckless moves made by Japan during WWII can never truly be quantified, but the industry created as a result changed the history of the global economy and environment forever.

Figure 2.1 World War II-era propaganda promoting recycling as a aiding the Allies' war-effort World War II-era propaganda promoting/inciting citizens to aid the war-effort via recycling.

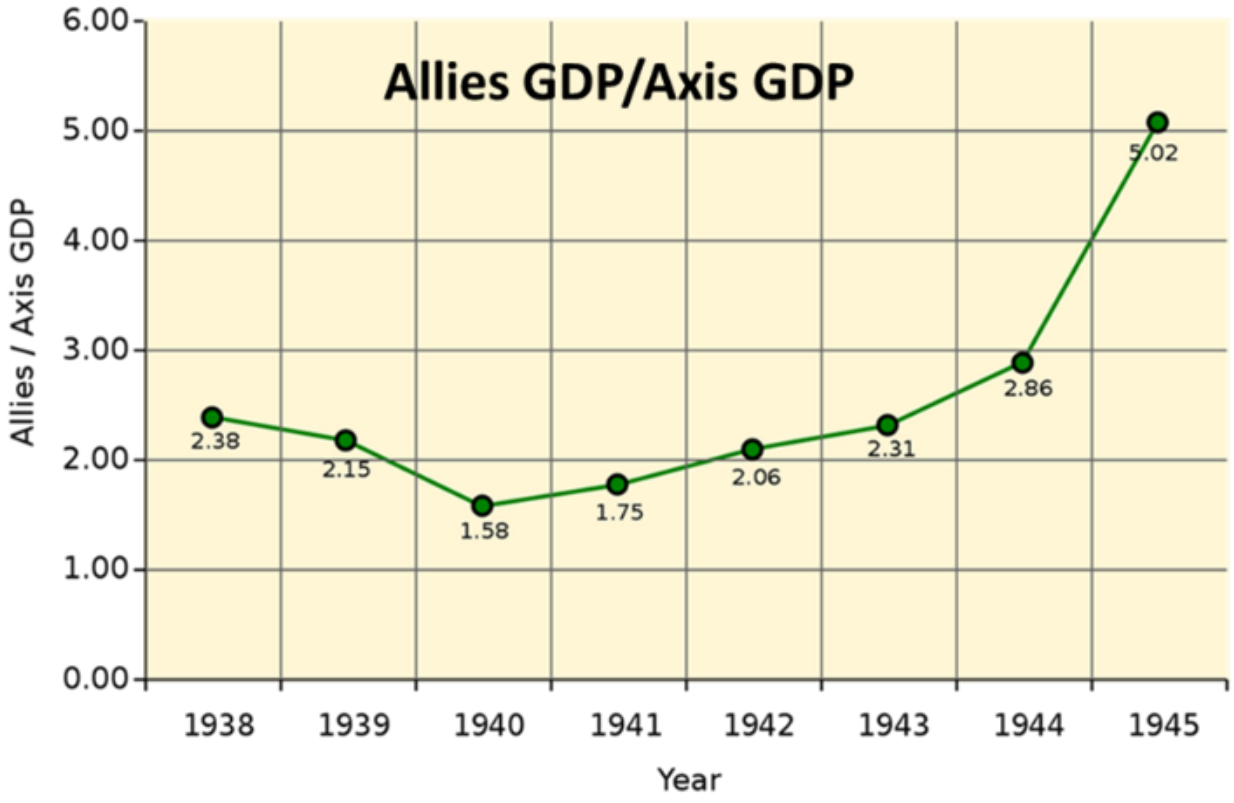

Figure 2.2 Snapshot of the GDP of both sides during WWII.

Contemporary society has become almost completely dependent on the products that allow us to perform our various day-to-day tasks such as cooking, working, and relaxing. Many of these consumer products are largely based on plastics and rubbers… a.k.a. polymers. Polymers dominate our daily lives as they generally provide a lower-cost, lighter weight alternative to traditional materials used in consumer-goods production. Polymers, more specifically synthetic polymers, have saturated modern society as they are employed in a wide number of capacities ranging from packaging to staple parts of modern products such as electronic casings, clothing textiles, and innumerable products in the food industry. This is possible due to the wide variety of polymers and their greatly varied material properties. Synthesis and tailoring of various polymer chemistries presents their greatest advantage as their material properties are somewhat easily altered through subtle changes in the polymer microstructure.[10–25] Polymer chemistries are like a puzzle that has an infinite number of pieces that can be put together in an infinite number of correct configurations to yield polymers of all sizes, shapes, colors, and functionality. The sheer number of combinations of polymer chemistries and microstructures makes understanding of property-relationships a very difficult task. The relationship of polymer microstructure to resulting material properties is the main topic of this document as it is the underlying common denominator amongst all of my research to date.

2.1- Polymer Microstructure

Our daily lives are governed by the consumer products which we use to survive, interact, and play. Many of these products are largely polymer-based and their constituent materials sometimes only differ by a few subtle changes at the molecular level. In other words, the way in which we choose to utilize certain consumer products is governed by the particular arrangement of molecules and how they respond to external stimuli.

Polyethylene will serve as our starting point for our discussion of polymer microstructure as it is the most commonly used polymer in modern society and has many derivatives utilized across a wide-variety of applications.[26] Unbeknownst to much of the general public, small changes in the underlying material microstructure and architecture can often yield materials with drastically different properties. For instance, polyethylene (the most common polymer used in society) comes in a variety of configurations ranging from low-density to high-density and the main difference is their extent of branching.[27] Even though they do not possess any different types of bonds, their inherent properties are drastically different. Furthermore, by choosing to substitute some of the hydrogens for fluorine or chlorine we observe other material properties such as high chemical or corrosion resistance. Namely, substitution of the hydrogens in the backbone for fluorine yields PTFE which, as we know, is highly abundant in our society.

If we revisit polyethylene and place double bonds between every other carbon, effectively removing half of the hydrogens, we induce yet another drastic change into the polymer backbone… π-orbital conjugation. Heeger et al. in 1972 discovered that polymers were not strictly the insulating material society had pegged them to be.[28] The presence of alternating single and double bonds allows for charges to transport across the polymer backbone. This is important since before this discovery, all conductive materials were thought to have been only metallic substances which provide good device performance but at a cost to processability and tunability. The microstructures of polyethylene and other similar polymers are shown in **Figure 2.3**.

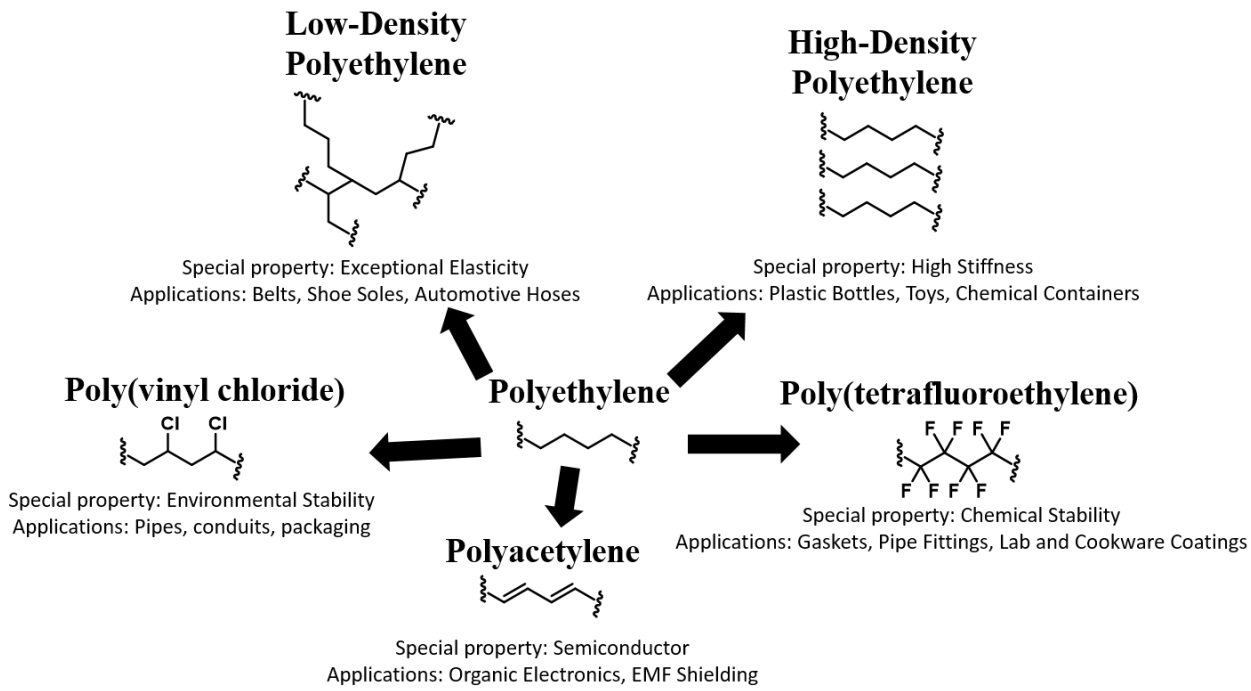

Figure 2.3 Microstructure of polyethylene and other similar polymers.[29,30]

2.2- Tuning and Tailoring of Polymer Properties

Generally, devices and technology based off polymer materials are flexible, lighter, less-costly, and easier to produce on large scales, and versatile in application as compared to their small molecule counterparts. Additionally, polymer properties can be tuned by making small changes to their synthetic routes. It has been shown many times throughout literature that by copolymerizing two or more distinct monomers, the properties of the resulting materials can be altered.[10,16–20,23,24,31–40] This aspect of polymer science is crucial as it typically provides a facile route to unlock previously inaccessible combinations of material properties as researchers seek to make use of advantageous homopolymers properties while minimizing any inherently negative properties. Additionally, the architecture or patterning of the copolymer backbone directly affects the resulting material properties and plays a critical role in determining the performance of the devices utilizing

the polymer material. Conveniently, copolymer backbones have been stereotyped into a few common types of additions, outlined in **Figure 2.4**.

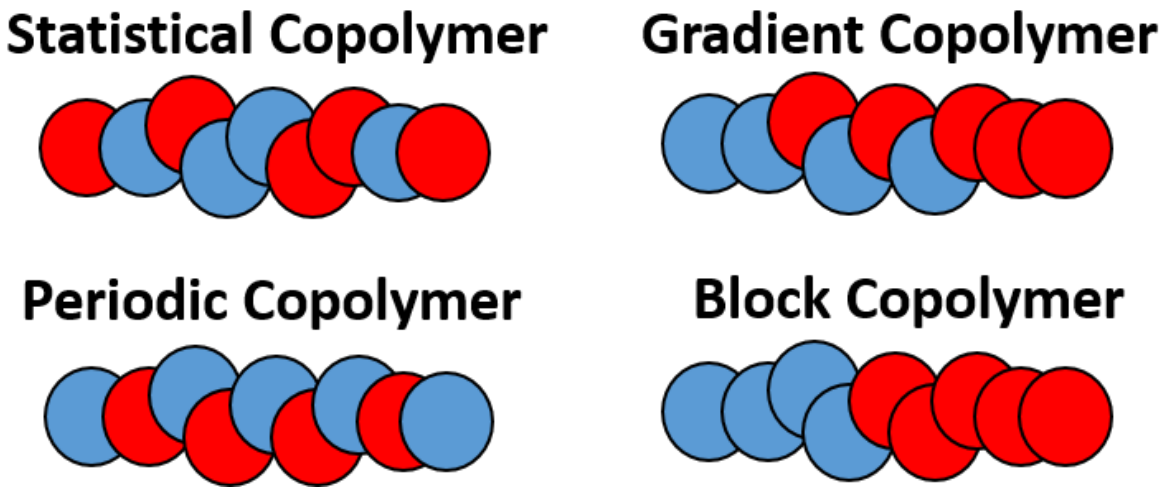

Figure 2.4 Example patterns of various copolymer architectures.[41]

Polymer chemistry, namely copolymer chemistry, is very complicated as polymer can have the same global composition but the manner in which the monomers were enchained can greatly affect the resulting material properties.[40,42–45] There are many experimental parameters that impact copolymer microstructure such as: reaction temperature, solvent environment, monomer functionality, catalytic moderators, initiation methods, and monomer charge timing (addition of monomers at discretely different reaction times).[31,46,47] A very common way to discuss copolymerization mechanisms is through the monomer propagation functionalities, and this is typically distinct from repeat unit functionality within the resulting polymer. For instance, in a perfectly alternating system (periodic), we would describe the monomer 1 as A-A and monomer 2 as B-B in which the backbone chemistry of monomer "1" is distinct from that of monomer "2". In this scenario, the group functionality A can only react with that of functionality B. This method

provides a facile route to decouple initial monomer concentration from that of resulting copolymer architecture. However, perfectly periodic copolymers are not always desired as other conformations can provide additional, and useful, material properties. For example, gradient copolymers can be utilized to enhance compatibility between two incompatible polymer phases by gradually evolving from one block-like phase to another.[39,40] One particularly, useful case of copolymer microstructure is that of block copolymers. Block copolymers can be thought of as two or more homopolymers (often times relatively short chain) that are covalently bonded together. They are utilized in a wide variety of applications ranging from micellar polymersomes for drug delivery to donor-acceptor structured semiconductive copolymers.[46,48–53]

The final type of linear copolymer architecture, the most relevant to this dissertation, are statistical copolymers. Statistical copolymers are typically synthesized by polymerizing two or more distinct monomers that typically possess the same propagation functionalities (A-B). Typically, statistical copolymers do not require any additional synthetic steps, with the exception of two or more monomer syntheses, as the copolymerization process is typically identical to that of the synonymous homopolymerization methodology.[15–17,36] In the scope of this work, statistical copolymerization of thiophene and thiophene derivatives is explored extensively and will be discussed in further detail in later sections and chapters.

2.3- Polymer Backbone Stereochemistry

Distinguishing between the different types of additions is many times difficult and sometimes impossible. Accurate determination of backbone architecture is crucial for understanding material behavior and the performance in its given application. An important historical example of the importance of stereochemistry is the 1950's era drug Thalidomide.[54] Thalidomide, much like many organic-based drugs and materials possesses two enantiomers, shown in **Figure 2.5**, that behave

completely different when processed by the body. R-Thalidomide performs as intended, to mitigate morning sickness symptoms in pregnant women, while S-Thalidomide is both ineffective, and produces birth defects and high mortality rates in the offspring of the subjected women.[54]

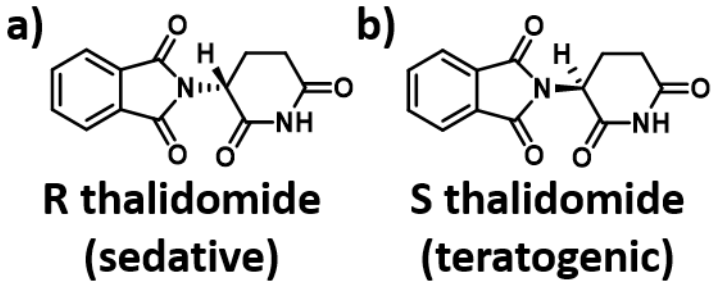

Figure 2.5 Microstructures of a) safe, sedative thalidomide enantiomer and b) unsafe teratogenic thalidomide enantiomer.

Similarly, polythiophenes can exhibit varied backbone stereochemistry that impact their material properties. Even slight changes such as the location of a side chain on the aromatic thiophene ring can greatly alter solid-state and solution properties.[55–57] One of the greatest microstructure issues facing poly(3-alkylthiophenes) is a characteristic known as regioregularity. Regioregularity designates the pattern in which the side chains sit on the polythiophene backbone as shown in **Figure 2.6** for poly(3-substituted thiophene)s. The conductive properties of regioregular polythiophenes are superior to regiorandom polythiophenes.[55–61] This is largely due to the ability of regioregular polythiophenes to interdigitate and form tightly packed lamellae. Non-regioregular poly(3-substituted thiophenes) lack the ability to form crystals due to sterics, which also inhibits the ability to form appreciable π-π stacking, the polymer characteristic that allows transport of charge carriers.

Not only does the relative position of the side chain play a critical role in the behavior of the polymers, the electron withdrawing behavior can also have a great impact on the resulting material properties.[11,55–70] Conflicting literature as to the exact effects of electron-withdrawing behavior on the Fermi energy levels is present.[68,69] Some cases present data in which electron-donating groups such as alkoxy-substituted thiophenes raises the HOMO energy levels (Mei et al) while others suggest that it lowers the HOMO energy levels (Cui et al).[68,69] As evidenced in literature, the electronic structures also affect more than the band gap, it also can also demonstrate the ability to self assemble as demonstrated by fluoroalkyl- and perfluoro-subsituted thiophene polymers and copolymers.[66–68]

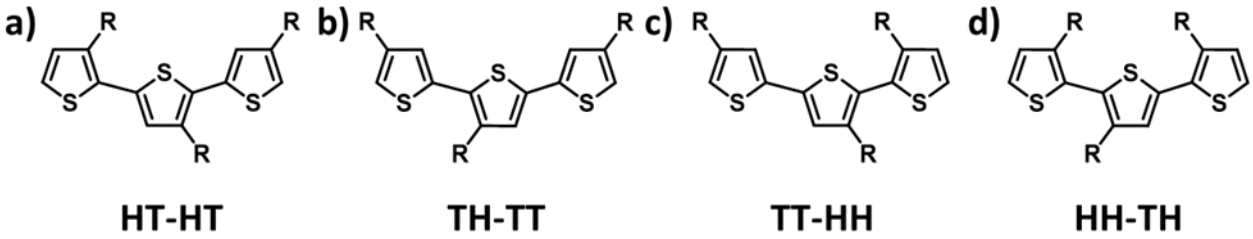

Figure 2.6 Microstructural triads of regioregular HT-HT substituted polythiophene (a) and regiorandom polythiophene conformations (b-d).

2.4- Semiconductive Polymers

Traditionally, electronic devices have been comprised of small molecule/ materials but recently polymers have begun to replace them as polymer properties meet or exceed specifications. Polymers can overcome some disadvantages of small molecule-based devices by allowing for devices that are tunable, flexible, and scalable for larger economic need. Semiconducting polymers enable the fabrication of polymer based electronic devices such as solar panels, thermoelectric generators, chemical sensors, and thin-film transistors by providing an organic active medium. Polythiophene, polyaniline, polypyrrole, and the previously mentioned polyacetylene are all

examples of semiconducting polymers that have found applications in organic electronic devices.[55,65,71–75] They are conductive due to their conjugated double bond structure, which allows for π-π stacking to occur.[15,16,76] Four common examples of semiconductive polymers are show in **Figure 2.7**.

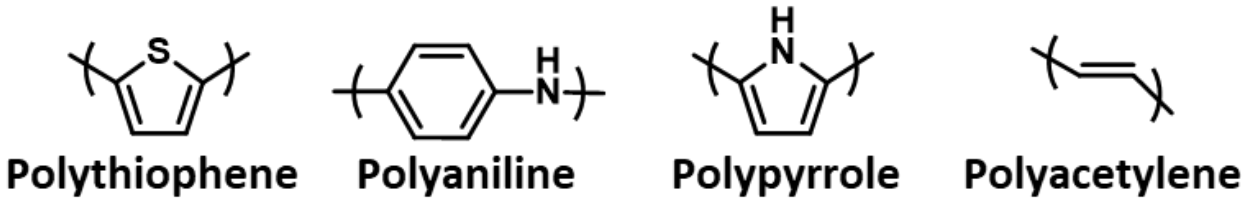

Figure 2.7 General microstructures of common semiconductive polymers.

While both polymers and inorganic materials can absorb energy from light (polymers typically from ultraviolet light), the mechanism for energy generation in these two classes of semiconductive materials differs. Inorganic materials release free electrons upon excitation by light energy while organic materials generate an electron-hole pair known as an exciton. The exciton is then transported along the polymer backbone through carbon-carbon stretching. Transportation of the exciton is enabled through coupling with a phonon in the backbone of the polymer. In order generate charge carriers and energy the exciton must be near an acceptor-donor interface to be able to dissociate into the respective carriers.[75,77,78] One problem with this is that the exciton is a neutral species which means that it will diffuse randomly. Having the interface with the appropriate band gap and distance from the point of generation is crucial to effective energy generation.

2.4.1- Introduction to Polythiophene

Polythiophenes have been widely studied due to their comparably good charge transport, appreciable chemical/environmental stability, tunable microstructures and properties, and compatibility with a wide variety of synthesis methods. Polythiophene was originally synthesized as a derivative of the nearly identical polypyrrole.[79] The substitution of the NH heteroatom in the aromatic ring for sulfur resulted in a much more oxidatively stable semiconductive polymer. Following the realization of unsubstituted polythiophene, which was likely synthesized via electropolymerization methods, substituted polythiophenes began to be explored. As discussed in section 2.3, 3-substituted polythiophenes suffered from lack of regio-contol and as such exhibited nearly unpredictable/non-repeatable results. McCullough et al. demonstrated a method known as Grignard Metathesis (GRIM) polymerization which provides a facile route for highly regioregular poly(3-alkylthiophenes) synthesis, shown in **Scheme 2.1**-**Scheme 2.3**. GRIM polymerization is a metathesis polymerization in which a sterically hindered Grignard selectively inserts magnesium into the bromine-carbon bond of the dibrominated monomer. **Scheme 2.1** shows the substitution reaction of the magnesium onto the aromatic thiophene ring; shown in **Chapters 6** and **8** are a more in-depth discussion of this mechanism.[17] Next a sterically hindered catalyst is added and selectively reacts with the same location as the t-butyl magnesium chloride; this is shown in **Scheme 2.2**. The result of this steric selectivity is highly uniform, or regioregular, poly(3-substituted thiophenes). Finally, the reaction can is terminated by, in a typical case, 6 M HCl but termination with other compounds can be useful for placing a functional group at the chain end; shown in **Scheme 2.3**.[76] This is a common route to the synthesis of block copolymers with a polythiophene block; termination typically with ethynyl magnesium bromide and subsequent reaction of azide-alkyne at the chain end.

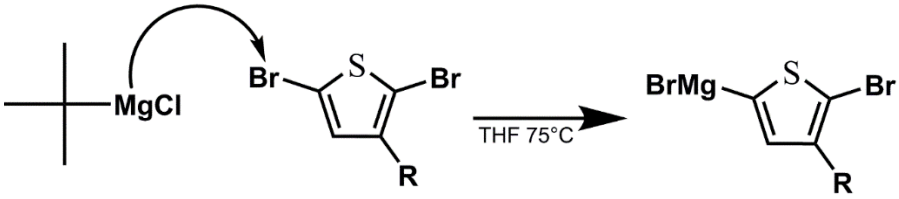

Scheme 2.1. Grignard Substitution of magnesium into the bromine-carbon bond of 2,5-dibromo-3-hexylthiophene by t-butyl magnesium chloride.

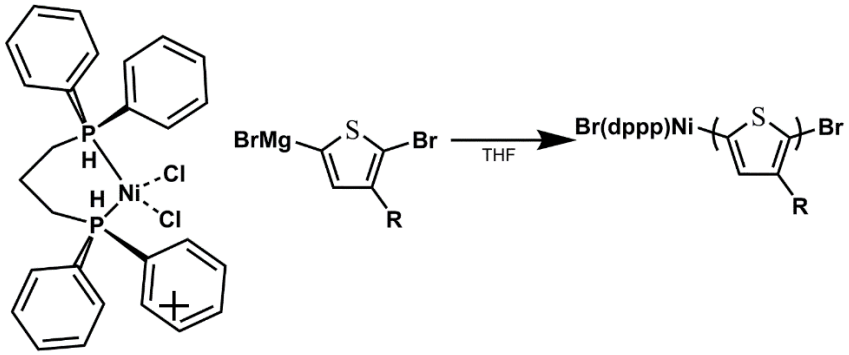

Scheme 2.2 Intermediate formation during GRIM polymerization upon reaction of 1,3-bis(diphenylphosphino)propane nickel(II) chloride with the Grignard on the aromatic ring.

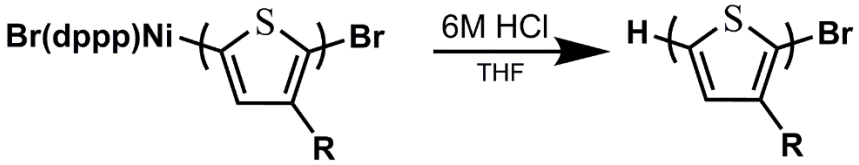

Scheme 2.3 Termination of intermediate GRIM reagent with 6 M HCl.

2.4.2- Microstructure of Polythiophenes

Polymer microstructure can greatly affect polymer material properties. In poly(3-alkylthiophene)'s microstructure and repeat unit chemistry affects their light absorbance, solubility, crystallinity, thermal transport, and conductivity.[11,15–17,21,36,60,62,65,70,75,76] There are several commonly used

substituted polythiophenes including fused ring and traditional 3-alkyl thiophenes. **Figure 2.8** shows unsubstituted polythiophene and some examples of various common polythiophene derivatives. As shown in **Figure 2.8**, the main differences in the structures are the side chains, and the functionality of the side chain is limited mostly by the imagination of the researcher involved in the synthesis.[68] Altering the structure of the single ring polythiophenes is pretty straight forward as it only requires modification of the substitution step in the monomer synthesis; discussed further in Chapters 6-8. Since alteration of polythiophene microstructure is well understood, a facile method for tuning of material properties via small microstructure modifications is copolymerization of two or more thiophene derivatives. This capacity is exploited in this dissertation as substituent groups are varied to synthesize a plethora of monomers amenable for polymerization via GRIM; Chapter 6-8. There are a very wide range of thiophenes and statistical copolymers of these thiophenes proves to be an easily accessible way to manipulate the material properties of interest. A few examples of these copolymers are shown in **Figure 2.9**.

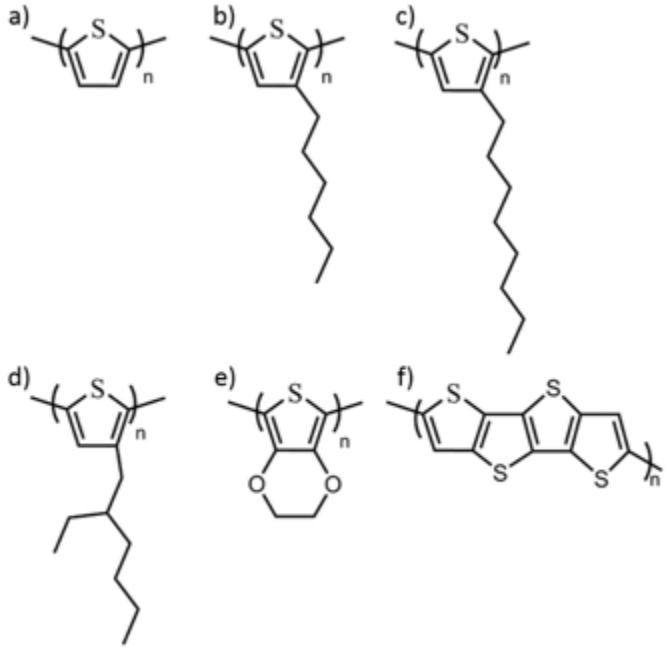

Figure 2.8 Various polythiophene derivatives a)polythiophene b) poly(3-hexylthiophene) c) poly(3-octylthiophene) d) poly(3-(2'-ethyl)hexylthiophene) e) poly(3,4-ethyldioxy thiophene) f) poly(quarter thiophene).

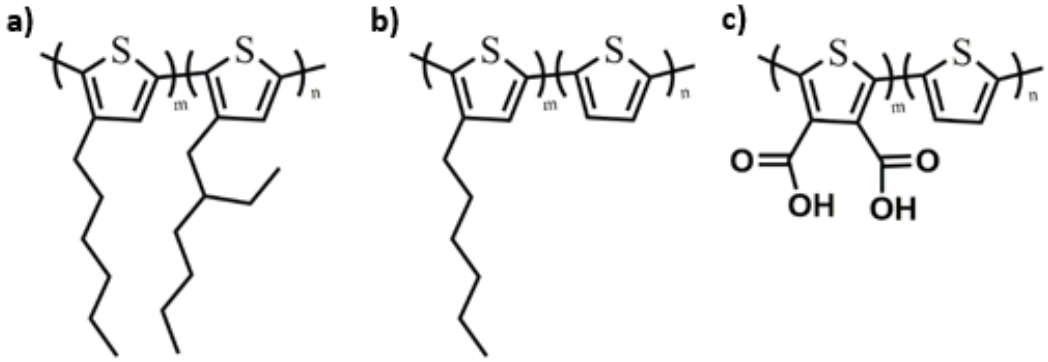

Figure 2.9 Various statistical copolymers a) poly(3-hexylthiophene-co-3-(2'-ethyl)hexylthiophene), b) poly(3-hexylthiophene-co-thiophene), and c) poly(3,4-carboxylic acid thiophene-co-thiophene).

Subtle changes in polymer microstructure yields polymers with a wide variety of properties. A prime example of this behavior for substituted polythiophenes are poly(3-hexylthiophene-co-3-(2'-ethyl)hexylthiophene) copolymers synthesized by Ho et al.[11] They synthesized a range of statistical copolymers of varying molecular composition and examine thermal and optoelectronic properties.[11] A near linear trend is observed in melting temperature from one homopolymer to the other; poly(3-hexylthiophene) melts at 228 °C and poly(3-(2'-ethyl)hexylthiophene) melts at 76 °C while their statistical range of copolymers all melt between the two copolymers.[11] While this may seem somewhat intuitive that the melting temperature and other various properties should shift from one homopolymers to the other throughout the statistical range, this is atypical behavior for semicrystalline polymers. Further reinforcing this atypical behavior, they also observed a similar trend in the optical properties of these various copolymers. Wherein the crystal structure assumes that of the majority constituent and two distinct domains are observed. Factors such as monomer asymmetry, crystallization rate, and solubility can affect the evaluation and characterization of these critical properties. By making use of the inherent chemical nature of various side chain substituents and copolymerizing various derivatives, properties and combinations of properties can be realized to further push the limits of polymer science. Statistical copolymers of polythiophene and its synonymous 3-substituted derivatives and their resulting material properties is a primary topic of this dissertation.

2.5- Modernization of Polymer Characterization

One other critical facet of copolymer chemistry is accurate characterization of copolymer backbone composition. In recent years, research groups have been opting to utilize in-house characterization equipment for a wide variety of reasons including shortened synthesis-to-property loops, tighter control of characterization techniques, cost-friendly experiments, and a larger

volume of experiments. There are many examples here at Auburn, as a few of the groups have in-house capabilities that only a few years ago were fairly inaccessible; for example, there is X-Ray diffraction, a compact mass-spectrometry setup, and our benchtop NMR spectrometer.

Benchtop/low-field nuclear magnetic resonance spectroscopy (LFNMR) has been used in an increasing manner over the last decade as instrument manufacturers move to producing more of these products with an ever-increasing number of capabilities. This trend is especially true for small molecule chemistry labs, as the instruments are often advertised as being specially made for those types of systems. However, some polymer-based materials have begun to make headway in the realm of benchtop NMR spectroscopy.[80–85] Typical benchtop NMR spectrometers operate at much lower field strengths and employ permanent magnets, in contrast to their high-field counterparts that require cryogenic fluids to cool superconducting magnetic coils. Additionally, low-field NMR spectrometers require significantly less floor space and do not require dedicated personnel for maintenance. Benchtop and low-field will be used interchangeably to discuss spectrometers/spectroscopy performed using magnetic fields with a strength of 1.6 T or less and no cryogenic cooling fluid. Benchtop NMR spectroscopy provides convenient, accessible characterization of chemical materials but at a cost to instrumental sensitivity.

For polymers, ^{1}H NMR spectroscopy is typically used for characterization of a variety of important properties such as absolute molecular weight, copolymer composition, polymerization reaction kinetics, polymer-backbone stereochemistry, and routine intermediate reagent synthesis characterization. There are a seemingly infinite number of studies that utilize these various functions of NMR spectroscopy for polymers or polymer-like compounds (lignins, proteins/peptides, etc.), but the majority of these studies utilize the aforementioned high-field spectrometers. Only recently has the application of LFNMR become an accepted method for the

characterization of polymer systems.[80–83,86] However, even though high-field NMR spectroscopy has its own heuristics and field-accepted methodology, the field of LFNMR with regards to polymers and other macromolecules is somewhat lacking synonymous principles and guidelines.[80–83,86]

In this document, I will discuss low-field NMR spectroscopy as it applies to the field of polymer science. In Chapters 4 and 5 demonstrate/benchmark the ability of a Pulsar 60 MHz ^{1}H NMR spectrometer to produce data that reasonably matches high-field spectrometer results. I will discuss the application of LFNMR to analyze a plethora of polymer systems including polymer blends, polymer block copolymers, statistical copolymers, and polymer synthesis intermediates.

2.6- References

(1) Donadio, S. American Recycling Born During World War II. *Power Recycling Inc.*, 2017.
(2) Make It Do - Scrap Drives in World War II http://www.sarahsundin.com/make-it-do-scrap-drives-in-world-war-ii-2/ (accessed Jul 25, 2019).
(3) WWII http://historyofrubber.weebly.com/wwii.html (accessed Jul 25, 2019).
(4) Wakefield, P. Polymer Advances in the Interwar Period: The Impact of Science on World War II http://www.almc.army.mil/alog/issues/Mar-Apr07/polymer_advan.html (accessed Nov 8, 2017).
(5) U.S. Synthetic Rubber Program - National Historic Chemical Landmark https://www.acs.org/content/acs/en/education/whatischemistry/landmarks/syntheticrubber.html (accessed Jan 8, 2020).
(6) Polyisoprene https://polymerdatabase.com/Elastomers/Isoprene.html (accessed Jan 8, 2020).
(7) Military Production during World War II. *Wikipedia*; 2019.
(8) Teflon - Ohio History Central https://ohiohistorycentral.org/w/Teflon (accessed Jan 8, 2020).
(9) IBISWorld - Industry Market Research, Reports, and Statistics https://www.ibisworld.com/default.aspx (accessed Jul 25, 2019).
(10) Xu, B.; Noh, S.; Thompson, B. C. Fine Tuning of Polymer Properties by Incorporating Strongly Electron-Donating 3-Hexyloxythiophene Units into Random and Semi-Random Copolymers. *Macromolecules* **2014**, *47* (15), 5029–5039. https://doi.org/10.1021/ma5012107.
(11) Ho, V.; Boudouris, B. W.; Segalman, R. A. Tuning Polythiophene Crystallization through Systematic Side Chain Functionalization. *Macromolecules* **2010**, *43* (19), 7895–7899. https://doi.org/10.1021/ma101697m.
(12) Kim, J.-S.; Kim, J.-H.; Lee, W.; Yu, H.; Kim, H. J.; Song, I.; Shin, M.; Oh, J. H.; Jeong, U.; Kim, T.-S.; Kim, B. J. Tuning Mechanical and Optoelectrical Properties of Poly(3-Hexylthiophene) through Systematic Regioregularity Control. *Macromolecules* **2015**, *48* (13), 4339–4346. https://doi.org/10.1021/acs.macromol.5b00524.
(13) Schwalm, R.; Häußling, L.; Reich, W.; Beck, E.; Enenkel, P.; Menzel, K. Tuning the Mechanical Properties of UV Coatings towards Hard and Flexible Systems. *Progress in Organic Coatings* **1997**, *32* (1), 191–196. https://doi.org/10.1016/S0300-9440(97)00060-X.
(14) Howard, J. B.; Noh, S.; Beier, A. E.; Thompson, B. C. Fine Tuning Surface Energy of Poly(3-Hexylthiophene) by Heteroatom Modification of the Alkyl Side Chains. *ACS Macro Lett.* **2015**, *4* (7), 725–730. https://doi.org/10.1021/acsmacrolett.5b00328.
(15) Son, S. Y.; Kim, J.-H.; Song, E.; Choi, K.; Lee, J.; Cho, K.; Kim, T.-S.; Park, T. Exploiting π–π Stacking for Stretchable Semiconducting Polymers. *Macromolecules* **2018**, *51* (7), 2572–2579. https://doi.org/10.1021/acs.macromol.8b00093.
(16) Smith, Z. C.; Wright, Z. M.; Arnold, A. M.; Sauvé, G.; McCullough, R. D.; Sydlik, S. A. Increased Toughness and Excellent Electronic Properties in Regioregular Random Copolymers of 3-Alkylthiophenes and Thiophene. *Advanced Electronic Materials* **2017**, *3* (1), 1600316. https://doi.org/10.1002/aelm.201600316.
(17) Minkler, M. J.; Beckingham, B. S. Statistical Copolymers of 3-Hexylthiophene and Thiophene: Impact of Thiophene Content on Optoelectronic and Thermal Properties.

Materials Today Communications **2019**, 100547. https://doi.org/10.1016/j.mtcomm.2019.100547.
(18) Gao, D.; Hollinger, J.; Seferos, D. S. Selenophene–Thiophene Block Copolymer Solar Cells with Thermostable Nanostructures. *ACS Nano* **2012**, *6* (8), 7114–7121. https://doi.org/10.1021/nn3021844.
(19) Thompson, B. C.; Kim, B. J.; Kavulak, D. F.; Sivula, K.; Mauldin, C.; Fréchet, J. M. J. Influence of Alkyl Substitution Pattern in Thiophene Copolymers on Composite Fullerene Solar Cell Performance. *Macromolecules* **2007**, *40* (21), 7425–7428. https://doi.org/10.1021/ma071649s.
(20) Burkhart, B.; Khlyabich, P. P.; Thompson, B. C. Influence of the Ethylhexyl Side-Chain Content on the Open-Circuit Voltage in Rr-Poly(3-Hexylthiophene- *Co* -3-(2-Ethylhexyl)Thiophene) Copolymers. *Macromolecules* **2012**, *45* (9), 3740–3748. https://doi.org/10.1021/ma300263a.
(21) Sivula, K.; Ball, Z. T.; Watanabe, N.; Fréchet, J. M. J. Amphiphilic Diblock Copolymer Compatibilizers and Their Effect on the Morphology and Performance of Polythiophene:Fullerene Solar Cells. *Advanced Materials* **2006**, *18* (2), 206–210. https://doi.org/10.1002/adma.200501787.
(22) Suggs, L. J.; Payne, R. G.; Yaszemski, M. J.; Alemany, L. B.; Mikos, A. G. Synthesis and Characterization of a Block Copolymer Consisting of Poly(Propylene Fumarate) and Poly(Ethylene Glycol). *Macromolecules* **1997**, *30* (15), 4318–4323. https://doi.org/10.1021/ma970312v.
(23) Yang, Y.-L.; Lee, Y.-H.; Lee, Y.-P.; Chiang, C.-J.; Shen, C.; Wu, C.-C.; Ohta, Y.; Yokozawa, T.; Dai, C.-A. Synthesis and Characterization of Poly(3-Hexylthiophene)–Poly(3-Hexyloxythiophene) Random Copolymers with Tunable Band Gap via Grignard Metathesis Polymerization. *Polymer International* **2014**, *63* (12), 2068–2075. https://doi.org/10.1002/pi.4744.
(24) Antinucci, S.; Guerra, G.; Oliva, L.; Ballesteros, O. R. de; Venditto, V. Pseudo-Hexagonal Crystallinity in Ethene-Styrene Random Copolymers. *Macromolecular Chemistry and Physics* **2001**, *202* (3), 382–387. https://doi.org/10.1002/1521-3935(20010201)202:3<382::AID-MACP382>3.0.CO;2-7.
(25) Rabiej, S. The Influence of Side Branches on the Structure of Crystalline Phase in Ethylene-1-Alkene Copolymers. *European Polymer Journal* **2005**, *41* (2), 393–402. https://doi.org/10.1016/j.eurpolymj.2004.09.016.
(26) Roy, A. Industrial Uses of Polyethylene | Kplintl Blog.
(27) The Differences (and Similarities) of LDPE and HDPE, 2016.
(28) Alan G. MacDiarmid, Alan J. Heeger, and Hideki Shirakawa https://www.sciencehistory.org/historical-profile/alan-g-macdiarmid-alan-j-heeger-and-hideki-shirakawa (accessed Jan 9, 2020).
(29) Mark, J. *Polymer Data Handbook*, 2nd ed.; Oxford University Press, 1999.
(30) Popular Applications for HDPE - A&C Plastics, Inc https://www.acplasticsinc.com:443/informationcenter/r/common-uses-of-hdpe (accessed Jan 9, 2020).
(31) Beckingham, B. S.; Register, R. A. Synthesis and Phase Behavior of Block-Random Copolymers of Styrene and Hydrogenated Isoprene. *Macromolecules* **2011**, *44* (11), 4313–4319. https://doi.org/10.1021/ma200913k.

(32) Davidson, E. C.; Segalman, R. A. Confined Crystallization within Cylindrical P3EHT Block Copolymer Microdomains. *Macromolecules* **2017**, *50* (16), 6128–6136. https://doi.org/10.1021/acs.macromol.7b01323.
(33) Davis, K. A.; Burdick, J. A.; Anseth, K. S. Photoinitiated Crosslinked Degradable Copolymer Networks for Tissue Engineering Applications. *Biomaterials* **2003**, *24* (14), 2485–2495. https://doi.org/10.1016/S0142-9612(02)00582-3.
(34) Iovu, M. C.; Craley, C. R.; Jeffries-EL, M.; Krankowski, A. B.; Zhang, R.; Kowalewski, T.; McCullough, R. D. Conducting Regioregular Polythiophene Block Copolymer Nanofibrils Synthesized by Reversible Addition Fragmentation Chain Transfer Polymerization (RAFT) and Nitroxide Mediated Polymerization (NMP). *Macromolecules* **2007**, *40* (14), 4733–4735. https://doi.org/10.1021/ma070406x.
(35) Davidson, E. C.; Beckingham, B. S.; Ho, V.; Segalman, R. A. Confined Crystallization in Lamellae Forming Poly(3-(2′-Ethyl)Hexylthiophene) (P3EHT) Block Copolymers. *Journal of Polymer Science Part B: Polymer Physics* **2016**, *54* (2), 205–215. https://doi.org/10.1002/polb.23904.
(36) Minkler, M. J.; Kim, J.; Lawson, K. E.; Ali, A.; Zhao, R.; Adamczyk, A. J.; Beckingham, B. S. Solution Processible Statistical Poly(3-Methoxythiophene)-Co-Poly(3-Hexylthiophene) Copolymer. *Materials Letters* **2019**, *256*, 126563. https://doi.org/10.1016/j.matlet.2019.126563.
(37) Showak, M. T.; Burns, A. B.; Stella, A. J.; Register, R. A. Counit Inclusion in Hydrogenated Polynorbornene Copolymer Crystals. *Macromolecules* **2013**, *46* (23), 9288–9295. https://doi.org/10.1021/ma401834t.
(38) Sauvé, G.; McCullough, R. D. High Field-Effect Mobilities for Diblock Copolymers of Poly(3-Hexylthiophene) and Poly(Methyl Acrylate). *Advanced Materials* **2007**, *19* (14), 1822–1825. https://doi.org/10.1002/adma.200602368.
(39) Mok, M. M.; Ellison, C. J.; Torkelson, J. M. Effect of Gradient Sequencing on Copolymer Order–Disorder Transitions: Phase Behavior of Styrene/n-Butyl Acrylate Block and Gradient Copolymers. *Macromolecules* **2011**, *44* (15), 6220–6226. https://doi.org/10.1021/ma201080n.
(40) Jakubowski, W.; Juhari, A.; Best, A.; Koynov, K.; Pakula, T.; Matyjaszewski, K. Comparison of Thermomechanical Properties of Statistical, Gradient and Block Copolymers of Isobornyl Acrylate and n-Butyl Acrylate with Various Acrylate Homopolymers. *Polymer* **2008**, *49* (6), 1567–1578. https://doi.org/10.1016/j.polymer.2008.01.047.
(41) Rinkenauer, A. C.; Schubert, S.; Traeger, A.; Schubert, U. S. The Influence of Polymer Architecture on in Vitro PDNA Transfection. *J. Mater. Chem. B* **2015**, *3* (38), 7477–7493. https://doi.org/10.1039/C5TB00782H.
(42) Sauvet, G.; Fortuniak, W.; Kazmierski, K.; Chojnowski, J. Amphiphilic Block and Statistical Siloxane Copolymers with Antimicrobial Activity. *Journal of Polymer Science Part A: Polymer Chemistry* **2003**, *41* (19), 2939–2948. https://doi.org/10.1002/pola.10895.
(43) Glöckner, G.; Müller, A. H. E. Gradient High-Performance Liquid Chromatography of Statistical and Block Copolymers of Styrene and t-Butyl Methacrylate. *Journal of Applied Polymer Science* **1989**, *38* (9), 1761–1774. https://doi.org/10.1002/app.1989.070380914.
(44) Yamada, K.; Minoda, M.; Fukuda, T.; Miyamoto, T. Amphiphilic Block and Statistical Copolymers with Pendant Glucose Residues: Controlled Synthesis by Living Cationic Polymerization and the Effect of Copolymer Architecture on Their Properties. *Journal of*

Polymer Science Part A: Polymer Chemistry **2001**, *39* (4), 459–467. https://doi.org/10.1002/1099-0518(20010215)39:4<459::AID-POLA1014>3.0.CO;2-E.
(45) Hollinger, J.; Sun, J.; Gao, D.; Karl, D.; Seferos, D. S. Statistical Conjugated Polymers Comprising Optoelectronically Distinct Units. *Macromolecular Rapid Communications* **2013**, *34* (5), 437–441. https://doi.org/10.1002/marc.201200777.
(46) Hodrokoukes, P.; Pispas, S.; Hadjichristidis, N. Controlling Micellar Properties of Styrene/Isoprene Copolymers by Altering the Monomer Arrangement along the Chain. *Macromolecules* **2002**, *35* (3), 834–840. https://doi.org/10.1021/ma011331e.
(47) Kotani, Y.; Kamigaito, M.; Sawamoto, M. Living Random Copolymerization of Styrene and Methyl Methacrylate with a Ru(II) Complex and Synthesis of ABC-Type "Block-Random" Copolymers. *Macromolecules* **1998**, *31* (17), 5582–5587. https://doi.org/10.1021/ma980294x.
(48) Shuai, X.; Ai, H.; Nasongkla, N.; Kim, S.; Gao, J. Micellar Carriers Based on Block Copolymers of Poly(ε-Caprolactone) and Poly(Ethylene Glycol) for Doxorubicin Delivery. *Journal of Controlled Release* **2004**, *98* (3), 415–426. https://doi.org/10.1016/j.jconrel.2004.06.003.
(49) Zhang, Q.; Cirpan, A.; Russell, T. P.; Emrick, T. Donor−Acceptor Poly(Thiophene-Block-Perylene Diimide) Copolymers: Synthesis and Solar Cell Fabrication. *Macromolecules* **2009**, *42* (4), 1079–1082. https://doi.org/10.1021/ma801504e.
(50) Kwon, G. S.; Kataoka, K. Block Copolymer Micelles as Long-Circulating Drug Vehicles. *Advanced Drug Delivery Reviews* **1995**, *16* (2), 295–309. https://doi.org/10.1016/0169-409X(95)00031-2.
(51) Ouhib, F.; Khoukh, A.; Ledeuil, J.-B.; Martinez, H.; Desbrières, J.; Dagron-Lartigau, C. Diblock and Random Donor/Acceptor "Double Cable" Polythiophene Copolymers *via* the GRIM Method. *Macromolecules* **2008**, *41* (24), 9736–9743. https://doi.org/10.1021/ma801934g.
(52) Sommer, M.; Lang, A. S.; Thelakkat, M. Crystalline–Crystalline Donor–Acceptor Block Copolymers. *Angewandte Chemie International Edition* **2008**, *47* (41), 7901–7904. https://doi.org/10.1002/anie.200802725.
(53) Sommer, M.; Huettner, S.; Thelakkat, M. Donor–Acceptor Block Copolymers for Photovoltaic Applications. *J. Mater. Chem.* **2010**, *20* (48), 10788–10797. https://doi.org/10.1039/C0JM00665C.
(54) Vargesson, N. Thalidomide-induced Teratogenesis: History and Mechanisms. *Birth Defects Res C Embryo Today* **2015**, *105* (2), 140–156. https://doi.org/10.1002/bdrc.21096.
(55) Khlyabich, P. P.; Burkhart, B.; Ng, C. F.; Thompson, B. C. Efficient Solar Cells from Semi-Random P3HT Analogues Incorporating Diketopyrrolopyrrole. *Macromolecules* **2011**, *44* (13), 5079–5084. https://doi.org/10.1021/ma2009386.
(56) Mohammad, A.; Mahmood, A.; Chin, K. T.; Danquah, M. K.; Stratan, S. van. Nano Silver Diffusion Behaviour on Conductive Polymer during Doping Process for High Voltage Application. *IOP Conf. Ser.: Mater. Sci. Eng.* **2017**, *206* (1), 012048. https://doi.org/10.1088/1757-899X/206/1/012048.
(57) Yu, L.; Davidson, E.; Sharma, A.; Andersson, M. R.; Segalman, R.; Müller, C. Isothermal Crystallization Kinetics and Time–Temperature–Transformation of the Conjugated Polymer: Poly(3-(2′-Ethyl)Hexylthiophene). *Chem Mater* **2017**, *29* (13), 5654–5662. https://doi.org/10.1021/acs.chemmater.7b01393.

(58) Barbarella, G.; Bongini, A.; Zambianchi, M. Regiochemistry and Conformation of Poly(3-Hexylthiophene) via the Synthesis and the Spectroscopic Characterization of the Model Configurational Triads. *Macromolecules* **1994**, *27* (11), 3039–3045. https://doi.org/10.1021/ma00089a022.
(59) Deng, P.; Wu, B.; Lei, Y.; Cao, H.; Ong, B. S. Regioregular and Random Difluorobenzothiadiazole Electron Donor–Acceptor Polymer Semiconductors for Thin-Film Transistors and Polymer Solar Cells. *Macromolecules* **2016**, *49* (7), 2541–2548. https://doi.org/10.1021/acs.macromol.5b02754.
(60) Wu, P.-T.; Ren, G.; Jenekhe, S. A. Crystalline Random Conjugated Copolymers with Multiple Side Chains: Tunable Intermolecular Interactions and Enhanced Charge Transport and Photovoltaic Properties. *Macromolecules* **2010**, *43* (7), 3306–3313. https://doi.org/10.1021/ma100006x.
(61) Yue, S.; Berry, G. C.; McCullough, R. D. Intermolecular Association and Supramolecular Organization in Dilute Solution. 1. Regioregular Poly(3-Dodecylthiophene). *Macromolecules* **1996**, *29* (3), 933–939. https://doi.org/10.1021/ma951008+.
(62) Yao, Z.; Hu, X.; Huang, B.; Zhang, L.; Liu, L.; Zhao, Y.; Wu, H.-C. Halochromism of a Polythiophene Derivative Induced by Conformational Changes and Its Sensing Application of Carbon Dioxide. *ACS Appl. Mater. Interfaces* **2013**, *5* (12), 5783–5787. https://doi.org/10.1021/am401761n.
(63) Himmelberger, S.; Duong, D. T.; Northrup, J. E.; Rivnay, J.; Koch, F. P. V.; Beckingham, B. S.; Stingelin, N.; Segalman, R. A.; Mannsfeld, S. C. B.; Salleo, A. Role of Side-Chain Branching on Thin-Film Structure and Electronic Properties of Polythiophenes. *Adv. Funct. Mater.* **2015**, *25* (17), 2616–2624. https://doi.org/10.1002/adfm.201500101.
(64) Hong, X.; Tyson, J. C.; Middlecoff, J. S.; Collard, D. M. Synthesis and Oxidative Polymerization of Semifluoroalkyl-Substituted Thiophenes. *Macromolecules* **1999**, *32* (13), 4232–4239. https://doi.org/10.1021/ma9900030.
(65) Faïd, K.; Leclerc, M. Functionalized Regioregular Polythiophenes: Towards the Development of Biochromic Sensors. *Chem. Commun.* **1996**, No. 24, 2761–2762. https://doi.org/10.1039/CC9960002761.
(66) Li, L.; Collard, D. M. Tuning the Electronic Structure of Conjugated Polymers with Fluoroalkyl Substitution: Alternating Alkyl/Perfluoroalkyl-Substituted Polythiophene. *Macromolecules* **2005**, *38* (2), 372–378. https://doi.org/10.1021/ma048510r.
(67) Li, L. Novel Conducting Polymeric Materials: 1. Fluoroalkylated Polythiophenes 2. Stacked Oligothiophenes as Models for the Interchain Charge Transfer in Conducting Polymers. **2004**.
(68) Mei, J.; Bao, Z. Side Chain Engineering in Solution-Processable Conjugated Polymers. *Chem. Mater.* **2014**, *26* (1), 604–615. https://doi.org/10.1021/cm4020805.
(69) Cui, C.; Wong, W.-Y. Effects of Alkylthio and Alkoxy Side Chains in Polymer Donor Materials for Organic Solar Cells. *Macromolecular Rapid Communications* **2016**, *37* (4), 287–302. https://doi.org/10.1002/marc.201500620.
(70) Sheina, E. E.; Khersonsky, S. M.; Jones, E. G.; McCullough, R. D. Highly Conductive, Regioregular Alkoxy-Functionalized Polythiophenes: A New Class of Stable, Low Band Gap Materials. *Chem. Mater.* **2005**, *17* (13), 3317–3319. https://doi.org/10.1021/cm050083o.
(71) Camurlu, P. Polypyrrole Derivatives for Electrochromic Applications. *RSC Advances* **2014**, *4* (99), 55832–55845. https://doi.org/10.1039/C4RA11827H.

(72) Salzner, U.; Lagowski, J. B.; Pickup, P. G.; Poirier, R. A. Comparison of Geometries and Electronic Structures of Polyacetylene, Polyborole, Polycyclopentadiene, Polypyrrole, Polyfuran, Polysilole, Polyphosphole, Polythiophene, Polyselenophene and Polytellurophene. *Synthetic Metals* **1998**, *96* (3), 177–189. https://doi.org/10.1016/S0379-6779(98)00084-8.
(73) Satoh, M.; Hasegawa, E. Polypyrrole: Synthesis and Electronic Device Application. *Macromol. Symp.* **1996**, *105* (1), 211–216. https://doi.org/10.1002/masy.19961050130.
(74) Wang, Y.; Yang, J.; Wang, L.; Du, K.; Yin, Q.; Yin, Q. Polypyrrole/Graphene/Polyaniline Ternary Nanocomposite with High Thermoelectric Power Factor. *ACS Appl. Mater. Interfaces* **2017**, *9* (23), 20124–20131. https://doi.org/10.1021/acsami.7b05357.
(75) Clark, J.; Chang, J.-F.; Spano, F. C.; Friend, R. H.; Silva, C. Determining Exciton Bandwidth and Film Microstructure in Polythiophene Films Using Linear Absorption Spectroscopy. *Appl. Phys. Lett.* **2009**, *94* (16), 163306. https://doi.org/10.1063/1.3110904.
(76) Loewe, R. S.; Ewbank, P. C.; Liu, J.; Zhai, L.; McCullough, R. D. Regioregular, Head-to-Tail Coupled Poly(3-Alkylthiophenes) Made Easy by the GRIM Method: Investigation of the Reaction and the Origin of Regioselectivity. *Macromolecules* **2001**, *34* (13), 4324–4333. https://doi.org/10.1021/ma001677+.
(77) Janse van Rensburg, E. J.; Guillet, J. E.; Whittington, S. G. Exciton Migration on Polymers. *Macromolecules* **1989**, *22* (11), 4212–4220. https://doi.org/10.1021/ma00201a013.
(78) Silbey, R.; Munn, R. Exciton States and Exciton Transport in Molecular Crystals. In *Photon, Electron, and Ion Probes of Polymer Structure and Properties*; ACS Symposium Series; American Chemical Society, 1981; Vol. 162, pp 45–56. https://doi.org/10.1021/bk-1981-0162.ch004.
(79) de Leon, A.; Advincula, R. C. Chapter 11 - Conducting Polymers with Superhydrophobic Effects as Anticorrosion Coating. In *Intelligent Coatings for Corrosion Control*; Tiwari, A., Rawlins, J., Hihara, L. H., Eds.; Butterworth-Heinemann: Boston, 2015; pp 409–430. https://doi.org/10.1016/B978-0-12-411467-8.00011-8.
(80) Papon, A.; Saalwächter, K.; Schäler, K.; Guy, L.; Lequeux, F.; Montes, H. Low-Field NMR Investigations of Nanocomposites: Polymer Dynamics and Network Effects. *Macromolecules* **2011**, *44* (4), 913–922. https://doi.org/10.1021/ma102486x.
(81) Vargas, M. A.; Cudaj, M.; Hailu, K.; Sachsenheimer, K.; Guthausen, G. Online Low-Field 1H NMR Spectroscopy: Monitoring of Emulsion Polymerization of Butyl Acrylate. *Macromolecules* **2010**, *43* (13), 5561–5568. https://doi.org/10.1021/ma1006599.
(82) Singh, K.; Blümich, B. Compact Low-Field NMR Spectroscopy and Chemometrics: A Tool Box for Quality Control of Raw Rubber. *Polymer* **2018**, *141*, 154–165. https://doi.org/10.1016/j.polymer.2018.02.057.
(83) Patel, J. P.; Hsu, S. L. Development of Low Field NMR Technique for Analyzing Segmental Mobility of Crosslinked Polymers. *Journal of Polymer Science Part B: Polymer Physics* **2018**, *56* (8), 639–643. https://doi.org/10.1002/polb.24583.
(84) Chakrapani, S. B.; Minkler, M. J.; Beckingham, B. S. Low-Field 1H-NMR Spectroscopy for Compositional Analysis of Multicomponent Polymer Systems. *Analyst* **2019**, *144* (5), 1679–1686. https://doi.org/10.1039/C8AN01810C.
(85) Minkler Jr, Michael J., Jung Min Kim, Vinita V. Shinde, and Bryan S. Beckingham. "Low-Field 1H NMR Spectroscopy: Factors Impacting Signal-to-Noise Ratio and Experimental Time in the Context of Mixed Microstructure Polyisoprenes." Magnetic Resonance in Chemistry (April 7, 2020). https://doi.org/10.1002/mrc.5022.

(86) Nordon, A.; Gemperline, P. J.; McGill, C. A.; Littlejohn, D. Quantitative Analysis of Low-Field NMR Signals in the Time Domain. *Anal. Chem.* **2001**, *73* (17), 4286–4294. https://doi.org/10.1021/ac0102866.

Chapter 3 - Experimental Methods

3.1- Polythiophenes

3.1.1- Materials

All chemicals were used as received unless otherwise specified. 3-hexylthiophene, 1,3-bis(diphenylphosphino)propane nickel(II) chloride, sodium methoxide, and tert-butyl magnesium chloride were obtained from TCI America. 3-bromothiophene was obtained from Acros Organics. Hydrochloric acid, tetrahydrofuran, methanol, chloroform, petroleum ether, and ethyl ether were obtained from BDH. Sodium thiosulfate was obtained from Amresco. Sodium chloride was obtained from Sigma Aldrich. Magnesium sulfate was obtained from Fisher Scientific. N-bromosuccinnimide was obtained from EMD Millipore. Tetrahydrofuran (THF) was degassed via freeze-pump-thaw, purified in a stille with sodium-benzophenone and collected in a flame-dried, air-free flask via vacuum distillation prior to use. 12 M HCl was diluted to 6 M HCl with Type 1 deionized water from a Labconco Water Pro BT.

3.1.2- Synthetic Methods

Synthesis of 2,5-dibromo-3-hexylthiophene (DB3HT). N-bromosuccinimide (NBS, 30.1 g, 0.17 mol) was added to 3-hexylthiophene (3HT, 10 mL, 0.056 mol) in purified THF (110 mL, 1.36 mol). The reaction was allowed to proceed overnight under nitrogen at room temperature. The reaction was quenched with 10 wt% sodium thiosulfate in water (120 mL, 6.65 mol) and stirred for one hour with an equal volume of ethyl ether (120 mL, 1.15 mol) to extract the product. The organic phase was extracted using a separatory funnel, washed with 10 wt% potassium hydroxide (125 mL, 6.93 mol) in water and 10 wt% NaCl in water (125 mL, 6.93 mol). The extracted product was dried with $MgSO_4$, and concentrated via rotary evaporation. The product was purified by column chromatography (eluent hexane) followed by rotary evaporation and vacuum distillation. The product, 2,5-dibromo-3-hexylthiophene (DB3HT) was verified by ^1H NMR spectroscopy with

a 60 MHz Oxford Pulsar NMR spectrometer. NMR samples were prepared with 1-5 drops of monomer in 1 mL of $CDCl_3$ and 1-3 drops of tetramethylsilane (TMS).

Synthesis of Poly(3-hexylthiophene-co-thiophene). The general procedure followed the GRIM method outlined by McCullough et al.[1,2]Anhydrous THF (100 mL, 1.23 mol), 2,5-dibromo-3-hexylthiophene (DB3HT, 4.924 g, 0.015 mol), 2,5-dibromothiophene (DBT, 0.1771 g, 0.00073 mol) were added to an oven-dried, vacuumed 3-neck 250 mL round bottom flask equipped with a condenser, and either an addition funnel with a septum or with two septa. Tert-butyl magnesium chloride 2 M in diethyl ether (tert-butyl MgCl, 7.67 mL, 0.015 mol) was added via cannula transfer to the addition funnel. After the addition of the tert-butyl MgCl, the reaction flask was vented to nitrogen and heated to 75-80 °C. The reaction was carried out for approximately 90 minutes; after the 90 minutes, the reaction flask was cooled to room temperature. Once the flask was appropriately cooled, $Ni(dppp)Cl_2$ (100 mg, 0.19 mmol) was added to the reaction flask by removing the septum on the unoccupied neck and adding the catalyst quickly in one shot. After the catalyst was added, the solution turned a deep red color for the remainder of the reaction, the reaction was allowed to proceed for 45 minutes at room temperature; the reaction was quenched with 6 M HCl (2.5 mL, 0.015 mol) and after the bubbling finished the reaction mixture was dumped into methanol (MeOH, 250 mL, 6.17 mol) to crystallize the polymer. The solution was allowed to sit overnight to allow for sufficient crystallization of the product. Once the crystallization was finished, the solution was filtered, and the filter paper was inserted into a Soxhlet apparatus. MeOH (350 mL, 8.64 mol) was ran through the Soxhlet followed by hexane (350 mL, 2.68 mol) and chloroform (350 mL, 4.37 mol). Finally, the product was heated to 40 °C for 2-4 hours and left to dry under vacuum overnight. A synonymous procedure was also utilized to synthesize poly(3-hexylthiophene-*co*-3-methoxythiophene).

For compositional drift analyses described in Chapter 8, 1 mL aliquots were collected and placed into scintillation vials containing 4 mL of MeOH and 1-2 drops of 6M HCl. Polymer at each time point was allowed to precipitate. The precipitated polymer was then filtered and subsequently rinsed with MeOH until the collected MeOH ran clear; this is to remove the Grignard salts but leave all polymer. Collected polymers were then weighed and prepared for NMR spectroscopy and gel-permeation chromatography as described in Section 3.1.3.

3.1.3- Characterization Methods

Macromolecular Characterization. The composition and regioregularity of synthesized thiophene copolymers synthesized in Chapters 6 and 7 were determined using either a Bruker 600 MHz NMR spectrometer or a Bruker 400 MHz NMR spectrometer. For aliquot-based polymer synthesis detailed in Chapter 8, all spectra were collected on a 500 MHz Bruker NMR spectrometer. NMR spectroscopy samples were prepared with 15-20 mg/mL of polymer in deuterated chloroform ($CDCl_3$). Molar compositions of *P3HT-co-T* copolymers were determined using ^{1}H NMR spectroscopy via the aromatic (δ, 6.96-7.20 ppm) and aliphatic (δ, 2.5-3.04 ppm) regions of the ^{1}H NMR spectrum. P3HT was used as the basis for the integration limits for the subsequent synthesized copolymers; 6.96-7.02 ppm for the aromatic 3-hexylthiophene proton and 7.03-7.20 ppm for the unsubstituted thiophene aromatic protons. Polymer chain regioregularity was calculated using the α-carbon proton region of the ^{1}H NMR spectrum through the peak attributed to regioregular (δ, 2.8 ppm) and non-regioregular (δ, 2.6 ppm) sequences.[3,4] Dispersity and polystyrene-equivalent molecular weight of the synthesized polymers were determined using gel-permeation chromatography on a Viscotek GPC setup with VE 7510 degasser, VE 1122 solvent delivery system, VE 3580 RI Detector, and a 270 dual detector. Samples were prepared by

dissolving 5-10 mg of polymer in THF extracted from the mobile phase source for the GPC instrument to make 1 mg/mL solutions.

Thermal Characterization. Melting temperatures and heats of fusion were determined using a TA Instruments Q20 differential scanning calorimeter. Approximately10 mg of each sample was weighed and hermetically sealed in an aluminum pan. All samples were ramped to 200 °C (with the exception of P3HT, which was ramped to 250 °C) and then subsequently cooled to 0 °C before allowing to crystallize for 15 hours to allow for sufficient crystallization. Following crystallization, the samples were ramped to 200 °C (250 °C for P3HT) at a rate of 10 °C/min.

Optoelectronic Characterization. The absorbance and theoretical band gap were determined using a Cary 60 UV/Vis spectrophotometer. 10 drops of chlorobenzene with 1 wt % polymer was spin cast onto VWR micro cover glass slides (Cat. No. 48368 085 Lot 16943) at a rate of 1500 rpm for 120 seconds. Following spin coating, the films were annealed at 20 °C below their melting temperatures (as determined by DSC) and subsequently allowed to crystallize at 6 °C for 72 hours. The polymer-coated slides were subjected to UV/Vis spectrophotometry and the results were analyzed using the Spano Model to obtain the theoretical band gaps and other key optoelectronic properties.[3,5]

Electronic Characterization. Cyclic voltammetry and four-point probe resistometry were used to determine the electronic behavior of all synthesized polythiophene copolymers. Polymers were solvated in toluene to 4 mg/mL and then passed through a syringe filter before spray coating. Room temperature, filtered solutions were spray coated onto substrates preheated to ~100 °C and at a at nozzle outlet pressure of 20 psi; substrates for CV were indium tin oxide-coated glass and standard microscope slides for four-point probe. Scattered white light interferometry was used to estimate film thickness of the four-point probe samples; surface roughness was taken as film thickness.

Crystal Structure Characterization. Samples were prepared by melt pressing polymer between two Kapton® sheets at 20 °C above melting temperature (as determined by DSC) and allowed to quiescently cool and were stored at room temperature (19-23 °C). Wide-angle X-ray scattering was performed on a Panalytical X-ray diffractometer scanning from 2-20 2θ at a step size of 0.013 degrees and dwell time of 60 seconds.

3.2-PEOD/DGEBA Copolymer Chemistries

3.2.1- Materials

All chemicals were used as received unless otherwise specified. Bisphenol a diglycidyl ether (DGEBA) was purchased from Alfa Aesar. Poly(ethylene glycol) (400) diglycidyl ether (PEOD) was purchased from Sigma Aldrich. Pentaerythritol tetra(3-mercaptopropionate) (4SH) was purchased from TCI America. 4-(dimethylamino)pyridine (DMAP) was purchased from EMD Millipore. All chemicals were used as received.

3.2.2- Synthesis Methods and Sample Preparation

Sample Preparation. Two systems were investigated with varied relative amounts of PEOD and DGEBA denoted as 10P for 10 mole % PEOD (90 mole % DGEBA) and 40P for 40 mole % PEOD (60 mole % DGEBA). Requisite quantities of DGEBA (10P: 3.16 g, 9.28 mmol) and PEOD (10P: 0.50 g, 1.25 mmol) were successively added to a scintillation vial. In a separate scintillation vial, DMAP (0.06 g, 0.49 mmol) and 4SH (2.35 g, 4.81 mmol) were mixed and agitated via manual stirring with a spatula until DMAP dissolves. It should be noted that the molar ratio of DMAP to reactants was kept constant but DMAP is observably less soluble in DGEBA and therefore did not fully solvate in systems with relatively high DGEBA content. Following solvation of DMAP in 4SH, the solution was quickly added to the PEOD/DGEBA mixture. The reaction media was vigorously stirred until a homogeneous mixture was observed. A sample of the mixture (~10 mg) was the transferred to a pre-weighed TA Tzero DSC pan. The pan was quickly capped and

quenched in liquid nitrogen to halt the reaction. Following liquid nitrogen quenching, the pan was reweighed and placed into the DSC (TA Instruments DSC Q20) for the appropriate experiment.

Bulk solid films of the polymer systems were also synthesized between two glass plates (6”x6”) separated by a Viton rubber spacer. PEOD, DGEBA, 4SH, and DMAP were weighed and mixed in a similar fashion to the aforementioned DSC preparation. Following mixing of the reaction media, the uncured mixture was quickly poured into the Viton spacer-glass plate setup (the gap between the plates was oriented vertically).

3.2.3- Cure Kinetics via Differential Scanning Calorimetry

Isothermal Cure Kinetics. A typical isothermal curing experiment consisted of the aforementioned sample preparation followed by a thermal sequence in which the DSC cell was held at a desired temperature (19, 25, 45, and 55 °C). Prior to the placement of the sample pan into the DSC, the DSC was equilibrated at the desired isothermal temperature to eliminate any equilibration effects. For the first run at each temperature, this hold was at least five hours to allow for determination of total cure time at a given temperature. The hold times of successive replicates at each temperature were shortened based on the first run kinetics. Following isothermal curing, the sample was (at 10 °C /min) cooled to -50 °C and then heated to 100 °C to allow for the extraction of the residual heat of reaction, if any.

Non-isothermal Cure Kinetics. Following the sample preparation procedure mentioned above, the sample was subjected to non-isothermal cure conditions. Prior to the placement of the sample pan into the DSC, the DSC was equilibrated at 40 °C. The sample was then heated at different rates (1, 3, 5, and 7 °C/min).

3.2.4- Material Characterization Methods

Rheology. An AR-G2 TA Universal Rheometer with parallel plate geometry (40 mm steel plate) was used to measure the viscosity of initial monomer mixtures (excluding the cross-linking agent and catalyst) at varied shear rates and composition. Steady-state flow tests were performed at 25 ºC within 1- 150 s^{-1} shear rates.

Dynamic Mechanical Analysis. Dynamic mechanical analysis (DMA) was performed using a TA Instruments RSA 3 dynamic mechanical analyzer in temperature sweep mode. Samples were cut into rectangular fractions and stored in scintillation vials. The DMA experiment was performed from -50 °C to 50 °C at a ramp rate of 5-10 °C/min. The tan delta damping factor was extracted from the resulting DMA plots and were used to compare the glass transition temperature (*Tg*) of the polymer systems; *Tg* was taken as the tan delta curve apex temperature. The polymer samples were aged in scintillation vials in air, acidified brine (pH 3.0), and basic brine (pH 10.0) for varying lengths of time.

3.3- Polyolefins for 60 MHz NMR Spectrometer Benchmarking

3.3.1- Materials

All chemicals were used as received unless otherwise specified. Styrene, cyclohexane, deuterated chloroform, and tetramethylsilane (TMS) were purchased from EMD Millipore Corporation. Isoprene was obtained from Acros Organics. Triethylamine, polystyrene-*b*-polyisoprene-*b*-polystyrene (SIS) symmetric triblock copolymer (catalog # 432415), polystyrene-*b*-polybutadiene-*b*-polystyrene (SBS) (catalog # 43249-0), *sec*-Butyllithium and 2,2'-azobis(2-methylpropionitrile) were used as received from Sigma Aldrich. 1,1 diphenylethylene, *n*-butyllithium and inhibitor removal column resin (catalog # 42489) were procured from Alfa Aesar. Methanol and chloroform were obtained from VWR International and tert-butyllithium was received from TCI America. Cyclohexane was stirred over diphenylhexyllithium (adduct of *sec*-

butyllithium and 1,1-diphenylethylene), degassed via freeze-pump-thaw (FPT) cycles, and vacuum transferred prior to use. Isoprene was stirred over *n*-butyllithium, degassed via FPT, and vacuum transferred prior to use. *Caution! sec-butyllithium and n-butyllithium are pyrophoric and moisture-sensitive materials and should be handled with appropriate care.* Styrene and methyl methacrylate were passed through the inhibitor removal column and degassed by FPT cycles prior to use. Methanol, for terminating the anionic polymerization of isoprene, was degassed via FPT cycles prior to use.

3.3.2- Polyisoprene, Polystyrene, and Poly(methyl methacrylate) Polymerization

All reactors were flamed out under vacuum. *tert*-butyllithium initiated anionic polymerization of isoprene was performed at 60 °C. *Caution! tert-butyllithium is a pyrophoric and moisture-sensitive material and should be handled with appropriate care.* Cyclohexane, isoprene and *tert*-butyllithium were charged to a reactor in a nitrogen-filled glovebox prior to removal and heating to 60 °C by submersion in a temperature-controlled water bath. Upon completion the polymerization was terminated with degassed methanol. Polystyrene (PS) and poly(methyl methacrylate) (PMMA) were synthesized by free radical polymerization at 70 °C, neat, using 2,2'-azobis(2-methylpropionitrile) (AIBN) as the initiator. AIBN and monomer were charged to a reactor in a nitrogen-filled glovebox prior to removal and heating to 60 °C by submersion in a temperature-controlled water bath. Upon completion the polymerizations were removed from the water bath, precipitated in methanol and the product collected and dried in vacuo.

3.3.3 – Instrumentation and Characterization Methods

Two NMR spectrometers were primarily used in this study to obtain ^{1}H NMR spectra. Spectra at 400 MHz (9.4 T) were collected on a Bruker Avance 400 spectrometer and spectra at 60 MHz (1.4 T) were collected on an Oxford Instruments Pulsar 60 MHz spectrometer. The spectrum at 250 MHz shown in Figure 1 was collected on a Bruker Avance II 250 MHz spectrometer. High-field NMR spectroscopy was performed on a Bruker 400 MHz Avance400 NMR spectrometer. Low-field NMR spectroscopy was performed on an Oxford Pulsar 60 MHz NMR spectrometer.

All NMR samples were prepared in Wilmad high-throughput class B NMR tubes (8" length, 5 mm outer diameter, 4 mm inner diameter). NMR spectroscopy samples were prepared by metering a desired quantity of polyisoprene into a scintillation vial and adding the appropriate amount of $CHCl_3$ or $CDCl_3$ to prepare solutions with target concentrations of 1, 10, 25, and 50 mg/mL for low-field spectroscopy and 50 mg/mL for high-field spectroscopy. It should be noted that due to the presence of ^{13}C satellite peaks from $CHCl_3$, CH/TEA-synthesized polyisoprene samples were prepared only in $CDCl_3$ to prevent overlap of these satellite peaks with the vinyl polyisoprene peaks.

3.3.4- NMR Spectral Analysis

Unless otherwise specified, all spectra were simply auto-phased and auto-baselined following Fourier-transformation of the FID to prevent overworking of the acquired data and to emulate typical high-field processing procedures. All spectra were shifted in order to position the non-deuterated chloroform peak at 7.26 ppm (relative to TMS standard peak at 0 ppm). Some of the spectra required that the baseline be manually selected as the software read the baseline well above the spectral line, in which case the baseline was selected by placing two points on either side of the area of interest. For polyisoprenes synthesized in neat cyclohexane, the backbone 1,4-

polyisoprene allylic (-CH=) peak was integrated from 4.93-5.33 ppm and the 3,4-polyisoprene terminal allyl (=CH2) peak was integrated from 4.59-4.83 ppm. Polyisoprenes synthesized in cyclohexane/triethylamine mixtures were integrated as follows: 3,4-polyisoprene terminal allyl (=CH2) peak from 4.47-4.87 ppm, 1,2-polyisoprene terminal allyl (=CH2) from 5.44-5.61 ppm, and a peak containing both 1,2-polyisoprene (-CH=) and 1,4-polyisoprene (-CH=) from 4.90-5.34 ppm. Note, presence of the 1,2-polyisoprene peak at 5.4-6.0 ppm is indicative of the need to account for this isomer.[6,7]

3.4- References

(1) McCullough, R. D.; Lowe, R. D.; Jayaraman, M.; Anderson, D. L. Design, Synthesis, and Control of Conducting Polymer Architectures: Structurally Homogeneous Poly(3-Alkylthiophenes). *J. Org. Chem.* **1993**, *58* (4), 904–912. https://doi.org/10.1021/jo00056a024.

(2) McCullough, R. D. The Chemistry of Conducting Polythiophenes. *Advanced Materials* **1998**, *10* (2), 93–116. https://doi.org/10.1002/(SICI)1521-4095(199801)10:2<93::AID-ADMA93>3.0.CO;2-F.

(3) Murphy, A. R.; Fréchet, J. M. J.; Chang, P.; Lee, J.; Subramanian, V. Organic Thin Film Transistors from a Soluble Oligothiophene Derivative Containing Thermally Removable Solubilizing Groups. *J. Am. Chem. Soc.* **2004**, *126* (6), 1596–1597. https://doi.org/10.1021/ja039529x.

(4) Son, S. Y.; Kim, Y.; Lee, J.; Lee, G.-Y.; Park, W.-T.; Noh, Y.-Y.; Park, C. E.; Park, T. High-Field-Effect Mobility of Low-Crystallinity Conjugated Polymers with Localized Aggregates. *J. Am. Chem. Soc.* **2016**, *138* (26), 8096–8103. https://doi.org/10.1021/jacs.6b01046.

(5) Son, S. Y.; Kim, J.-H.; Song, E.; Choi, K.; Lee, J.; Cho, K.; Kim, T.-S.; Park, T. Exploiting π–π Stacking for Stretchable Semiconducting Polymers. *Macromolecules* **2018**. https://doi.org/10.1021/acs.macromol.8b00093.

(6) Beckingham, B. S.; Register, R. A. Synthesis and Phase Behavior of Block-Random Copolymers of Styrene and Hydrogenated Isoprene. *Macromolecules* **2011**, *44* (11), 4313–4319. https://doi.org/10.1021/ma200913k.

(7) Santee, E. R.; Chang, R.; Morton, M. 300 MHz Proton NMR of Polybutadiene: Measurement of Cis-Trans Isomeric Content. *Journal of Polymer Science: Polymer Letters Edition* **1973**, *11* (7), 449–452. https://doi.org/10.1002/pol.1973.130110704.

Chapter 4 - Critical Factors Impacting Signal-to-Noise Ratio and Experimental Time in Low-Field NMR Spectroscopy

Reproduced in part with permission from Jung Min Kim, Vinita V. Shinde, and Bryan S. Beckingham.
(Invited Special Issue) Reproduced by permission of Magnetic Resonance in Chemistry:
Minkler Jr, Michael J., Jung Min Kim, Vinita V. Shinde, and Bryan S. Beckingham. "Low-Field 1H NMR Spectroscopy: Factors Impacting Signal-to-Noise Ratio and Experimental Time in the Context of Mixed Microstructure Polyisoprenes." Magnetic Resonance in Chemistry, April 7, 2020. https://doi.org/10.1002/mrc.5022.

4.1- Introduction

Nuclear magnetic resonance (NMR) spectroscopy of polymeric systems has almost exclusively been performed on NMR spectrometers identified as 300 MHz or higher (at least since their inception).[1–9] This is due to their high sensitivity, repeatable experiments, and ability to produce distinguishable peaks in spectra of systems with many chemically similar protons. However, these high-field instruments often have very high capital and operating costs associated with them. Specially-trained, dedicated personnel are required to operate these instruments as they are very sensitive to their environments and require daily maintenance to prevent mishaps such as quenching of the superconductive magnetic coils. Modern day high-field NMR spectrometers require cryogenic fluids such as helium to remain operational.[10] This fact is problematic as recently prices of cryogenics like helium have begun to increase due to shortages. In addition to the high capital and operating costs, high field spectrometers also require significant square footage and room ventilation as the magnets themselves are relatively large in size and require ample space around them to prevent harm from potential stray magnetic fields and the potential of an unexpected magnet quenching event. The final drawback of these instruments is that they require the researcher to either send in a sample or commute to a centralized location of the high-field magnet. This places the NMR tube and the contained sample in conditions outside of the

environment in which it was prepared, placing it under additional risk (for example heat or UV exposure) and consuming time that could be utilized for other critical laboratory operations.

More recently, low-field NMR spectrometers have begun to make a comeback as a viable means to analyze complex systems.[11–18] Earlier versions of NMR spectrometers are what we now identify as low-field NMR spectrometers, and differ mainly via their mode of operation and lack of digital analysis equipment. Given the advances in modern technology, current-day low-field NMR spectrometers operate more analogous to high-field spectrometers by pulsing magnetic waves through a sample rather than a singular continuous pulse. This repeated excitation and relaxation enhances the obtained signal and improves the overall sensitivity of low-field spectrometers. Operationally, low-field spectrometers have a few advantages over their high-field counterparts such as no required cryogenic cooling, relatively small lab footprint, ability (typically) to use non-deuterated solvents, and overall more accessible usage. Arguably the largest advantage of low-field spectrometers is their potential accessibility within research laboratories as this can save enormous amounts of time. This proximity also allows for sample characterization to remain in-house; effectively eliminating large queue times and allowing researchers to more easily maintain sample possession. However, due to the lower field strength low-field spectrometers are not as sensitive as high-field spectrometers. This stigma has limited the viability of low-field NMR spectrometers in both academia and industry as researchers strive to obtain the best quality data possible. But when used under the correct operating conditions, they can provide data that is comparable to that of high-field instruments.[16,18,19]

Many factors, both instrumental- and sample-based, impact the spectral data quality obtained from an NMR spectroscopy experiment.[20,21] The instrumental parameters chosen for a given experiment—including spectral width, relaxation delay, the number of data points per scan, and

number of scans per experiment—directly affect the resulting spectrum. Given the lack of necessity for dedicated personnel, the effects of these parameters can remain somewhat obscure to a person new to the field of NMR spectroscopy trying to obtain high quality spectra from a low-field spectrometer. Further compounding this problem, sample preparation and the type of sample also directly impact the resulting spectra. For instance, the sample concentration, chosen solvent, and polymer molecular weight all directly affect the NMR spectra of a polymer.[20,21] Lastly, after a successful NMR spectroscopy experiment, the researcher still must process the data in a facile and repeatable manner without over-manipulating the spectra and skewing the results; an unfortunate drawback to the ease of digital data processing.

In this work we aim to examine the impact of instrumental parameters and sample characteristics on signal-to-noise ratio (SNR), experimental time, and extracted polymer composition of mixed microstructure polyisoprenes using a 60 MHz low-field NMR spectrometer. We chose polyisoprene as our polymer of interest due to its complicated microstructure (three distinct polymer repeat units) and its importance as a commercial polymer. Here, we investigate the impact of four instrumental parameters (spectral width, number of data points per scan, relaxation delay, and number of scans per run) and two sample characteristics (polymer concentration and molecular weight) and examine the resulting spectral quality using extracted signal-to-noise ratio and polyisoprene microstructure in comparison with results from a high-field (400 MHz) spectrometer.

4.2 - Experimental Methods

Materials. All chemicals were used as received unless otherwise specified. Cyclohexane, deuterated chloroform, and tetramethylsilane (TMS) were purchased from EMD Millipore. Isoprene was obtained from Acros Organics. Triethylamine (TEA), *n*-butyllithium, and 1,1-diphenylethylene were purchased from Alfa Aesar. Methanol and chloroform were obtained from

VWR International and *tert*-butyllithium was received from TCI America. *Caution! tert-butyllithium and n-butyllithium are pyrophoric and moisture-sensitive materials and should be handled with appropriate care.* Cyclohexane and triethylamine were stirred over diphenylhexyllithium (adduct of *n*-butyllithium and 1,1-diphenylethylene), degassed via freeze–pump–thaw (FPT) cycles, and vacuum transferred prior to use. Isoprene was stirred over *n*-butyllithium, degassed via FPT, and vacuum transferred prior to use. Methanol was degassed via FPT cycles prior to use.

Synthesis of Polyisoprenes. All reaction vessels were flamed out under vacuum prior to use. *Tert*-Butyllithium initiated anionic polymerization of isoprene was performed at room temperature over 20 hours to achieve >99.9% conversion.[22] Cyclohexane (100 mL, 0.92 mols), isoprene (10 g, 0.15 mols), and *tert*-butyllithium (0.73 mL, 0.0014 mols) were charged to a reactor and polymerized in a nitrogen-filled glovebox. *Caution! tert-butyllithium is pyrophoric and moisture-sensitive materials and should be handled with appropriate care.* The polymerization was terminated by addition of degassed methanol and recovered by precipitation into methanol. An analogous procedure was followed for anionic polymerization of isoprene in a 50/50 vol/vol mixture of cyclohexane/TEA.

Molecular Characterization. Gel permeation chromatography (GPC) was conducted using a Malvern Omnisec Resolve tetradetection system with THF as the mobile phase, and calibrated with narrow-distribution polystyrene standards. The apparent "polystyrene-equivalent" molecular weight obtained by GPC was converted to absolute molecular weight by correcting for the differences in hydrodynamic volume between polystyrene and polyisoprene.[22,23] The results from GPC can be found in **Figure 4.13**.

NMR Sample Preparation and Analysis. High-field NMR spectroscopy was performed on a Bruker 400 MHz Avance400 NMR spectrometer. Low-field NMR spectroscopy was performed on an Oxford Pulsar 60 MHz NMR spectrometer. All NMR samples were prepared in Wilmad high-throughput class B NMR tubes (8" length, 5 mm outer diameter, 4 mm inner diameter). NMR spectroscopy samples were prepared by metering a desired quantity of polyisoprene into a scintillation vial and adding the appropriate amount of $CHCl_3$ (for low-field) or $CDCl_3$ (for high-field) to prepare solutions with target concentrations of 1, 10, 25, and 50 mg/mL for low-field spectroscopy and 50 mg/mL for high-field spectroscopy. It should be noted that due to the presence of ^{13}C satellite peaks from $CHCl_3$, TEA-synthesized polyisoprene samples were prepared in $CDCl_3$ to prevent overlap of these satellite peaks with the vinyl polyisoprene peaks.

Unless otherwise specified, all spectra were simply auto-phased and auto-baselined following Fourier-transformation of the FID to prevent overworking of the acquired data and to emulate typical high-field processing procedures. All spectra were shifted in order to position the non-deuterated chloroform peak at 7.26 ppm (relative to TMS standard peak at 0 ppm). Some of the spectra required that the baseline be manually selected as the software read the baseline well above the spectral line, in which case the baseline was selected by placing two points on either side of the area of interest. For polyisoprenes synthesized in neat cyclohexane, the backbone 1,4-polyisoprene allylic (-CH=) peak was integrated from 4.93-5.33 ppm and the 3,4-polyisoprene terminal allyl ($=CH_2$) peak was integrated from 4.59-4.83 ppm. Polyisoprenes synthesized in cyclohexane/triethylamine mixtures were integrated as follows: 3,4-polyisoprene terminal allyl ($=CH_2$) peak from 4.47-4.87 ppm, 1,2-polyisoprene terminal allyl ($=CH_2$) from 5.44-5.61 ppm, and a peak containing both 1,2-polyisoprene (-CH=) and 1,4-polyisoprene (-CH=) from 4.90-5.34

ppm. Note, presence of the 1,2-polyisoprene peak at 5.4-6.0 ppm is indicative of the need to account for this isomer.[22,23]

4.3- Results and Discussion

In order to examine the impact of instrumental and sample parameters on the quality of low-field NMR spectra, we chose to utilize polyisoprene as our polymer of interest. Depending on the mode of addition as repeat units are incorporated into the growing polymer chain, three distinct polyisoprene repeat units (Figure 1) are formed; 1,4-, 1,2- and 3,4-polyisoprene, so named for the isoprene carbon positions that covalently link the repeat unit to the polymer chain. Here, we synthesize two sets of polyisoprenes using alkyllithium-initiated anionic polymerization where the solvent environment was altered to produce polyisoprenes with two different microstructures (relative fraction of addition modes). Three polyisoprenes of varied molecular weight (14.3 kg/mol, 29.3 kg/mol, and 35.1 kg/mol) were synthesized in neat cyclohexane (referred to herein as PICH's) and as such has a majority 1,4-addition and no 1,2-addition content.[22,23] Three polyisoprenes of varied molecular weight (11.2 kg/mol, 26.0 kg/mol, and 42.9 kg/mol) were synthesized in a 50/50 mixture of TEA/cyclohexane resulting in a higher vinyl content with nearly equimolar 1,4-addition and 3,4-addition and a small amount of 1,2-addition.[22] Three molecular weights of each type of polyisoprene were synthesized to investigate the effects of polymer molecular weight on the acquired spectral data. One of the synthesized polyisoprenes (29.3 kg/mol PICH) was subjected to a variety of experiments to determine the effects of the instrumental parameters on the resulting spectral data quality and accuracy.

4.3.1-Impact of Instrumental Parameters

One advantage of low-field NMR spectrometers is their ability to utilize a "soft-lock" which uses advanced software algorithms to prevent spectral drift over a series of scans. This soft-lock enables

non-deuterated solvents to be utilized for data analysis. This is advantageous as it eliminates the need for the comparably much more expensive deuterated solvents but it also enables direct tracking of reaction progress without sample manipulation; change in concentrations by addition of solvent or additives. Additionally, for reaction monitoring the presence of a large solvent peak of known shift can be used as the reference peak; eliminating the need for the addition of an additive such as tetramethylsilane (TMS). Note, chemical shifts (δ, Equation 4.1) are determined based on the frequency (v_i) of the spectrometer, sample and an arbitrary reference (typically TMS).

$$\delta(ppm) = \frac{\nu_{reference}(Hz) - \nu_{sample}(Hz)}{\nu_{spectrometer}(MHz)} \tag{4.1}$$

For instance, the spectrum in **Figure 4.1** is shifted based on the peak furthest downfield as this peak is attributed to chloroform and thereby shifted to its known '*standard'* location (7.26 ppm) relative to TMS having a chemical shift of zero.

A successful NMR spectroscopy experiment typically involves a lot of "behind-the-scenes" setup on the part of the computer and instrument. This is especially true for high-field spectrometers, where many parameters are automatically manipulated or often buried within lines of standard code utilized by a user as outlined in a run procedure at a central instrumental facility. In the case of low-field spectrometers, like the Oxford Pulsar 60 MHz NMR spectrometer used here, the instrument software (Spinflow 2.3.0) is graphics-based and many of the instrumental parameters are visually presented to the operator; parameters shown in **Table 4.1**. Even an experiment as simple as a 1-dimensional (1D), free-induction decay (FID) ^{1}H NMR experiment involves the use of at least nine parameters; of which five are typically operator-adjusted. The other four parameters can be adjusted if desired, however these are set by the routine shimming and calibration routines and user-adjustment outside these routines is imprudent. Here, we are interested in the impact of

four of the five adjustable settings: spectral width (referred to as Filter in Spinflow 2.3.0, corresponding to the total window of observed frequency in Hz), number of scans (*n*), relaxation delay (*RD*, time between scans), and the number of points per scan (*NP*). Depending on their selected values, these four parameters can dramatically affect the resulting NMR spectra. The signal-to-noise ratio (*SNR*) is both a critical and an easy to understand characteristic used to describe the quality of an NMR spectra. The SNR (Equation 4.2) is governed by the magnetic field strength ($B_{0,}$ in Tesla), the number of scans (*n*), and the number of spins (*N*) which is related to the sample concentration.[20,21]

$$\frac{Signal}{Noise} \alpha N B_0^{\frac{3}{2}} \sqrt{n} \tag{4.2}$$

As the SNR is a useful quantitative metric for spectral quality, we calculate the SNR for a series of ^{1}H NMR spectra of the 29.3 kg/mol PICH at a concentration of 50 mg/mL. We perform an array of experiments independently varying one parameter around a base case 65536 points per scan, 5000 Hz spectral width, and 1 second relaxation delay. We then extract the experimental time and SNR for each experiment with varied number of points per scan, spectral width, and relaxation time (**Figure 2a-c**). Note that experimental time refers to the total experimental time in the spectrometer for all scans while the relaxation delay refers to the time between sequential scans. For instance, the experimental time (*ET*) is related to the acquisition time (*AT*)—where *ET = AT * n*)—which is a function of both the spectral width (*SW*), number of points per scan (*NP*), and correspondingly the signal resolution (*R*) as described by Equation 4.3.[20] Conversely, relaxation delay is itself an instrumental parameter of the instrument that can be directly set by the user.

While SNR and spectral resolution (*R*) are related, they are distinct concepts. SNR is a measured result of a spectra that can vary due to numerous experimental parameters whereas spectral

resolution is describing the density of data points and is dictated by the selected parameters (Equation 4.3). Examining the SNRs and experimental times in **Figure 4.2**, a couple of trends emerge concerning the tradeoff between these two experimental considerations. Experimental time, as expected from Equation 4.3, increases with increasing number of points per scan (**Figure 4.2a**) and decreases with increasing spectral width (**Figure 4.2b**). Experimental time also increases with increasing relaxation delay as the relaxation delay increases the time required for each scan sequence. Due to the interconnected nature of the parameters discussed in this work clear, distinct trends in SNR are somewhat absent and prevent the use of a parametric grid to demonstrate the effects of the selected experimental variables. However, we do observe consistently improved SNR for larger spectral width as expected; as spectral width is directly proportional to spectral resolution (*R*, in Equation 4.3). Additionally, a higher SNR is achieved for lower relaxation delay as the polyisoprene relaxation times are much shorter than that of chloroform, allowing for enhanced signal recovery. We also observe a decrease in SNR at high number of points per scan (**Figure 4.2a**), likely due to the higher data point density capturing a higher fraction of the low-probability, high-amplitude noise and acquiring noise for longer time after the polymer relaxation.[20,24]

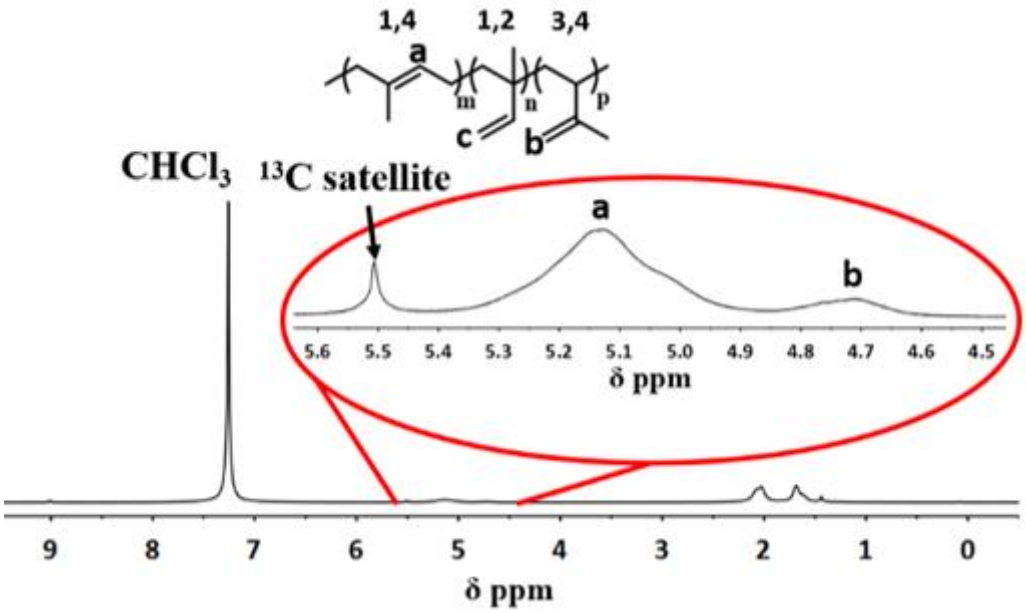

Figure 4.1 Polyisoprene structure and ^{1}H NMR spectrum shifted based on the $CHCl_3$ peak position (7.26 ppm) relative to a TMS reference shift at zero.

Table 4.1 List of common parameters available in NMR spectroscopy.

Name	Abbreviation	User Tunable
Spectral Width	SW	X
Number of Scans	n	X
Spectrometer Offset Frequency [Hz]	O1	X
90 Degree Pulse Length [μs]	P90	
Relaxation Delay [seconds]	RD	X
Receiver Attenuation [dB]	RGA	
Number of Points Per Scan	NP	X
Transmit Pulse Amplitude	RFA0	
Spectrometer Base Frequency [MHz]	SF	

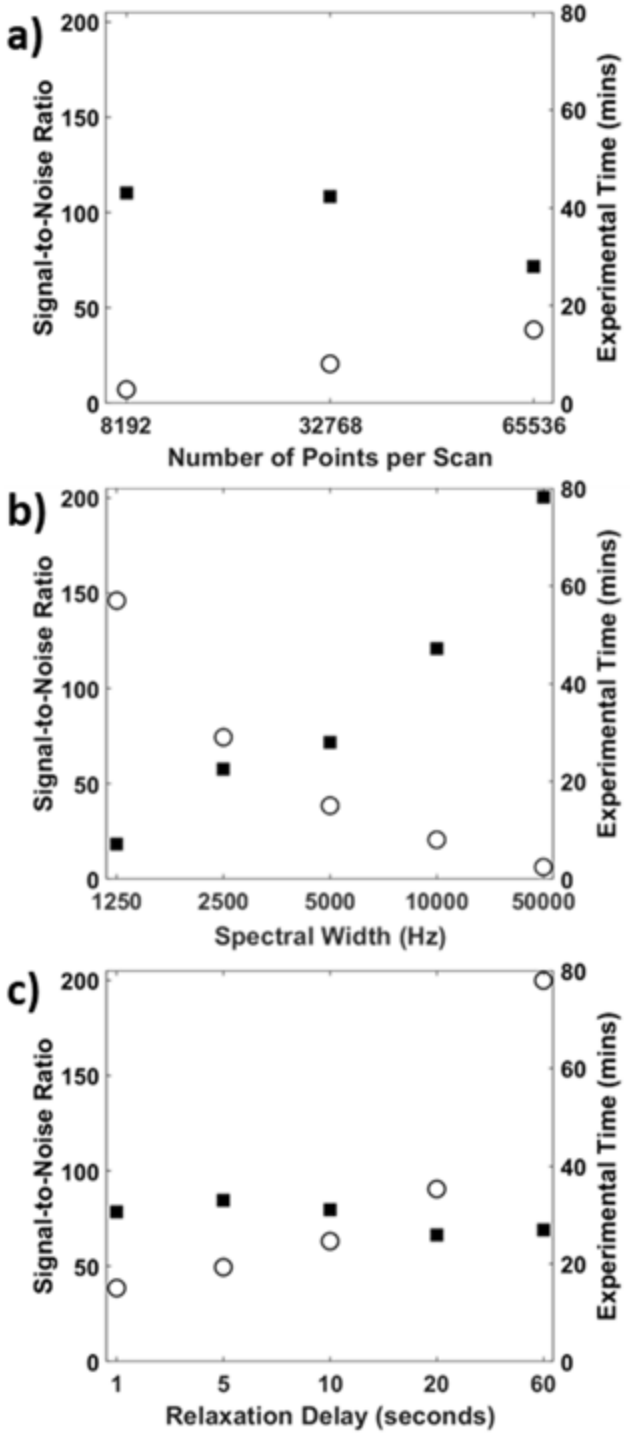

Figure 4.2 SNR (filled squares, left vertical axes) and experimental time (open circles, right vertical axes) versus (a) varied number of points per scan (spectral width 5000 Hz, relaxation delay 1 second, 64 scans), (b) varied spectral width (65,536 points per scan and 1 second relaxation delay, 64 scans), and (c) varied relaxation delay (spectral width 5000 Hz and 65,536 points per scan, 64 scans) for 29.3 kg/mol PICH at a concentration of 50 mg/mL.

$$R = \frac{1}{AT} = \frac{2 * SW}{NP} \tag{4.3}$$

Next, we examine the spectra for characterizing the polyisoprene microstructure (**Figure 4.3**). Each of the ^{1}H NMR experiments with varied number of points per scan, spectral width, and relaxation delay are integrated (see section 4.2 for integration limits) to determine the polyisoprene microstructure of this 29.3 kg/mol PICH and the results are compared to those obtained using a 400 MHz spectrometer (solid line on **Figure 4.3 a,c,e**). These are the most important results from this type of data collection as the ability to distinguish and quantify different isomeric repeat units within a polymer backbone is the purpose for conducting these ^{1}H NMR experiments. We find excellent agreement between the polyisoprene microstructures extracted from the low-field and high-field spectrometers with nearly all of the results within 1% for the range of instrumental parameters investigated here. These findings are consistent with findings in **Chapter 5**, where we evaluate the capability of a 60 MHz spectrometer (Pulsar) to consistently producing compositional data within 2% of the extracted high-field values for high 1,4-polyisoprene as well as select block copolymers and polymer blends.[18] Even the shortest experiment here, ~3 minutes, is capable of producing quantitatively consistent compositional results which is encouraging for the application of these instruments in quality control applications.

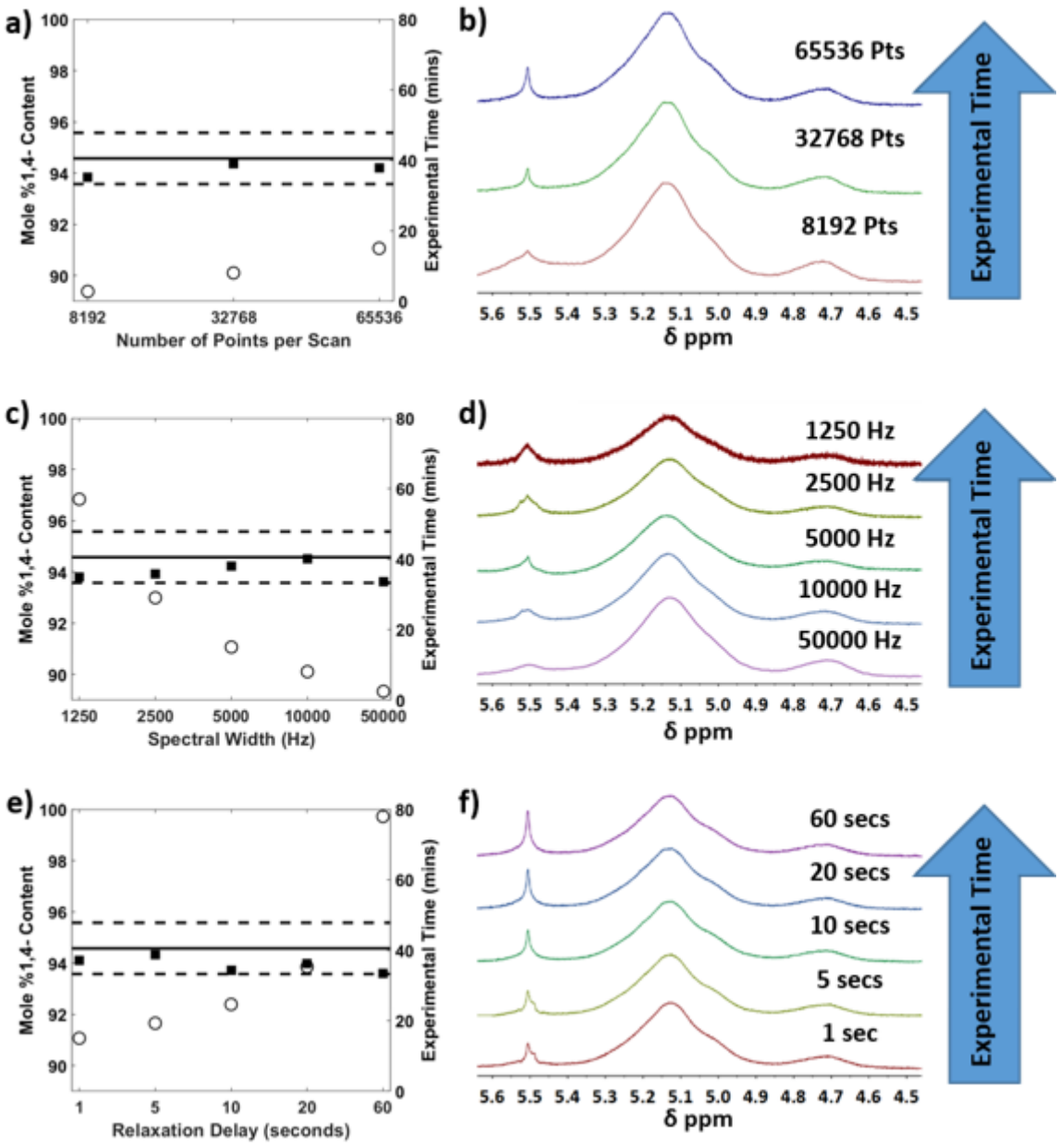

Figure 4.3 Extracted polyisoprene compositions (filled squares, left vertical axis), experimental time (open circles, right vertical axis) and the corresponding ^{1}H NMR spectra for a,b) varied number of points per scan (spectral width 5000 Hz, relaxation delay 1 second), c,d) varied spectral width (65,536 points per scan and 1 second relaxation delay), and e,f) varied relaxation delay (spectral width 5000 Hz and 65,536 points per scan) for 29.3 kg/mol PICH. See **Figure 4.6** for 400 MHz spectra.

4.3.2- Impact of Sample Characteristics

In addition to the complex relationships between user-tunable settings onboard an NMR spectrometer, sample preparation also plays a critical role in the quality of spectral data obtained from an experiment. It is known that both viscosity and the physical state of a sample directly affect the quality of NMR data. Here, the series of polyisoprenes (PICHs) with varying molecular weights (14.3 kg/mol, 29.3 kg/mol, and 35.1 kg/mol) synthesized in neat cyclohexane are solvated to varying concentration (1, 10, 25, and 50 mg/mL) to illustrate the impact of both polymer concentration and molecular weight on spectral quality. Additionally, we examine the impact of the number of scans (1, 4, 16, 64, and 256 scans) for each PICH at each concentration on SNR as this is arguably the most commonly user-varied parameter for 1D NMR experiments (**Figure 4.4**). As shown in **Figure 4.4**, both concentration and number of scans impact the SNR. As expected, an increase in concentration yielded an enhanced SNR (Equation 4.2) across all polymer compositions and molecular weight. Overall, the results in **Figure 4.4** suggest a more concentrated polymer sample is desirable and we thereby recommend the use of 50 mg/mL polymer samples for routine analysis of this type, when possible. The acquired spectra with varied number of scans are then analyzed to extract the polyisoprene microstructure (**Figure 4.5**); see **Figure 4.6**-**Figure 4.10** for corresponding spectra. As shown in **Figure 4.8b**, an unfortunate drawback of minimal digital workup is the potential for phase drift. This is apparent as the experiment with 4 scans went out of phase and appears to overlap with the 16-scan experiment. Again, we find excellent agreement between the 60 MHz results and 400 MHz results across all number of scans with all compositions within 1% of the 400 MHz result. This demonstrates that capability of low-field spectrometers for producing quantitative results for a wide variety of sample conditions and run parameters. Additionally, our results demonstrate that extensively long NMR experiments are not necessary for determination of polymer compositions.

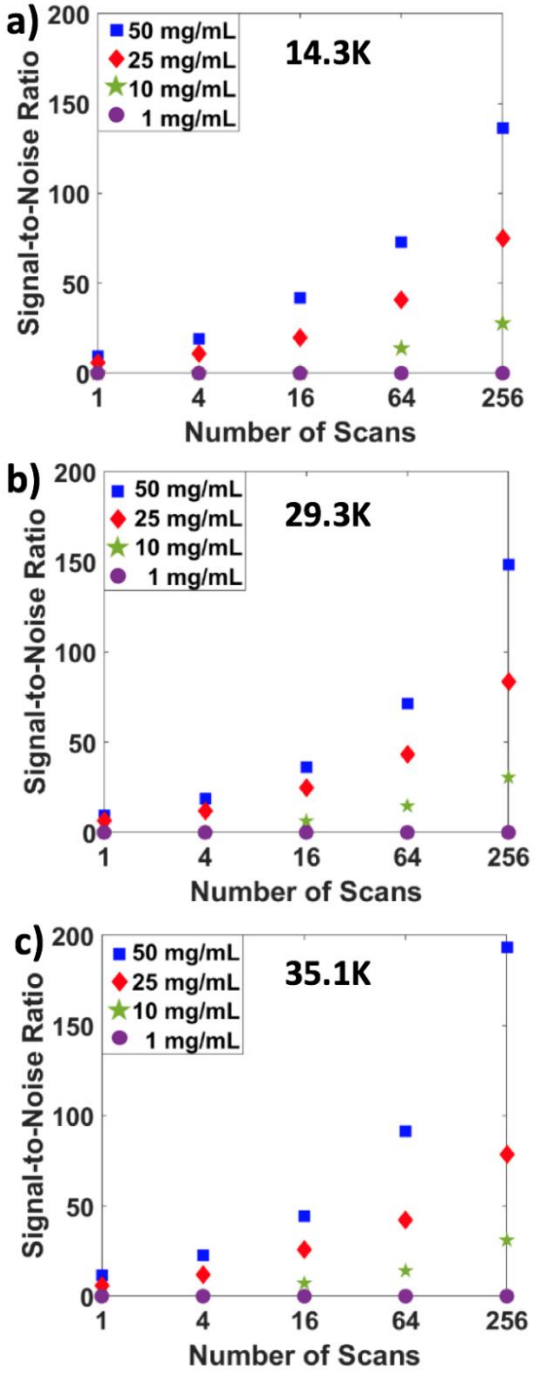

Figure 4.4 Enhancement of SNR via concentration and MW tuning of a) 14.3 kg/mol (14.3K) PICH, b) 29.3 kg/mol (29.3K) PICH, and c) 35.1 kg/mol (35.1K) PICH. See Figure 4.7-Figure 4.10 for corresponding spectra.

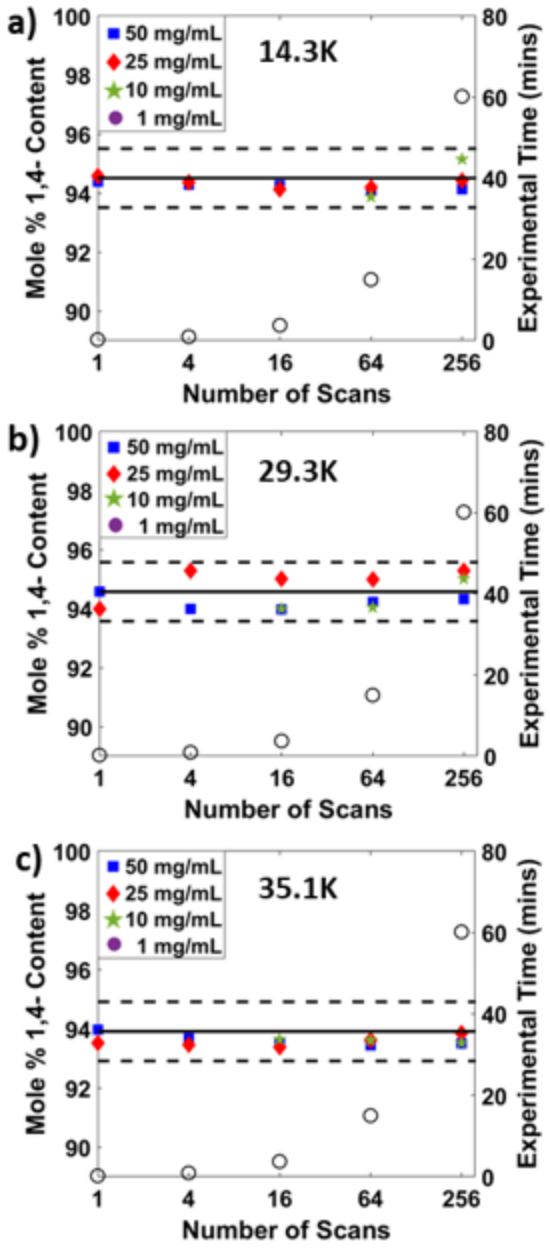

Figure 4.5 Mole percent 1,4-content of polyisoprene for varied concentrations and scans of of a) 14.3 kg/mol (14.3K) PICH, b) 29.3 kg/mol (29.3K) PICH, and c) 35.1 kg/mol (35.1K) PICH; see Figure 4.6-Figure 4.10 for corresponding spectra**.** Empty circles correspond to experimental time.

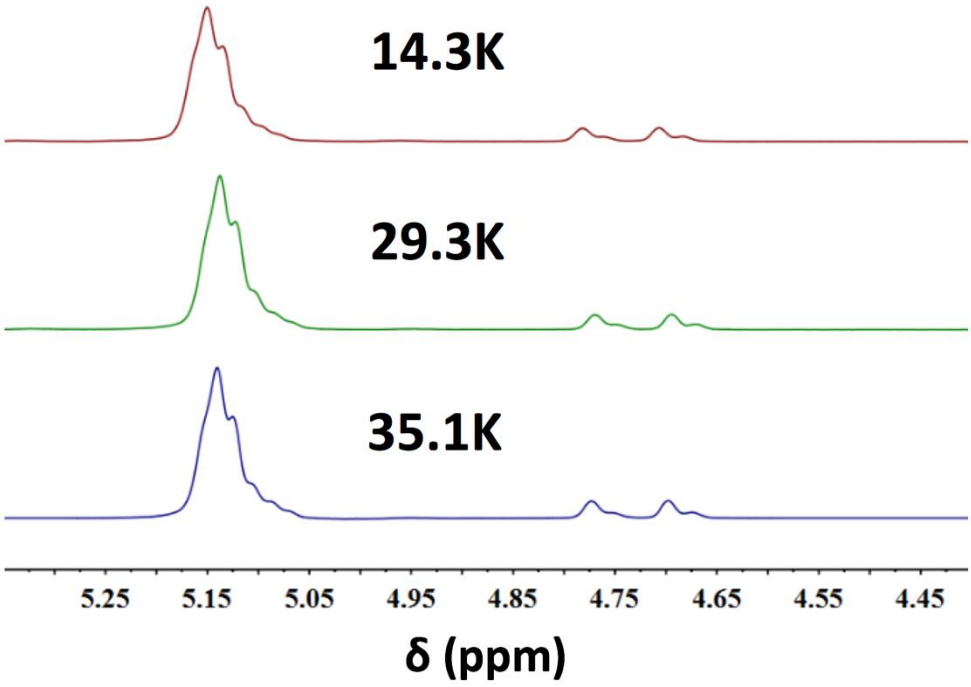

Figure 4.6 400 MHz spectra (16 scans) for PICH's at 50 mg/mL in deuterated chloroform; 14.3 kg/mol (14.3K), 29.3 kg/mol (29.3K) and 35.1 kg/mol (35.1K).

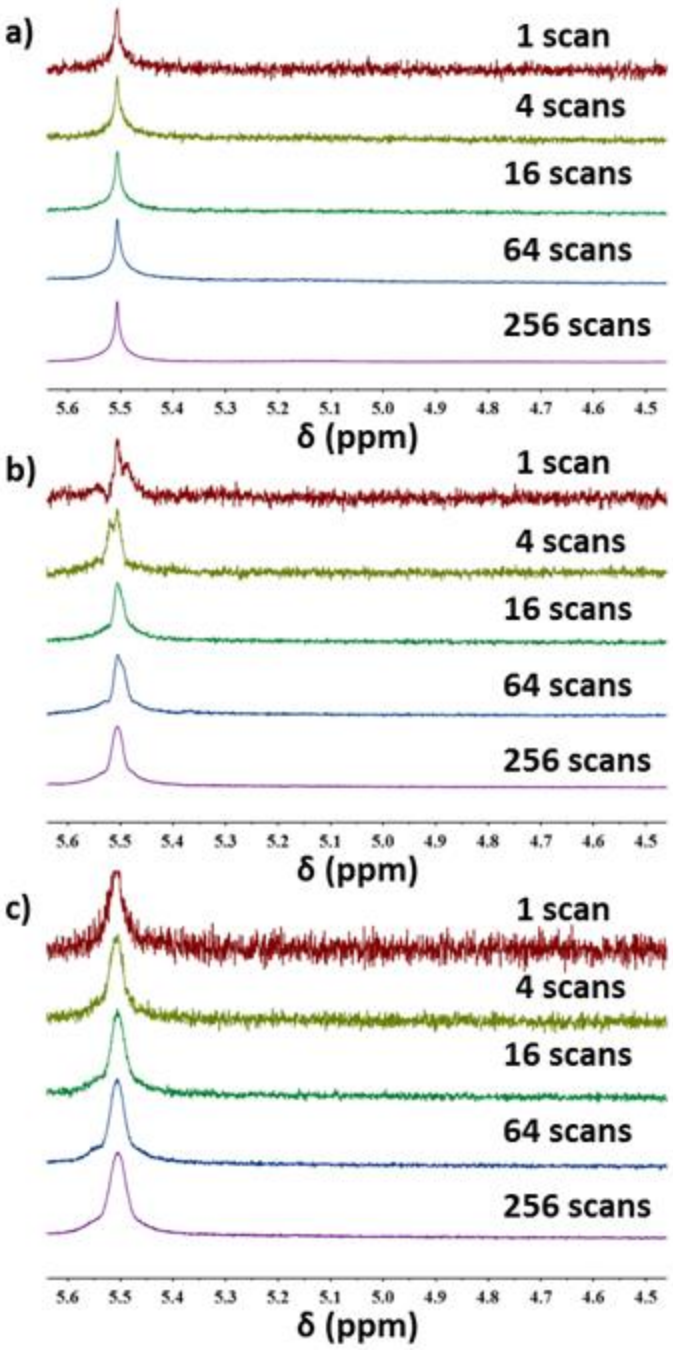

Figure 4.7 60 MHz spectra (varied scans, 5000 Hz spectral width, 1 second relaxation delay, 65536 points per scan) of a) 14.3 kg/mol PICH, b) 29.3 kg/mol PICH, and c) 35.1 kg/mol PICH at 1 mg/mL polymer concentration in chloroform.

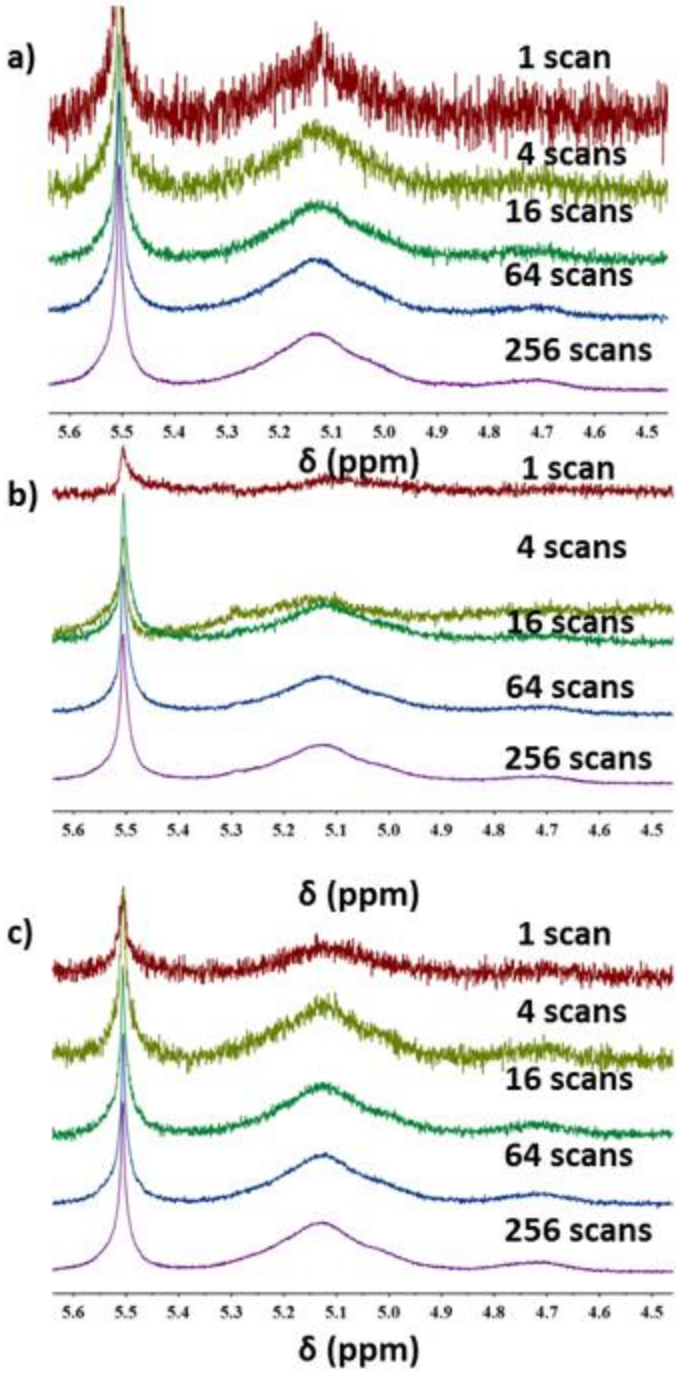

Figure 4.8 60 MHz spectra (varied scans, 5000 Hz spectral width, 1 second relaxation delay, 65536 points per scan) of a) 14.3 kg/mol PICH, b) 29.3 kg/mol PICH, and c) 35.1 kg/mol PICH at 10 mg/mL polymer concentration in chloroform.

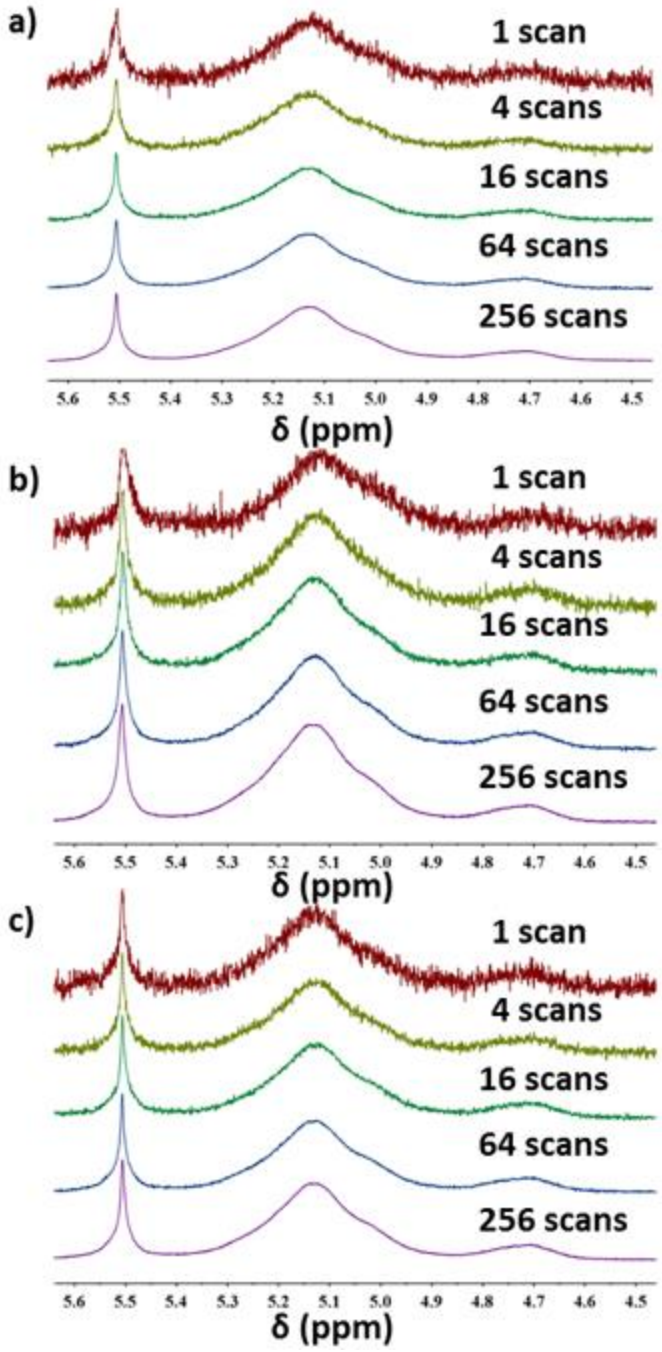

Figure 4.9 60 MHz spectra (varied scans, 5000 Hz spectral width, 1 second relaxation delay, 65536 points per scan) of a) 14.3 kg/mol PICH, b) 29.3 kg/mol PICH, and c) 35.1 kg/mol PICH at 25 mg/mL polymer concentration in chloroform.

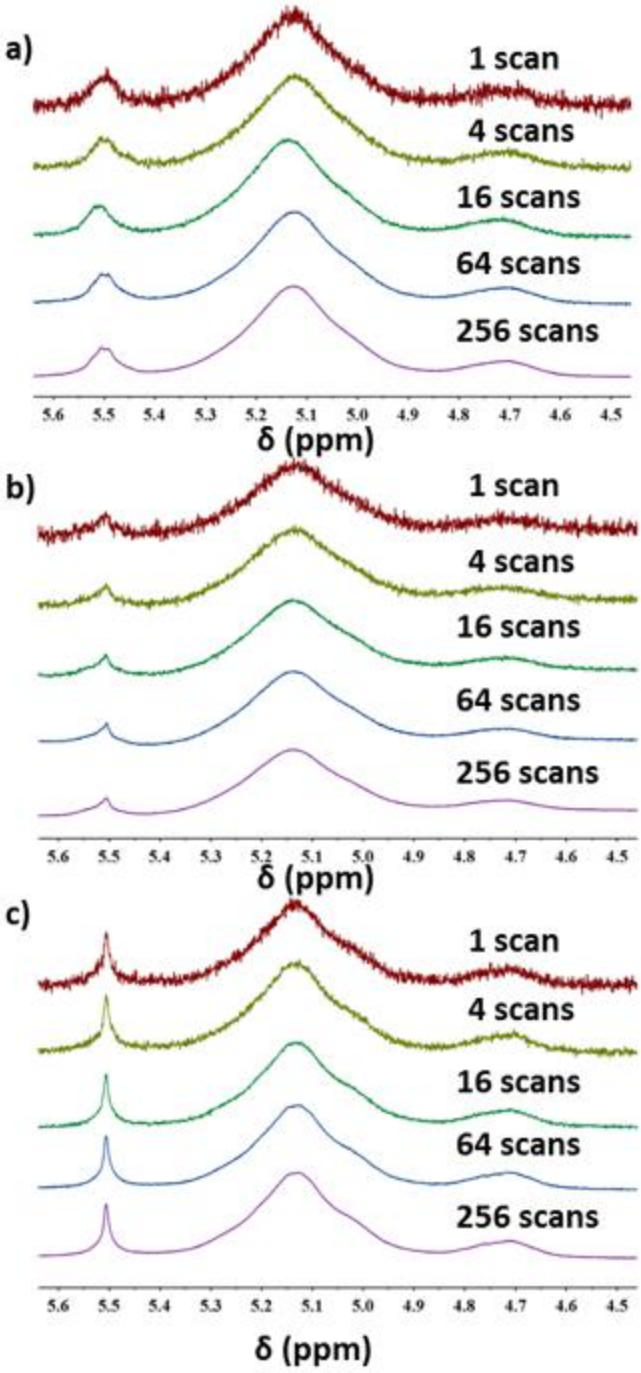

Figure 4.10 60 MHz spectra (varied scans, 5000 Hz spectral width, 1 second relaxation delay, 65536 points per scan) of a) 14.3 kg/mol PICH, b) 29.3 kg/mol PICH, and c) 35.1 kg/mol PICH at 50 mg/mL polymer concentration in chloroform.

4.3.3- Analysis of PICT, Presence of a Low Molar Concentration Constituent

Lastly, we examine three polyisoprenes of varied molecular weight (11.2 kg/mol, 26.0 kg/mol, and 42.9 kg/mol) synthesized in a mixture of cyclohexane and triethylamine (these polymers are referred to as PICT's). This series of polyisoprenes is important as the presence of TEA leads to a more balanced 1,4- vs 3,4-polyisoprene microstructure and the incorporation of 1,2-addition polyisoprene in low molar quantities. This allows for examination of the ability of the 60 MHz spectrometer to detect and quantitatively determine the presence of a trace minority component (less than 5%). PICT samples were prepared at a concentration of 50 mg/mL per our recommendation above and spectra obtained using the 60 MHz spectrometer for 256 scans, 5000 Hz spectral width, and a relaxation delay of 1 second. These parameters were chosen to give a good balance of experimental time and SNR. The extracted compositions (1,4-, 3,4-, and 1,2-) for these three PICTs obtained using the 60 MHz spectrometer are in excellent agreement with the high-field results with nearly all microstructure components within 1%; **Figure 4.11** (corresponding spectra in **Figure 4.12**). We note the differences increase as molecular weight increases with the largest discrepancy for 42.9 kg/mol PICT; behavior we hope to probe further as we test the limits of the 60 MHz spectrometer. Overall, these results validate the use of low-field spectrometers for characterizing mixed microstructure polyisoprenes of this type with good quantitative precision relative to higher-field spectrometers and likely signifies the capability to quantitatively determine polyisoprene microstructure across the compositional space including the presence of low microstructure contents (here, ~2 mole percent).

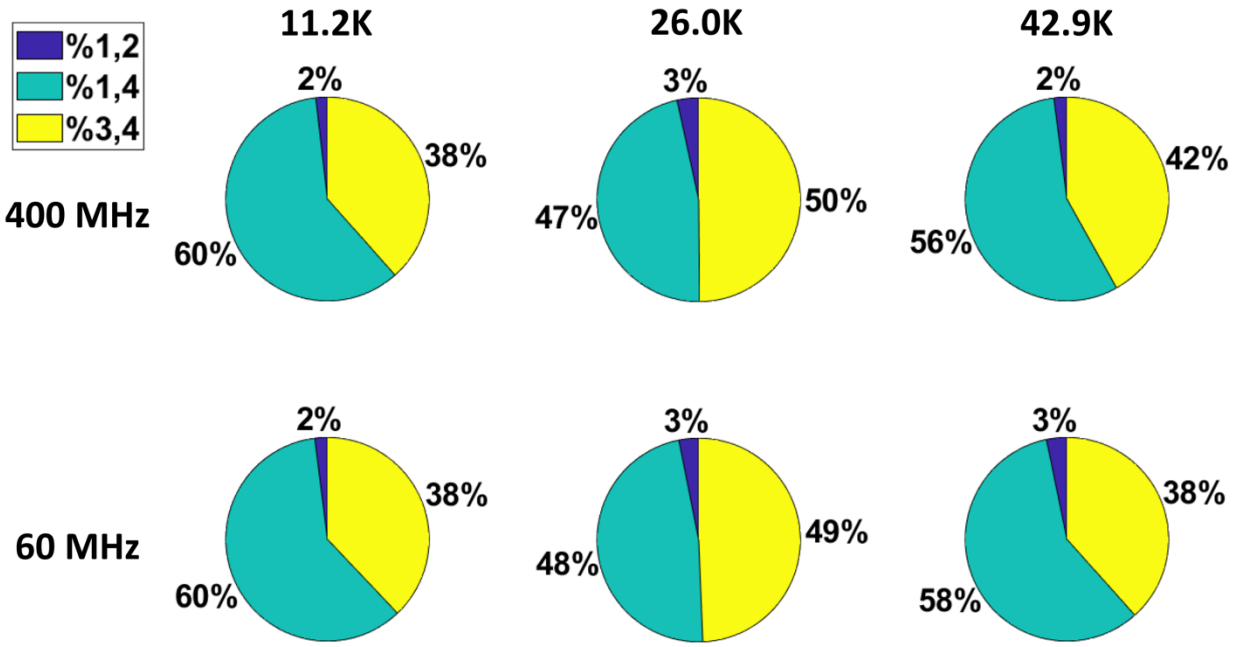

Figure 4.11 Extracted polyisoprene microstructure compositions for 11.2 kg/mol (11.2K) PICT, 26.0 kg/mol (26.0K) PICT, and 42.9 kg/mol (42.9K) PICT; see **Figure 4.12** for spectra.

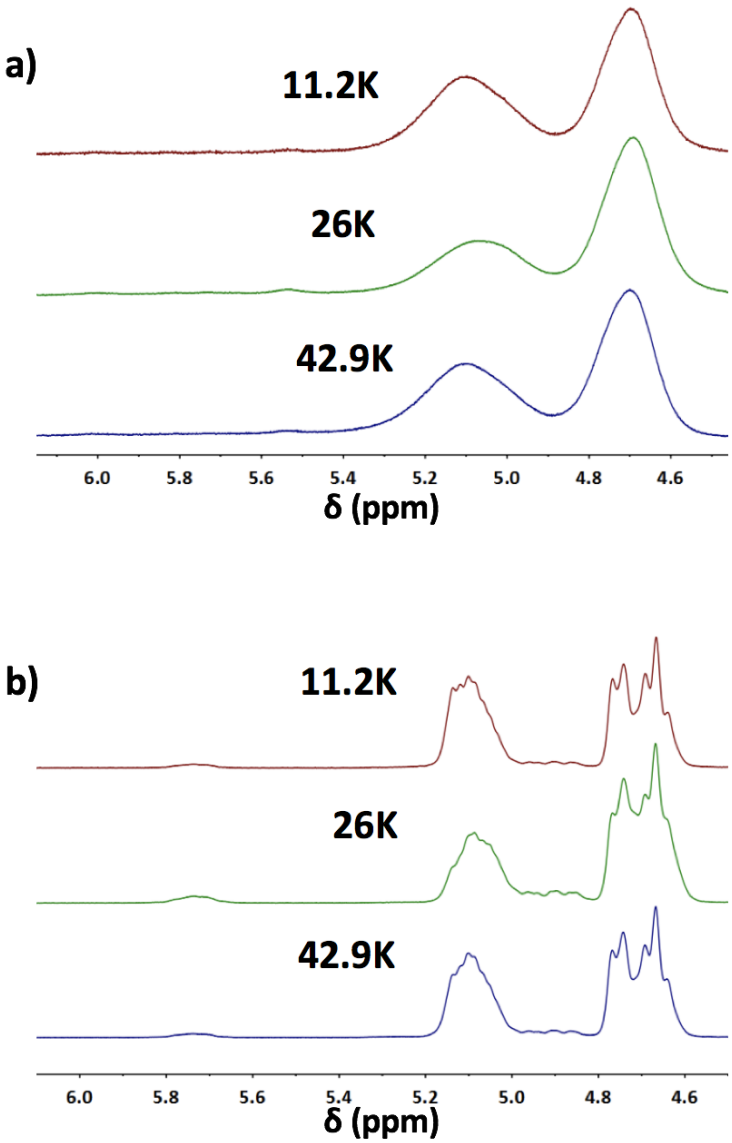

Figure 4.12 a) 60 MHZ spectra (256 scans, 5000 Hz spectral width, 1 second relaxation delay, 65536 points per scan) and b) 400 MHz spectra (16 scans) of PICT polymers at 50 mg/mL in deuterated chloroform; 11.2 kg/mol (11.2K), 26.0 kg/mol (26K) and 42.9 kg/mol (42.9K).

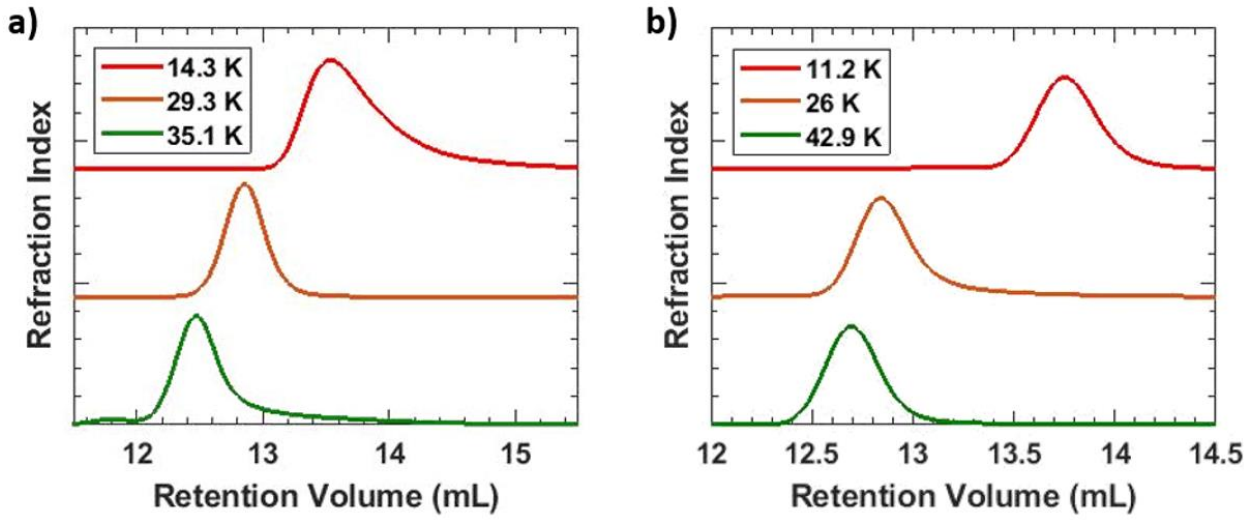

Figure 4.13 GPC traces of synthesized polyisoprenes. a) PICH's and b) PICT's.

4.4- Conclusions

Two sets of polyisoprenes of varied molecular weight and microstructure were synthesized and analyzed using both a 60 MHz low-field NMR spectrometer and a 400 MHz high-field spectrometer. Four instrumental parameters were varied (number of points per scan, spectral width, relaxation delay and number of scans) and their impact on SNR and total experimental time examined. Overall, we find excellent quantitative agreement with nearly all results obtained using the 60 MHz spectrometer within 1% agreement of those obtained using the 400 MHz spectrometer. These results validate the use of lower-field NMR spectrometers for the analysis of these complex polymer microstructures even for detecting and quantitatively determining the composition of low content structures (here 2-3 mole percent of 1,2-polyisoprene). While not tested here, we anticipate our findings to be generally true for low-field spectrometers of this field strength. The use of low-field NMR spectrometers is a true low-cost alternative to higher-field analysis without the need for central facilities, specialized personnel and, in many cases, deuterated solvents for the analysis of polymer systems. Methods such as low-field NMR spectroscopy are part of a growing industry of in-house characterization that will eventually prove to both enhance research quality and hasten the pace in which research can be performed.

4.5- References

(1) Tanaka, Y.; Takeuchi, Y.; Kobayashi, M.; Tadokoro, H. Characterization of Diene Polymers. I. Infrared and NMR Studies: Nonadditive Behavior of Characteristic Infrared Bands. *Journal of Polymer Science Part A-2: Polymer Physics* **1971**, *9* (1), 43–57. https://doi.org/10.1002/pol.1971.160090104.

(2) Stuart, B. H. *Polymer Analysis*; John Wiley & Sons, 2008.

(3) Gu, K.; Onorato, J.; Xiao, S. S.; Luscombe, C. K.; Loo, Y.-L. Determination of the Molecular Weight of Conjugated Polymers with Diffusion-Ordered NMR Spectroscopy. *Chemistry of Materials* **2018**, *30* (3), 570–576. https://doi.org/10.1021/acs.chemmater.7b05063.

(4) Zhang, Y.; Tajima, K.; Hashimoto, K. Nanostructure Formation in Poly(3-Hexylthiophene-Block-3-(2-Ethylhexyl)Thiophene)s. *Macromolecules* **2009**, *42* (18), 7008–7015. https://doi.org/10.1021/ma9013065.

(5) Ouhib Farid; Dkhissi Ahmed; Iratçabal Pierre; Hiorns Roger C.; Khoukh Abdel; Desbrières Jacques; Pouchan Claude; Dagron-Lartigau Christine. Electronic Structure and Optical Properties of Poly[3-(4-octylphenoxy)Thiophene]: Experimental and Theoretical Studies. *Journal of Polymer Science Part A: Polymer Chemistry* **2008**, *46* (22), 7505–7516. https://doi.org/10.1002/pola.23056.

(6) Davis, K. A.; Burdick, J. A.; Anseth, K. S. Photoinitiated Crosslinked Degradable Copolymer Networks for Tissue Engineering Applications. *Biomaterials* **2003**, *24* (14), 2485–2495. https://doi.org/10.1016/S0142-9612(02)00582-3.

(7) Hyberts, S. G.; Robson, S. A.; Wagner, G. Exploring Signal-to-Noise Ratio and Sensitivity in Non-Uniformly Sampled Multi-Dimensional NMR Spectra. *J Biomol NMR* **2013**, *55* (2), 167–178. https://doi.org/10.1007/s10858-012-9698-2.

(8) Suggs, L. J.; Payne, R. G.; Yaszemski, M. J.; Alemany, L. B.; Mikos, A. G. Synthesis and Characterization of a Block Copolymer Consisting of Poly(Propylene Fumarate) and Poly(Ethylene Glycol). *Macromolecules* **1997**, *30* (15), 4318–4323. https://doi.org/10.1021/ma970312v.

(9) Spiess, H. W. 50th Anniversary Perspective: The Importance of NMR Spectroscopy to Macromolecular Science. *Macromolecules* **2017**, *50* (5), 1761–1777. https://doi.org/10.1021/acs.macromol.6b02736.

(10) Cho, A. Helium-3 Shortage Could Put Freeze On Low-Temperature Research. *Science* **2009**, *326* (5954), 778–779. https://doi.org/10.1126/science.326_778.

(11) Eccles, C. Low Field NMR Methods and Applications. In *Encyclopedia of Spectroscopy and Spectrometry (Second Edition)*; Lindon, J. C., Ed.; Academic Press: Oxford, 2010; pp 1357–1371. https://doi.org/10.1016/B978-0-12-374413-5.00018-X.

(12) Nordon, A.; Gemperline, P. J.; McGill, C. A.; Littlejohn, D. Quantitative Analysis of Low-Field NMR Signals in the Time Domain. *Anal. Chem.* **2001**, *73* (17), 4286–4294. https://doi.org/10.1021/ac0102866.

(13) Papon, A.; Saalwächter, K.; Schäler, K.; Guy, L.; Lequeux, F.; Montes, H. Low-Field NMR Investigations of Nanocomposites: Polymer Dynamics and Network Effects. *Macromolecules* **2011**, *44* (4), 913–922. https://doi.org/10.1021/ma102486x.

(14) Vargas, M. A.; Cudaj, M.; Hailu, K.; Sachsenheimer, K.; Guthausen, G. Online Low-Field 1H NMR Spectroscopy: Monitoring of Emulsion Polymerization of Butyl Acrylate. *Macromolecules* **2010**, *43* (13), 5561–5568. https://doi.org/10.1021/ma1006599.

(15) Ruan, R. R.; Long, Z.; Song, A.; Chen, P. L. Determination of the Glass Transition Temperature of Food Polymers Using Low Field NMR. *LWT - Food Science and Technology* **1998**, *31* (6), 516–521. https://doi.org/10.1006/fstl.1998.0409.
(16) Singh, K.; Blümich, B. Compact Low-Field NMR Spectroscopy and Chemometrics: A Tool Box for Quality Control of Raw Rubber. *Polymer* **2018**, *141*, 154–165. https://doi.org/10.1016/j.polymer.2018.02.057.
(17) Patel, J. P.; Hsu, S. L. Development of Low Field NMR Technique for Analyzing Segmental Mobility of Crosslinked Polymers. *Journal of Polymer Science Part B: Polymer Physics* **2018**, *56* (8), 639–643. https://doi.org/10.1002/polb.24583.
(18) Chakrapani, S. B.; Minkler, M. J.; Beckingham, B. S. Low-Field 1H-NMR Spectroscopy for Compositional Analysis of Multicomponent Polymer Systems. *Analyst* **2019**, *144* (5), 1679–1686. https://doi.org/10.1039/C8AN01810C.
(19) Isaac-Lam, M. F. Determination of Alcohol Content in Alcoholic Beverages Using 45 MHz Benchtop NMR Spectrometer https://www.hindawi.com/journals/ijs/2016/2526946/ (accessed Sep 30, 2019). https://doi.org/10.1155/2016/2526946.
(20) Günther, H. *NMR Spectroscopy: Basic Principles, Concepts and Applications in Chemistry*; John Wiley & Sons, 2013.
(21) Skoog, D.; Holler, F.; Crouch, S. *Instrumental Analysis*, Indian Edition.; Cengage Learning.
(22) Beckingham, B. S.; Register, R. A. Synthesis and Phase Behavior of Block-Random Copolymers of Styrene and Hydrogenated Isoprene. *Macromolecules* **2011**, *44* (11), 4313–4319. https://doi.org/10.1021/ma200913k.
(23) Santee, E. R.; Chang, R.; Morton, M. 300 MHz Proton NMR of Polybutadiene: Measurement of Cis-Trans Isomeric Content. *Journal of Polymer Science: Polymer Letters Edition* **1973**, *11* (7), 449–452. https://doi.org/10.1002/pol.1973.130110704.
(24) Keeler, J. *Understanding NMR Spectroscopy*; John Wiley & Sons, 2011.

Chapter 5 - Low-field NMR Spectroscopy of Polymers

Reproduced in part with permission from Sneha B. Chakrapani and Bryan S. Beckingham.
Reproduced by permission of The Royal Society of Chemistry:
Chakrapani, Sneha B., Michael J. Minkler, and Bryan S. Beckingham. "Low-Field 1H-NMR Spectroscopy for Compositional Analysis of Multicomponent Polymer Systems." Analyst 144, no. 5 (2019): 1679–86. https://doi.org/10.1039/C8AN01810C.

Chapter 5.1 - Introduction

Polymeric materials are ubiquitous in our daily lives due to the breadth of material properties afforded by variation in molecular architecture, chemical microstructure and functionality. A classic and industrially important method for tuning material properties for target applications using polymeric materials is by mixing two chemically dissimilar polymers forming a polymer blend.[1–5] One such classic example is the polymerization of polystyrene or styrene-acrylonitrile copolymers in the presence of rubber to produce high impact polystyrene or ABS respectively which have greatly improved mechanical properties compared to any of the homopolymers or mechanically prepared blends.[6–8] Another example are blends of polystyrene and poly(phenylene ether), i.e. Noryl^{TM}, which possesses the high heat resistance, high dielectric strength, and hydrolytic stability attributed to PPO resin in combination with lower cost, lower glass-transition termperature (T_g), and ease of processing due to the presence of polyisoprene in the blend.[9] In the analysis of multicomponent polymer systems, such as polymer blends and statistical copolymers, the composition of the polymer blend and individual polymer chains is crucial. Typically, the composition of multicomponent polymer systems is characterized with ^{1}H Nuclear Magnetic Resonance (NMR) Spectroscopy.[10–12] ^{1}H NMR spectroscopy is particularly useful for polymer chemical structure and composition as nearly all polymers have abundant and distinct protons for analysis. Additionally, ^{1}H NMR spectroscopy yields

quantitative chemical group concentrations without prior calibration. This has led ^{1}H NMR spectroscopy to become a routine method for the molecular characterization of polymers. Over the last several decades NMR spectrometers have improved significantly, and current state-of-the-art spectrometers have increasingly high magnetic fields (i.e. Bruker Aeon 1 GHz Spectrometer).[13] It is currently common practice to refer to these high-field magnets by their corresponding magnetic field strength for hydrogen. Equations 5.1 and 5.2 show the relationship between gyromagnetic ratio (γ_n) and spectrometer field strength (B_0):

$$\frac{\gamma_n}{2\pi} = \frac{\mu_N g_n}{h} \tag{5.1}$$

$$f = \frac{\gamma_n}{2\pi} B_0 \tag{5.2}$$

where μ_N is the nuclear magneton, g_n is the g-factor for a nucleus, h is Planck's constant, f is frequency (MHz).[14] To determine the frequency of a particular NMR spectrometer, the user needs only multiply the field strength of the magnet (in Tesla) by $\gamma_n/2\pi$ or 42.577 MHz T^{-1} for hydrogen (i.e. 1 GHz spectrometer has a field strength of 23.5 T).[14] The increase in magnetic field strength has led to several orders of magnitude improvement in sensitivity.[13,15] This increase in sensitivity is typically characterized as a signal to noise ratio which is proportional to both field strength and the number of scans acquired (n); as shown in Equation 5.3 (analogous to Equation 4.2).

$$\frac{Signal}{Noise} \alpha B_0^{\frac{3}{2}} \sqrt{n} \tag{5.3}$$

Thus, spectrometers with higher field strengths require less sample and will produce spectra with significantly sharper peaks.[14] High-field—where here we denote high-field as > 5.8 T

field strength (or alternatively > 250 MHz) NMR spectrometers require cryogenic cooling due to their superconducting magnets and advanced probes as well as staffing by dedicated professionals due to the numerous, and at times very complex, NMR experiments that can be performed and the associated upkeep and maintenance requirements.[13] Unfortunately, due to the high capital and operating costs associated with high-field spectrometers, NMR spectroscopy is not commonly considered a low-cost analysis technique. This is especially true for routine materials verification such as quality control in industrial settings that commonly lack on-site advanced instrumentation facilities.

The recent development of commercially available low-field benchtop NMR spectrometers may provide a less expensive alternative to higher field, and costlier, NMR spectrometers once validated for desired analyzes.[16–18] These low-field NMR spectrometers or compact "benchtop" NMR spectrometers feature permanent magnets with typical magnetic field strengths of 20-80 MHz (0.46-1.88 T), a lower capital cost, little to no operating expense, and have a small physical footprint. As a consequence of the lower field strength these spectrometers have lower overall sensitivity and spectral dispersion.[13,15,19] For the analysis of polymers, where peaks are characteristically broader than small molecule analogs, the lower spectral dispersion exacerbates issues with resonance overlap.[19] This resonance overlap can impede quantitative analysis of polymer materials with closely situated peak signatures using 1D ^{1}H NMR spectra much more at low-field than at high-field. **Figure 5.1a** shows spectra acquired with a 60 MHz benchtop spectrometer, a 250 MHz spectrometer, and a 400 MHz spectrometer. The spectra are reasonably similar; however, the spectra produced by higher field strength spectrometers appear cleaner with less visible noise. It should be noted that all three spectra were produced with 16 scans, standard acquisition

parameters, and the data produced were processed in the same manner using MNOVA. The difference in the data is due to the frequencies at which protons are detected in each of the spectrometers. These differences can also be visualized by plotting the data in frequency space as shown in **Figure 5.1b**. This illustrates how at the expanded frequency space at higher field strength leads to improved resolution upon transformation into the same range of ppm space; i.e. the weaker the magnet, the narrower the spectrum in frequency space.

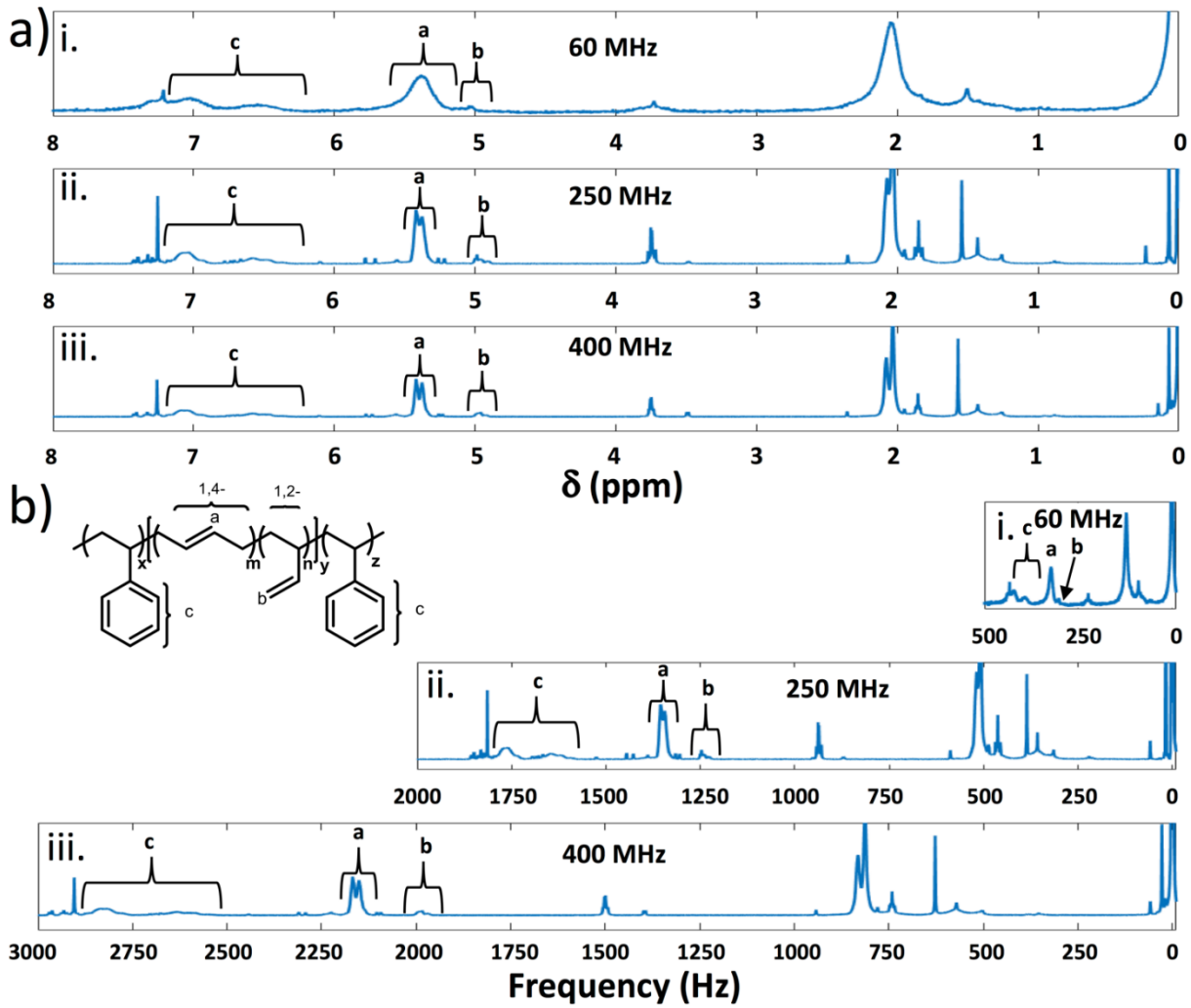

Figure 5.1 ^{1}H NMR spectra of SBS acquired with a i) 60 MHz spectrometer, ii) 250 MHz spectrometer, and iii) 400 MHz spectrometer. b) Frequency shift spectra of SBS acquired with a i) 60 MHz spectrometer, ii) 250 MHz spectrometer, and iii) 400 MHz spectrometer.

The above mentioned issues with spectra quality notwithstanding, due to a recent surge in commercial availability of these instruments there has been increased interest in the application of low-field NMR spectroscopy and efforts have been made to benchmark and validate these instruments for applications both old and new.[19–23] For instance, low-field spectrometers have recently been applied to quality control aspects of agricultural products (beef authenticity, oil adulteration, alcohol content, etc.).[23–26] For characterizing synthetic polymer materials, low-field NMR spectrometers have been applied to a variety of applications including monitoring polymerization kinetics, crystallization kinetics and crystallite/amorphous morphology, nanocomposite miscibility and dynamics, network crosslink density and swelling, composition and glass transition.[17,19,20,26–31] Low-field ^{1}H NMR spectroscopy has also been coupled with gel permeation chromatography for chemical identity mapping with molecular weight distributions.[32–34] In the analysis of multicomponent polymer systems, Singh and Blümich recently investigated the ability of a 43 MHz (1 T) compact NMR spectrometer outfitted with both ^{1}H and ^{13}C probes for quality control of styrene-butadiene rubber (SBR) production.[35] By using 1D ^{1}H and ^{13}C spectra in combination with a partial least squares regression they found they could determine the S/B relative composition and the polybutadiene microstructure quantitatively.[35] Additionally, they were able to distinguish differences within lots and across production processes and suppliers as a proof of concept of this approach for quality control in industrial SBR production.[35] However, the total acquisition time for each sample was quite long—1 minute and 5.7 hours for ^{1}H and ^{13}C spectra acquisition respectively—and a multivariate calibration model which calibrates for the prediction of composition in unknown samples from known samples.[35] These complexities may hinder application such that a faster and

model-free process would be desirable. For our primary purposes in the synthesis and characterization of various polymers, statistical copolymers and block copolymers, accurate characterization of copolymer composition and microstructure is paramount and so we set out to benchmark low-field ^{1}H NMR for composition and microstructural analysis.

Here, we investigate the utility of low-field 1D ^{1}H NMR spectroscopy as a stand-alone technique for quantitative molecular characterization of a set of polymer blends and block copolymers. In particular, we investigate (1) microstructure analysis of polyisoprene (2) compositional and polydiene microstructural analysis of commercially available poly(styrene-*b*-isoprene-*b*-styrene) (SIS) and poly(styrene-*b*-butadiene-*b*-styrene) (SBS) triblock copolymers, and (3) compositional analysis of a series of polystyrene/polyisoprene (PS/PI) and polystyrene/poly(methyl methacrylate) (PS/PMMA) polymer blends as proxies for statistical and block copolymer analysis. The ability to conduct routine analyses such as these of polymer blends and copolymers at comparatively low cost in-house has potential implications for polymer instrumentation in academic and industrial research laboratories as well as industrial implications in quality control scenarios.

5.2- Results and Discussion

In order to assess the utility of low-field benchtop spectrometers for routine applications in polymer characterization, we examined three common operations. First, we examined the characterization of polyisoprene (PI) microstructure using PI synthesized via alkyllithium-initiated anionic polymerization in cyclohexane. Next, we examined the compositional analysis and polydiene microstructural analysis of two commercially available triblock block copolymers, polystyrene-*b*-polybutadiene-*b*-polystyrene (SBS) and polystyrene-*b*-

polyisoprene-*b*-polystyrene (SIS). Lastly, we synthesized polystyrene and poly(methyl methacrylate) via free-radical polymerization and examined the composition of prepared polymer blends based on these three common polymers (PS/PI and PS/PMMA) at a range of relative compositions. In each of the above cases, we characterized the samples with ^{1}H NMR spectroscopy using both a 60 MHz and a 400 MHz spectrometer. Importantly, to prevent sample preparation, metering or other experimental errors, each prepared sample was characterized using both spectrometers in order to directly compare the results.

The results obtained from analysis of the spectra acquired at 400 MHz are taken as the "true" values and used to benchmark the performance of the 60 MHz spectrometer. In all the samples examined deuterated solvent was included in order to obtain a lock when acquiring spectra with the 400 MHz spectrometer. However, the 60 MHz spectrometer does not require a locking signal such that spectra can be obtained using standard non-deuterated chloroform or other non-deuterated solvents; a definitive cost and ease of use advantage for the 60 MHz spectrometer. However, in order to properly reference the spectra obtained at 60 MHz, TMS was included to provide for consistent spectral shift in ppm during the spectra analysis with the MestreNova Software.

5.2.1- Polyisoprene Microstructural Characterization

Polymers such as polyisoprene (PI) and polybutadiene (PB) are essentially copolymer structures due to the different modes of addition during polymerization; 1,4-, 1,2-, and 3,4-polyisoprene and 1,2- and 1,4-polybutadiene. We synthesized polyisoprene in cyclohexane using anionic polymerization to yield a high 1,4-content polyisoprene analogous to that typically present in commercially available SIS triblock copolymers. The polyisoprene product was dissolved in deuterated chloroform, doped with TMS and analyzed using ^{1}H NMR spectroscopy at both 400 MHz and 60 MHz **Figure 5.2**.

Comparing the spectra in **Figure 5.2**, clearly distinguishable peaks are observed in both with the 60 MHz spectra peaks appearing broader, less defined, with slight overlap. As mentioned above, the sharpness and contrast of the peaks is directly dependent on both field strength and the number of scans. By increasing the number of scans and thereby improving the signal-to-noise ratio (Equation 5.3), the spectra quality improves visually as shown in **Figure 5.3a**. Of interest for polyisoprene microstructural characterization are the peaks at 4.7 ppm, 5.1 ppm, and 5.7 ppm corresponding to 3,4-, 1,4- & 1,2-, and 1,2-addition respectively. Based on these peak areas, the microstructure can be determined. In both the 400 MHz and 60 MHz spectra no 1,2-PI content is observed, i.e. no peak at 5.7 ppm, as expected for the synthetic route chosen.

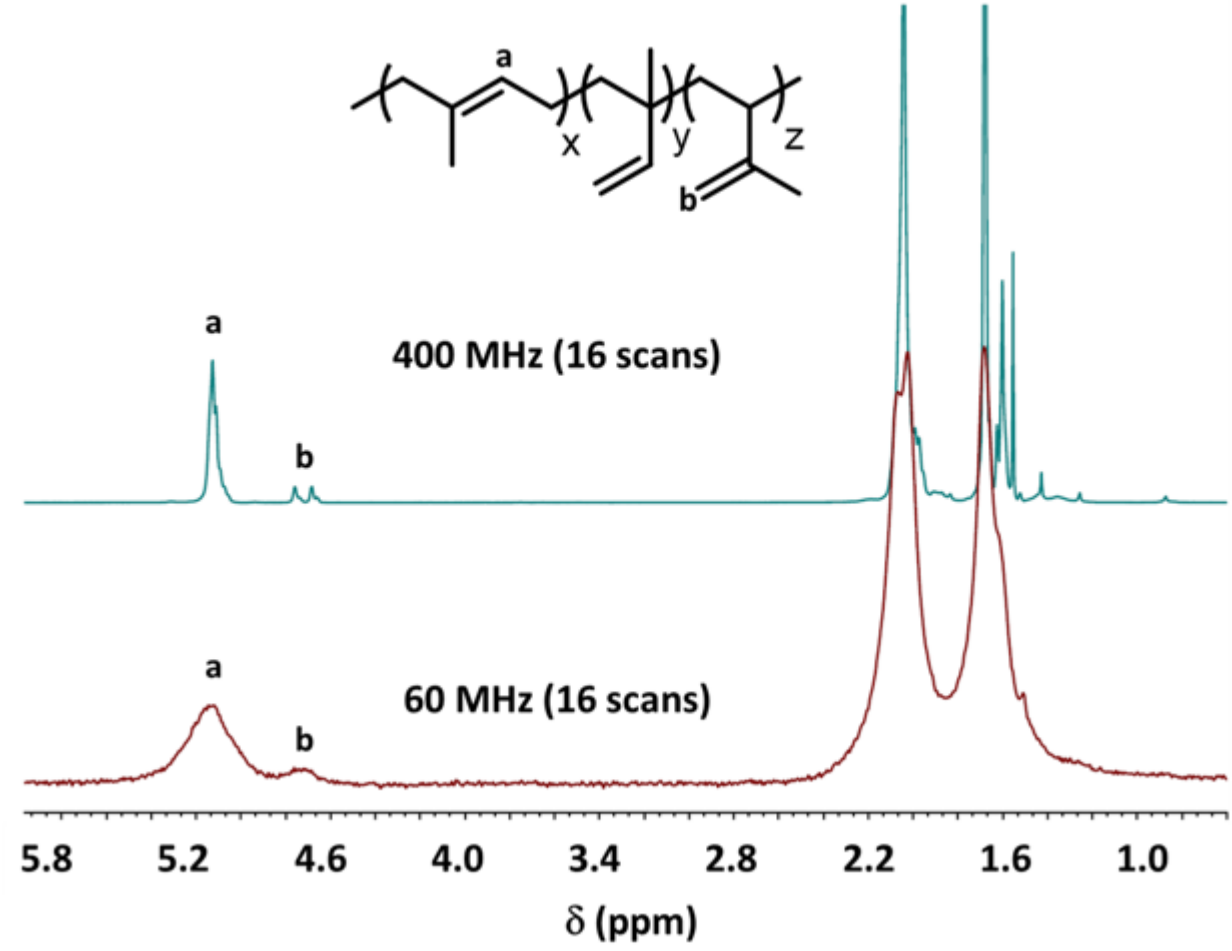

Figure 5.2 ^{1}H NMR spectrum of PI acquired at a) 400 MHz and b) 60 MHz.

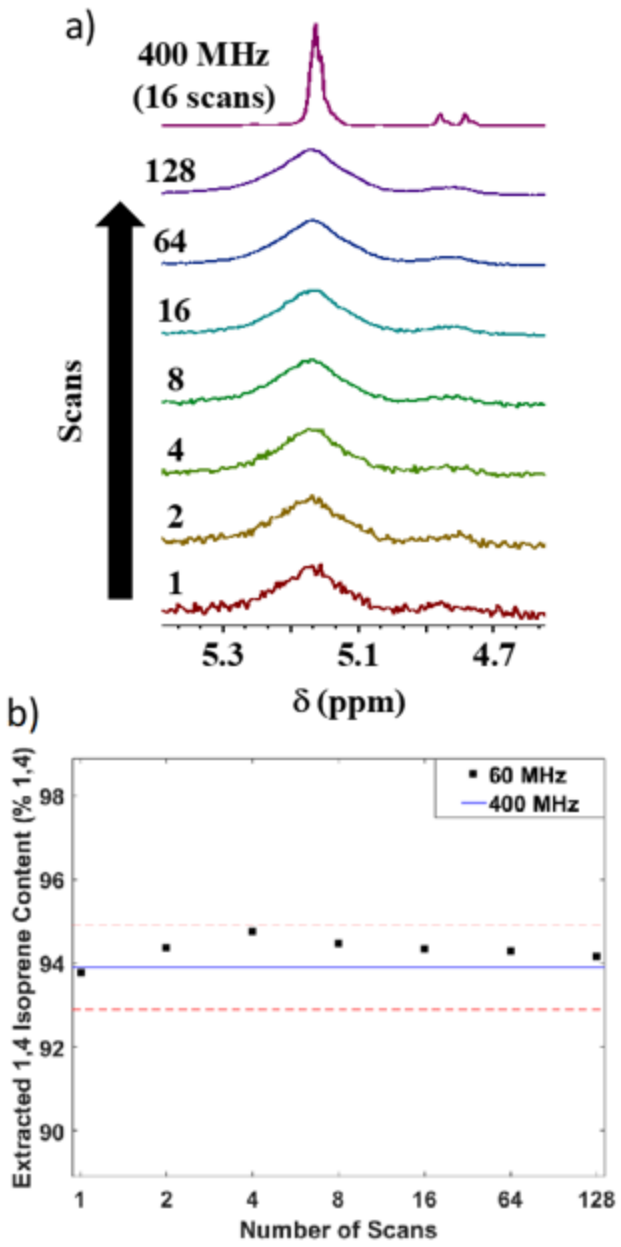

Figure 5.3. a) Polyisoprene high-field ^{1}H NMR spectrum acquired at 400 MHz (top) compared to 60 MHz spectra of varied number of scans. b) Polyisoprene microstructure (% 1,4-addition) obtained from 60 MHz spectra at varied number of scans. The solid horizontal line indicates the % 1,4-addition obtained from the 400 MHz spectrum with dotted horizontal lines indicating +/- 1 % around the 400 MHz value.

In the absence of 1,2-PI, the 1,4- and 3,4-content can be calculated directly from the peaks at 4.7 ppm and 5.1 ppm according to Equations 5.4 and 5.5, where I_i is the area of the peak at *i* ppm, yielding the results shown in **Figure 5.3b**.[10]

$$\%1,4\ (=CH-) = 100 * \frac{I_{5.1}}{I_{5.1} + \frac{I_{4.7}}{2}} \tag{5.4}$$

$$\%3,4\ (=CH_2) = 100 * \frac{\frac{I_{4.7}}{2}}{I_{5.1} + \frac{I_{4.7}}{2}} \tag{5.5}$$

As shown in **Figure 3b**, excellent agreement is obtained, within 1 %, between the 60 MHz and 400 MHz spectra. For instance, at the same number of scans as a typical high-field experiment (16 scans), we find excellent agreement between the 60 MHz (94.3 % 1,4-PI) and 400 MHz (93.9 % 1,4-PI) results. As relative polymer compositions are typically rounded to the nearest percent, 94 % 1,4-polyisoprene is extracted from both spectra. Notably, even at a single scan excellent agreement is achieved even though the spectrum is considerably noisier. Overall, we find the 60 MHz spectrometer capable of performing this characterization quantitatively as desired.

5.2.2- Symmetric Triblock Compositional Analysis

The block copolymers SBS and SIS are commercially available thermoplastic elastomers and utilized in a wide variety of applications from footwear to asphalt modification. Here, SBS and SIS triblock copolymers are purchased from Sigma Aldrich, dissolved in deuterated chloroform, and doped with TMS and ^{1}H NMR spectra were obtained at both 400 MHz and 60 MHz. Both ^{1}H NMR spectra are shown in Figure 4 for SIS while SBS is

shown in Figure 1 for SBS (see **Figure 5.5** for expanded SBS spectra analogous to **Figure 5.4**).

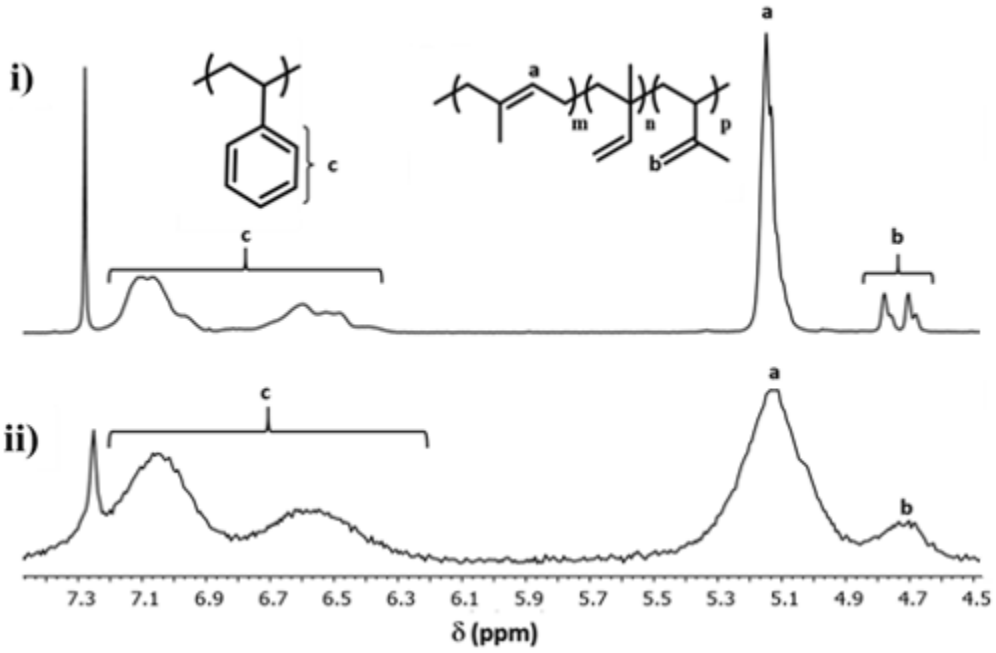

Figure 5.4. ^{1}H NMR spectra of SIS triblock copolymer at i) 400 MHz and ii) 60 MHz.

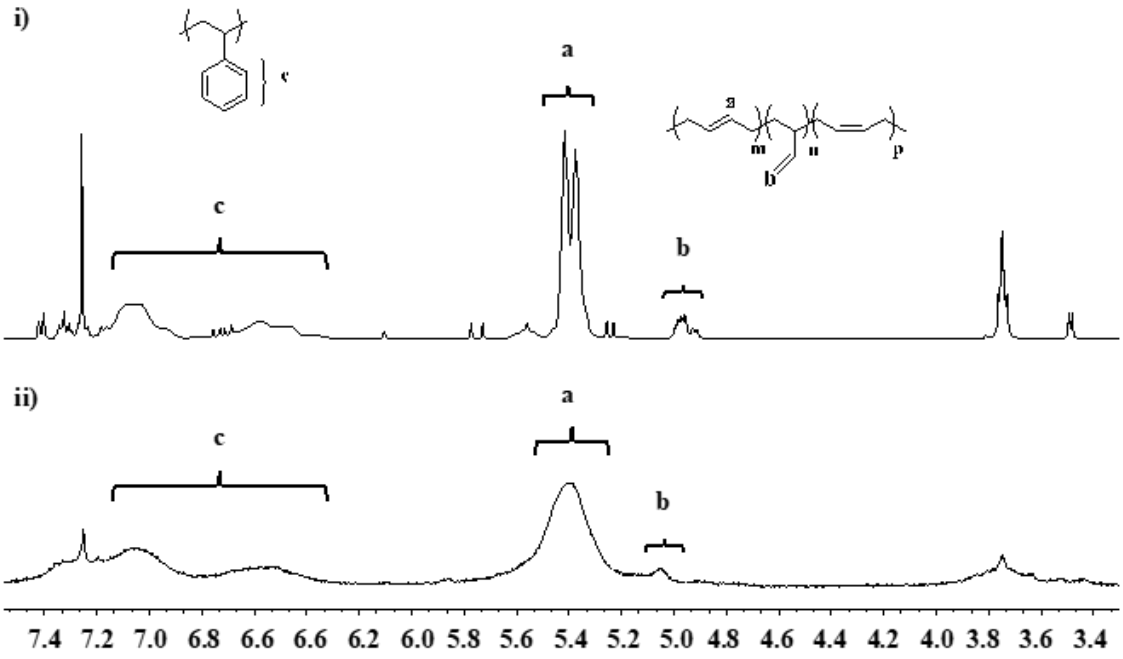

Figure 5.5. ^{1}H NMR spectra of SBS triblock copolymer at i) 400 MHz and ii) 60 MHz.

At 400 MHz clear distinct peaks are obtained, whereas at 60 MHz peaks appear broader and less defined. Both the polydiene microstructure and the relative composition of styrene and diene are extracted from the spectra. For SIS, the peak regions for the polystyrene aromatic protons (6.3-7.2 ppm) and the polyisoprene allylic protons (4.7 ppm, and 5.1 ppm) are integrated and the microstructure and composition determined for SIS using Equations 5.44-6. Analogous equations for SBS characterization are given in Equations 5.7-9.

$$\%S(in\,SIS) = 100 * \frac{\frac{I_7}{5}}{I_{5.1} + \frac{I_{4.7}}{2} + \frac{I_7}{5}} \tag{5.6}$$

$$\%S(in\,SBS) = 100 * \frac{\frac{I_7}{5}}{I_{5.4} + I_{5.6} + \frac{I_7}{5}} \tag{5.7}$$

$$\%1,2\ (=CH_2) = 100 * \frac{I_{5.6}}{I_{5.4} + I_{5.6}} \tag{5.8}$$

$$\%1,4\ (=CH-) = 100 * \frac{I_{5.4}}{I_{5.4} + I_{5.6}} \tag{5.9}$$

The spectrum acquired at 60 MHz again clearly possesses adequate capability to detect polystyrene peaks at 6.2-7.3 ppm, as well as both 1,4- and 3,4- polyisoprene configurations and no 1,2- content (5.7 ppm) is visible in either spectrum.

Using the polydiene microstructures and polystyrene content obtained at 400 MHz as the "true" value, we find excellent agreement. Both SBS and SIS are high in 1,4-content as expected for these commercial triblock copolymers, which are typically synthesized via anionic polymerization in hydrocarbon solvents. For SBS, we find a composition of 10.1 % polystyrene with 95.4 % 1,4-polybutadiene using the 400 MHz spectra, while the 60 MHz spectra yields 12.2 % styrene with 98.7 % 1,4-polybutadiene. At 400 MHz we determine the SIS to be 16.4 % polystyrene with 94.3 % 1,4-polyisoprene compared to 15.5

% polystyrene with 92.9 % 1,4-polyisoprene at 60 MHz. This is excellent agreement as, generally, the confidence in compositional analysis performed using high-field NMR spectrometers in this manner for polymers is +/- 1 %. Here, the 60 MHz results fall within this typical experimental confidence for SIS while SBS is just outside with a 2 % difference in composition.

Overall, the 60 MHz results are quantitatively the same for SIS with slight deviation for SBS. This level of accuracy at lower cost and increased accessibility could find use for quality control, research characterization and other applications and is acceptable for validating the use of these low-field instruments for this analysis.

5.2.3- Polymer Blend Compositional Analysis

To assess the utility of low-field ^{1}H NMR spectroscopy for the compositional analysis of polymer blends and other block copolymer systems, polystyrene and poly(methyl methacrylate) (PMMA) were synthesized using AIBN-initiated free-radical polymerization to complement the previously discussed PI. PS/PI and PS/PMMA mixtures were prepared gravimetrically at varied relative compositions, dissolved in deuterated chloroform to a concentration of 10-50 mg/ml as described in **Chapter 3** and their ^{1}H NMR spectra obtained at both 400 MHz and 60 MHz (see **Figure 5.7** and **Figure 5.8** for corresponding spectra). The overall polymer composition for each blend was determined analogous to the triblock copolymers using the PMMA methyl protons on the acrylate side chain (3.6 ppm) and the aforementioned polystyrene aromatic and polyisoprene allylic peaks (Equation 5.10).[36]

$$\%S(in\,PS/PMMA) = 100 * \frac{\frac{I_7}{5}}{\frac{I_{3.9}}{3} + \frac{I_7}{5}} \tag{5.10}$$

Compositions determined using the spectra obtained with the 60 MHz spectrometer are plotted against those obtained from the 400 MHz spectrometer for both PS/PS and PS/PMMA; **Figure 5.6a** and **Figure 5.6b** respectively (see **Table 5.1** Composition extracted from analysis of each spectra for both PS/PI and PS/PMMA blends.for the composition values and **Figure 5.7**-**Figure 5.8** for the spectra used to construct **Figure 5.6**). We find excellent agreement between the 400 MHz and 60 MHz results for both PS/PI and PS/PMMA blends as nearly all points in **Figure 5.6** lie along the identity line. For five of the nine PS/PI blends the compositions obtained using the 60 MHz spectra are equivalent to those from the 400 MHz spectra, after rounding to the nearest percent, with the remaining 4 differing by only 1 %. Similarly, for PS/PMMA blends equivalent results are found for four of the nine blends, four differ by 1 % and one differs by 2 %. Overall, the average difference between the extracted compositions at 60 MHz and 400 MHz is 0.48 % for PS/PI blends and 0.66 % percent for PS/PMMA blends. These findings demonstrate the utility of low-field spectrometers for the quantitative determination of relative composition in these polymer blends.

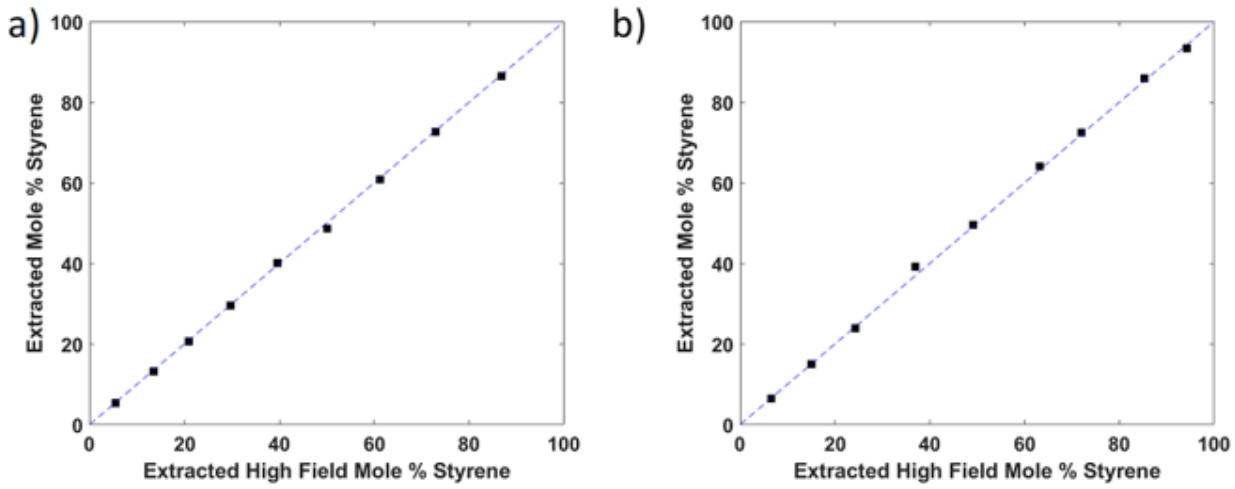

Figure 5.6. Extracted composition values from 60 MHz spectra plotted against values extracted from 400 MHz spectra for polymer blends of a) polystyrene and polyisoprene and b) polystyrene and poly(methyl methacrylate). Dashed line represents the identity line; y = x.

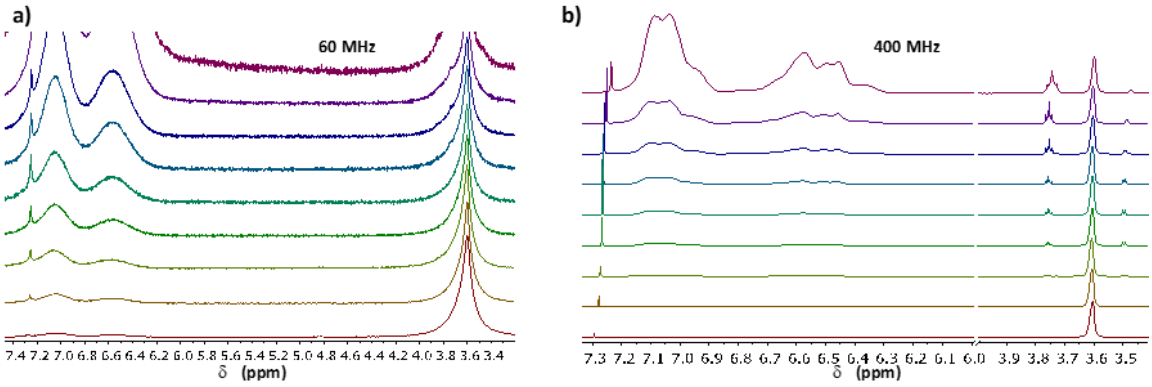

Figure 5.7. [1]H NMR spectra of PS/PI polymer blends at varied relative composition at a) 60 MHz and b) 400 MHz.

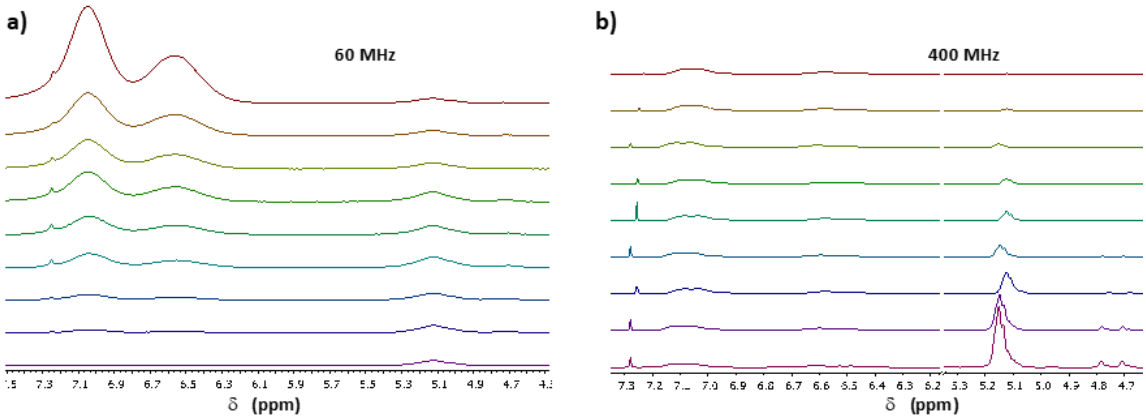

Figure 5.8. [1]H NMR spectra of PS/PMMA polymer blends at varied relative composition at a) 400 MHz and b) 60 MHz.

Table 5.1 Composition extracted from analysis of each spectra for both PS/PI and PS/PMMA blends.

Sample	Frequency (MHz)	Mole % Polystyrene	Sample	Frequency (MHz)	Mole % Polystyrene
PSPI-6	60	5.4	**PSPMMA-7**	60	6.5
	400	5.6		400	6.6
PSPI-14	60	13.2	**PSPMMA-15**	60	15.0
	400	13.5		400	15.1
PSPI-21	60	20.6	**PSPMMA-24**	60	23.9
	400	20.9		400	24.3
PSPI-30	60	29.6	**PSPMMA-37**	60	39.2
	400	29.7		400	37.0
PSPI-40	60	40.0	**PSPMMA-50**	60	49.4
	400	39.6		400	49.1
PSPI-50	60	48.6	**PSPMMA-64**	60	64.1
	400	50.2		400	63.2
PSPI-61	60	60.7	**PSPMMA-72**	60	72.4
	400	61.2		400	72.0
PSPI-73	60	72.6	**PSPMMA-85**	60	86.0
	400	72.9		400	85.2
PSPI-87	60	86.4	**PSPMMA-94**	60	93.4
	400	86.8		400	94.2

5.3- Conclusions

^{1}H NMR spectroscopy is a powerful tool for the characterization of polymer structures and the relative compositions of repeat unit structures within multicomponent polymer systems. In this work we assessed the potential of a low-field spectrometer (60 MHz) to perform routine polymer characterizations; polydiene microstructure, triblock copolymer composition and polymer blend compositional analysis. While the 60 MHz spectrometer is less sensitive, with broader peaks due to the narrower frequency of acquisition, the acquired spectra possess distinct peaks containing the requisite relative concentration information for performing the desired compositional analysis. Five different polymer systems were analyzed and the results obtained using a 60 MHz spectrometer and a 400 MHz spectrometer were compared. A majority of results obtained for each sample using both spectrometers are within the typical experimental error anticipated for high-field spectrometers (+/- 1 %). Extracted compositions are within 3 % in all cases with a majority (26/31 or 84%) within 1 %. These results validate the use of 60 MHz ^{1}H NMR spectrometers for the polymer systems analyzed here. However, we note that additional systems of interest should be similarly validated before application of these instruments for quantitative analyses. Overall, ^{1}H NMR spectroscopy at low-field strength is a promising tool for the routine characterization of multicomponent polymer systems.

5.4- References

(1) Krishnamoorti, R.; Graessley, W. W.; Dee, G. T.; Walsh, D. J.; Fetters, L. J.; Lohse, D. J. Pure Component Properties and Mixing Behavior in Polyolefin Blends. *Macromolecules* **1996**, *29* (1), 367–376. https://doi.org/10.1021/ma950754b.

(2) Wu, S. Phase Structure and Adhesion in Polymer Blends: A Criterion for Rubber Toughening. *Polymer* **1985**, *26* (12), 1855–1863. https://doi.org/10.1016/0032-3861(85)90015-1.

(3) Coleman, M. M.; Painter, P. C. Hydrogen Bonded Polymer Blends. *Progress in Polymer Science* **1995**, *20* (1), 1–59. https://doi.org/10.1016/0079-6700(94)00038-4.

(4) Barlow, J. W.; Paul, D. R. Polymer Blends and Alloys—a Review of Selected Considerations. *Polymer Engineering & Science* **1981**, *21* (15), 985–996. https://doi.org/10.1002/pen.760211502.

(5) *Polymer Blends Handbook*, 2nd ed.; Utracki, L. A., Wilkie, C., Eds.; Springer Netherlands, 2014.

(6) Fryling, C. F. High Impact Polystyrene. US3144420A, August 11, 1964.

(7) Gilbert, D. G.; Donald, A. M. Toughening Mechanisms in High Impact Polystyrene. *J Mater Sci* **1986**, *21* (5), 1819–1823. https://doi.org/10.1007/BF01114745.

(8) Hobbs, S. Y. The Effect of Rubber Particle Size on the Impact Properties of High Impact Polystyrene (HIPS) Blends. *Polymer Engineering & Science* **1986**, *26* (1), 74–81. https://doi.org/10.1002/pen.760260112.

(9) Hay, A. S. Polymerization by Oxidative Coupling: Discovery and Commercialization of PPO® and Noryl® Resins. *Journal of Polymer Science Part A: Polymer Chemistry* **1998**, *36* (4), 505–517. https://doi.org/10.1002/(SICI)1099-0518(199803)36:4<505::AID-POLA1>3.0.CO;2-O.

(10) Tanaka, Y.; Takeuchi, Y.; Kobayashi, M.; Tadokoro, H. Characterization of Diene Polymers. I. Infrared and NMR Studies: Nonadditive Behavior of Characteristic Infrared Bands. *Journal of Polymer Science Part A-2: Polymer Physics* **1971**, *9* (1), 43–57. https://doi.org/10.1002/pol.1971.160090104.

(11) Stuart, B. H. *Polymer Analysis*; John Wiley & Sons, 2008.

(12) Santee, E. R.; Chang, R.; Morton, M. 300 MHz Proton NMR of Polybutadiene: Measurement of Cis-Trans Isomeric Content. *Journal of Polymer Science: Polymer Letters Edition* **1973**, *11* (7), 449–452. https://doi.org/10.1002/pol.1973.130110704.

(13) Kovacs, H.; Moskau, D.; Spraul, M. Cryogenically Cooled Probes—a Leap in NMR Technology. *Progress in Nuclear Magnetic Resonance Spectroscopy* **2005**, *46* (2), 131–155. https://doi.org/10.1016/j.pnmrs.2005.03.001.

(14) Günther, H. *NMR Spectroscopy: Basic Principles, Concepts and Applications in Chemistry*; John Wiley & Sons, 2013.

(15) Spiess, H. W. 50th Anniversary Perspective: The Importance of NMR Spectroscopy to Macromolecular Science. *Macromolecules* **2017**, *50* (5), 1761–1777. https://doi.org/10.1021/acs.macromol.6b02736.

(16) Blümich, B. Introduction to Compact NMR: A Review of Methods. *TrAC Trends in Analytical Chemistry* **2016**, *83*, 2–11. https://doi.org/10.1016/j.trac.2015.12.012.

(17) Adams, A. Analysis of Solid Technical Polymers by Compact NMR. *TrAC Trends in Analytical Chemistry* **2016**, *83*, 107–119. https://doi.org/10.1016/j.trac.2016.04.003.

(18) Donaldson, M.; Freed, D.; Mandal, S.; Song, Y.-Q. Chemical Analysis Using Low-Field Magnetic Resonance. *TrAC Trends in Analytical Chemistry* **2016**, *83*, 84–93. https://doi.org/10.1016/j.trac.2016.03.008.
(19) Nordon, A.; Gemperline, P. J.; McGill, C. A.; Littlejohn, D. Quantitative Analysis of Low-Field NMR Signals in the Time Domain. *Anal. Chem.* **2001**, *73* (17), 4286–4294. https://doi.org/10.1021/ac0102866.
(20) Hertlein, C.; Saalwächter, K.; Strobl, G. Low-Field NMR Studies of Polymer Crystallization Kinetics: Changes in the Melt Dynamics. *Polymer* **2006**, *47* (20), 7216–7221. https://doi.org/10.1016/j.polymer.2006.03.117.
(21) Eccles, C. Low Field NMR Methods and Applications. In *Encyclopedia of Spectroscopy and Spectrometry (Second Edition)*; Lindon, J. C., Ed.; Academic Press: Oxford, 2010; pp 1357–1371. https://doi.org/10.1016/B978-0-12-374413-5.00018-X.
(22) Dalitz, F.; Cudaj, M.; Maiwald, M.; Guthausen, G. Process and Reaction Monitoring by Low-Field NMR Spectroscopy. *Progress in Nuclear Magnetic Resonance Spectroscopy* **2012**, *60*, 52–70. https://doi.org/10.1016/j.pnmrs.2011.11.003.
(23) Parker, T.; Limer, E.; Watson, A. D.; Defernez, M.; Williamson, D.; Kemsley, E. K. 60 MHz 1H NMR Spectroscopy for the Analysis of Edible Oils. *Trends Analyt Chem* **2014**, *57* (100), 147–158. https://doi.org/10.1016/j.trac.2014.02.006.
(24) Isaac-Lam, M. F. Determination of Alcohol Content in Alcoholic Beverages Using 45 MHz Benchtop NMR Spectrometer https://www.hindawi.com/journals/ijs/2016/2526946/ (accessed Sep 30, 2019). https://doi.org/10.1155/2016/2526946.
(25) Jakes, W.; Gerdova, A.; Defernez, M.; Watson, A. D.; McCallum, C.; Limer, E.; Colquhoun, I. J.; Williamson, D. C.; Kemsley, E. K. Authentication of Beef versus Horse Meat Using 60MHz 1H NMR Spectroscopy. *Food Chemistry* **2015**, *175*, 1–9. https://doi.org/10.1016/j.foodchem.2014.11.110.
(26) Ruan, R. R.; Long, Z.; Song, A.; Chen, P. L. Determination of the Glass Transition Temperature of Food Polymers Using Low Field NMR. *LWT - Food Science and Technology* **1998**, *31* (6), 516–521. https://doi.org/10.1006/fstl.1998.0409.
(27) Elipe, M. V. S.; Milburn, R. R. Monitoring Chemical Reactions by Low-Field Benchtop NMR at 45 MHz: Pros and Cons. *Magnetic Resonance in Chemistry* **2016**, *54* (6), 437–443. https://doi.org/10.1002/mrc.4189.
(28) Pedroza, O. J. O.; Tavares, M. I. B.; Preto, M. The Use of Spin-Lattice Relaxation Time in the Investigation of Polystyrene/Acrylic Acid Copolymerization. *Polymer Testing* **2006**, *25* (2), 246–248. https://doi.org/10.1016/j.polymertesting.2005.10.003.
(29) Preto, M.; Tavares, M. I. B.; Silva, E. P. da. Low-Field NMR Study of Nylon 6/Silica Composites. *Polymer Testing* **2007**, *26* (4), 501–504. https://doi.org/10.1016/j.polymertesting.2007.01.009.
(30) Papon, A.; Saalwächter, K.; Schäler, K.; Guy, L.; Lequeux, F.; Montes, H. Low-Field NMR Investigations of Nanocomposites: Polymer Dynamics and Network Effects. *Macromolecules* **2011**, *44* (4), 913–922. https://doi.org/10.1021/ma102486x.
(31) Patel, J. P.; Hsu, S. L. Development of Low Field NMR Technique for Analyzing Segmental Mobility of Crosslinked Polymers. *Journal of Polymer Science Part B: Polymer Physics* **2018**, *56* (8), 639–643. https://doi.org/10.1002/polb.24583.
(32) Cudaj, M.; Guthausen, G.; Hofe, T.; Wilhelm, M. Online Coupling of Size-Exclusion Chromatography and Low-Field 1H NMR Spectroscopy. *Macromolecular Chemistry and Physics* **2012**, *213* (18), 1933–1943. https://doi.org/10.1002/macp.201200290.

(33) Cudaj, M.; Guthausen, G.; Hofe, T.; Wilhelm, M. SEC-MR-NMR: Online Coupling of Size Exclusion Chromatography and Medium Resolution NMR Spectroscopy. *Macromolecular Rapid Communications* **2011**, *32* (8), 665–670. https://doi.org/10.1002/marc.201000760.
(34) Höpfner, J.; Ratzsch, K.-F.; Botha, C.; Wilhelm, M. Medium Resolution 1H-NMR at 62 MHz as a New Chemically Sensitive Online Detector for Size-Exclusion Chromatography (SEC–NMR). *Macromolecular Rapid Communications* **2018**, *39* (7), 1700766. https://doi.org/10.1002/marc.201700766.
(35) Singh, K.; Blümich, B. Compact Low-Field NMR Spectroscopy and Chemometrics: A Tool Box for Quality Control of Raw Rubber. *Polymer* **2018**, *141*, 154–165. https://doi.org/10.1016/j.polymer.2018.02.057.

Chapter 6 - Statistical Copolymer of 3-hexylthiophene and Thiophene

Reproduced in part with permission from Bryan S. Beckingham.
Reproduced by permission of Materials Communications Today:
"Minkler, Michael J., and Bryan S. Beckingham. "Statistical Copolymers of 3-Hexylthiophene and Thiophene: Impact of Thiophene Content on Optoelectronic and Thermal Properties." Materials Today Communications, June 18, 2019, 100547. https://doi.org/10.1016/j.mtcomm.2019.100547."

6.1 – Introduction

Conjugated polymers have attracted extensive attention as functional materials for use in organic electronic devices. Due to their well-controlled and tolerant synthesis by Grignard Metathesis (GRIM) polymerization, substituted polythiophenes present abundant opportunities to alter their properties via a variety of other substitutions to the 3-position of the aromatic thiophene ring.[1–5] Many substituent groups such as hydrocarbons of varying lengths or alkoxy groups with higher electron affinities, which impact thermal and optoelectronic properties, have been employed.[3–5] Poly(3-alkylthiophenes) (P3ATs) where an alkyl chain of various lengths have been incorporated at the three position are a commonly-studied family of conjugated polymers for organic electronics (in thin-film transistors, chemical sensors, thermoelectric generators, and bulk-heterojunction solar panels).[1–5] Poly(3-hexylthiophene) (P3HT) is the most prominent and widely-studied member of this group for application in both high-performance organic field-effect transistors and organic photovoltaics.[6–11] Importantly, side chain chemistry plays a crucial role in setting material characteristics of substituted polythiophenes such as crystal packing, solubility, and charge transport.[1–8] For instance, while the melting temperature of P3HT is close to its thermal degradation temperature, the melting transitions of P3ATs can be lowered with longer (such as dodecyl) or bulkier (such as 2-ethyl-hexyl) side-chain groups.[3,6,11] This lower melting transition has proven valuable for controlling the nanoscale morphology in block copolymers while also providing useful route for studying structure-property relationships in P3ATs.[12–19]

While the polymerization of thiophenes via Grignard Metathesis is well controlled, there are still many facets of this method that are not well understood and do not translate between various thiophene derivatives. Given the potential for enhanced charge transport of unsubstituted thiophene-containing polymers, block copolymers consisting of a solubilizing 3-substituted thiophene and unsubstituted thiophene have been synthesized to take advantage of the potential enhanced charge transport properties.[19–21] Statistical copolymers consisting of more than one type of thiophene repeat unit have also been investigated as a route to varying thermal and optoelectronic properties.[4–6,22–26] Statistical ranges of copolymers consisting of 3HT and other 3-alkyl-substituted, 3-alkoxy substituted or unsubstituted thiophene have been synthesized by varying the relative molar amounts of the monomers in the GRIM polymerization method.[11,21,23,25–30] For instance, Ho et al. synthesized a range of statistical copolymers of 3-hexylthiophene (3HT) and 3-(2'-ethylhexylthiophene) (3EHT) and observed a smooth transition from the melting temperature of poly(3-hexylthiophene) (P3HT) to that of poly(3-(2'-ethylhexyl)thiophene) (P3EHT) while optoelectronic properties tracked with those of the majority comonomer.[6] Conversely, Wu et al. synthesized statistical copolymers containing 3-butylthiophene and 3-octylthiophene and observed very different behavior.[22] Instead of a smooth transition from the melting temperature of poly(3-butylthiophene) (P3BT) to poly(3-octylthiophene) (P3OT), they observed melting transitions that behaved more like the dominant comonomer.[22] In both these cases, the thermal and optoelectronic behavior of the resulting copolymers is closely tied to the copolymer chemistries and comonomer compositions illustrating the potential utility of copolymerization strategies for tailoring the thermal and optoelectronic properties of conjugated polymers such as polythiophenes.[6,22] Polythiophene itself has potentially promising electronic properties such as high charge carrier mobility, however, suffers from insolubility beyond

oligomers (6 repeat units).[27] This lack of solubility of polythiophene has in many aspects driven the synthesis of 3-substituted thiophenes in order to improve solubility by incorporation of alkyl and other side-chains. However, copolymers containing unsubstituted thiophene remain relatively unexplored, and so the literature pertaining to statistical thiophene-based copolymers is almost wholly concerning 3-substituted thiophenes.[6,11,22,26,29,30]

Recently, the incorporation of thiophene units into copolymers with 3-hexylthiophene has been investigated by two groups and were found to have improved charge carrier transport properties and increased toughness compared to P3HT copolymer.[21,25] Unfortunately, across both studies only a few copolymers (5) were synthesized over a relatively narrow compositional range; 79-49 mol % P3HT.[21,25] Herein, we synthesize nine copolymers of 3-hexylthiophene with unsubstituted thiophene using a modified GRIM procedure over a broader compositional range (44-95 % P3HT). Synthesized poly(3-hexylthiophene-*co*-thiophene) copolymers are fully characterized for their macromolecular structure by GPC and ^{1}H NMR spectroscopy and their thermal and optoelectronic properties examined using differential scanning calorimetry and UV-Vis spectroscopy.

Placing our results in the context of the limited previous studies of P3HT/PT statistical copolymers, we observe similar behavior with regards to an apparent increase in copolymer dispersity with increased thiophene content, analogous thermal behavior with composition and our absorption data agree with the results of Son et al., where a cluster of optical bands with an initial blue shift followed by a red shift with increasing unsubstituted thiophene content.[23,27,28] However, in comparison with traditional copolymers of 3-substituted thiophenes we observe more complex thermal and optical behavior due to the lack of steric control during copolymerization.

6.2 - Results and Discussion

6.2.1 - Synthesis and Macromolecular Characterization

A series of copolymers of 3-hexylthiophene and unsubstituted thiophene copolymers were synthesized using the Grignard Metathesis (GRIM) polymerization route developed by McCullough and coworkers by varying the initial monomer ratio (3HT:T).[1,2] Molecular characteristics of the synthesized copolymers are given in **Table 6.1** (denoted P3HT:PT-X where X is the molar content of 3HT in the copolymer). Analysis by gel permeation chromatography (GPC) yielded polystyrene equivalent molecular weights and confirmed fairly consistent and relatively low dispersity ($Đ$ < 1.76) for each of the synthesized copolymers. Composition, and overall regioregularity were determined by ^{1}H NMR spectroscopy. Copolymer compositions were determined using the relative areas of the peaks of the aromatic protons (δ:6.96-7.02 ppm for 3-hexylthiophene units and δ:7.03-7.20 ppm for thiophene units). Lastly, overall chain regioregularity was determined by analysis of the α-carbon proton region of the ^{1}H NMR spectrum through the peak attributed to regioregular (δ, 2.8 ppm) and non-regioregular (δ, 2.6 ppm) sequences.[1,2,27]

As was also observed by Smith et al, following Soxhlet extraction, an insoluble phase of polymer was left behind in the thimble.[23] The fraction of polymer that was able to be extracted demonstrated little to no effect on solubility until approximately 40 mol percent 3-hexylthiophene. Additionally, we observe a general increase in the dispersity of the copolymers as compared to P3HT, suggesting a difference in monomer reactivity ratios; a topic to be considered elsewhere.[23,27,28]

An important facet of polythiophene chemistry is the microstructure and, in particular, the regiochemistry of the polymer repeat units along the backbone. Regiochemistry is determined by the intermediates formed during GRIM polymerization as shown in **Scheme 6.1**. As shown in **Scheme 6.1a**, unsubstituted thiophene has two sterically unhindered reaction sites compared to a

single unhindered reaction site for 3-hexylthiophene which leads to the synthesis of highly regioregular P3HT as demonstrated in the literature.[1,2,27,28]

Previously shown by McCullough, P3HT microstructure can consist of four different triads depending on how units are incorporated into the polymer chain; **Figure 6.1**.[1,2] However, copolymerization of 3-hexylthiophene with thiophene complicates this backbone regiochemistry as upon addition of thiophene units, eight more triads are possible. These additional microstructural sequences are readily apparent in the ^{1}H NMR spectra (δ, 2.6-2.75 ppm), where additional peaks and shoulders are observed and clearly impacts polymer regioregularities extracted using an approach analogous to that used for P3HT or copolymers of 3-subsituted thiophene monomers.[27] Examining these potential triad structures, there are five additional triad sequence possibilities and thereby additional signals in the ^{1}H NMR spectra as shown in Figure 1b; HT-HT (one configuration), TH-TT (four configurations), TT-HH (two configurations), HH-TH (one configuration), HT-TH (one configuration), and TT-TT (three configurations).

This additional complexity is readily apparent in the ^{1}H NMR spectra shown in Figure 2, where upon increasing addition of unsubstituted thiophene, additional peaks are observed in the aliphatic portion of the spectrum (δ, 2.5-2.65 ppm). This assignment is used in determining the overall regioregularity (**Figure 6.2b**). Overall, the amount of non-regioregular content increases as the amount of thiophene comonomer included increases as reflected in Figure 2b. This change in regioregularity will, as has been shown for P3HT, have an impact on the crystallite formation, packing and thermal behavior of these copolymers as discussed below. Additionally, we note that the regioregularity reported in **Table 6.1** and **Figure 6.2b** is a quantification of *local* sequence regioregularity and does not consider the potential for down-chain changes in orientation of regioregular sequences due to the presence of unsubstituted thiophene units. Additionally, as

previously shown, the presence of two or more chemically similar thiophene units disallows the facile calculation of absolute molecular weight from ^{1}H NMR spectroscopy.[27]

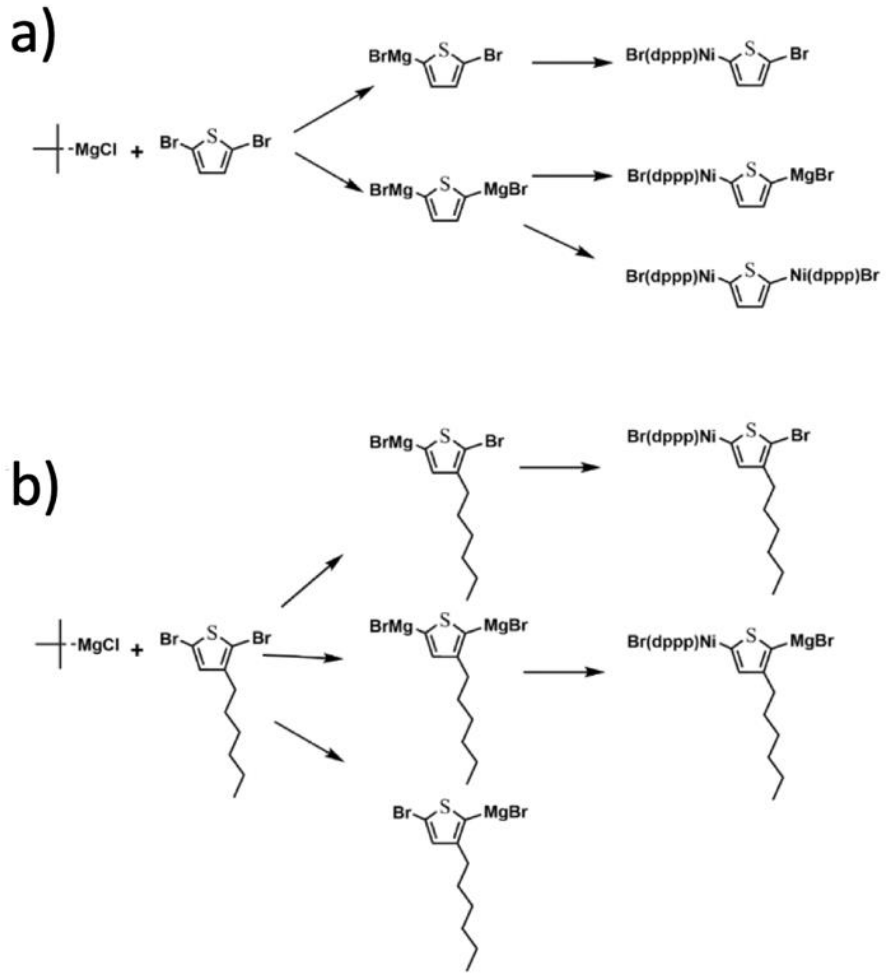

Scheme 6.1 a) Potential monomer addition routes for unsubstituted thiophene via GRIM polymerization. b) GRIM polymerization of 3-hexylthiophene as discussed by McCullough et al.[1,2]

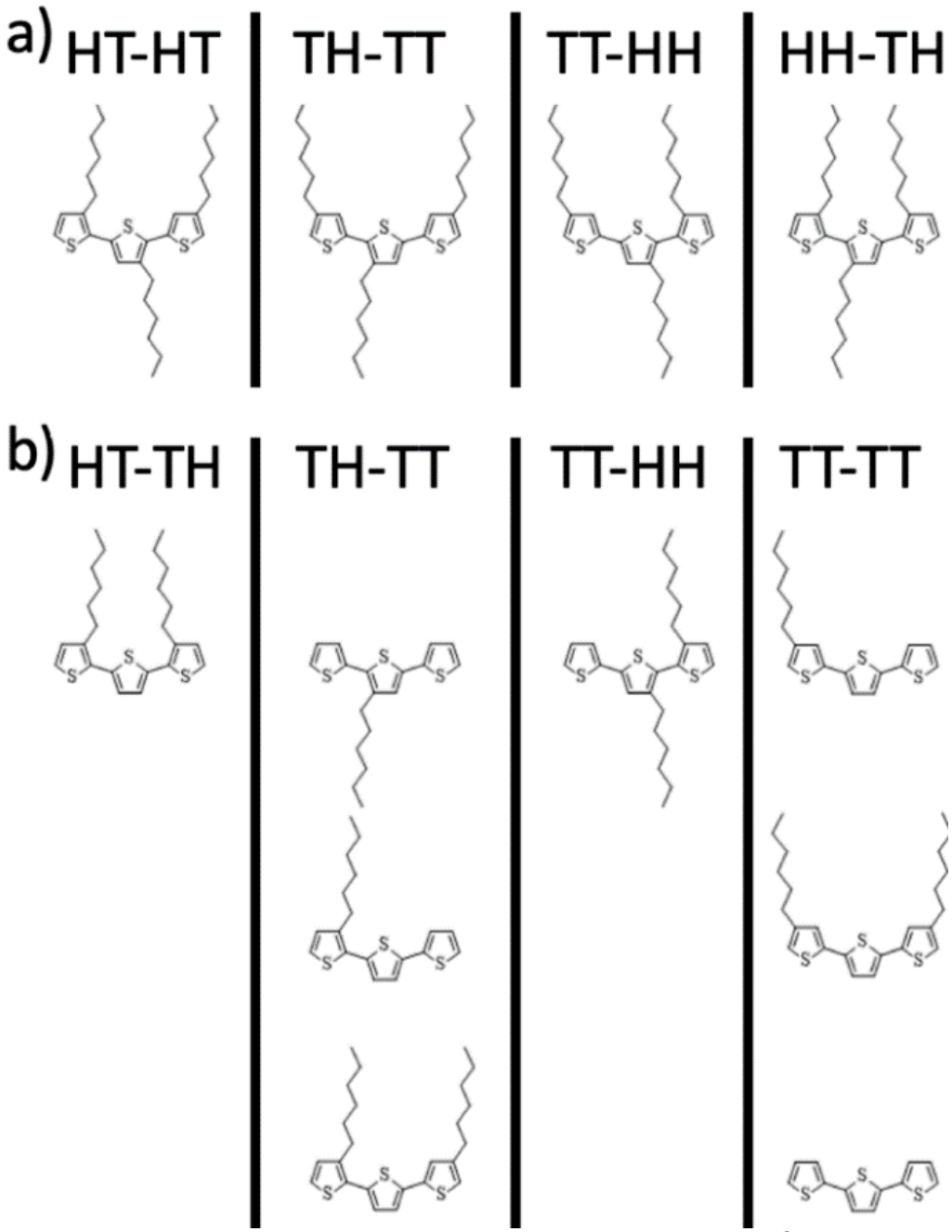

Figure 6.1 a) Possible triads of P3HT as shown by McCullough et al.[1,2,23] and b) Possible triad configurations of P3HT-co-PT statistical copolymers.

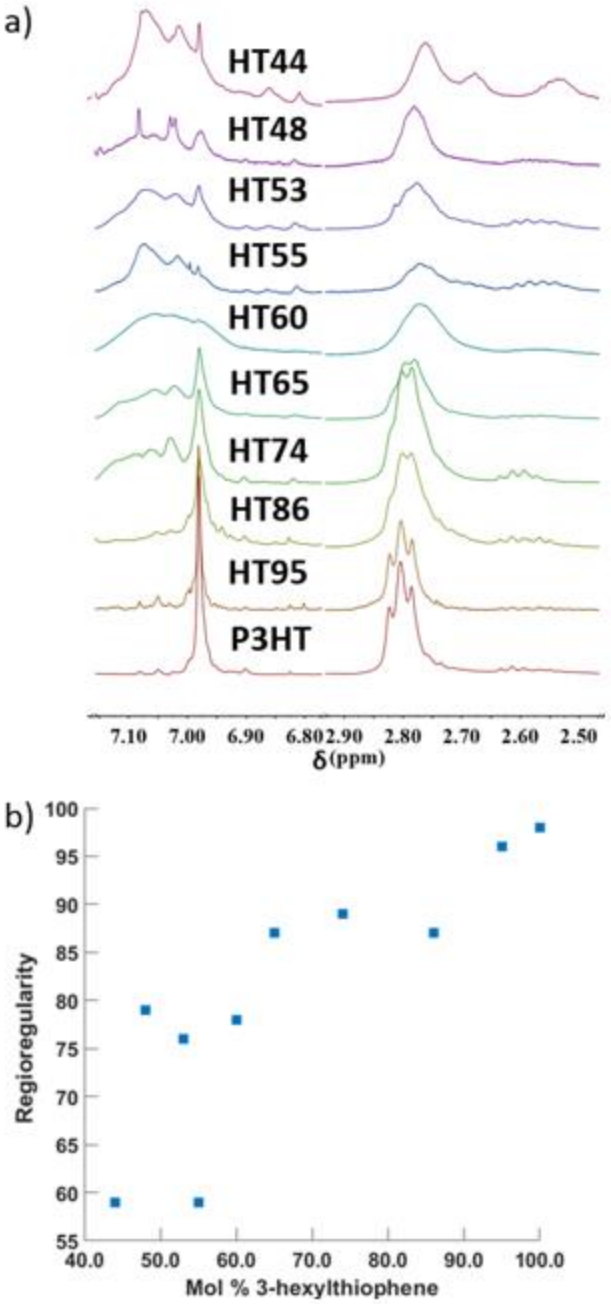

Figure 6.2 a) 1H NMR spectra of the synthesized statistical poly(3-hexylthiophene-co-thiophene) copolymers. The copolymers are denoted here listing only their molar 3-hexylthiophene content; where HTXX denotes the molar content of P3HT and b) calculated regioregularity.

6.2.2 - Thermal Behavior

The thermal behavior of the synthesized P3HT-*co*-PT copolymers was investigated with differential scanning calorimetry (DSC). Copolymers were first heated to 200-250 °C before quenching to 0 °C and isothermal crystallization for 15 hours. After isothermal crystallization, copolymers were subsequently ramped to 200-250 °C at a rate of 10 °C/min and the resulting DSC traces examined. Copolymer melting temperatures (Tm), calculated as the temperature at the inflection point of the dH/dT thermogram curve, were extracted and are shown in **Table 6.1** and **Figure 6.3**; see **Figure 6.4** and **Figure 6.5** for DSC thermograms and **Table 6.1** for melting enthalpies (via peak integration). The obtained melting temperature of P3HT is consistent with literature values while the obtained copolymer melting temperatures are consistently lower.[17] The copolymers exhibit an initial drop in T_m from that of P3HT with increasing unsubstituted thiophene content. This depression in melting temperature is likely due to the decrease in overall chain regioregularity and the presence of unsubstituted thiophene defects disrupting the P3HT crystallites. Analogous behavior is also observed at the other end of the composition window as the melting temperature increases as the composition approaches polythiophene homopolymer. It should be noted that the P3HT:PT-44 has a relatively low melting temperature, we attribute this to its comparatively lower molecular weight as compared to the other synthesized polymer. Due to the complex nature of the aforementioned copolymerization, direct comparisons between our values presented here and those presented by previous groups should be lightly drawn as compositions, dispersity and synthesis methods vary slightly.[23,27,28] However, we find good overall agreement between our molar content and thermal data presented in the two previous studies.

Table 6.1 Molecular and Thermal Characteristics of Poly(3-hexylthiophene-co-thiophene) copolymers.

Polymer	M_n (kg/mol)[b]	Đ[b]	Regioregularity[c] (%)	T_m (°C)[d]	ΔH (J/g)[e]
P3HT	8.7	1.13	98	223	24.6
P3HT:PT-95	7.6	1.29	96	179	11.1
P3HT:PT-86	21.8	1.29	87	106	12.0
P3HT:PT-74	7.1	1.48	89	134	2.29
P3HT:PT-65	12.9	1.56	87	112	15.1
P3HT:PT-60	32.0	1.38	78	139	4.72
P3HT:PT-55	16.9	1.38	59	164	0.70
P3HT:PT-53	6.5	1.68	76	196	1.82
P3HT:PT-48	5.0	1.53	79	145	1.23
P3HT:PT-44	1.8	1.56	59	97	6.52
P3HT:PT-30*	Insoluble	Insoluble	Insoluble	199	11.02
P3HT:PT-20*	Insoluble	Insoluble	Insoluble	192	4.04
P3HT:PT-10*	Insoluble	Insoluble	Insoluble	230	0.109

[a]P3HT:PT-*X* indicates the molar content of 3HT of the copolymer as calculated by ^{1}H-NMR spectroscopy.
*P3HT:PT-X indicates the molar content of 3HT of the initial reaction media.
[b]As determined by GPC in polystyrene equivalents; GPC traces shown in Figure 6.6 and Figure 6.7.
[c]As determined by ^{1}H NMR spectroscopy.
[d]Peak temperature of endothermic peak.
[e]Integrated area of the observed endothermic peak.

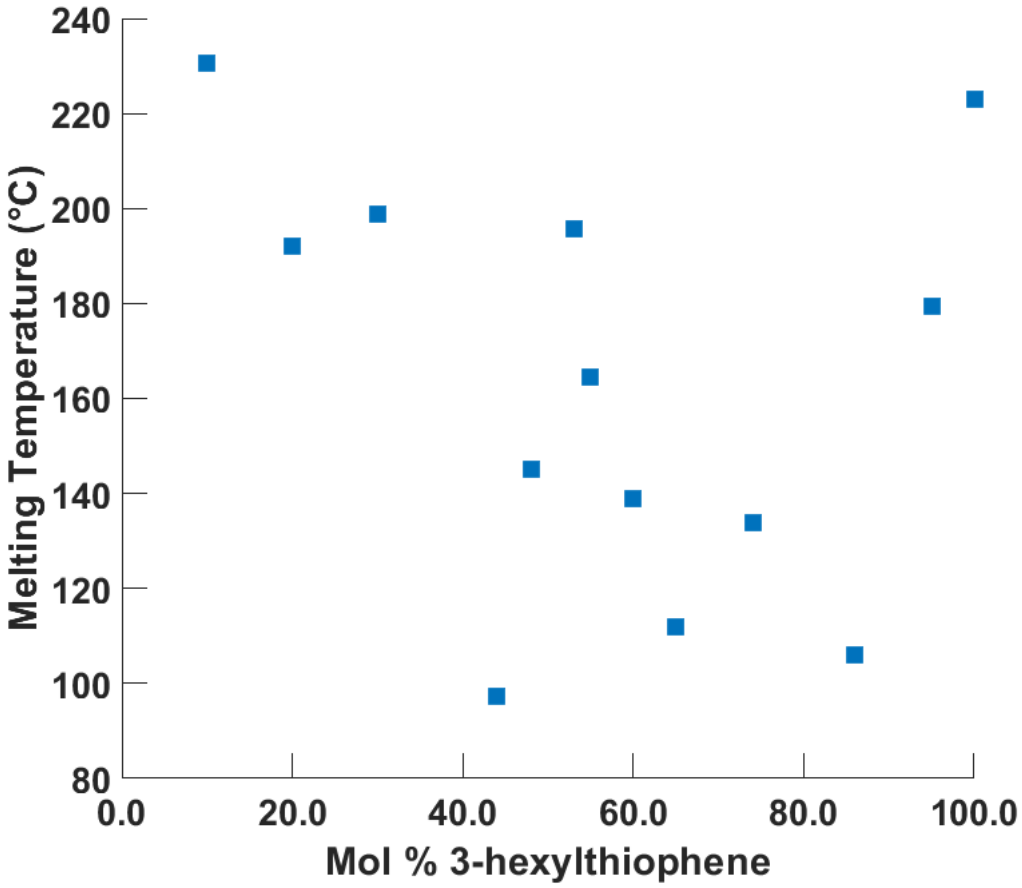

Figure 6.3 Melting temperatures vs. 3-hexylthiophene content.

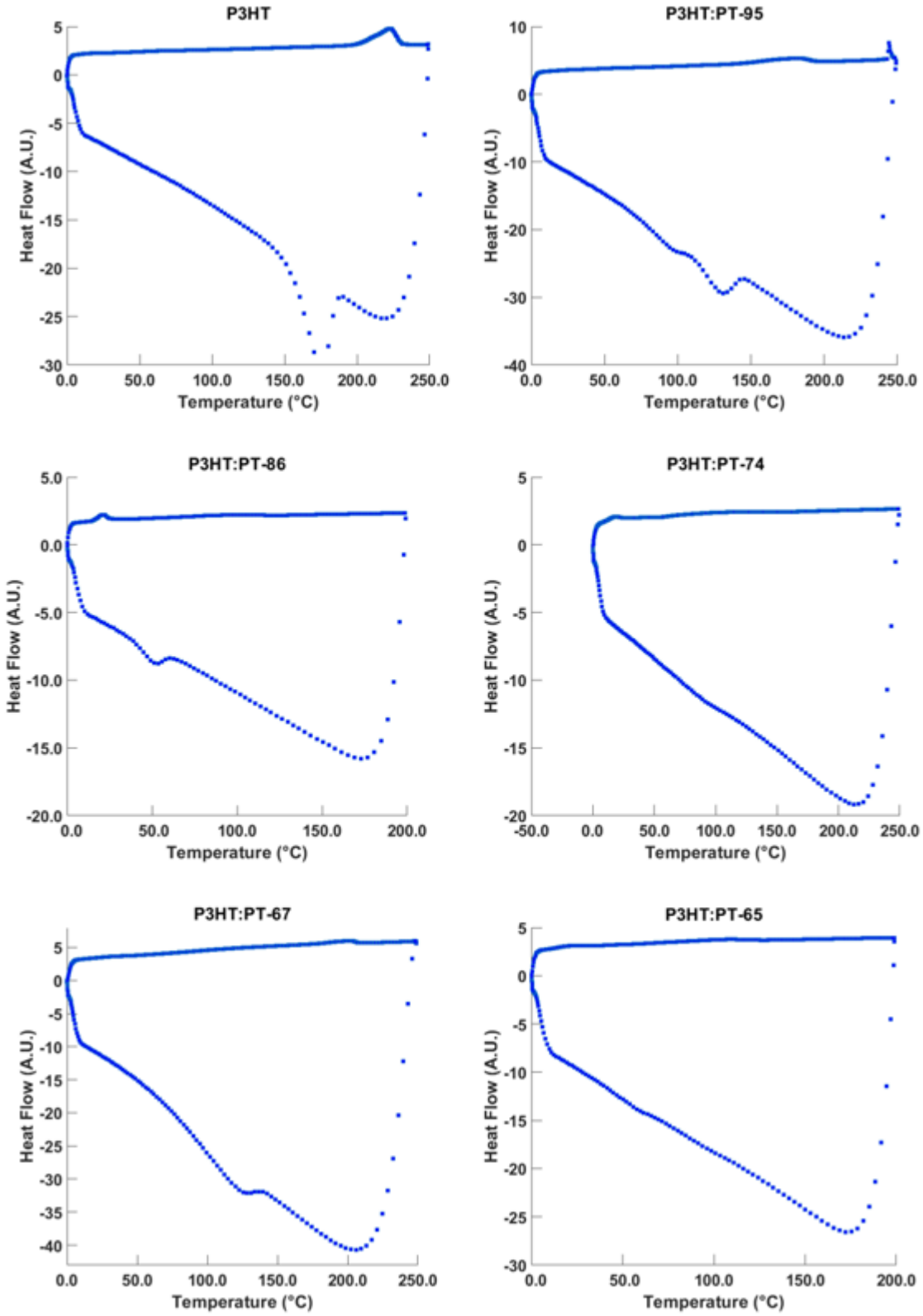

Figure 6.4 DSC thermograms of synthesized P3HT and poly(3-hexylthiophene-co-thiophene) statistical copolymers.

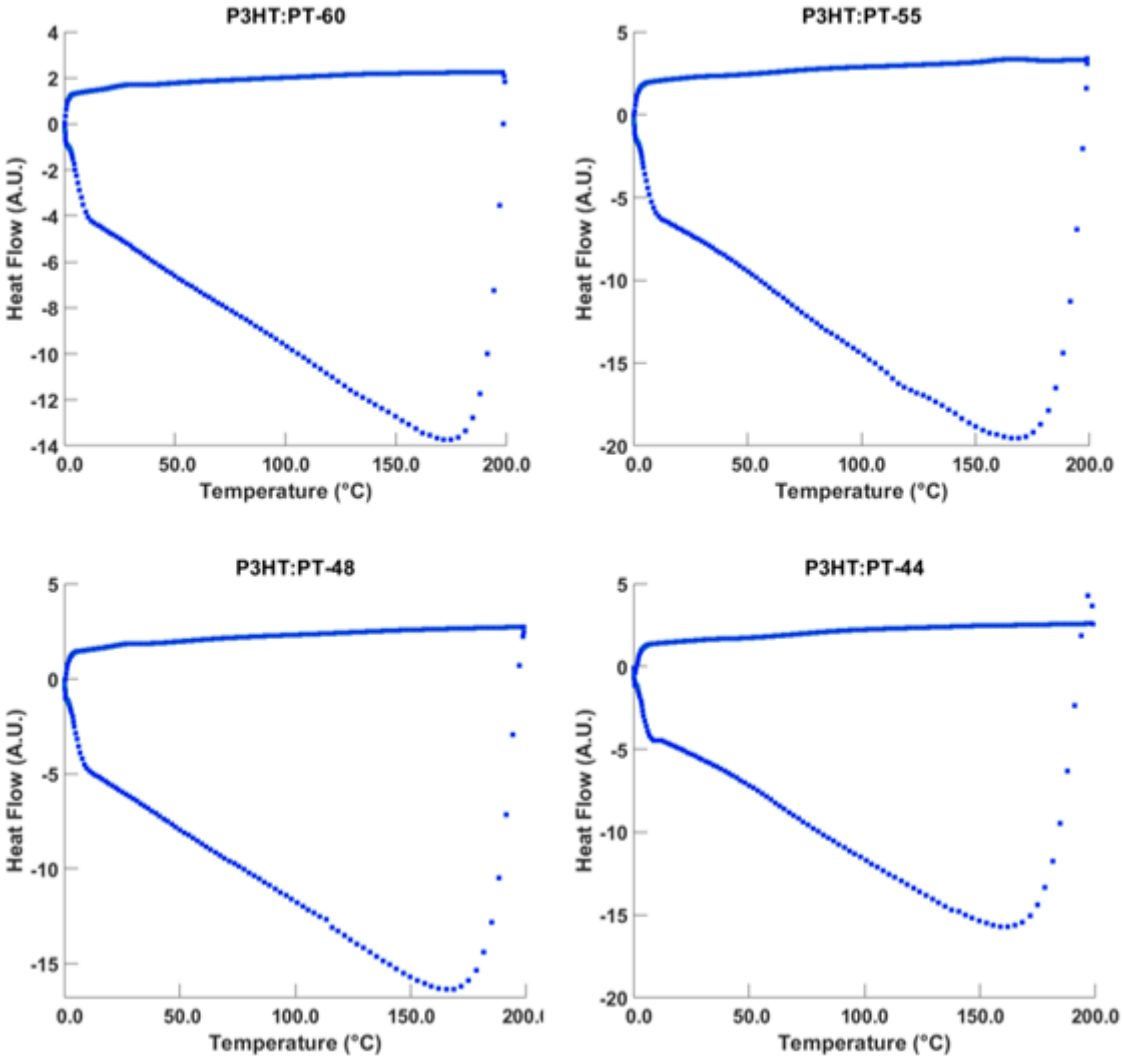

Figure 6.5 DSC thermograms of synthesized P3HT-co-T statistical copolymers.

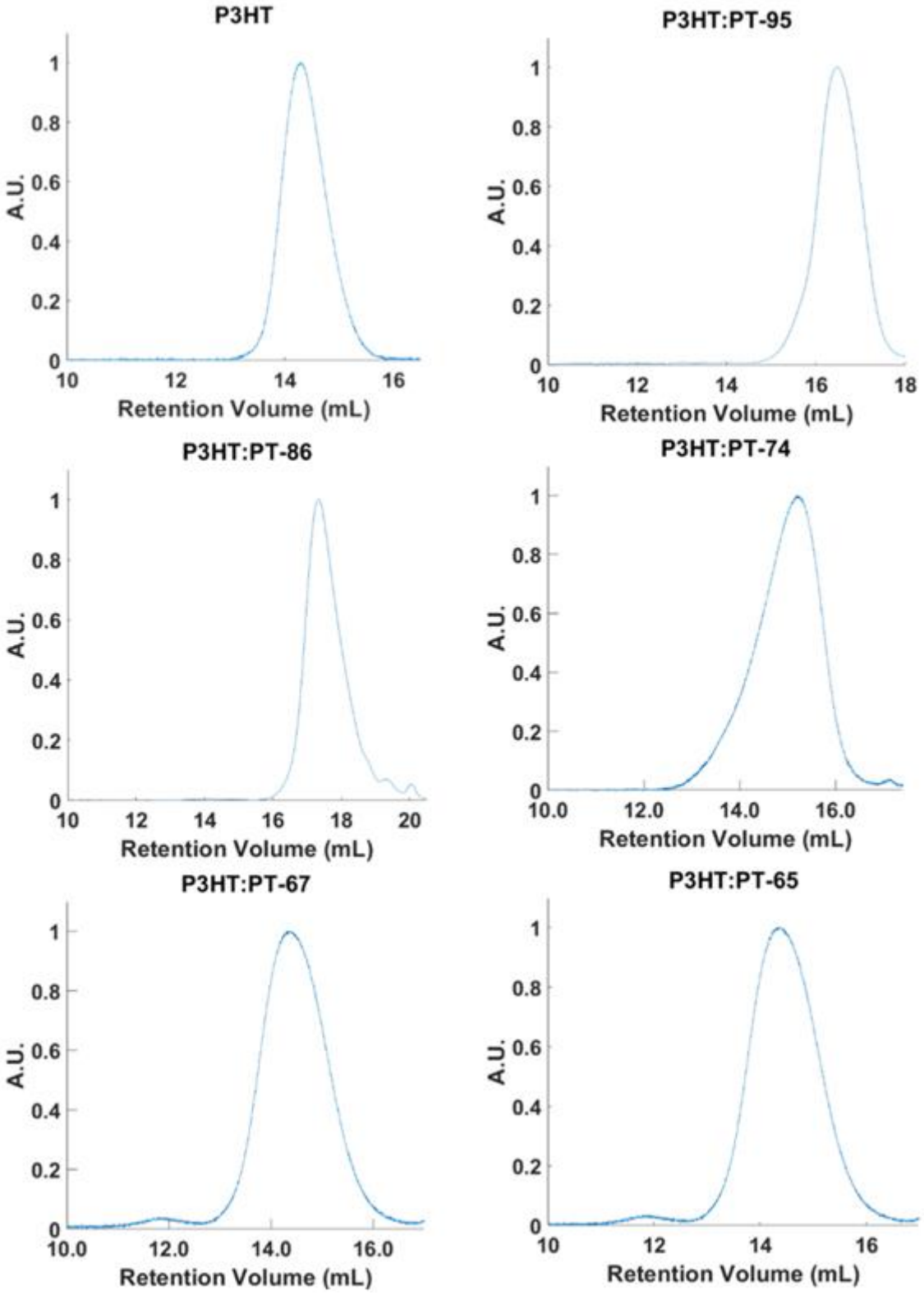

Figure 6.6 Gel permeation chromatographs for soluble synthesized soluble poly(3-hexylthiophene-co-thiophene) statistical copolymers.

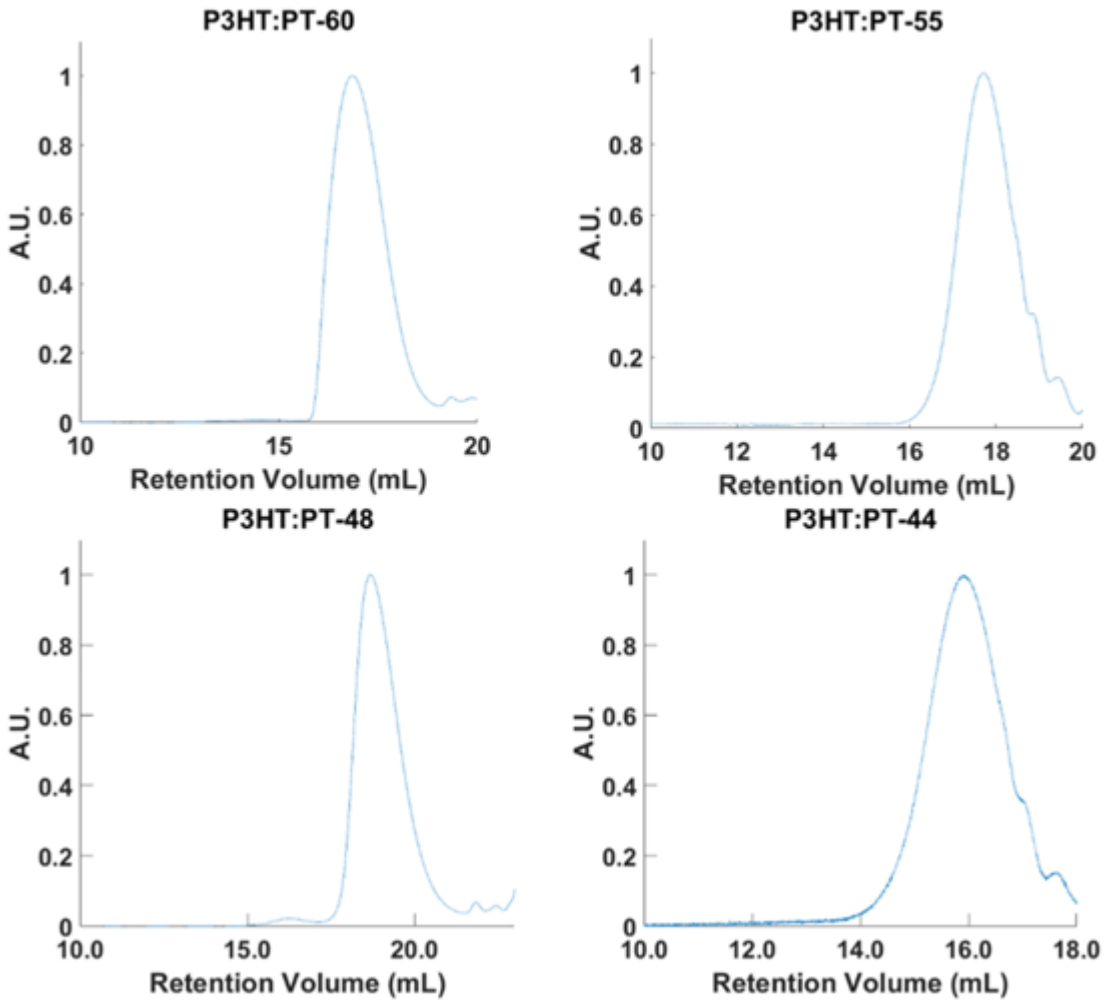

Figure 6.7 Gel permeation chromatographs for soluble synthesized soluble poly(3-hexylthiophene-co-thiophene) statistical copolymers.

6.2.3 - Optoelectronic Properties

Optoelectronic properties of the synthesized (P3HT-PT) copolymers were examined via UV-Vis spectrophotometry (**Figure 6.8**) and their optical band gaps, excitonic band widths, carbon stretching modes, and stretching mode energies extracted using the Spano Model. The optical band gaps of the statistical copolymers demonstrate interesting behavior compared to previously synthesized copolymers of 3-hexylthiophene-containing statistical copolymers.[6] Wu et al. synthesized poly((3-octyl thiophene)-*co*-(3-butyl thiophene)) (P3OT-*co*-P3BT) and observed behavior in which two band gaps domains were formed. In the work of Ho et al., the optical band gaps of poly((3-hexylthiophiene)-*co*-(3-(2'-ethyl)hexylthiophene)) (P3HT-*co*-P3EHT) copolymers possessed distinct regimes where the compositionally dominant comonomers set the behavior.[6] P3HT-*co*-P3EHT copolymers with 50% or more of EHT comonomer possessed band gaps analogous to that of P3EHT homopolymer while the converse of this statement is true for the case of the HT dominant copolymers. As shown in **Figure 6.9**, the polymers synthesized here also exhibit two regimes of behavior, however they do not strictly follow the dominant comonomer behavior as exhibited by P3EHT-*co*-P3HT or P3OT-*co*-P3BT copolymers.[6,22] Instead, we observe dominant copolymer behavior for very P3HT-rich copolymers (86 mol % and above) and composition dependent behavior for copolymers with less than 86 mol% P3HT (generally increasing with increasing polythiophene content). We attribute this more complicated behavior to the additional complexity in chain regiochemistry with incorporation of sterically unhindered thiophene units as compared with copolymers consisting of wholly 3-substituted thiophene derivatives.

UV-Vis absorption curves can be analyzed using the Spano Model to estimate the optical band gaps of semiconducting materials by fitting the area under the curve with various vibrational states and absorption states resulting from the aggregated and amorphous regions. As shown in **Figure**

6.8, the P3HT-*co*-PT absorption bands form two main clusters and upon application of the Spano Model two band gap regimes are readily apparent; those with band gaps above 2.0 eV and those with band gaps 1.7 or below as shown in **Figure 6.9**. The copolymers with 86 mole percent or more 3HT monomer content exhibit behavior much like P3HT while the rest of the copolymers exhibit depressed bandgaps which increase as P3HT content decreases. The optical band gaps of the statistical copolymers demonstrate interesting behavior compared to previously synthesized copolymers of 3-hexylthiophene-containing statistical copolymers.[6] Wu et al. synthesized poly((3-octyl thiophene)-*co*-(3-butyl thiophene)) (P3OT-*co*-P3BT) and observed behavior in which two band gaps domains were formed. In the work of Ho et al., the optical band gaps of poly((3-hexylthiophiene)-*co*-(3-(2'-ethyl)hexylthiophene)) (P3HT-*co*-P3EHT) copolymers possessed distinct regimes where the compositionally dominant comonomers set the behavior.[6] P3HT-*co*-P3EHT copolymers with 50% or more of EHT comonomer possessed band gaps analogous to that of P3EHT homopolymer while the converse of this statement is true for the case of the HT dominant copolymers. As shown in **Figure 6.9**, the polymers synthesized here also exhibit two regimes of behavior, however they do not strictly follow the dominant comonomer behavior as exhibited by P3EHT-*co*-P3HT or P3OT-*co*-P3BT copolymers.[6,22] Instead, we observe dominant copolymer behavior for very P3HT-rich copolymers (86 mol % and above) and composition dependent behavior for copolymers with less than 86 mol% P3HT (generally increasing with increasing polythiophene content). We attribute this more complicated behavior to the additional complexity in chain regiochemistry with incorporation of sterically unhindered thiophene units as compared with copolymers consisting of wholly 3-substituted thiophene derivatives.

Table 6.2 Fitting parameters to UV-vis spectra of thin films

Polymer	W (nm)	E0-0 (ev)	Ep	σ
P3HT	0.12	2.03	0.18	0.08
P3HT:PT-95	0.14	2.04	0.18	0.08
P3HT:PT-86	0.26	2.04	0.21	0.10
P3HT:PT-74	2.40	1.40	0.37	0.14
P3HT:PT-65	1.58	1.49	0.32	0.09
P3HT:PT-60	1.47	1.52	0.34	0.11
P3HT:PT-55	1.12	1.70	0.28	0.12
P3HT:PT-53	2.05	1.36	0.40	0.10
P3HT:PT-48	1.19	1.60	0.28	0.09
P3HT:PT-44	1.15	1.68	0.31	0.12

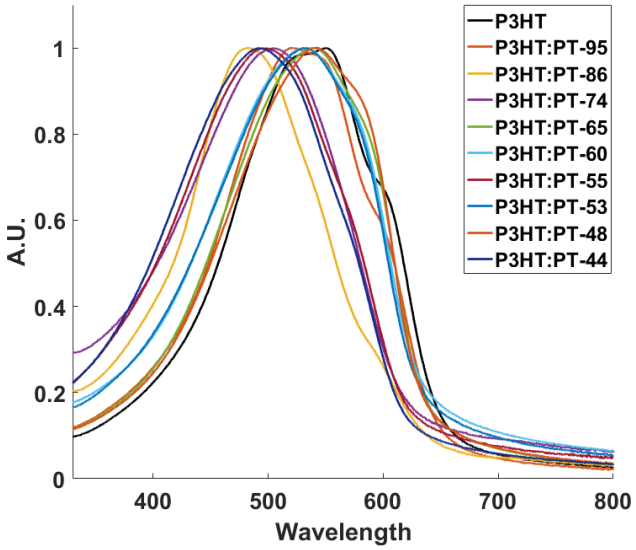

Figure 6.8 UV-Vis absorption spectra of annealed synthesized polymer films.

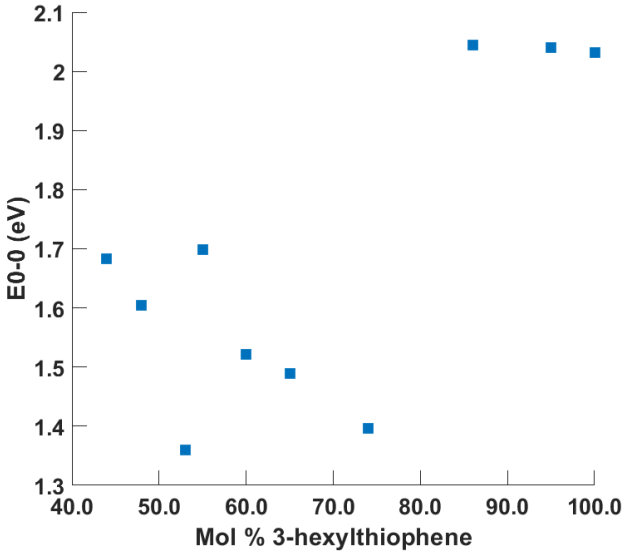

Figure 6.9 Extracted optical band gaps of synthesized polymer films from Spano Model.

6.2.4 – Electronic Behavior

Cyclic voltammetry was used to determine the HOMO energy levels to provide further insight into the electronic bandgaps determined by the Spano Model. Cyclic voltammograms are shown in **Figure 6.10** and **Figure 6.11** while the extracted HOMO energy levels are shown in **Figure 6.12**. **Figure 6.12** shows that the copolymers have relatively similar HOMO energy levels. LUMO energy levels were estimated by subtracting the optical band gap from the HOMO energy levels. As expected, there is a general narrowing of electronic band gap with lower 3HT content observed in **Figure 6.12**.[23,28]

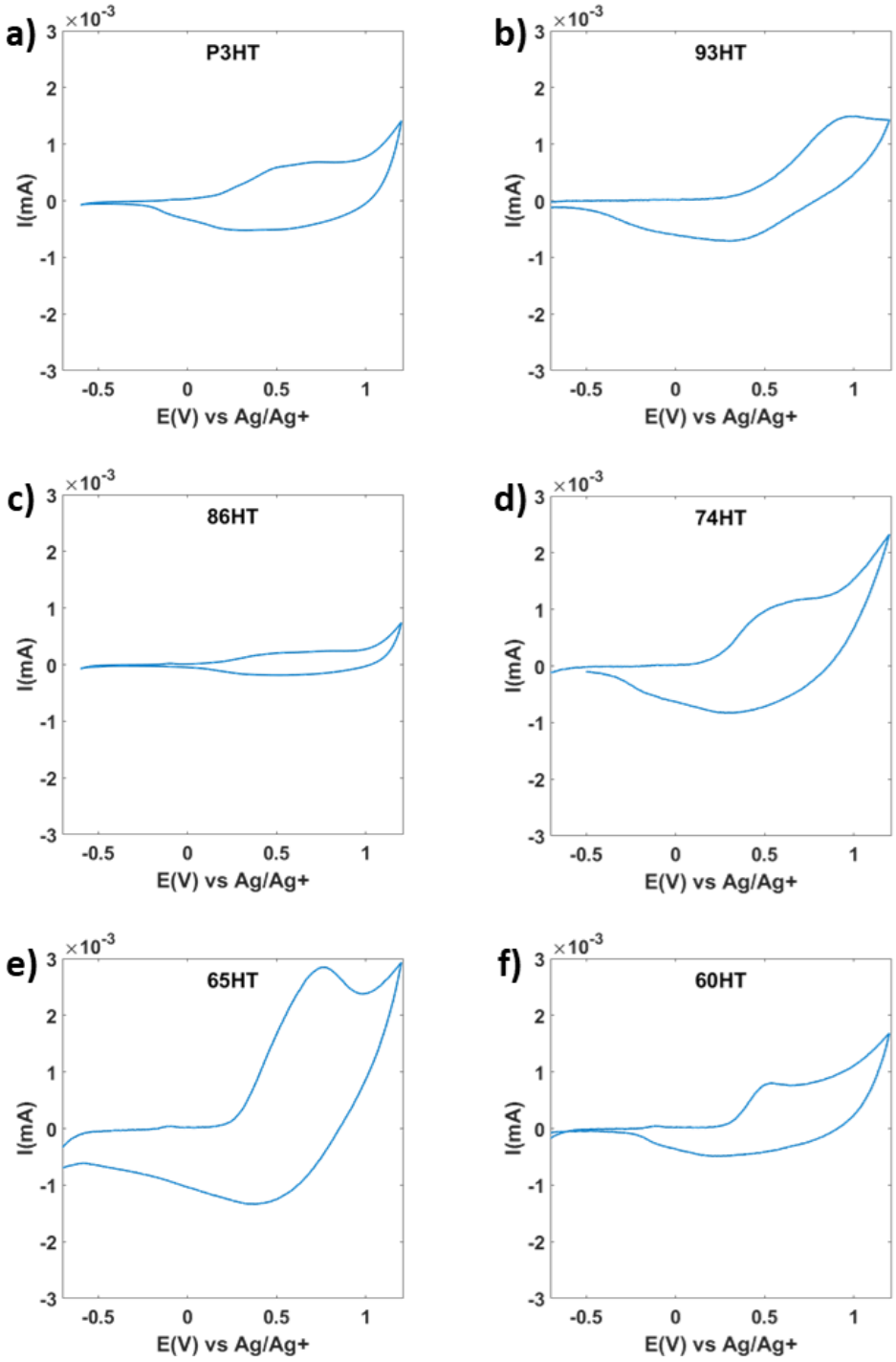

Figure 6.10 Cyclic voltammagrams for a) P3HT, b) 93HT, c) 86HT, d) 74HT, e) 65HT, and f) 60HT statistical copolymers.

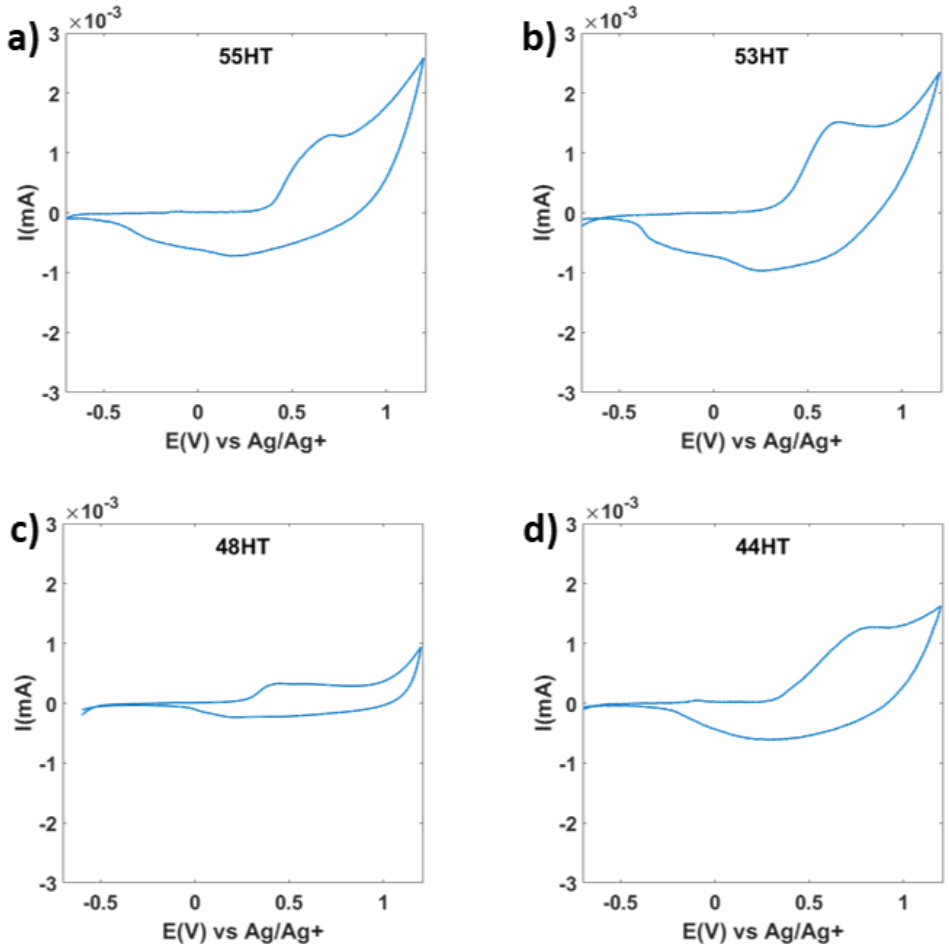

Figure 6.11 Cyclic voltammagrams for a) 55HT, b) 53HT, c) 48HT, d) 44HT statistical copolymers.

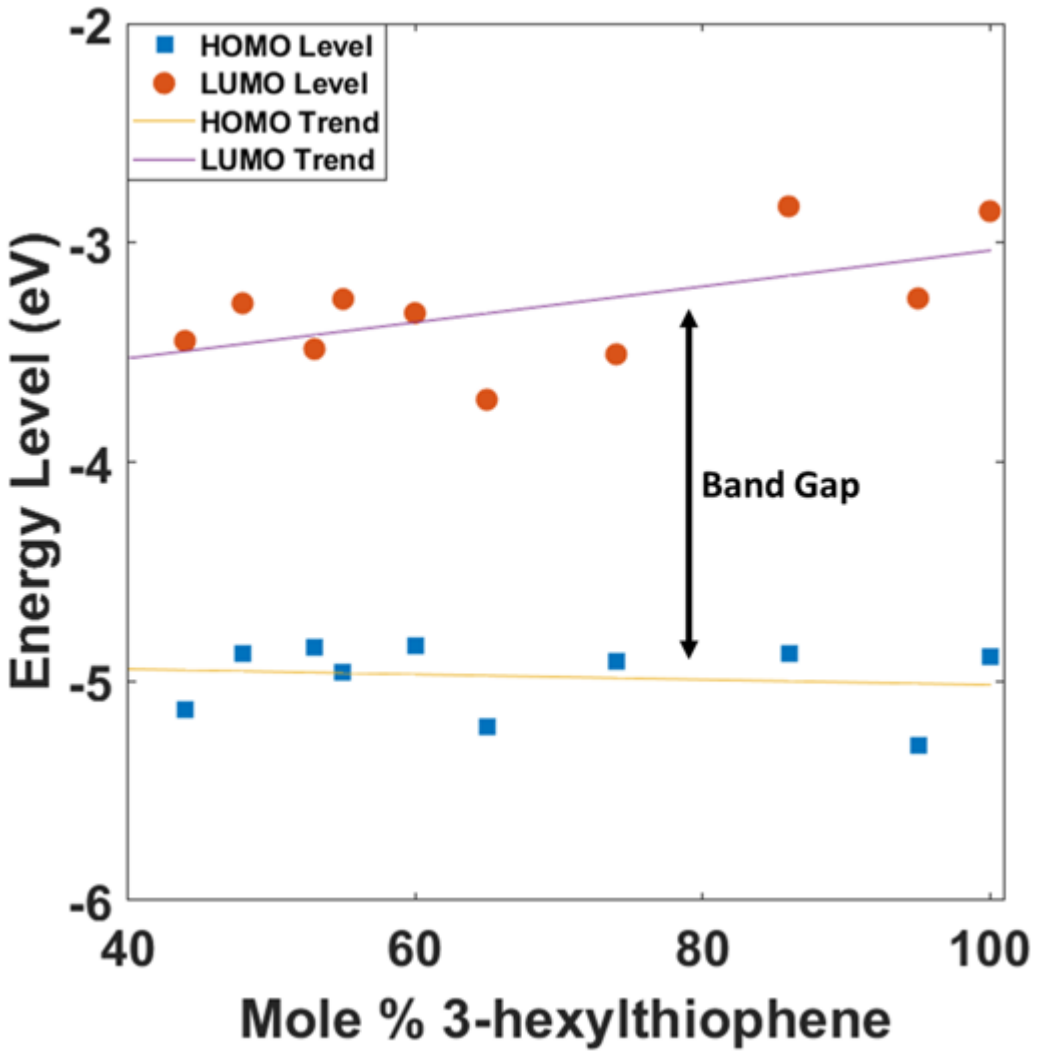

Figure 6.12 Extracted HOMO and LUMO energy levels for P3HT-*co*-PT statistical copolymers. Note that LUMO values were determined by subtracting the optical band gaps from the HOMO energy levels.

6.2.5 – Copolymer Crystal Structure

X-Ray Diffraction (XRD) at wide-angles, wide-angle X-ray Scattering (WAXS), was performed on the P3HT-*co*-T statistical copolymers and the characteristic crystal domains are shown in **Figure 6.13**. As expected, the WAXS patterns exhibited by the statistical copolymers, shown in **Figure 6.14**, varied greatly with some copolymers exhibiting order similar to that of P3HT and others exhibiting little to no order. As discussed in Chapter 6.2.1, the difference in these patterns is likely due to the complicated regioregularity in the statistical copolymer backbones. Upon comparison of WAXS patterns for copolymers with at least 65 mole % 3HT, we find good agreement with the available literature on these copolymers.[11,23,28] The presence of the (100) peaks and the (200) peaks in the P3HT WAXS pattern demonstrates lamellar packing and high regioregularity. Similar to the shifting behavior observed in other similar systems, the XRD patterns for P3HT through 65HT exhibit shifting towards a higher angle; indicating diminished side chain bulkiness.[23,28] The (010) peak (not present in this data) is commonly attributed to π-π stacking from regularly spaced thiophene units and should be investigated in the future with in-plane WAXS or WAXS with a 2D scattering detector.[11,23,28] The absence of this peak in the copolymers suggests that little to no long-range ordering/lamellar packing is observed as noted by Son et al and Smith et al.[23,28] As is shown for the 60HT-48HT copolymers, in place of the (100) peak, a much broader peak is observed. We attribute this peak to be a result of highly ordered amorphous fractions of the polymer as the signal is not absent but is also not distinct as is the case for the other polymers shown.[33–35]

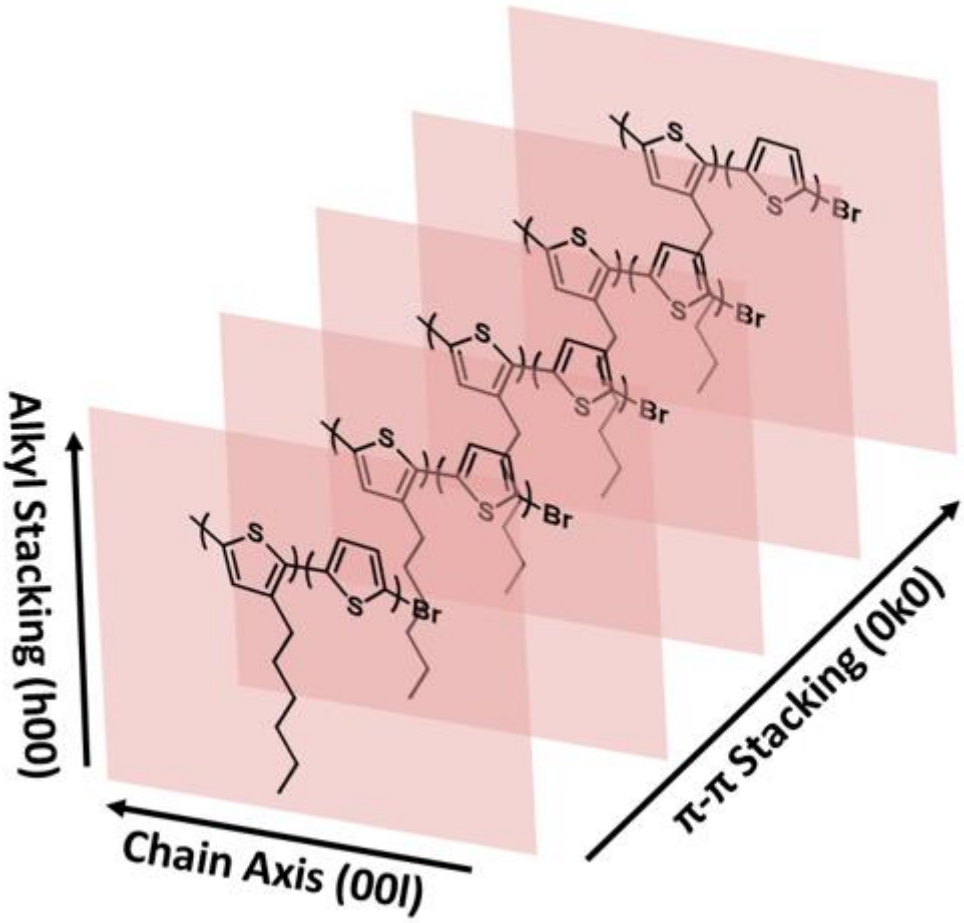

Figure 6.13 Illustration of hierarchical ordering in P3HT-*co*-T statistical copolymers.

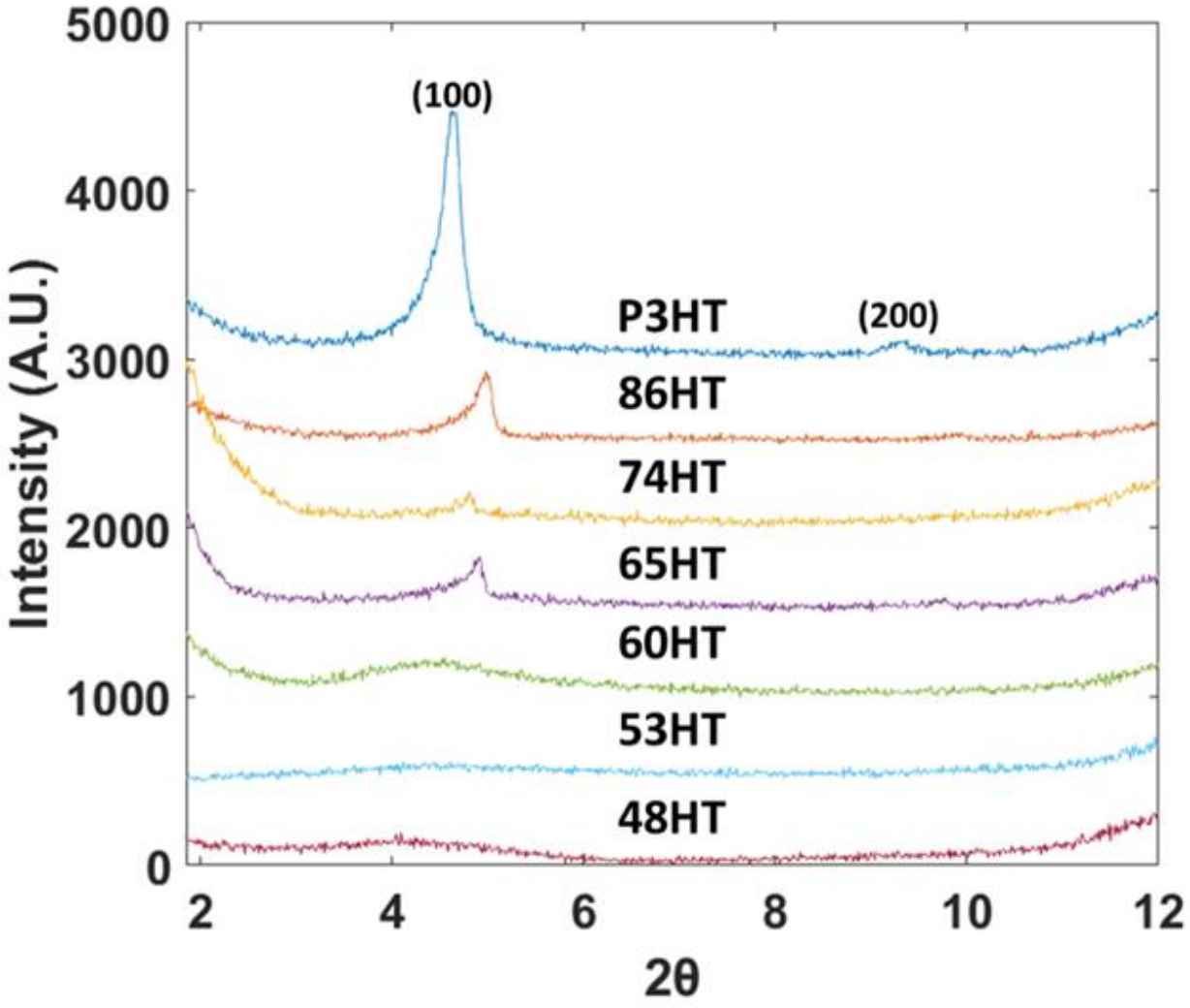

Figure 6.14 WAXS patterns of P3HT-*co*-T statistical copolymers.

6.3- Experiments Delayed Due to the COVID-19 Pandemic

As discussed in the previous two sections, there are a few experiments that are delayed due to the outbreak of COVID-19 and subsequent closures of relevant research facilities. These experiments are included in **Table 6.3.**

Table 6.3 Experiments delayed by COVID-19 outbreak.

Experiment	Copolymers	Reason
XRD (WAXS)[a]	95HT, 55HT,44HT	Crystal Structure
Modulated DSC	All	RAF Verification
Four-Point Probe	All	Conductivity
Scattered White Light Interferometry[b]	All	Film Thickness
Polarized Light Optical Microscopy[c]	All	Birefringent Behavior

[a] Georgia Institute of Technology Materials Characterization Facility.
[b] Dr. Kyle Schulze's Lab in Mechanical Engineering at Auburn University.
[c] Dr. Virginia Davis' Lab in Chemical Engineering at Auburn University.

These experiments would have contributed additional data that could more completely describe the material behavior of the polymers discussed in this chapter. It should be noted that the three polymers that need to be subjected to XRD were going to be rerun as the original samples were not well suited for analysis and the resulting X-ray patterns were difficult to obtain and unclear. New samples have been prepared and are to be sent out for data collection by the staff at the Georgia Institute of Technology facility. XRD samples were prepared as discussed in **Chapter 3**. The same samples were also to be used for four-point probe resistometry, scattered white light interferometry, and polarized light optical microscopy. The samples were prepared as follows: polymer was weighed into a scintillation vial and subsequently solvated to 4 mg/mL in toluene. The samples were passed through a syringe filter and then spin coated onto 3 by 1-inch microscope slides. Room temperature filtered samples were sprayed at an outlet pressure of 20 psi onto preheated slides (~100 °C).

6.4 - Conclusions.

We synthesized a series of P3HT-*co*-PT copolymers of varied composition and examined the molecular characteristics, thermal and optoelectronic behavior of these statistical copolymers. The incorporation of unsubstituted thiophene greatly complicates the reaction chemistry as it lacks the steric hindrance of a 3-position substituent group for directing monomer addition to the polymer chain. This leads to lower regioregularities due to the lack of control over monomer addition as unsubstituted thiophene content increases. The incorporation of a small number of unsubstituted thiophene units leads to defects to the chain regioregularity altering the thermal behavior (lower melting temperature) while maintaining the optical band gap analogous to P3HT. In particular, incorporation of unsubstituted units initially results in a smooth decrease in melting temperature while the optical band gap remains unchanged; behavior analogous to that for copolymers of 3-substituted thiophenes. However, at increasingly high levels of unsubstituted content (> 15 %) the resulting complexity of the polymer microstructure due to the lack of steric hinderance by thiophene monomer results in more complex thermal behavior and optical band gap behavior. We anticipate that even the copolymers with reduced crystallinity will exhibit appreciable conductivity. Their respective conductivities will likely be related to their band gaps, specifically their LUMO levels as all copolymers have approximately equal HOMO levels.

6.5- References

(1) McCullough, R. D.; Lowe, R. D.; Jayaraman, M.; Anderson, D. L. Design, Synthesis, and Control of Conducting Polymer Architectures: Structurally Homogeneous Poly(3-Alkylthiophenes). *J. Org. Chem.* **1993**, *58* (4), 904–912. https://doi.org/10.1021/jo00056a024.

(2) McCullough, R. D. The Chemistry of Conducting Polythiophenes. *Advanced Materials* **1998**, *10* (2), 93–116. https://doi.org/10.1002/(SICI)1521-4095(199801)10:2<93::AID-ADMA93>3.0.CO;2-F.

(3) Beckingham, B. S.; Ho, V.; Segalman, R. A. Melting Behavior of Poly(3-(2′-Ethyl)Hexylthiophene). *Macromolecules* **2014**, *47* (23), 8305–8310. https://doi.org/10.1021/ma501915v.

(4) Xu, B.; Noh, S.; Thompson, B. C. Fine Tuning of Polymer Properties by Incorporating Strongly Electron-Donating 3-Hexyloxythiophene Units into Random and Semi-Random Copolymers. *Macromolecules* **2014**, *47* (15), 5029–5039. https://doi.org/10.1021/ma5012107.

(5) Keheze, F. M.; Raithel, D.; Wu, T.; Schiefer, D.; Sommer, M.; Hildner, R.; Reiter, G. Signatures of Melting and Recrystallization of a Bulky Substituted Poly(Thiophene) Identified by Optical Spectroscopy. *Macromolecules* **2017**, *50* (17), 6829–6839. https://doi.org/10.1021/acs.macromol.7b01080.

(6) Ho, V.; Beckingham, B. S.; Ng, H. H.; Segalman, R. A. Control of Thermal and Optoelectronic Properties in Conjugated Poly(3-Alkylthiophenes). *MRS Communications* **2014**, *4* (2), 45–50. https://doi.org/10.1557/mrc.2014.9.

(7) Malik, S.; Nandi, A. K. Crystallization Mechanism of Regioregular Poly(3-Alkyl Thiophene)s. *Journal of Polymer Science Part B: Polymer Physics* **2002**, *40* (18), 2073–2085. https://doi.org/10.1002/polb.10272.

(8) Boudouris, B. W.; Ho, V.; Jimison, L. H.; Toney, M. F.; Salleo, A.; Segalman, R. A. Real-Time Observation of Poly(3-Alkylthiophene) Crystallization and Correlation with Transient Optoelectronic Properties. *Macromolecules* **2011**, *44* (17), 6653–6658. https://doi.org/10.1021/ma201316a.

(9) Sheina, E. E.; Khersonsky, S. M.; Jones, E. G.; McCullough, R. D. Highly Conductive, Regioregular Alkoxy-Functionalized Polythiophenes: A New Class of Stable, Low Band Gap Materials. *Chem. Mater.* **2005**, *17* (13), 3317–3319. https://doi.org/10.1021/cm050083o.

(10) Sivula, K.; Ball, Z. T.; Watanabe, N.; Fréchet, J. M. J. Amphiphilic Diblock Copolymer Compatibilizers and Their Effect on the Morphology and Performance of Polythiophene:Fullerene Solar Cells. *Advanced Materials* **2006**, *18* (2), 206–210. https://doi.org/10.1002/adma.200501787.

(11) Ho, V.; Boudouris, B. W.; Segalman, R. A. Tuning Polythiophene Crystallization through Systematic Side Chain Functionalization. *Macromolecules* **2010**, *43* (19), 7895–7899. https://doi.org/10.1021/ma101697m.

(12) Burkhart, B.; Khlyabich, P. P.; Thompson, B. C. Influence of the Ethylhexyl Side-Chain Content on the Open-Circuit Voltage in Rr-Poly(3-Hexylthiophene- *Co* -3-(2-Ethylhexyl)Thiophene) Copolymers. *Macromolecules* **2012**, *45* (9), 3740–3748. https://doi.org/10.1021/ma300263a.

(13) Davidson, E. C.; Beckingham, B. S.; Ho, V.; Segalman, R. A. Confined Crystallization in Lamellae Forming Poly(3-(2′-Ethyl)Hexylthiophene) (P3EHT) Block Copolymers. *Journal of Polymer Science Part B: Polymer Physics* **2016**, *54* (2), 205–215. https://doi.org/10.1002/polb.23904.
(14) Davidson, E. C.; Segalman, R. A. Confined Crystallization within Cylindrical P3EHT Block Copolymer Microdomains. *Macromolecules* **2017**, *50* (16), 6128–6136. https://doi.org/10.1021/acs.macromol.7b01323.
(15) Yu, L.; Davidson, E.; Sharma, A.; Andersson, M. R.; Segalman, R.; Müller, C. Isothermal Crystallization Kinetics and Time–Temperature–Transformation of the Conjugated Polymer: Poly(3-(2′-Ethyl)Hexylthiophene). *Chem Mater* **2017**, *29* (13), 5654–5662. https://doi.org/10.1021/acs.chemmater.7b01393.
(16) Ho, V.; Boudouris, B. W.; McCulloch, B. L.; Shuttle, C. G.; Burkhardt, M.; Chabinyc, M. L.; Segalman, R. A. Poly(3-Alkylthiophene) Diblock Copolymers with Ordered Microstructures and Continuous Semiconducting Pathways. *Journal of the American Chemical Society* **2011**, *133* (24), 9270–9273. https://doi.org/10.1021/ja2035317.
(17) Sauvé, G.; McCullough, R. D. High Field-Effect Mobilities for Diblock Copolymers of Poly(3-Hexylthiophene) and Poly(Methyl Acrylate). *Advanced Materials* **2007**, *19* (14), 1822–1825. https://doi.org/10.1002/adma.200602368.
(18) Iovu, M. C.; Craley, C. R.; Jeffries-EL, M.; Krankowski, A. B.; Zhang, R.; Kowalewski, T.; McCullough, R. D. Conducting Regioregular Polythiophene Block Copolymer Nanofibrils Synthesized by Reversible Addition Fragmentation Chain Transfer Polymerization (RAFT) and Nitroxide Mediated Polymerization (NMP). *Macromolecules* **2007**, *40* (14), 4733–4735. https://doi.org/10.1021/ma070406x.
(19) Luebben, S. D.; Elliott, B.; Wilson, C. Poly(Heteroaromatic) Block Copolymers with Electrical Conductivity. US7279534B2, October 9, 2007.
(20) McCullough, R.; Liu, J.; Ewbank, P.; Sheina, E. Polythiophenes, Block Copolymers Made Therefrom, and Methods of Forming the Same. US20050187370A1, August 25, 2005.
(21) Wu, P.-T.; Ren, G.; Jenekhe, S. A. Crystalline Random Conjugated Copolymers with Multiple Side Chains: Tunable Intermolecular Interactions and Enhanced Charge Transport and Photovoltaic Properties. *Macromolecules* **2010**, *43* (7), 3306–3313. https://doi.org/10.1021/ma100006x.
(22) Zhang, Y.; Tajima, K.; Hashimoto, K. Nanostructure Formation in Poly(3-Hexylthiophene-Block-3-(2-Ethylhexyl)Thiophene)s. *Macromolecules* **2009**, *42* (18), 7008–7015. https://doi.org/10.1021/ma9013065.
(23) Smith, Z. C.; Wright, Z. M.; Arnold, A. M.; Sauvé, G.; McCullough, R. D.; Sydlik, S. A. Increased Toughness and Excellent Electronic Properties in Regioregular Random Copolymers of 3-Alkylthiophenes and Thiophene. *Adv. Electron. Mater.* **2017**, *3* (1), n/a-n/a. https://doi.org/10.1002/aelm.201600316.
(24) Howard, J. B.; Noh, S.; Beier, A. E.; Thompson, B. C. Fine Tuning Surface Energy of Poly(3-Hexylthiophene) by Heteroatom Modification of the Alkyl Side Chains. *ACS Macro Lett.* **2015**, *4* (7), 725–730. https://doi.org/10.1021/acsmacrolett.5b00328.
(25) Yang, Y.-L.; Lee, Y.-H.; Lee, Y.-P.; Chiang, C.-J.; Shen, C.; Wu, C.-C.; Ohta, Y.; Yokozawa, T.; Dai, C.-A. Synthesis and Characterization of Poly(3-Hexylthiophene)–Poly(3-Hexyloxythiophene) Random Copolymers with Tunable Band Gap via Grignard Metathesis Polymerization. *Polymer International* **2014**, *63* (12), 2068–2075. https://doi.org/10.1002/pi.4744.

(26) Murphy, A. R.; Fréchet, J. M. J.; Chang, P.; Lee, J.; Subramanian, V. Organic Thin Film Transistors from a Soluble Oligothiophene Derivative Containing Thermally Removable Solubilizing Groups. *J. Am. Chem. Soc.* **2004**, *126* (6), 1596–1597. https://doi.org/10.1021/ja039529x.
(27) Son, S. Y.; Kim, Y.; Lee, J.; Lee, G.-Y.; Park, W.-T.; Noh, Y.-Y.; Park, C. E.; Park, T. High-Field-Effect Mobility of Low-Crystallinity Conjugated Polymers with Localized Aggregates. *J. Am. Chem. Soc.* **2016**, *138* (26), 8096–8103. https://doi.org/10.1021/jacs.6b01046.
(28) Son, S. Y.; Kim, J.-H.; Song, E.; Choi, K.; Lee, J.; Cho, K.; Kim, T.-S.; Park, T. Exploiting π–π Stacking for Stretchable Semiconducting Polymers. *Macromolecules* **2018**, *51* (7), 2572–2579. https://doi.org/10.1021/acs.macromol.8b00093.
(29) Ouhib, F.; Khoukh, A.; Ledeuil, J.-B.; Martinez, H.; Desbrières, J.; Dagron-Lartigau, C. Diblock and Random Donor/Acceptor "Double Cable" Polythiophene Copolymers *via* the GRIM Method. *Macromolecules* **2008**, *41* (24), 9736–9743. https://doi.org/10.1021/ma801934g.
(30) Mescoloto, A. de F.; Pulcinelli, S. H.; Santilli, C. V.; Gonçalves, V. C. Structural and Thermal Properties of Carboxylic Acid Functionalized Polythiophenes. *Polímeros Ciência e Tecnologia* **2014**, *24* (ESP), 31–35. https://doi.org/10.4322/polimeros.2014.049.
(31) Duong, D. T.; Toney, M. F.; Salleo, A. Role of Confinement and Aggregation in Charge Transport in Semicrystalline Polythiophene Thin Films. *Phys. Rev. B* **2012**, *86* (20), 205205. https://doi.org/10.1103/PhysRevB.86.205205.
(32) Spano, F. C. Modeling Disorder in Polymer Aggregates: The Optical Spectroscopy of Regioregular Poly(3-Hexylthiophene) Thin Films. *J Chem Phys* **2005**, *122* (23), 234701. https://doi.org/10.1063/1.1914768.
(33) Beckingham, B. S.; Ho, V.; Segalman, R. A. Formation of a Rigid Amorphous Fraction in Poly(3-(2′-Ethyl)Hexylthiophene). *ACS Macro Lett.* **2014**, *3* (7), 684–688. https://doi.org/10.1021/mz500262d.
(34) Kolesov, I.; Androsch, R. The Rigid Amorphous Fraction of Cold-Crystallized Polyamide 6. *Polymer* **2012**, *53* (21), 4770–4777. https://doi.org/10.1016/j.polymer.2012.08.017.
(35) Di Lorenzo, M. L.; Gazzano, M.; Righetti, M. C. The Role of the Rigid Amorphous Fraction on Cold Crystallization of Poly(3-Hydroxybutyrate). *Macromolecules* **2012**, *45* (14), 5684–5691. https://doi.org/10.1021/ma3010907.

Chapter 7 - Poly(3-methoxythiophene-*co*-3-hexylthiophene)

Reproduced in part with permission from Jihyuk Kim, Rong Zhao, Katherine Lawson, Ashraf Ali, Andrew Adamczyk, and Bryan S. Beckingham.
Reproduced by permission of Materials Letters
(https://doi.org/10.1016/j.matlet.2019.126563)

7.1-Introduction

As discussed in **Chapter 6**, of the different types of conjugated polymers, polythiophene and its derivatives are of great interest for use as p-type semiconductors in electronic devices such as transistors, chemical sensors, and thermoelectric generators due to the high stability of its (un)doped states, ease of structural modification, and solution processability.[1,2] Alkoxy-functionalized polythiophenes are of interest as they exhibit desirable band gaps, low oxidation potentials, and a highly stable conducting state with additional electron-donating character of the oxygen atom on the sidechain.[3,4] Poly(3-methoxythiophene) (PMoT) is the shortest sidechain alkoxythiophene, however, poor solubility has been reported due to this sidechain shortness.[5,6] Altering of polythiophene microstructure by varying thiophene ring side-chain chemistry or copolymerization of two or more dissimilar thiophene monomers allows for modification of solid-state and optoelectronic properties of polythiophenes.[7-14] In this work we synthesize PMoT and to improve solubility in organic solvents, a copolymer of PMoT with poly(3-hexylthiophene) (P3HT) using Grignard Metathesis polymerization. P3HT is a prominent and widely-studied semiconducting polymer for high-performance organic field-effect transistors and organic photovoltaics.[7,15-20] The synthesized copolymer is soluble in common organic solvents, is characterized experimentally for its melting and optoelectronic properties in comparison with P3HT. Differences in electronic properties were probed using DFT calculations of homo-oligomers and successfully extended to the co-oligomers using linear mixing rules

7.2- Experimental Methods

7.2.1- Synthesis of 3-methoxythiopehene and its (co)polymerization

Copper bromide (1.123 g, 7.796 mmol) was added to a 250 mL two-neck flask in a distillation apparatus (condenser and septa) and evacuated for 10 min. Sodium methoxide in methanol (3 M, 41.95 mL, 125.8 mmol) was canula transferred to the reactor while stirring. Next, 3-bromothiophene (7.305 mL, 78.0 mmol) was added to the reactor via syringe and stirred at 65 °C overnight before cooling to room temperature and quenching with 150 mL of Type I DI water. The mixture was washed with 150 mL of diethyl ether, dried with magnesium sulfate and concentrated by rotary evaporation before purifying by column chromatography using petroleum ether. The product, 3-methoxythiophene (MoT), was verified via ^{1}H NMR spectroscopy. 2,5-dibromo 3-methoxythiophene and subsequent polymer and copolymer were synthesized as discussed for the alkyl thiophene derivatives discussed in Chapter 3.1.2.

7.2.2- Density Functional Theory Calculations

P3HT and PMoT homo-oligomer electronic structures were optimized using Density Functional Theory (DFT) at the B3LYP/CEP-31G level of theory using Gaussian 16 software.[23,24] HOMO-LUMO energy gaps for P3HT and PMoT homo-oligomers were calculated as a difference between the HOMO and LUMO energy levels.[25] Linear mixing rules were then applied to estimate the HOMO-LUMO energy gap and HOMO energy level of the PMoT-co-P3HT oligomers.

7.3- Results and Discussion

The synthetic approaches taken to prepare 3-methoxythiophene (MoT), PMoT and PMoT-co-P3HT are shown in **Figure 7.1** and the synthesis of P3HT used here was described previously.[13] Synthesis of MoT was confirmed using ^{1}H NMR spectroscopy as shown in **Figure 7.1c**. Peaks at 3.76, 6.2, 6.75 and 7.18 ppm correspond to the main protons in the MoT and their relative peak integrals (1:1:3; b':c':d') confirm successful MoT synthesis. Synthesized MoT was brominated at the aromatic 2 and 5 positions with completion verified by ^{1}H NMR spectroscopy via the disappearance of the corresponding proton signals; **Figure 7.1c**.

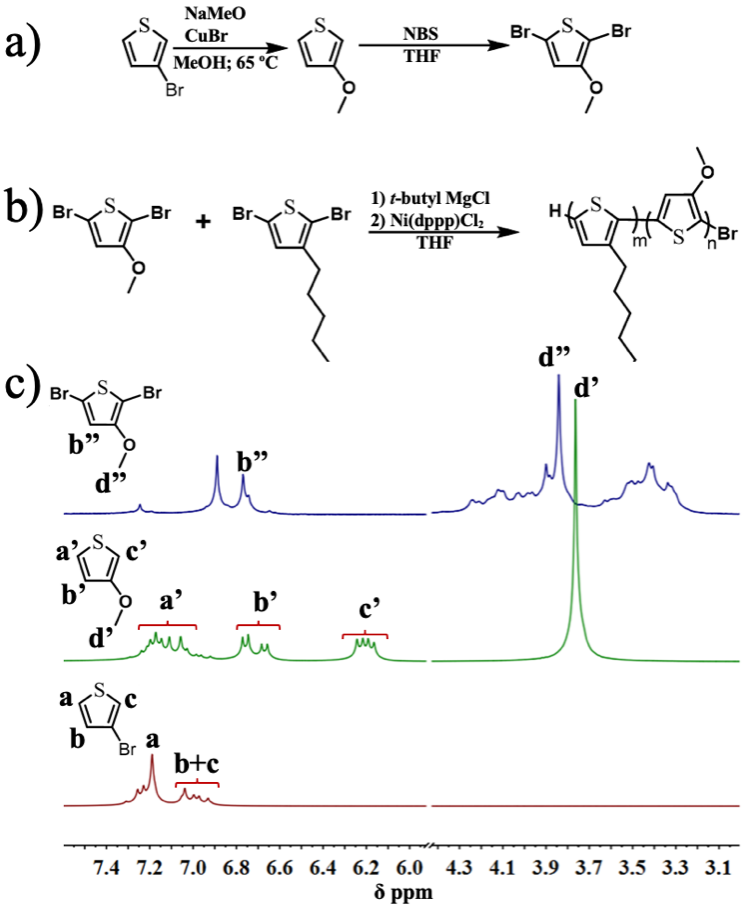

Figure 7.1 a) Synthesis route for 2,5-dibromo-3-methoxythiophene and b) poly((3-methoxythiophene)-co-(hexylthiophene). c) ^{1}H NMR spectrum of (top) dibrominated MoT monomer, middle MoT monomer, and bottom 3-bromothiophene.

With monomer synthesis confirmed, PMoT was synthesized using Grignard Metathesis (GRIM) polymerization followed by purification by Soxhlet extraction to remove Grignard salts, catalyst, and small polymers and oligomers. As solubility is important for both molecular characterization and processability for devices, the solubility of PMoT in a series of solvents (chlorobenzene, THF, chloroform, petroleum ether, ethyl ether, cyclohexane and water) was examined (**Figure 7.2**). Unfortunately, as has been reported using other synthesis routes, PMoT is insoluble in petroleum ether, ethyl ether, cyclohexane, and DI water and only showed dispersion-like behavior upon attempted solvation in chlorobenzene, THF, and chloroform.[6] As PMoT is insoluble in these common solvents, and thereby not-solution processable no further characterization was performed.

To improve solubility, MoT was copolymerized with 3-hexylthiophene (3HT). The inclusion of an alkyl side chain on thiophene is a commonly-used approach for improving solubility for device fabrication.[26-29] MoT and 3HT were statistically copolymerized (30/70 mol/mol MoT/3HT feed) with the solution turning a dark red color as the reaction progressed. Improved solubility was confirmed during Soxhlet extraction as chloroform was able to extract polymer from the thimble. In the ^{1}H NMR spectra (**Figure 7.3**), characteristic 3HT peaks are present and consistent with P3HT. The peaks corresponding to PMoT (~3.9-4.25 ppm, -OC**H**$_3$- and 5.0-5.5 ppm =C**H**-) appear in the expected ratio of 3:1 and a copolymer composition of 10 mol% PMoT is extracted. Macromolecular size and dispersity were examined with gel permeation chromatography (GPC) (**Figure 7.4**) yielding a polystyrene-equivalent M_n of 17.3 kg/mol and dispersity of 1.54; both reasonable for the synthetic route used. Thermal behavior was investigated with differential scanning calorimetry (DSC) (**Figure 7.5**) with an observed copolymer melting temperature (206 °C) confirming semicrystallinity, however with a slightly depressed melting temperature compared to P3HT (223 °C), and a decreased overall melting enthalpy as shown in **Figure 7.5**.

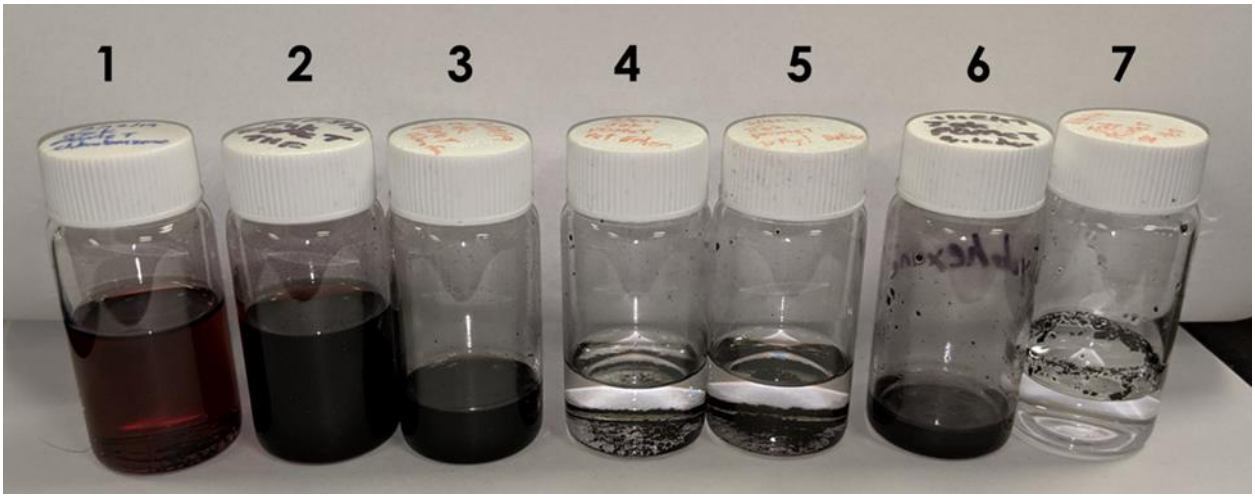

Figure 7.2 PMoT in a range of solvents: 1) chlorobenzene 2) tetrahydorfuran 3) chloroform 4) petroleum ether 5) ethyl ether 6) cyclohexane 7) type 1 deionized water.

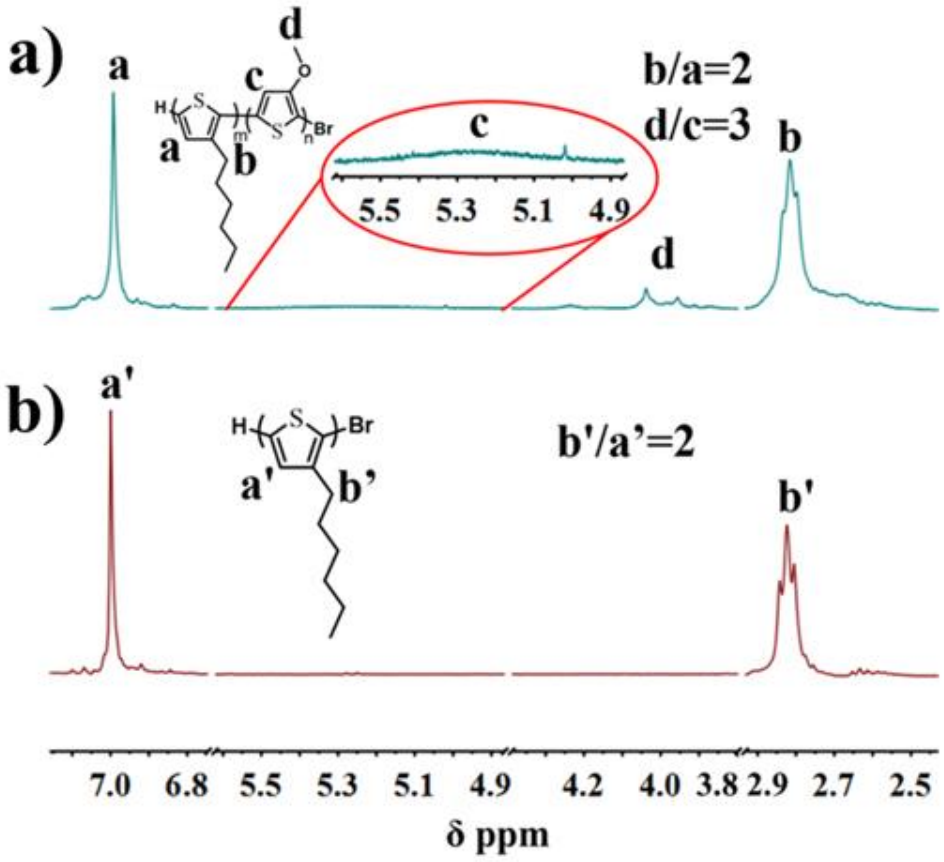

Figure 7.3 ^{1}H NMR spectrum of a) PMoT-3HT and b) PMoT.

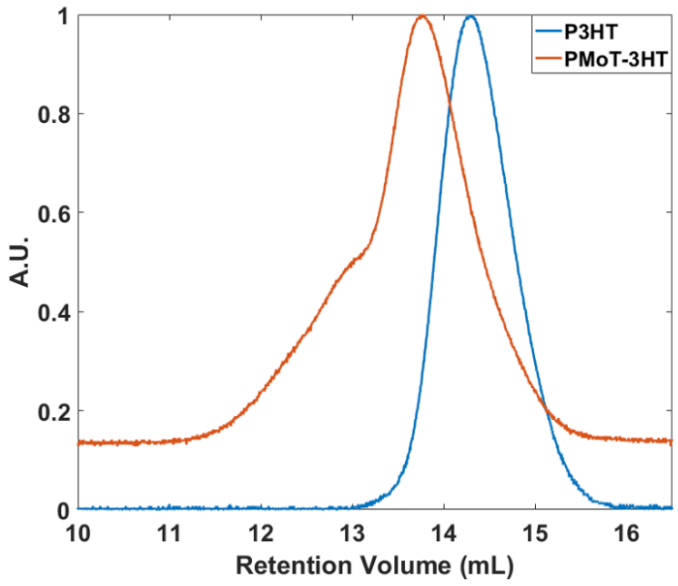

Figure 7.4 GPC traces of P3HT and PMoT-3HT.

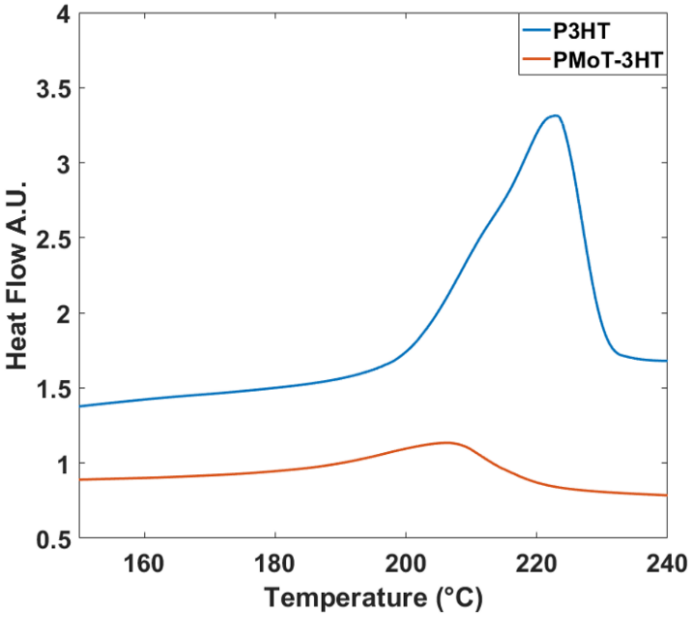

Figure 7.5 DSC thermograms of P3HT and PMoT-3HT.

Optoelectronic properties were investigated using UV/Vis spectroscopy (**Figure 7.6**) on spun cast, annealed films. The copolymer exhibits enhanced overall absorption compared to P3HT while its right band edge is essentially unchanged. The optical band gap and excitonic band widths are obtained using the Spano Model.[1] The Spano Model estimates optical band gap and other optoelectronic properties of semiconducting materials by modeling absorption from aggregates in the weak excitonic coupling regime by fitting Gaussian vibrational and absorption states in semiconductive thin films; Spano Model Equation shown in Equation 7.1.[7,30-34]

$$A \propto \left(\frac{e^{-S}S^m}{m!}\right)\left(1 - \frac{We^{-S}}{2E_p}\sum_{n\neq m}\frac{S^n}{n!(n-m)}\right) exp\left(-\frac{\left(E - E_{0-0} - mE_p - \frac{1}{2}WS^m e^{-S}\right)^2}{2\sigma^2}\right) \quad \textbf{(7.1)}$$

where *S* is the Huang-Rhys factor, m and n are vibrational states, *W* is the excitonic bandwidth, E_p is the energy of the C=C stretching mode, $E_{0\text{-}0}$ is the energy of the 0-0 transition, and σ is the Gaussian line width. The model was fit to the collected absorption data and the results for parameters of interest given in **Table 7.1**.

Table 7.1 Fitting parameters to UV-vis spectra of thin films (P3HT and PMoT-P3HT).

Polymer	*W* (meV)	$E_{0\text{-}0}$ (eV)	E_p (meV)	σ (meV)
P3HT	0.12	2.03	0.18	0.08
PMoT-P3HT	0.18	2.01	0.24	0.13

The optical band gap for the copolymer (PMoT-co-P3HT, 2.01 eV) is found to be similar to P3HT (P3HT, 2.03 eV) and the largest optoelectronic parameter differences being in the excitonic band width (PMoT-co-P3HT, 0.18 nm and P3HT, 0.12 nm) and stretching mode energy (PMoT-co-

P3HT, 0.223 eV and P3HT, 0.18 eV). Cyclic voltammetry was used to determine HOMO levels for PMoT-co-P3HT (-4.76 eV) and P3HT (-4.89 eV); shown in **Figure 7.7**.

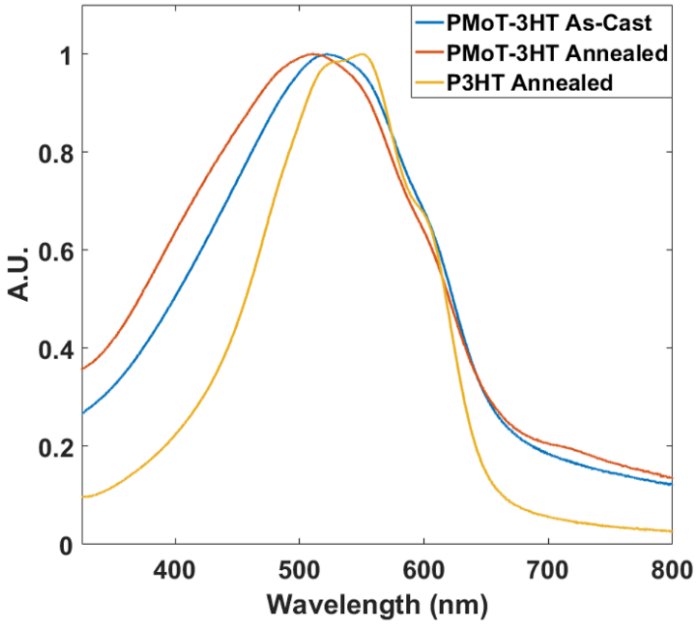

Figure 7.6 UV/Vis absorption spectra of PMoT-3HT and P3HT films.

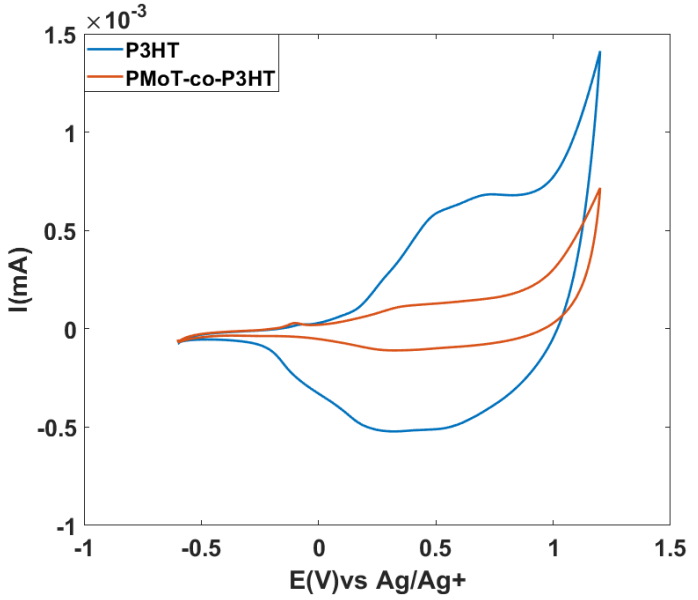

Figure 7.7 PMoT-*co*-P3HT vs P3HT cyclic voltammograms.

DFT electronic structure calculations were performed for P3HT and PMoT homo-oligomers. The correlation between HOMO-LUMO energy gap and oligomer chain length followed the asymptotic trend (**Figure 7.8**). A chain length of twelve monomeric units was sufficient to capture the experimental band gap of this study (**Table 7.2**). Additionally, using linear mixing rules and the HOMO-LUMO energy gap of the homo-oligomers P3HT and PMoT, the PMoT-co-P3HT oligomer is estimated to have a HOMO-LUMO energy gap equal to the experimental value. Similar analysis is performed for the HOMO energy level estimation for both homo-oligomers and extended to the co-oligomer using linear mixing rules (**Table 7.2**), which qualitatively follows the experimental trend between the P3HT homo-oligomer and the co-oligomer.

Copolymerization of PMoT with P3HT yielded a copolymer with wider absorption band edges and similar band gap energy. Despite the fact that both comonomers were 3-subsituted, PMoT-P3HT exhibited apparent depressed melting temperature and apparent crystallinity as evidenced in the DSC thermogram (**Figure 7.5**). Additionally, methoxy thiophene content in the initial reaction media did not result in a copolymer with similar composition. This proves problematic as synthesis of a statistical range of these copolymers would be very difficult as the resulting polymer compositions would likely be random and might overlap.

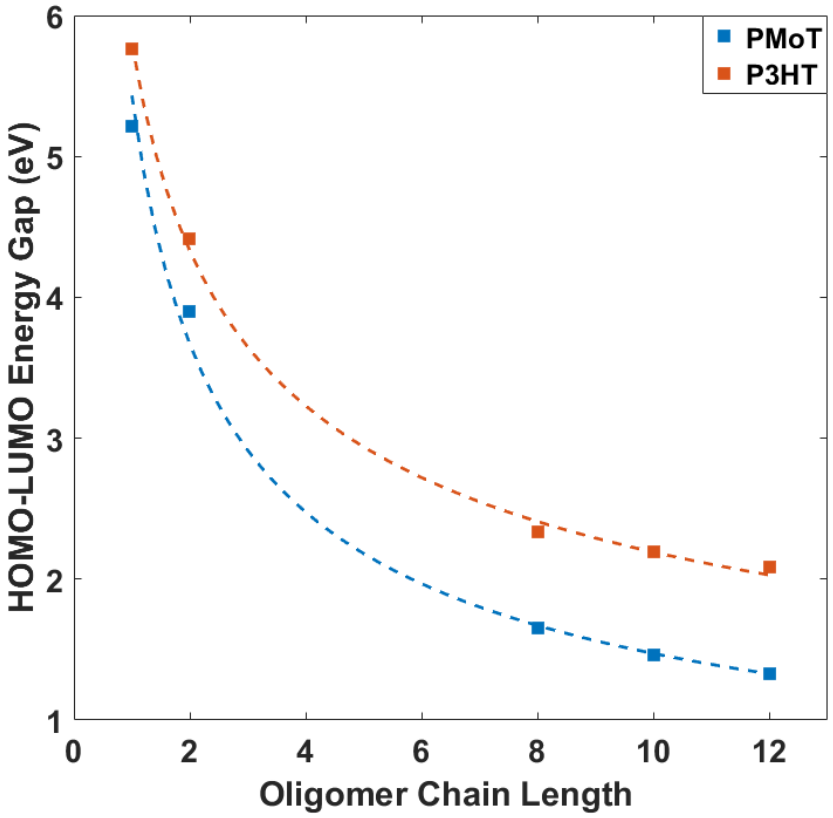

Figure 7.8 Calculated HOMO-LUMO energy gap as a function of oligomer chain length at the B3LYP/CEP-31G level of theory for P3HT and PMoT homo-oligomers.

Table 7.2 HOMO-LUMO energy gap and HOMO energy values experimental values from this study in parentheses.

	HOMO-LUMO energy gap[a] (eV)	**HOMO energy level[a] (eV)**
P3HT	2.08 (2.03)	-4.58 (-4.89)
PMoT	1.33 (NA)	-3.90 (NA)
PMoT-co-P3HT	2.01 (2.01)	-4.51 (-4.76)

[a]experimental values from this study in parentheses. NA denotes value is not available from this study due to inability to form films using solution processing.

7.4- Conclusions

3-methoxythiophene was synthesized and polymerized to form poly(3-methoxythiophene) and poly((3-methoxythiophene)-*co*-(3-hexylthiophene)) using Grignard Metathesis polymerization. PMoT was not soluble in common solvents, prohibiting many standard characterization techniques. However, PMoT-*co*-P3HT is fully soluble in common organic solvents due to the presence of the alkyl side chains on P3HT. PMoT-*co*-P3HT exhibited a slightly depressed but distinct melting transition confirming the copolymer to be semicrystalline and fairly high-melting. Optoelectronic properties were examined using UV/Vis spectroscopy, cyclic voltammetry and DFT modeling. PMoT-*co*-P3HT exhibits enhanced absorption compared to P3HT, similar optical band gaps and stretching mode energies but a lower exitonic band width and a lower HOMO level. DFT electronic structure calculations were found to predict very well the HOMO-LUMO energy gap of the both the P3HT homo-oligomer and PMoT-*co*-P3HT oligomer to within 0.05 eV or less of experimental values with comparable accuracy for the HOMO energy level prediction. Overall, copolymerization of PMoT with P3HT yielded a solution processable semiconducting polymer with comparable optoelectronic properties and enhanced overall absorption compared to the widely studied P3HT.

7.5- References

(1) Sheina, E. E.; Khersonsky, S. M.; Jones, E. G.; McCullough, R. D. Highly Conductive, Regioregular Alkoxy-Functionalized Polythiophenes: A New Class of Stable, Low Band Gap Materials. *Chem. Mater.* **2005**, *17*, 3317–3319.

(2) Barbarella, G.; Bongini, A.; Zambianchi, M. Regiochemistry and Conformation of Poly(3-Hexylthiophene) via the Synthesis and the Spectroscopic Characterization of the Model Configurational Triads. *Macromolecules* **1994**, *27*, 3039–3045.

(3) Yang, Y.-L.; Lee, Y.-H.; Lee, Y.-P.; Chiang, C.-J.; Shen, C.; Wu, C.-C.; Ohta, Y.; Yokozawa, T.; Dai, C.-A. Synthesis and Characterization of Poly(3-Hexylthiophene)-Poly(3-Hexyloxythiophene) Random Copolymers with Tunable Band Gap via Grignard Metathesis Polymerization. *Polym. Int.* **2014**, *63*, 2068–2075.

(4) Zhang, Z.-B.; Fujiki, M. Synthesis and Molecular Weight Dependent Optical Properties of Mono-Alkoxy Substituted Polythiophenes. *Polym J* **2001**, *33*, 597–601.

(5) Chang, A. C.; Blankespoor, R. L.; Miller, L. L. Characterization and Spectroelectrochemical Studies of Soluble Polymerized 3-Methoxythiophene. *J. Electroanal. Chem* **1987**, *236*, 239–252.

(6) Hu, X.; Xu, L. Structure and Properties of 3-Alkoxy Substituted Polythiophene Synthesized at Low Temperature. *J. Electroanal. Chem* **2000**, *41*, 9147–9154.

(7) Ho, V.; Beckingham, B. S.; Ng, H. H.; Segalman, R. A. Control of Thermal and Optoelectronic Properties in Conjugated Poly(3-Alkylthiophenes). *MRC* **2014**, *4*, 45–50.

(8) Somanathan, N.; Radhakrishnan, S.; Thelakkat, M.; Schmidt, H. W. Studies on 3-(2-Ethylhexyl)Thiophene Polymers. *Macromol. Mater. Eng.* **2002**, *287*, 236–238.

(9) Smith, Z. C.; Wright, Z. M.; Arnold, A. M.; Sauvé, G.; McCullough, R. D.; Sydlik, S. A. Increased Toughness and Excellent Electronic Properties in Regioregular Random Copolymers of 3-Alkylthiophenes and Thiophene. *Advanced Electronic Materials* **2016**, *3*, 1600316–1600319.

(10) Burkhart, B.; Khlyabich, P. P.; Thompson, B. C. Influence of the Ethylhexyl Side-Chain Content on the Open-Circuit Voltage in Rr-Poly(3-Hexylthiophene- Co-3-(2-Ethylhexyl)Thiophene) Copolymers. *Macromolecules* **2012**, *45*, 3740–3748.

(11) Xu, B.; Noh, S.; Thompson, B. C. Fine Tuning of Polymer Properties by Incorporating Strongly Electron-Donating 3-Hexyloxythiophene Units into Random and Semi-Random Copolymers. *Macromolecules* **2014**, *47*, 5029–5039.

(12) Hardeman, T.; Koeckelberghs, G. The Synthesis of Poly(Thiophene- Co-Fluorene) Gradient Copolymers. *Macromolecules* **2015**, *48*, 6987–6993.

(13) Matuszewska, A.; Uchman, M.; Adamczyk-Woźniak, A.; Sporzyński, A.; Pispas, S.; Kováčik, L.; Štěpánek, M. Glucose-Responsive Hybrid Nanoassemblies in Aqueous Solutions: Ordered Phenylboronic Acid Within Intermixed Poly(4-Hydroxystyrene)-Block-Poly(Ethylene Oxide) Block Copolymer. *Biomacromolecules* **2015**, *16*, 3731–3739.

(14) Beckingham, B. S.; Ho, V.; Segalman, R. A. Melting Behavior of Poly(3-(2′-Ethyl)Hexylthiophene). *Macromolecules* **2014**, *47*, 8305–8310.

(15) Boudouris, B. W.; Ho, V.; Jimison, L. H.; Toney, M. F.; Salleo, A.; Segalman, R. A. Real-Time Observation of Poly(3-Alkylthiophene) Crystallization and Correlation with Transient Optoelectronic Properties. *Macromolecules* **2011**, *44*, 6653–6658.

(16) Sivula, K.; Ball, Z. T.; Watanabe, N.; Fréchet, J. M. J. Amphiphilic Diblock Copolymer Compatibilizers and Their Effect on the Morphology and Performance of Polythiophene: Fullerene Solar Cells. *Adv. Mater.* **2006**, *18*, 206–210.
(17) Segalman, R. A.; McCulloch, B.; Kirmayer, S.; Urban, J. J. Block Copolymers for Organic Optoelectronics. *Macromolecules* **2009**, *42*, 9205–9216.
(18) Beckingham, B. S.; Ho, V.; Segalman, R. A. Formation of a Rigid Amorphous Fraction in Poly(3-(2′-Ethyl)Hexylthiophene). *ACS Macro Lett.* **2014**, *3*, 684–688.
(19) Davidson, E. C.; Beckingham, B. S.; Ho, V.; Segalman, R. A. Confined Crystallization in Lamellae Forming Poly(3-(2 '-Ethyl)Hexylthiophene) (P3EHT) Block Copolymers. *Journal of Polymer Science Part B: Polymer Physics* **2016**, *54*, 205–215.
(20) Minkler, M. J.; Beckingham, B. S. Statistical Copolymers of 3-Hexylthiophene and Thiophene Impact of Thiophene Content on Optoelectronic and Thermal Properties. *Materials Today Communications* **2019**, 100547.
(21) McCullough, R. D. The Chemistry of Conducting Polythiophenes. **1998**, *10*, 93–116.
(22) McCullough, R. D.; Lowe, R. D.; Jayaraman, M.; Anderson, D. L. Design, Synthesis, and Control of Conducting Polymer Architectures: Structurally Homogeneous Poly(3-Alkylthiophenes). *J. Org. Chem.* **1993**, *58*, 904–912.
(23) Frisch, M.J.; Trucks, G.W.; Schlegel, H.B.; Scuseria, G.E.; Robb, M.A.; Cheeseman, J.R.; Scalmani, G.; Barone, V.; Petersson, G.A.; Nakatsuji, H.; Li, X.; Caricato, M.; Marenich, A.V.; Bloino, J.; Janesko, B.G.; Gomperts, R.; Mennucci, B.; Hratchian, H.P.; Ortiz, J.V.; Izmaylov, A.F.; Sonnenberg, J.L.; Williams; Ding, F.; Lipparini, F.; Egidi, F.; Goings, J.; Peng, B.; Petrone, A.; Henderson, T.; Ranasinghe, D.; Zakrzewski, V.G.; Gao, J.; Rega, N.; Zheng, G.; Liang, W.; Hada, M.; Ehara, M.; Toyota, K.; Fukuda, R.; Hasegawa, J.; Ishida, M.; Nakajima, T.; Honda, Y.; Kitao, O.; Nakai, H.; Vreven, T.; Throssell, K.; Montgomery Jr., J.A.; Peralta, J.E.; Ogliaro, F.; Bearpark, M.J.; Heyd, J.J.; Brothers, E.N.; Kudin, K.N.; Staroverov, V.N.; Keith, T.A.; Kobayashi, R.; Normand, J.; Raghavachari, K.; Rendell, A.P.; Burant, J.C.; Iyengar, S.S.; Tomasi, J.; Cossi, M.; Millam, J.M.; Klene, M.; Adamo, C.; Cammi, R.; Ochterski, J.W.; Martin, R.L.; Morokuma, K.; Farkas, O.; Foresman, J.B.; Fox, D.J. *Gaussian 16 Rev. B.01*, Wallingford, CT, 2016.
(24) Al-anber, M. J.; Ali, A. M.; Al-Mailky, N. S.; World, A. A.-M. S.; 2013. Theoretical DFT Study the Opto-Electronic Properties of Poly (3, 4-Ethylenedioxythiophene).
(25) Choi, Y.; Adamczyk, A. J. Tuning Hydrogenated Silicon, Germanium, and SiGe Nanocluster Properties Using Theoretical Calculations and a Machine Learning Approach. *The Journal of Physical Chemistry A* **2018**.
(26) Ho, V.; Boudouris, B. W.; Segalman, R. A. Tuning Polythiophene Crystallization Through Systematic Side Chain Functionalization. *Macromolecules* **2010**, *43*, 7895–7899.
(27) Roesing, M.; Howell, J.; Boucher, D. Solubility Characteristics of Poly(3-Hexylthiophene). *Journal of Polymer Science Part B: Polymer Physics* **2017**, *55*, 1075–1087.
(28) Howell, J. S.; Boucher, D. S. Temperature Dependence of the Convex Solubility Parameters of Organic Semiconductors. *Journal of Polymer Science Part B: Polymer Physics* **2015**, *54*, 81–88.
(29) Johnson, C. E.; Boucher, D. S. Poly(3-Hexylthiophene) Aggregate Formation in Binary Solvent Mixtures: an Excitonic Coupling Analysis. *Journal of Polymer Science Part B: Polymer Physics* **2014**, *52*, 526–538.

(30) Murphy, A. R.; Fréchet, J. M. J.; Chang, P.; Lee, J.; Subramanian, V. Organic Thin Film Transistors From a Soluble Oligothiophene Derivative Containing Thermally Removable Solubilizing Groups. *Journal of the American Chemical Society* **2004**, *126*, 1596–1597.
(31) Son, S. Y.; Kim, J.-H.; Song, E.; Choi, K.; Lee, J.; Cho, K.; Kim, T.-S.; Park, T. Exploiting Π–Π Stacking for Stretchable Semiconducting Polymers. *Macromolecules* **2018**, *51*, 2572–2579.
(32) Spano, F. C. Modeling Disorder in Polymer Aggregates: The Optical Spectroscopy of Regioregular Poly(3-Hexylthiophene) Thin Films. *J. Chem. Phys.* **2005**, *122*, 234701–234715.
(33) Turner, S. T.; Pingel, P.; Steyrleuthner, R.; Crossland, E. J. W.; Ludwigs, S.; Neher, D. Quantitative Analysis of Bulk Heterojunction Films Using Linear Absorption Spectroscopy and Solar Cell Performance. *Adv. Funct. Mater.* **2011**, *21*, 4640–4652.
(34) Spano, F. C. Absorption in Regio-Regular Poly(3-Hexyl)Thiophene Thin Films: Fermi Resonances, Interband Coupling and Disorder. *Chemical Physics* **2006**, *325*, 22–35.

Chapter 8 - Compositional Drift Analysis of GRIM-Synthesized Copolymers

8.1- Introduction

Since their inception in the late 20th century, polythiophenes have garnered much interest for a wide variety of applications such as thin-film transistors, thermoelectric generators, and organic-based photovoltaics. 3-substituted polythiophene derivatives are widely studied due to their relatively facile synthetic methods and tunable material properties. Much of the focus has been on making subtle but distinct to the polythiophene microstructure via modification of the 3-position of thiophene monomer and subsequent polymerization steps. The substituent groups play a crucial role in many of the polythiophene properties such as optical band gaps, melting temperatures, and electronic properties.[1–6] While there are many methods to synthesize polythiophenes (such as Rieke synthesis, oxidative methods, Grignard Metathesis, and electropolymerization), they all have their own inherent advantages and drawbacks.[5,7,8] Grignard Metathesis polymerization (GRIM) has been shown to consistently produce polythiophenes with highly regioregular backbones at relatively mild conditions and at a reasonably large scale.[9–11] Though the method of GRIM is well documented and explained in literature, many aspects of the underlying mechanisms remain elusive for this polymerization technique. Many (most) researchers thoroughly characterize thiophene monomers and the resulting polymers but little to no work has been performed examining the down-chain composition of thiophene copolymer chains.[3,4,8,10–16]

As discussed in **Chapter 6**, one critical aspect of thiophene copolymers is the overall chain regioregularity. In general, GRIM polymerized 3-subsituted polythiophenes are highly regioregular due to the steric hindrance of the 2-position presented by the substituent group. Less explored however, is the effect of 3-substituent groups on the reactivity ratios of various thiophene monomers. Scarce, if any, research has been performed on polythiophene statistical copolymer

kinetics. This is likely due to the fact that the standard monomer concentration used in GRIM synthesis is very dilute compared to other systems and it is often very difficult to distinguish between thiophene variants, especially at such low concentrations. These factors greatly complicate tracking of GRIM-synthesis copolymers during polymerization.

There are two methods involving aliquots that can be used to track the reaction progress of these polymer systems and they are as follows. The first method is to monitor monomer content by drawing aliquots from the active reaction media over time. This method is difficult for thiophene copolymers and great care needs to be taken as the monomer concentration is on the order of 10^{-1} mol/L for each monomer. It is also important for the polymer formed at each point in the reaction to be either extracted or allowed to settle to the bottom of the aliquot vessel as the monomer and polymer signatures of interest during characterization by ^{1}H NMR are overlapping. Another drawback of this method is you must assume that the supernatant is well-mixed when drawn and must have an internal standard for comparing across aliquots. This internal standard can be the solvent, however THF (the typical solvent) is very volatile such that the assumption of constant relative THF content is tenuous at best. The second method is to analyze the polymer composition as a function of reaction time. This method is more straight-forward as the polymer in each aliquot can be precipitated, purified, and analyzed quantitatively without an internal standard. It should be noted that it is important to not completely purify the polymer as obtaining a holistic representation of the polymer formed at each step is critically important for accurate characterization. In other words, during removal of the Grignard salts, care should be taken to not remove any of the smaller molecular weight polymer present as these should also contribute to the observed compositional drift.

Accurate characterization of composition along the backbone of polythiophenes is critical as even copolymers with similar compositions can yield different material properties as discussed in **Chapter 2**. In addition to this, many thiophene copolymers are described as random copolymers and this is likely inaccurate for GRIM synthesized copolymers which instead form statistical copolymers, especially in the case of 3-substituted thiophenes.[1,11,17]

The most synonymous work to this is by Iovu et al. in which they sought to determine the exact nature of GRIM synthesis through tracking of homopolymerization kinetics.[18] In their work, they determined that initial monomer concentration and catalyst concentration both affect the consumption rate of 3-hexylthiophene. Importantly, for the two lower concentrations (0.02 and 0.04 mol/L, the conversion never approaches 100% even for a "high" concentration (0.08 mol/L) and an extended reaction time of up to nearly 3 hours.[18] This is critical as often in copolymerizations, the total monomer concentration is kept to that of the literature values for homopolymers; constituting lowered concentrations for minority constituent comonomers. In addition to this, comonomer functionality and microstructure likely also play a role in the ability of a monomer to add on to a chain. We anticipate that the addition of unsubstituted thiophene at least partially randomizes the reaction kinetics as the lack of any substituents yields a monomer with equally reactive sites; and would expect the same for other symmetrically 3- and 4-substituted thiophene monomers such as 3,4-ethylenedioxythiophene. This notion of random versus statistical copolymerization of thiophene comonomers is important as it could be the underlying reason for the differences observed between copolymers of similar composition.

8.2- Results and Discussion

We elected to investigate a variety of thiophene copolymer systems to characterize the effect of thiophene 3-substitutent groups on the relative reactivities. These systems include copolymers of

3EHT, 3HT, 3MoT, and unsubstituted thiophene. We first examined the supernatant of aliquots drawn from a 3EHT-3HT copolymer with initial reactor charge of 40 mole % 3HT and 60 mole % 3EHT. Reaction conditions were performed as detailed in **Chapter 3** (according to literature) and aliquots were drawn at various timepoints throughout the reaction.[5,6] Aliquots of 1 mL were drawn at various time points during GRIM synthesis and quenched into 4 mL of MeOH doped with 1-2 drops of 6 M HCl. The results are shown in **Figure 8.1** and were plotted against the Beckingham-Sanoja-Lynd (BSL) model; equations 8.1 and 8.2.[19] In the BSL model, p_i represents the conversion of monomer species "i", n_i represents initial concentration of monomer "*i*", and r_i represents the reactivity ratio of monomer species "i". The BSL model was selected as we anticipate that the reactivity of the nickel-complexed intermediate formed during GRIM synthesis propagation is dependent only on the chemistry of the approaching monomer, effectively negating any effect of the already-formed chain composition.[19]

$$p_{ab}(p_a) = 1 - n_a(1 - p_a) - (1 - n_a)(1 - p_a)^{r_b} \tag{8.1}$$

$$p_{ab}(p_b) = 1 - n_a(1 - p_b)^{r_a} - (1 - n_a)(1 - p_b) \tag{8.2}$$

As is shown in **Figure 8.1a**, the monomer conversion tapers off around 80% and 45 mins, similar to that of Iovu et al. for homopolymer P3HT.[18] Additionally, we note the monomer that is in higher concentration (3EHT) is preferentially consumed by the reaction; **Figure 8.1b**. It is also apparent that after sufficient monomer conversion, the relative monomer consumption approaches the random line (**Figure 8.1b**); likely due to the concentration limitations observed by Iovu et al. for homopolymer P3HT.[18] This suggests that the relative concentration of each monomer plays a role in their respective rates of addition, as demonstrated in the same work by Iovu et al..[18] Preparation and analysis of this data was quite cumbersome and required a great deal of time and effort so to

address this we decided to repeat with similar experiments using the produced polymer at each time point instead. More specifically, the similarity of monomer chemistries and very low concentration of each monomer in the supernatant, accurate detection is very difficult.

Next, we analyzed the forming polymer during each time point for a complimentary system, 70/30 3HT/3EHT; shown in **Figure 8.2**. Similar to the data shown in **Figure 8.1**, the composition of the polymers begins to shift towards (3EHT) until a sort of equilibrium was reached (~64 mole % 3HT). This suggests that 3EHT may be more reactive than 3HT as it is the minority constituent in this reaction setup. It should be noted that there is a significant time gap between the third and fourth data points in **Figure 8.2**, this gap is a result of the COVID-19 pandemic interrupting workflow. The aliquots necessary to fill in this gap were taken and just require work up via NMR spectroscopy and GPC. The selected data points were taken to gain a preliminary snapshot of the polymer composition evolution over the course of the entire (extended) reaction. This particular experiment, and a few others that were not presented here, were extended out to 2 hours to gather additional data points at essentially depleted reactive monomer concentrations in the reaction media.

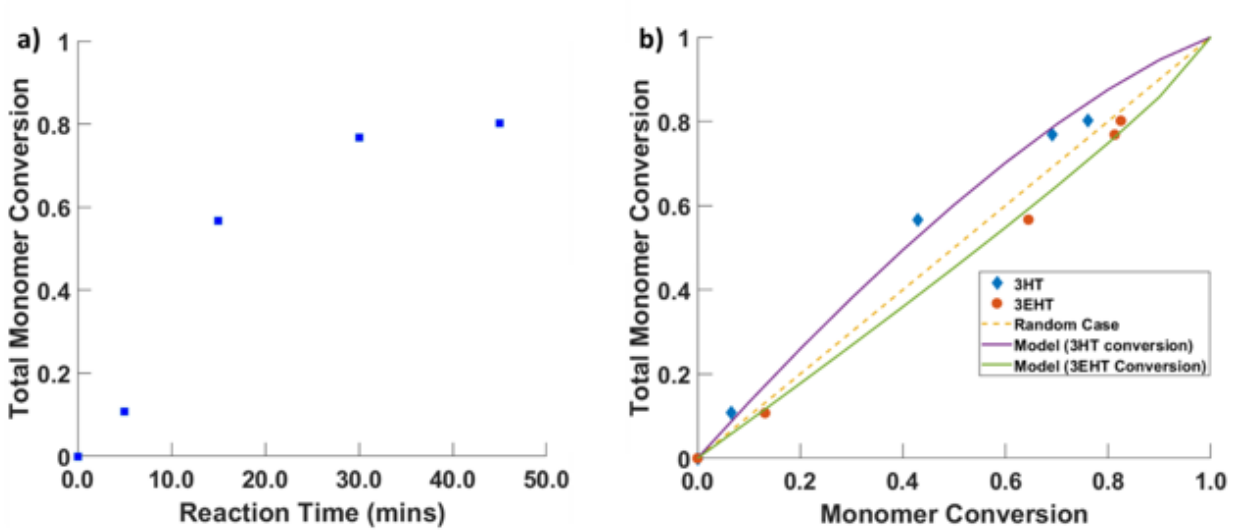

Figure 8.1 a) Total monomer conversion and b) individualized conversion for 3EHT and 3HT.

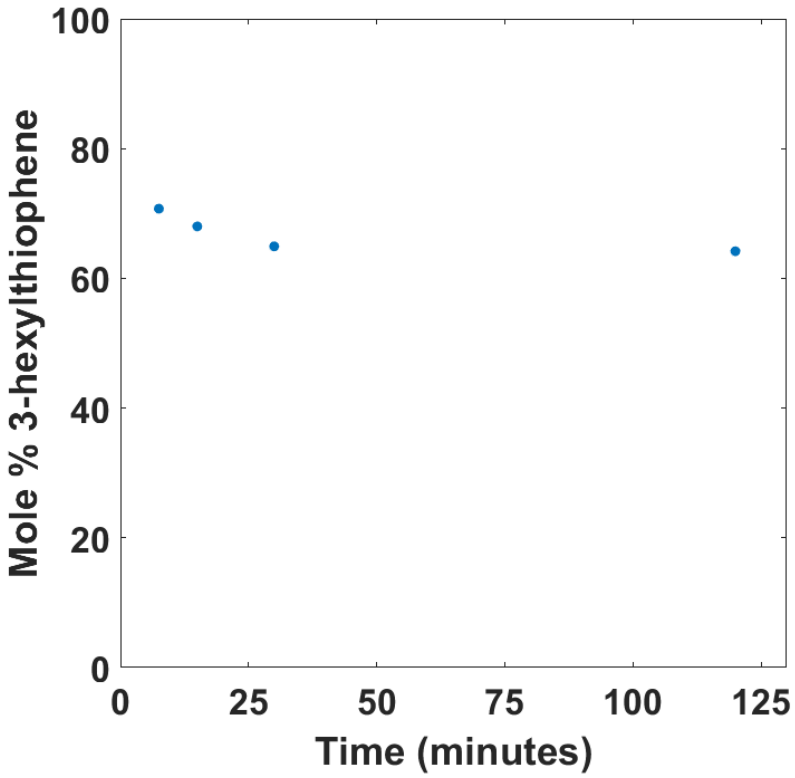

Figure 8.2 Polymer composition as a function of time for 70/30 3HT/EHT charge.

The data presented in **Figure 8.1** and **Figure 8.2** illustrate that perhaps the 3EHT dominance was exaggerated in the first experiment by its concentration. Following the interesting results from the 3EHT/3HT copolymerizations, we investigated the compositional drift of polymers formed during GRIM polymerization for a 3HT-unsubsituted thiophene copolymer, namely the 74HT copolymer from **Chapter 6**. This polymer was selected as a matter of timing, it was one of the last of the P3HT-co-T statistical copolymers to be synthesized (around the same point in time we decided to investigate reactivity ratios).[5] The results of the compositional drift are shown in **Figure 8.3**. Similar to the behavior observed in **Figure 8.2**, the minority constituent (unsubstituted thiophene) is consumed at a much higher rate than the majority constituent initially. The observed exaggerated behavior is likely due, in part, to the ability of unsubstituted thiophene to facilitate multiple reaction sites as discussed in **Chapter 6** and our published work.[5] It should be noted that **Figure 8.2** and **Figure 8.3** would be more complete with polymer molecular weight as this would also allow for the extraction of monomer conversion and subsequently, reactivity ratios. This additional data is discussed in the next section, Section 8.3.

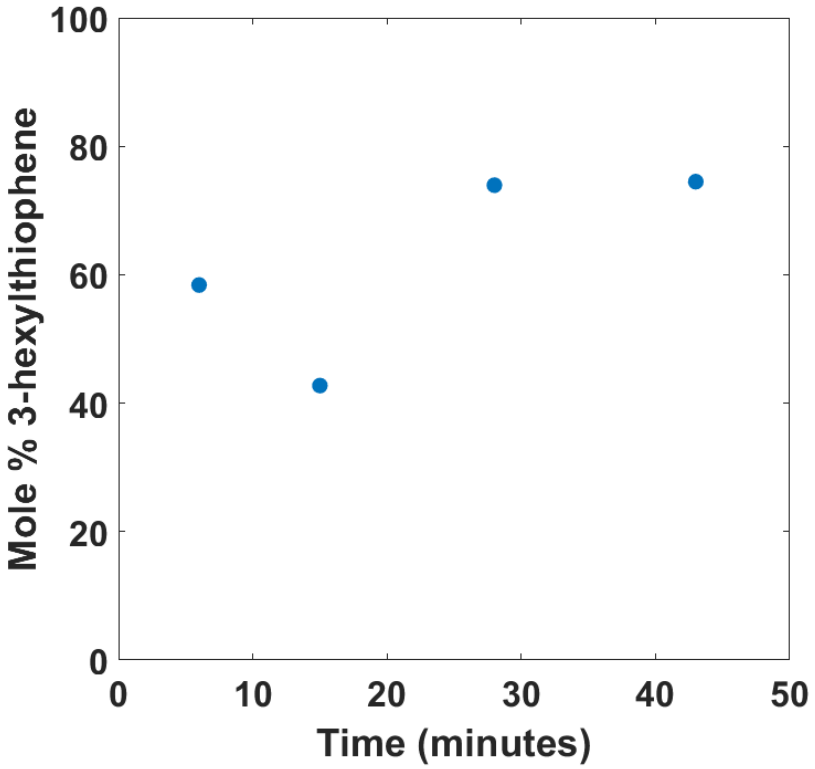

Figure 8.3 Compositional drift for GRIM polymerization of 3HT and unsubstituted thiophene.

8.3- Experiments Delayed Due to the COVID-19 Pandemic

As noted in **Chapter 6**, the global COVID-19 pandemic has set back many aspects of finalizing my research and inhibited certain critical experiments that would allow for a more complete picture of the works detailed within this document. I have prepared and was in preparation of several experiments to more completely finish the work described within this chapter. The remaining experiments to be performed upon a return to some sense of normalcy are detailed in **Table 8.1**.

Table 8.1 Pertinent experiments delayed by COVID-19 for compositional drift analysis.

Experiment	Copolymer	Reason
NMR Spectroscopy	70/30 3EHT/3HT 70/30 3EHT/T 70/30 3HT/3MoT	Track Copolymer Composition
Gel-Permeation Chromatography	All Systems	Track Copolymer Molecular Weight

I would like to note that the synthesis for all of the copolymer systems listed here have already been performed and the aliquots stored at 5-7 °C in MeOH. I find it pertinent to also note that additional data points of the 70/30 3HT/3EHT and 74HT systems should be collected to fill in the gaps between the data points shown in **Figure 8.2** and **Figure 8.3**.

I expect to find that the relative reactivity of each monomer discussed within this chapter will be highly dependent on three aspects of monomer chemistries (in decreasing order of importance): relative comonomer concentration, sterics, and dipole moment of intermediate complexes. I expect relative monomer concentration to play the largest role as a monomer with significantly higher concentration is naturally more accessible to the propagating chain. If additional syntheses are performed, the relative initial comonomer concentrations should be close to 50/50 to highlight the

effects of sterics and complexed monomer dipole moments during the GRIM synthesis halogen dance mechanism.

8.4- Conclusions

Through analysis of the manner in which monomers are added to the growing polymer chains, a better understanding of the relationship between initial reaction charge and resulting copolymer composition can be gained. This aspect of polythiophene chemistry is critical for high-performance device fabrication as many of the copolymer properties are dependent upon the polymer backbone composition and architecture. It is also clear that, according to the data presented here, copolymerization of thiophene monomers is not random. Determination of the exact nature of comonomer propagation will prove to be a useful tool for the design and fabrication of organic-based electronics with specific functions and properties.

8.5- References

(1) Howard, J. B.; Thompson, B. C. Design of Random and Semi-Random Conjugated Polymers for Organic Solar Cells. *Macromolecular Chemistry and Physics* **2017**, *218* (21), 1700255. https://doi.org/10.1002/macp.201700255.

(2) Wu, P.-T.; Ren, G.; Jenekhe, S. A. Crystalline Random Conjugated Copolymers with Multiple Side Chains: Tunable Intermolecular Interactions and Enhanced Charge Transport and Photovoltaic Properties. *Macromolecules* **2010**, *43* (7), 3306–3313. https://doi.org/10.1021/ma100006x.

(3) Yang, Y.-L.; Lee, Y.-H.; Lee, Y.-P.; Chiang, C.-J.; Shen, C.; Wu, C.-C.; Ohta, Y.; Yokozawa, T.; Dai, C.-A. Synthesis and Characterization of Poly(3-Hexylthiophene)–Poly(3-Hexyloxythiophene) Random Copolymers with Tunable Band Gap via Grignard Metathesis Polymerization. *Polymer International* **2014**, *63* (12), 2068–2075. https://doi.org/10.1002/pi.4744.

(4) Smith, Z. C.; Wright, Z. M.; Arnold, A. M.; Sauvé, G.; McCullough, R. D.; Sydlik, S. A. Increased Toughness and Excellent Electronic Properties in Regioregular Random Copolymers of 3-Alkylthiophenes and Thiophene. *Advanced Electronic Materials* **2017**, *3* (1), 1600316. https://doi.org/10.1002/aelm.201600316.

(5) Minkler, M. J.; Beckingham, B. S. Statistical Copolymers of 3-Hexylthiophene and Thiophene: Impact of Thiophene Content on Optoelectronic and Thermal Properties. *Materials Today Communications* **2019**, 100547. https://doi.org/10.1016/j.mtcomm.2019.100547.

(6) Minkler, M. J.; Kim, J.; Lawson, K. E.; Ali, A.; Zhao, R.; Adamczyk, A. J.; Beckingham, B. S. Solution Processible Statistical Poly(3-Methoxythiophene)-Co-Poly(3-Hexylthiophene) Copolymer. *Materials Letters* **2019**, *256*, 126563. https://doi.org/10.1016/j.matlet.2019.126563.

(7) Chen, T.-A.; Wu, X.; Rieke, R. D. Regiocontrolled Synthesis of Poly(3-Alkylthiophenes) Mediated by Rieke Zinc: Their Characterization and Solid-State Properties. *J. Am. Chem. Soc.* **1995**, *117* (1), 233–244. https://doi.org/10.1021/ja00106a027.

(8) Hong, X.; Tyson, J. C.; Middlecoff, J. S.; Collard, D. M. Synthesis and Oxidative Polymerization of Semifluoroalkyl-Substituted Thiophenes. *Macromolecules* **1999**, *32* (13), 4232–4239. https://doi.org/10.1021/ma9900030.

(9) McCullough, R. D.; Lowe, R. D.; Jayaraman, M.; Anderson, D. L. Design, Synthesis, and Control of Conducting Polymer Architectures: Structurally Homogeneous Poly(3-Alkylthiophenes). *J. Org. Chem.* **1993**, *58* (4), 904–912. https://doi.org/10.1021/jo00056a024.

(10) Loewe, R. S.; Ewbank, P. C.; Liu, J.; Zhai, L.; McCullough, R. D. Regioregular, Head-to-Tail Coupled Poly(3-Alkylthiophenes) Made Easy by the GRIM Method: Investigation of the Reaction and the Origin of Regioselectivity. *Macromolecules* **2001**, *34* (13), 4324–4333. https://doi.org/10.1021/ma001677+.

(11) Ouhib, F.; Khoukh, A.; Ledeuil, J.-B.; Martinez, H.; Desbrières, J.; Dagron-Lartigau, C. Diblock and Random Donor/Acceptor "Double Cable" Polythiophene Copolymers *via* the GRIM Method. *Macromolecules* **2008**, *41* (24), 9736–9743. https://doi.org/10.1021/ma801934g.

(12) Hundt, N.; Hoang, Q.; Nguyen, H.; Sista, P.; Hao, J.; Servello, J.; Palaniappan, K.; Alemseghed, M.; Biewer, M. C.; Stefan, M. C. Synthesis and Characterization of a Block

Copolymer Containing Regioregular Poly(3-Hexylthiophene) and Poly(γ-Benzyl-L-Glutamate). *Macromolecular Rapid Communications* **2011**, *32* (3), 302–308. https://doi.org/10.1002/marc.201000502.
(13) McCullough, R.; Liu, J.; Ewbank, P.; Sheina, E. Polythiophenes, Block Copolymers Made Therefrom, and Methods of Forming the Same. US20050187370A1, August 25, 2005.
(14) Al-Ibrahim, M.; Roth, H.-K.; Schroedner, M.; Konkin, A.; Zhokhavets, U.; Gobsch, G.; Scharff, P.; Sensfuss, S. The Influence of the Optoelectronic Properties of Poly(3-Alkylthiophenes) on the Device Parameters in Flexible Polymer Solar Cells. *Organic Electronics* **2005**, *6* (2), 65–77. https://doi.org/10.1016/j.orgel.2005.02.004.
(15) Beckingham, B. S.; Ho, V.; Segalman, R. A. Melting Behavior of Poly(3-(2′-Ethyl)Hexylthiophene). *Macromolecules* **2014**, *47* (23), 8305–8310. https://doi.org/10.1021/ma501915v.
(16) Barbarella, G.; Bongini, A.; Zambianchi, M. Regiochemistry and Conformation of Poly(3-Hexylthiophene) via the Synthesis and the Spectroscopic Characterization of the Model Configurational Triads. *Macromolecules* **1994**, *27* (11), 3039–3045. https://doi.org/10.1021/ma00089a022.
(17) Khlyabich, P. P.; Burkhart, B.; Ng, C. F.; Thompson, B. C. Efficient Solar Cells from Semi-Random P3HT Analogues Incorporating Diketopyrrolopyrrole. *Macromolecules* **2011**, *44* (13), 5079–5084. https://doi.org/10.1021/ma2009386.
(18) Iovu, M. C.; Sheina, E. E.; Gil, R. R.; McCullough, R. D. Experimental Evidence for the Quasi-"Living" Nature of the Grignard Metathesis Method for the Synthesis of Regioregular Poly(3-Alkylthiophenes). *Macromolecules* **2005**, *38* (21), 8649–8656. https://doi.org/10.1021/ma051122k.
(19) Beckingham, B. S.; Sanoja, G. E.; Lynd, N. A. Simple and Accurate Determination of Reactivity Ratios Using a Nonterminal Model of Chain Copolymerization. *Macromolecules* **2015**, *48* (19), 6922–6930. https://doi.org/10.1021/acs.macromol.5b01631.

Chapter 9 - Curing Kinetics of Thiol Crosslinked PEOD/DGEBA Copolymers

Reproduced in part with permission from Xinyu Hou, Nima Alizadeh, Maria Auad, Anton K. Schindler, Lauren E. Beckingham, and Bryan S. Beckingham.
Submitted to Polymer, In Review.

9.1 - Introduction

Hydraulic fracturing and other enhanced oil recovery techniques have enabled increased production of domestic petroleum resources by enabling their recovery from deposits deep within the earth. Unfortunately, leakage of brine, hydrocarbons, or other injected components through both operational and abandoned wellbores poses a risk to overlying resources, including drinking water, and the health of humans and surface environments.[1–3] Problems with wellbore integrity occur primarily due to material performance failure over wellbore lifetime, improper installation, or due to environmental response and leakage pathways can develop through both plugged and operational wellbores.[4–6] Of particular interest recently is evolution of these leakage pathways in CO_2-rich subsurface regions including, CO_2-sequestration wells, or CO_2-enhanced oil-recovery scenarios due to the acidification of the subsurface brine.[2,3,7,8] In order to prevent these undesirable leakage events, environmentally stable cements or remediating sealants that can be effectively deployed into crevices of fractured wellbores are critical.[2,9–14] Traditional materials such as cement-based slurries are easily deployed through squeeze cementing operations, however, the inherent particulate size of conventional cements (10-200 microns) can be problematic to effectively seal fractures that occur in the wellbore walls.[15,16] This has led to the need to investigate materials, such as polymers, which can infiltrate and fill fracture crevices to completely seal off the potential leakage site.[14,17–20]

Crosslinked polymer networks present one potential opportunity for in-field deployable wellbore-fracture sealants with tunable properties that include particle sizes, crosslink densities, and curing

kinetics. Network precursors can be injected into the leakage pathways and then solidify in-place. The properties of crosslinked polymer networks can be tuned by altering the constituents of the network such as the crosslinker and the various monomers/polymers used in the architecture of the network.[21–36] For instance, crosslink density and glass transition temperature can widely be tuned through judicious choice of the selected polymer network constituents; as monomers of greater molecular weight (macromers) generally decrease the crosslinking density while enhancing flexibility. Additionally, by varying crosslinking density the curing reaction rate can be manipulated by either concentrating the reaction sites or more sparsely scattering them within the material.[1,7,13,16–19] Epoxide-based polymer systems are one class of commonly available resins implemented as crosslinked polymer networks in paints, adhesives, sealants and a wide variety of other products. As many epoxy-based polymer systems require more than one component which must be mixed immediately prior to use, they are useful due to their long shelf-life without unwanted reaction. Depending on the chemical nature of the resin system, the resin set-times, stiffness, and environmental stability will vary. Additionally, epoxide-based resins are fairly low viscosity fluids facilitating pumping into subsurface wellbore leakage pathways; which offers a key advantage over particle- or slurry-based sealing techniques.[1,14,18,37–39]

In this work, we evaluate the curing kinetics and physical properties of a copolymer resin consisting of poly(ethylene glycol) (400 Mn) diglycidyl ether (PEOD) and bisphenol-A diglycidyl ether (DGEBA). DGEBA-based copolymer systems have been shown to demonstrate the aforementioned desirable properties of tunable cure kinetics and readily apparent differences in the material properties directly dependent on the presence of a comonomer or lack thereof.[22,40,41] DGEBA is commonly copolymerized with a functionally reactive, small molecular weight polymer to vary the stiffness and glass transition temperature; as DGEBA-only polymer systems

are stiff and have relatively high glass transition temperatures (T_gs). Herein, we use a short chain polyether (PEOD) as the comonomer to provide flexibility while also tuning the curing reaction kinetics. Curing kinetics are examined through both isothermal and dynamic differential scanning calorimetry (DSC) experiments which mimic the thermal conditions and thereby curing behavior for storage, injection and stable subsurface scenarios.

9.2 - Experimental Methods

Materials. Bisphenol-A diglycidyl ether (DGEBA) was purchased from Alfa Aesar. Poly(ethylene glycol) (400) diglycidyl ether (PEOD) was purchased from Sigma Aldrich. Pentaerythritol tetra(3-mercaptopropionate) (4SH) was purchased from TCI America. 4-(dimethylamino)pyridine (DMAP) was purchased from EMD Millipore. All chemicals were used as received.

Sample Preparation. Two systems were investigated with varied relative amounts of PEOD and DGEBA denoted as 10P for 10 mole % PEOD (90 mole % DGEBA) and 40P for 40 mole % PEOD (60 mole % DGEBA). Requisite quantities of DGEBA (10P: 3.16 g, 9.28 mmol) and PEOD (10P: 0.50 g, 1.25 mmol) were successively added to a scintillation vial. In a separate scintillation vial, DMAP (0.06 g, 0.49 mmol) and 4SH (2.35 g, 4.81 mmol) were mixed and agitated via manual stirring with a spatula until DMAP dissolved. It should be noted that the molar ratio of DMAP to reactants was kept constant, but DMAP is observably less soluble in DGEBA and therefore did not fully solvate in systems with relatively high DGEBA content. Following solvation of DMAP in 4SH, the solution was quickly added to the PEOD/DGEBA mixture. The reaction media was vigorously stirred until a homogeneous mixture was observed. A sample of the mixture (~10 mg) was the transferred to a pre-weighed TA Tzero DSC pan. The pan was quickly capped and quenched in liquid nitrogen to halt the reaction. Following liquid nitrogen quenching, the pan was reweighed and placed into the DSC (TA Instruments DSC Q20) for testing.

Bulk solid films of the polymer systems were also synthesized between two glass plates (6”x6”) separated by a Viton rubber spacer. PEOD, DGEBA, 4SH, and DMAP were weighed and mixed in a similar fashion to the aforementioned DSC preparation. Following mixing of the reaction media, the uncured mixture was quickly poured into the Viton spacer-glass plate setup (the gap between the plates was oriented vertically) for curing.

Isothermal Cure Kinetics. A typical isothermal curing experiment consisted of the aforementioned sample preparation followed by a thermal sequence in which the DSC cell was held at a desired temperature (19, 25, 45, and 55 °C). Prior to the placement of the sample pan into the DSC, the DSC was equilibrated at the desired isothermal temperature to eliminate any equilibration effects. For the first run at each temperature this hold was at least five hours to allow for determination of total cure time at a given temperature. The hold times of successive replicates at each temperature were shortened based on the first run kinetics. Following isothermal curing, the sample was (at 10 °C/min) cooled to -50 °C and then heated to 100 °C to allow for the extraction of the residual heat of reaction, if any.

Non-isothermal Cure Kinetics. Following the sample preparation procedure mentioned above, the sample was subjected to non-isothermal cure conditions. Prior to the placement of the sample pan into the DSC, the DSC was equilibrated at 40 °C. The sample was then heated at different rates (1, 3, 5, and 7 °C/min) to a sufficiently high temperature (typically ~150 °C).

Rheology. An AR-G2 TA Universal Rheometer with parallel-plate geometry (40 mm steel plate) was used to measure the viscosity of initial monomer mixtures (excluding the crosslinking agent and catalyst) at varied shear rates and composition. Steady-state flow tests were performed at 25 ^{o}C within 1-150 s^{-1} shear rates.

Dynamic Mechanical Analysis. Dynamic mechanical analysis (DMA) was performed using a TA Instruments RSA 3 dynamic mechanical analyzer in temperature sweep mode. Samples were cut into rectangular sections and stored in scintillation vials. The DMA experiment was performed from -50 °C to 50 °C at a ramp rate of 5-10 °C/min. The tan delta damping factor was extracted from the resulting DMA plots and were used to compare the glass transition temperature (T_g) of the polymer systems; In this work, the extracted T_g's were taken as the tan delta curve apex temperature.

9.3 - Results and Discussion

Here, we utilize a tetrathiol crosslinker, a reaction promoter (DMAP), and two chosen monomers (PEOD and DGEBA) which are statistically varied to tune reaction cure kinetics and the resulting material properties; structures shown in **Figure 9.1a**. We examine two systems based on the composition of monomer (PEOD and DGEBA) named for the percentage of PEOD that constitutes the monomer; 10P and 40P for 10% PEOD and 40% PEOD, respectively. In order to examine the curing behavior of the proposed PEOD/DGEBA wellbore sealant, differential scanning calorimetry experiments were performed to monitor the curing reaction kinetics. Two modes of curing were examined (isothermal and non-isothermal) and are designed to emulate common thermal conditions that would be encountered upon application as wellbores sealants. As shown in **Figure 9.1b**, the injected sealant media will travel down the shaft of the well and encounter a thermal gradient that will impact the curing behavior and ultimately the ability of the sealant to penetrate and seal small fractures. Isothermal curing experiments mimic rapid injection into a thermally stable subsurface as well as the system stability after mixing at varied surface temperatures. Alternatively, non-isothermal curing experiments mimic comparatively slow injection.

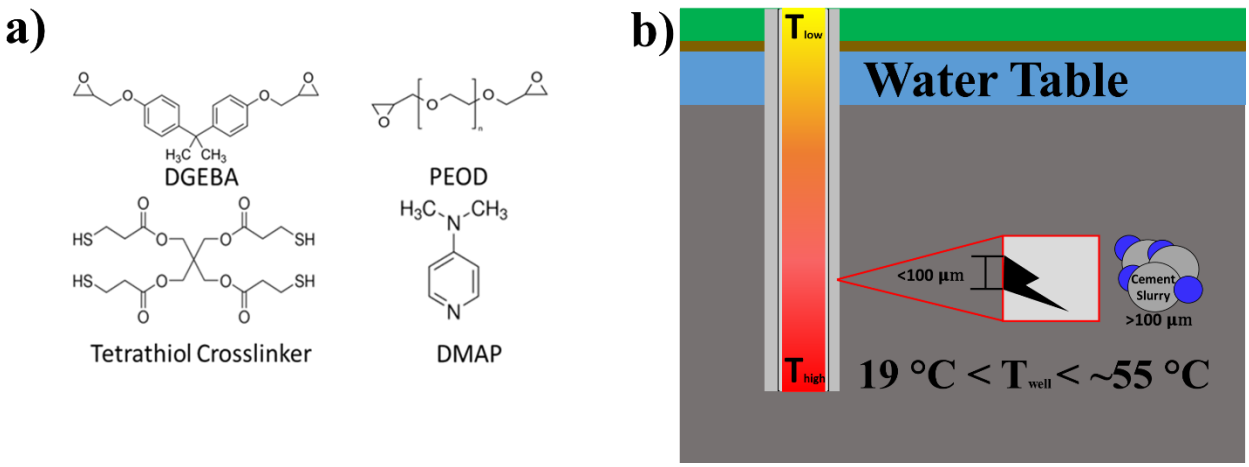

Figure 9.1 a) Representative visualization for sealant application and b) chemical structures of epoxy system components.

To visualize the curing process, the 40P polymer system was cured at room temperature (19-22 °C) and successive photographs taken until the polymer solution solidified (**Figure 9.2**). The initial reaction solution was viscous due to the presence of DGEBA, but remained fluid until around 50 minutes of cure time; at which time the reaction mixture lost all fluidity and stuck to the bottom of the scintillation vial. This process is expedited for reaction mixtures containing higher amounts of DGEBA as the higher reaction site density accelerates the curing process. The drawback to higher amounts of DGEBA with regards to application in the field is a faster cure rate combined with higher viscosity might prevent the reaction mixture from penetrating the necessary depth into a fracture prior to solidification.

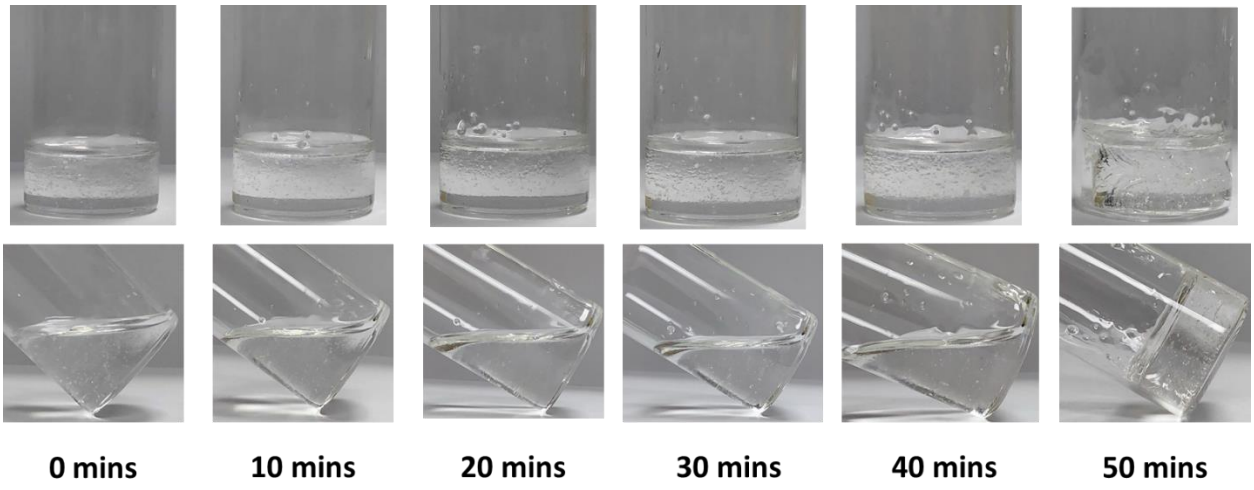

Figure 9.2 Visualized reaction progress for 40P at ~19-22 °C (room temperature).

9.3.1 - Isothermal Cure Kinetics

Isothermal DSC experiments were performed to determine the effect of temperature and mixture composition on the curing reaction kinetics. **Figure 9.3** displays the resulting thermograms and extracted degree of cure determined using Equation 9.1.

$$\alpha = \frac{H(t) - H_{Residual}}{H_{Total}} \tag{9.1}$$

where *H(t)* is the total enthalpy evolved at a given time, H_{Total} is the total enthalpy evolved during the isothermal hold, and $H_{Residual}$ is the residual heat of reaction observed during the thermal sweep succeeding isothermal curing. The reagents in this work react without any external driving force; however, the addition of energy in the form of heat has been demonstrated to alter curing kinetics of other similar systems.[23-25] The isothermal curing enthalpy peak times and total enthalpy evolution during curing (H_T) are shown in **Table 9.1** for each of the four isothermal curing temperatures.

Table 9.1 Isothermal curing peak times and enthalpy evolved

Polymer[a]	**Isothermal Peak Cure Time (mins), [H_{Total} (J/g)]**			
	19 °C	**25 °C**	**45 °C**	**55 °C**
40P	293 ± 65 [223 ± 13]	145 ± 23 [294 ± 42]	38 ± 11 [260 ± 47]	15 ± 2 [204 ± 26]
10P	144 ± 46 [364 ± 3]	90 ± 16 [330 ± 23]	25 ± 3 [312 ± 44]	6 ± 1 [387 ± 31]

[a]Number represents the mole percent PEOD of total monomer in initial reaction media; makeup percentage is DGEBA.

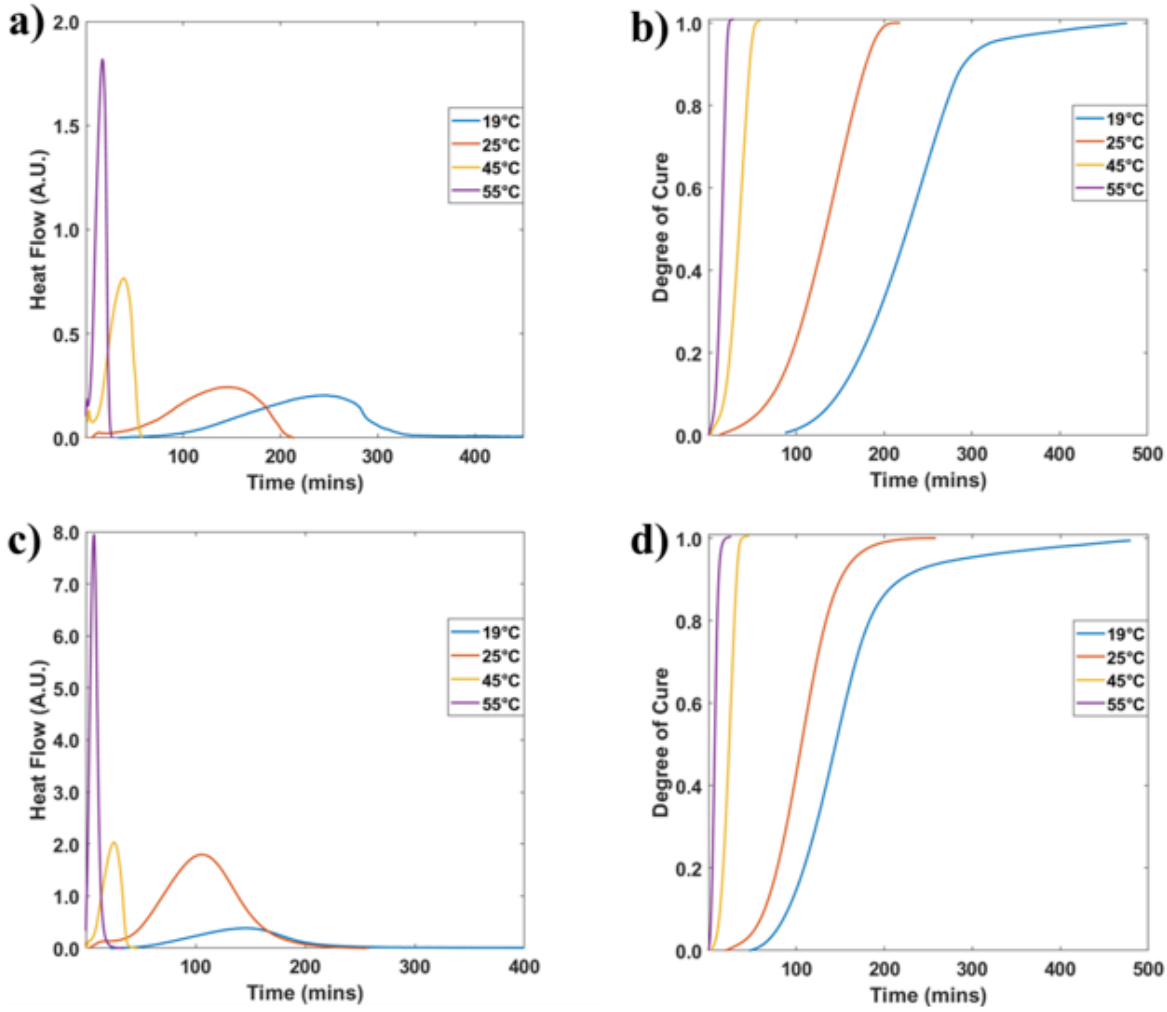

Figure 9.3 Representative isothermal curing thermograms and reaction progress timelines for (a and b) 40P and (c and d) 10P copolymer systems.

Expectedly, as the isothermal curing temperature increases a corresponding increase in the reaction rate is observed. For both systems, curing at 19 °C resulted in broad, low-intensity exothermic peaks while curing at 55 °C yielded sharp peaks with high-intensity. The increased reaction site density of the 10P system results in consistently faster curing behavior compared to the 40P system as evidenced by reduced peak enthalpy times and increased enthalpies of reaction. However, the difference in peak enthalpy times shrink as the isothermal curing temperature increases which is

because the viscosity of the monomers is decreased with higher cure temperatures; allowing for faster reaction times.

9.3.2 - Non-isothermal Cure Kinetics

As described above, for systems intended as injectable wellbore fracture sealants, it is necessary to consider the temperature gradient the mixture could experience as it is penetrating the wellbore to the subsurface fractures. To examine the impact of such temperature gradients on curing behavior, the two polymer systems were subjected to a series of non-isothermal DSC experiments as proxies for an increasing thermal profile upon injection. The resulting thermograms and degrees of cure are shown in **Figure 9.4**, and extracted peak cure temperatures and curing exotherm peak areas are given in **Table 9.2**. In the following sections, we apply two frameworks to examine the observed curing behavior: the Kissinger Model and Ozawa-Flynn-Wall Model-free analysis. Both of these approaches allow for estimation of the reaction activation energy.

Table 9.2 Non-isothermal peak cure temperatures and peak areas

Polymer	**Non-isothermal Peak Cure Temperature (°C), [H_{Total} (J/g)]**			
	1 °C/min	**3 °C/min**	**5 °C/min**	**7 °C/min**
40P	63 ± 5 [283 +/- 39]	78 ± 2 [283 ± 20]	89 ± 8 [269 ± 28]	93 ± 4 [261 ± 19]
10P	53 ± 4 [284 +/- 55]	67 ± 6 [306 ± 34]	79 ± 9 [255 ± 23]	88 ± 5 [280 ± 39]

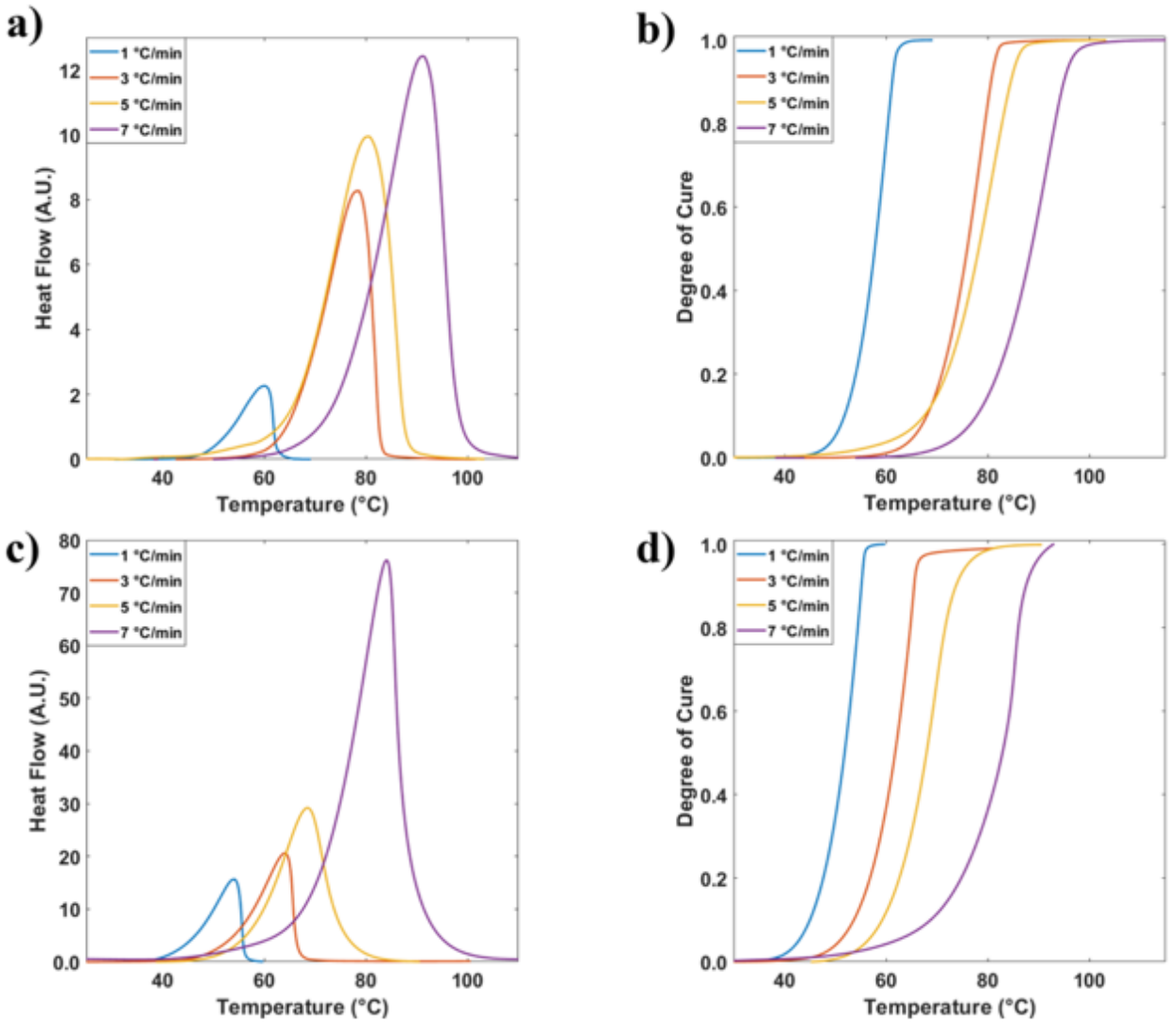

Figure 9.4 Representative thermograms and reaction progress for 40P (a and b) and 10P (c and d) under non-isothermal curing conditions.

9.3.3 - Kissinger Method

As expected from other similar systems in the literature[22,27,42], both the 40P and 10P systems examined here exhibit shifted peak temperatures, broad exotherms, and greater exotherm magnitude with increasing ramp rate; as shown in **Figure 9.4a** and **Figure 9.4c**. This type of curing behavior allows for the use of the Kissinger Model (Equation 9.2):

$$ln\left(\frac{\beta}{T_p^2}\right) = ln\left(\frac{AR}{E_\alpha}\right) - \frac{E_\alpha}{RT_p} \tag{9.2}$$

where β is the heating rate (K/min), T_p is the peak temperature of the highest exotherm (K), E_α is the activation energy of the curing system (kJ/mol), A is the pre-exponential factor, and R (kJ/K mol) is the universal gas constant.[23,28,43] To apply this model, it is necessary to perform several curing experiments as the model regression analysis relies on the underlying chemical activation energy versus the energy input from the DSC itself; in the form of a varied heating rate. Both copolymer systems exhibit similar behavior under non-isothermal curing conditions with the 10P system curing at a slightly faster rate compared to the 40P system. As shown previously, plotting of $\ln(\beta/T_P^2)$ vs $1/T_p$ allows for the calculation of the activation energy and pre-exponential factor from the slope and y-intercepts respectively. **Figure 9.5a** and **Figure 9.5b** show the Kissinger Plots for the 40P and 10P systems respectively.[24] The calculated activation energy for the two systems are 57.5kJ/mol and 51.6 kJ/mol for 40P and 10P, respectively. Comparing the two activation energies determined by the Kissinger Model, it is readily apparent that increasing the amount of DGEBA within the system increases the rate of reaction by reducing the activation energy. This is also reflected in the isothermal curing behavior in **Figure 9.4**. Additionally, both values fall within a reasonable range according to other similar systems.[22,27,42,43]

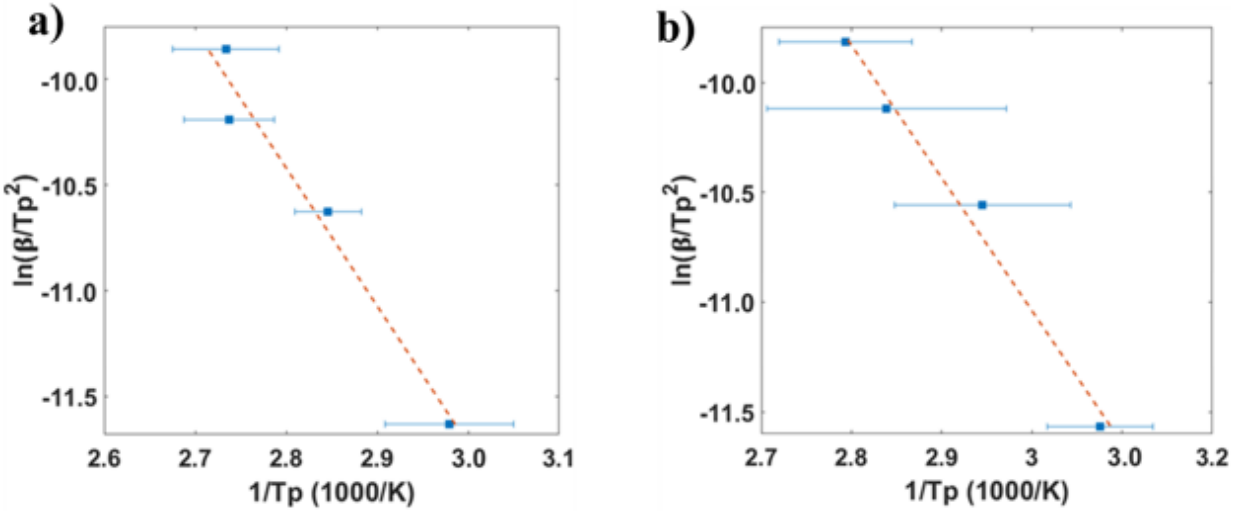

Figure 9.5 (a) Kissinger Model plot for 40P. (b) Kissinger Model plot for 10P.

9.3.4 - Ozawa-Flynn-Wall (OFW) Analysis

Crosslinked networks such as those discussed in this work tend to exhibit slight fluctuations in activation energy throughout the course of the curing process.[22,27,42] This behavior is attributed to a decrease in the reaction site density as the viscosity increases during curing and the solution lattice becomes more restrictive.[22,27,42,43] This behavior can be quantitatively observed by examining the activation energy at different extents of curing conversion as a function of the non-isothermal heating rate. In order to extract activation energies, the relationship between heating rate (β) and *Tp* is examined as shown in **Figure 9.6a** and **Figure 9.6b**. The linear fit at each point of conversion show no overlap, suggesting that this method is valid for both systems. Conveniently, OFW analysis allows for extraction of the activation energy at each point of conversion from the slopes of the trendlines at each degree of cure in Figure 6. These activation energies are shown for both 40P and 10P in **Figure 9.7a** and **Figure 9.7b** respectively as a function of degree of curing as determined by the OFW method. As shown in **Figure 9.7**, the 40P system exhibits behavior similar the autocatalytic effect observed by Hardis et al. while the 10P system did not.[22] The activation energy of 40P as calculated by the Kissinger Model (57.5 kJ/mol) is ~1-2 kJ/mol lower than that of the activation energy determined by OFW, while the results for the 10P system are in good agreement between the two methods.

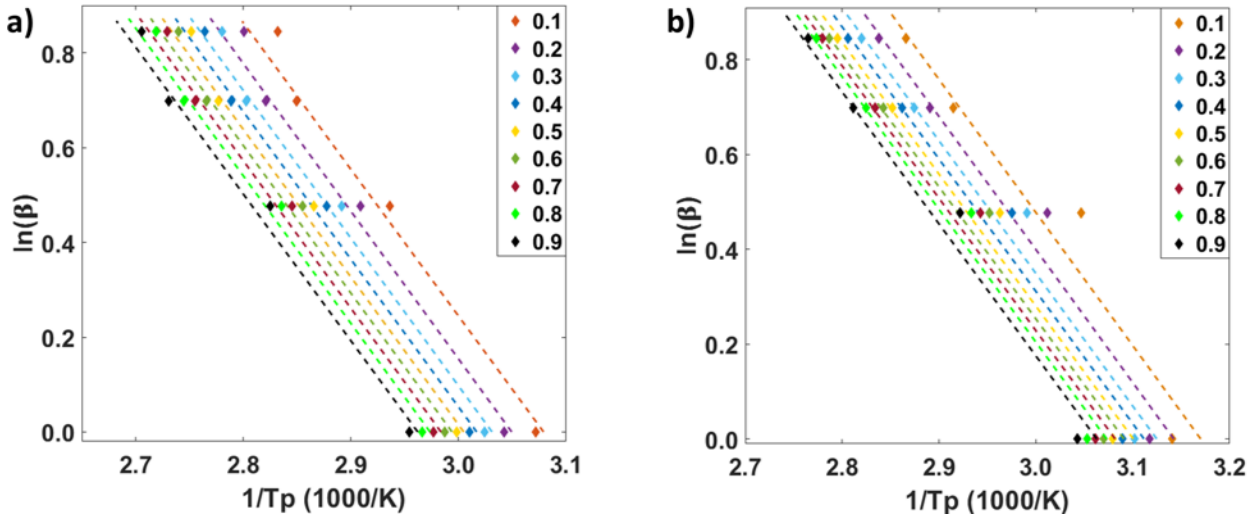

Figure 9.6 OFW plot for (a) 40P and (b) 10P showing heating rate versus peak temperature. The dotted lines represent fits the various scanning rates at a specific conversion.

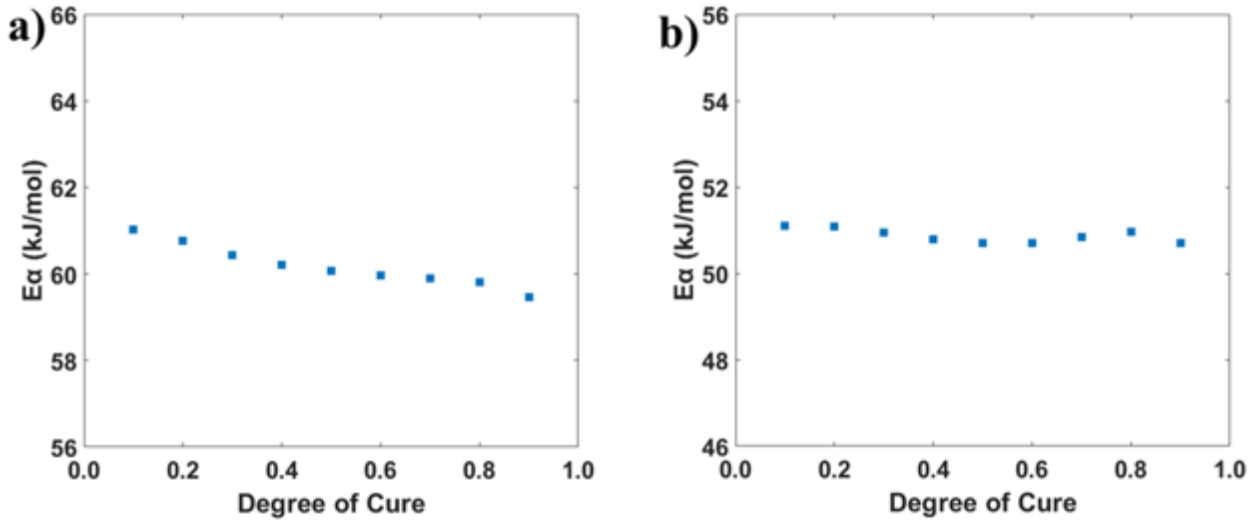

Figure 9.7 Activation energy versus degree of cure for (a) 40P and (b) 10P.

9.3.5 - Physical Properties

In addition to reaction kinetics being affected by the reaction media composition, the resulting material properties are also altered by varying the initial reaction media. Effective penetration of the reaction mixture into the wellbore is highly dependent on its viscosity. The viscosity of the system here is tunable via the composition of the two monomer constituents; PEOD is a short chain polymer, while DGEBA is a highly viscous small molecule. If the viscosity is too high, the mixture will not penetrate deep enough before hardening. In addition, if the crosslink density is not high enough (i.e. a mixture containing a higher percentage of the less viscous PEOD), the sealant may not perform as expected and would yield a higher chance of chemical seepage into the surrounding environment since contaminants would be spatially more free to elute through the plug. Thus, optimization of the interplay between viscosity and crosslink density is necessary for adequate performance of the sealant material. Shown in **Figure 9.8** and **Figure 9.9** are the viscosities of a statistical range of monomer mixtures. These viscosities do not include the 4SH or DMAP, as introduction of these constituents would initiate the curing process. As expected, the viscosity increases with increasing DGEBA content. The addition of PEOD to pure DGEBA has a much more exaggerated effect on the viscosity than addition of DGEBA to pure PEOD. The same compositions were then polymerized and subjected to DMA to extract their corresponding glass transition temperatures, as shown in **Figure 9.10a**, where glass transition temperatures are extracted from the apex of the tan delta curves as shown in **Figure 9.10b**. The Flory-Fox Equation predicts glass transition temperatures that are reasonably close to the experimental values extracted from DMA.

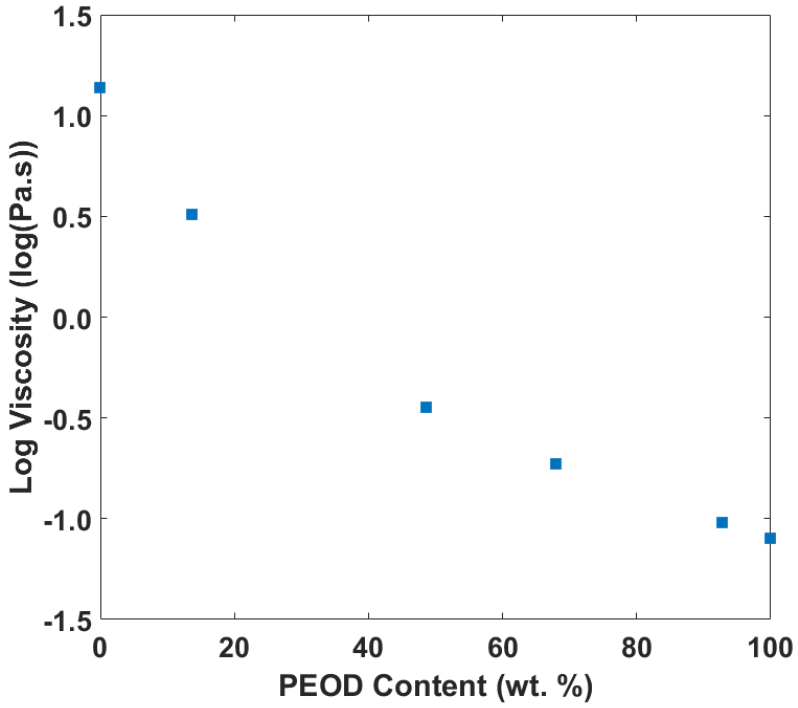

Figure 9.8 Viscosities of monomer pre-reaction PEOD/DGEBA mixtures; 4SH and DMAP are not present in these mixtures.

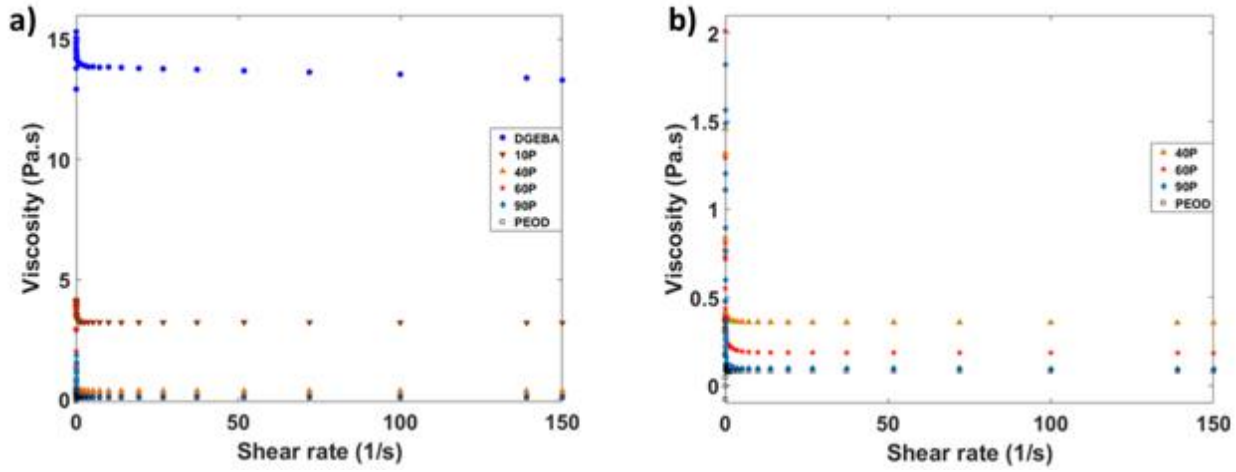

Figure 9.9 Shear rate vs viscosity for all copolymers. b) zoomed image for 40P, 60P, 90P, and PEOD systems.

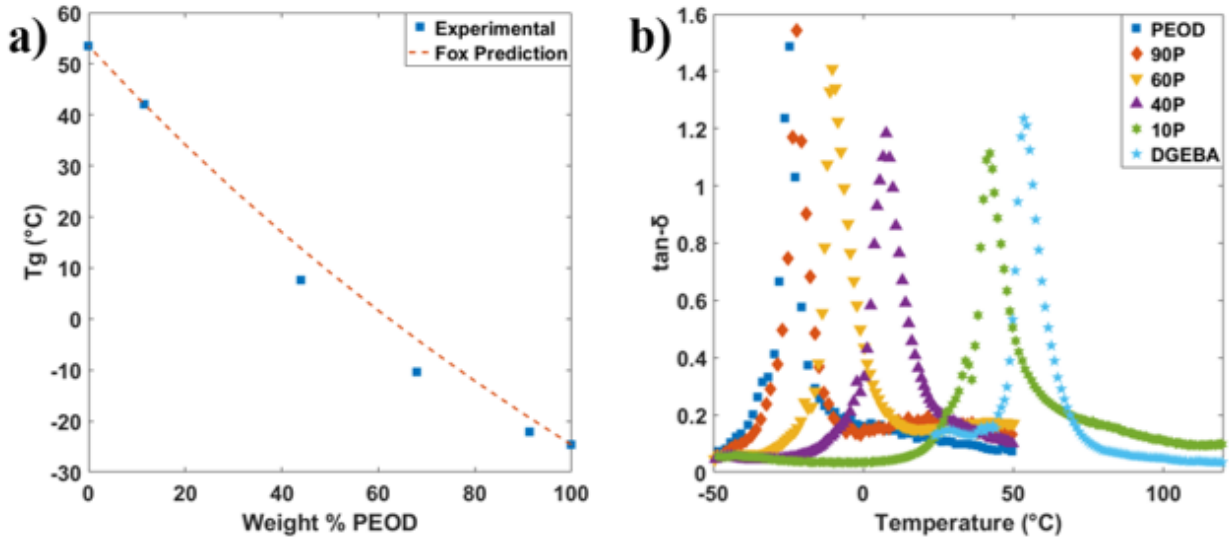

Figure 9.10 a) Comprehensive plots for glass transition temperatures of PEOD/DGEBA copolymers. Dotted line represents Flory-Fox equation predictions. b) tan-δ plots acquired via DMA for the statistical range of PEOD/DGEBA copolymers cured for 24 hours at room temperature.

As with their respective viscosities, the glass transition temperatures are also a function of the relative molar amounts of DGEBA/PEOD. T_g increases with increasing DGEBA content, which indicates stiffening of the resulting polymer material. The polymer sealant should have some flexibility to accommodate changes in the fractured cement and subsurface vibration events over time. In addition, as shown in Figure 9b, the magnitude of tan delta varies with copolymer composition. The 90P system exhibits slightly less elastic behavior than the homopolymer PEOD system and overall the elasticity decreases with increasing DGEBA content until the homopolymer composition is reached; in which case, the pure DGEBA system suffers a loss of elasticity.

9.4 - Conclusions

In this study we have investigated the curing kinetics (isothermal and non-isothermal) and physical properties (Tg and viscosities) for a DGEBA/PEOD comonomer system. We show how the system curing behavior and physical properties can be tuned by variation of the comonomer composition. A higher relative amount of PEOD yields a low viscosity reaction media, polymer networks with lower Tg's, and longer total cure times. By careful selection of the reaction media composition, sealants with tunable set-times and material properties can be appropriately engineered to prevent potential contamination of the environments immediately around wellbores.

9.5 - References

(1) Todorovic, J.; Raphaug, M.; Lindeberg, E.; Vrålstad, T.; Buddensiek, M.-L. Remediation of Leakage through Annular Cement Using a Polymer Resin: A Laboratory Study. *Energy Procedia* **2016**, *86*, 442–449. https://doi.org/10.1016/j.egypro.2016.01.045.

(2) Davies, R. J.; Almond, S.; Ward, R. S.; Jackson, R. B.; Adams, C.; Worrall, F.; Herringshaw, L. G.; Gluyas, J. G.; Whitehead, M. A. Oil and Gas Wells and Their Integrity: Implications for Shale and Unconventional Resource Exploitation. *Mar. Pet. Geol.* **2014**, *56*, 239–254. https://doi.org/10.1016/j.marpetgeo.2014.03.001.

(3) Abid, K.; Gholami, R.; Choate, P.; Nagaratnam, B. H. A Review on Cement Degradation under CO2-Rich Environment of Sequestration Projects. *J. Nat. Gas Sci. Eng.* **2015**, *27*, 1149–1157. https://doi.org/10.1016/j.jngse.2015.09.061.

(4) Bruant, R. G.; Jr., Jr.; Celia, M. A.; Guswa, A. J.; Peters, C. A. Peer Reviewed: Safe Storage of CO2 in Deep Saline Aquifiers. *Environ. Sci. Technol.* **2002**, *36* (11), 240A-245A. https://doi.org/10.1021/es0223325.

(5) Little, M. G.; Jackson, R. B. Potential Impacts of Leakage from Deep CO2 Geosequestration on Overlying Freshwater Aquifers. *Environ. Sci. Technol.* **2010**, *44* (23), 9225–9232. https://doi.org/10.1021/es102235w.

(6) Wilkin, R. T.; DiGiulio, D. C. Geochemical Impacts to Groundwater from Geologic Carbon Sequestration: Controls on PH and Inorganic Carbon Concentrations from Reaction Path and Kinetic Modeling. *Environ. Sci. Technol.* **2010**, *44* (12), 4821–4827. https://doi.org/10.1021/es100559j.

(7) Omosebi, O.; Maheshwari, H.; Ahmed, R.; Shah, S.; Osisanya, S.; Hassani, S.; DeBruijn, G.; Cornell, W.; Simon, D. Degradation of Well Cement in HPHT Acidic Environment: Effects of CO2 Concentration and Pressure. *Cem. Concr. Compos.* **2016**, *74*, 54–70. https://doi.org/10.1016/j.cemconcomp.2016.09.006.

(8) Tongwa, P.; Nygaard, R.; Blue, A.; Bai, B. Evaluation of Potential Fracture-Sealing Materials for Remediating CO2 Leakage Pathways during CO2 Sequestration. *Int. J. Greenh. Gas Control* **2013**, *18*, 128–138. https://doi.org/10.1016/j.ijggc.2013.06.017.

(9) Beharie, C.; Francis, S.; Øvestad, K. H. Resin: An Alternative Barrier Solution Material; Society of Petroleum Engineers, 2015. https://doi.org/10.2118/173852-MS.

(10) Cole, R. C. Epoxy Sealant For Combating Well Corrosion; Society of Petroleum Engineers, 1979. https://doi.org/10.2118/7874-MS.

(11) Estévez, E.; Valle, L.; del Barrio, D.; Blázquez, G.; Kovács, T.; Blázquez, V. Cements of Improved Sealing Capacity in CO₂ Geological Storage; International Society for Rock Mechanics and Rock Engineering, 2014.

(12) Genedy, M.; Stormont, J.; Matteo, E.; Taha, M. R. Examining Epoxy-Based Nanocomposites in Wellbore Seal Repair for Effective CO2 Sequestration. *Energy Procedia* **2014**, *63*, 5798–5807. https://doi.org/10.1016/j.egypro.2014.11.612.

(13) Morris, K.; Deville, J. P.; Jones, P. Resin-Based Cement Alternatives for Deepwater Well Construction; Society of Petroleum Engineers, 2012. https://doi.org/10.2118/155613-MS.

(14) Childers, M. I.; Nguyen, M.-T.; Rod, K. A.; Koech, P. K.; Um, W.; Chun, J.; Glezakou, V.-A.; Linn, D.; Roosendaal, T. J.; Wietsma, T. W.; Huerta, N. J.; Kutchko, B. G.; Fernandez, C. A. Polymer-Cement Composites with Self-Healing Ability for Geothermal and Fossil Energy Applications. *Chem. Mater.* **2017**, *29* (11), 4708–4718. https://doi.org/10.1021/acs.chemmater.7b00344.

(15) Goodwin, K. J. Principles of Squeeze Cementing; Society of Petroleum Engineers, 1984. https://doi.org/10.2118/12603-MS.
(16) Pang, X. Effects of Curing Temperature and Pressure on the Chemical, Physical, and Mechanical Properties of Portland Cement, Columbia University, 2011. https://doi.org/10.7916/D8RF620F.
(17) Rod, K. A.; Nguyen, M.-T.; Elbakhshwan, M.; Gills, S.; Kutchko, B.; Varga, T.; Mckinney, A. M.; Roosendaal, T. J.; Childers, M. I.; Zhao, C.; Chen-Wiegart, Y. K.; Thieme, J.; Koech, P. K.; Um, W.; Chun, J.; Rousseau, R.; Glezakou, V.-A.; Fernandez, C. A. Insights into the Physical and Chemical Properties of a Cement-Polymer Composite Developed for Geothermal Wellbore Applications. *Cem. Concr. Compos.* **2019**, *97*, 279–287. https://doi.org/10.1016/j.cemconcomp.2018.12.022.
(18) Schütz, M. K.; dos Santos, L. M.; Coteskvisk, P. M.; Menezes, S. C.; Einloft, S.; Dalla Vecchia, F. Evaluation of CO2 Attack in Wellbore Class G Cement: Influence of Epoxy Resins, Composites and Minerals as Additives. *Greenh. Gases Sci. Technol.* **2019**, *n/a* (n/a). https://doi.org/10.1002/ghg.1928.
(19) Ho, J. F.; Patterson, J. W.; Tavassoli, S.; Shafiei, M.; Balhoff, M. T.; Huh, C.; Bommer, P. M.; Bryant, S. L. The Use of a PH-Triggered Polymer Gelant to Seal Cement Fractures in Wells; Society of Petroleum Engineers, 2015. https://doi.org/10.2118/174940-MS.
(20) Bachu, S.; Bennion, D. B. Experimental Assessment of Brine and/or CO2 Leakage through Well Cements at Reservoir Conditions. *Int. J. Greenh. Gas Control* **2009**, *3* (4), 494–501. https://doi.org/10.1016/j.ijggc.2008.11.002.
(21) Li, Q.; Li, X.; Meng, Y. Curing of DGEBA Epoxy Using a Phenol-Terminated Hyperbranched Curing Agent: Cure Kinetics, Gelation, and the TTT Cure Diagram. *Thermochim. Acta* **2012**, *549*, 69–80. https://doi.org/10.1016/j.tca.2012.09.012.
(22) Hardis, R.; Jessop, J. L. P.; Peters, F. E.; Kessler, M. R. Cure Kinetics Characterization and Monitoring of an Epoxy Resin Using DSC, Raman Spectroscopy, and DEA. *Compos. Part Appl. Sci. Manuf.* **2013**, *49*, 100–108. https://doi.org/10.1016/j.compositesa.2013.01.021.
(23) Macan, J.; Brnardić, I.; Ivanković, M.; Mencer, H. J. DSC Study of Cure Kinetics of DGEBA-Based Epoxy Resin with Poly(Oxypropylene) Diamine. *J. Therm. Anal. Calorim.* **2005**, *81* (2), 369–373. https://doi.org/10.1007/s10973-005-0794-3.
(24) Brnardic, I.; Ivankovic, M.; Ivankovic, H.; Mencer, H. J. Isothermal and Nonisothermal Cure Kinetics of an Epoxy/Poly(Oxypropylene)Diamine/Octadecylammonium Modified Montmorillonite System. *J. Appl. Polym. Sci.* **2006**, *100* (3), 1765–1771. https://doi.org/10.1002/app.23080.
(25) McCoy, J. D.; Ancipink, W. B.; Clarkson, C. M.; Kropka, J. M.; Celina, M. C.; Giron, N. H.; Hailesilassie, L.; Fredj, N. Cure Mechanisms of Diglycidyl Ether of Bisphenol A (DGEBA) Epoxy with Diethanolamine. *Polymer* **2016**, *105*, 243–254. https://doi.org/10.1016/j.polymer.2016.10.028.
(26) Cai, H.; Li, P.; Sui, G.; Yu, Y.; Li, G.; Yang, X.; Ryu, S. Curing Kinetics Study of Epoxy Resin/Flexible Amine Toughness Systems by Dynamic and Isothermal DSC. *Thermochim. Acta* **2008**, *473* (1), 101–105. https://doi.org/10.1016/j.tca.2008.04.012.
(27) Sheng, X.; Akinc, M.; Kessler, M. R. Cure Kinetics of Thermosetting Bisphenol E Cyanate Ester. *J. Therm. Anal. Calorim.* **2008**, *93* (1), 77–85. https://doi.org/10.1007/s10973-007-8803-3.
(28) Zhao, X.; Huang, Z.; Song, P.; Chen, H.; Yang, H.; Zhang, Y. Effect of Isophorone Diamine on Curing Kinetics and Mechanical Properties of 2-Ethyl-4-

Methylimidazole/Epoxy Resin Crosslinked Network. *Thermochim. Acta* **2019**, *680*, 178380. https://doi.org/10.1016/j.tca.2019.178380.
(29) Lee, K.-M.; Woo, J.-Y.; Jee, B.-C.; Hwang, Y.-K.; Yun, C.; Moon, S.-B.; Chung, J.-H.; Kang, A.-S. Effect of Cross-Linking Agent and Heteropolyacid (HPA) Contents on Physicochemical Characteristics of Covalently Cross-Linked Sulfonated Poly(Ether Ether Ketone)/HPAs Composite Membranes for Water Electrolysis. *J. Ind. Eng. Chem.* **2011**, *17* (4), 657–666. https://doi.org/10.1016/j.jiec.2011.02.017.
(30) Seidel, C.; Kulicke, W.-M.; Heß, C.; Hartmann, B.; Lechner, M. D.; Lazik, W. Influence of the Cross-linking Agent on the Gel Structure of Starch Derivatives. *Starch - Stärke* **2001**, *53* (7), 305–310. https://doi.org/10.1002/1521-379X(200107)53:7<305::AID-STAR305>3.0.CO;2-Z.
(31) Xiao, H.-W.; Huang, S.-Q.; Jiang, T. Morphology, Rheology, and Mechanical Properties of Dynamically Cured EPDM/PP Blend: Effect of Curing Agent Dose Variation. *J. Appl. Polym. Sci.* **2004**, *92* (1), 357–362. https://doi.org/10.1002/app.20026.
(32) Cauich-Rodriguez, J. V.; Deb, S.; Smith, R. Effect of Cross-Linking Agents on the Dynamic Mechanical Properties of Hydrogel Blends of Poly(Acrylic Acid)-Poly(Vinyl Alcohol-Vinyl Acetate). *Biomaterials* **1996**, *17* (23), 2259–2264. https://doi.org/10.1016/0142-9612(96)00058-0.
(33) Lin, S.-T.; Huang, S. K. Synthesis and Impact Properties of Siloxane–DGEBA Epoxy Copolymers. *J. Polym. Sci. Part Polym. Chem.* **1996**, *34* (10), 1907–1922. https://doi.org/10.1002/(SICI)1099-0518(19960730)34:10<1907::AID-POLA8>3.0.CO;2-L.
(34) van der Sanden, M. C. M.; Meijer, H. E. H. Deformation and Toughness of Polymeric Systems: 3. Influence of Crosslink Density. *Polymer* **1993**, *34* (24), 5063–5072. https://doi.org/10.1016/0032-3861(93)90249-A.
(35) Jin, F.-L.; Park, S.-J. Impact-Strength Improvement of Epoxy Resins Reinforced with a Biodegradable Polymer. *Mater. Sci. Eng. A* **2008**, *478* (1), 402–405. https://doi.org/10.1016/j.msea.2007.05.053.
(36) Tripathi, G.; Srivastava, D. Studies on the Physico-Mechanical and Thermal Characteristics of Blends of DGEBA Epoxy, 3,4 Epoxy Cyclohexylmethyl, 3′,4′-Epoxycylohexane Carboxylate and Carboxyl Terminated Butadiene Co-Acrylonitrile (CTBN). *Mater. Sci. Eng. A* **2008**, *496* (1), 483–493. https://doi.org/10.1016/j.msea.2008.06.035.
(37) Aggarwal, L. K.; Thapliyal, P. C.; Karade, S. R. Properties of Polymer-Modified Mortars Using Epoxy and Acrylic Emulsions. *Constr. Build. Mater.* **2007**, *21* (2), 379–383. https://doi.org/10.1016/j.conbuildmat.2005.08.007.
(38) Djouani, F.; Connan, C.; Delamar, M.; Chehimi, M. M.; Benzarti, K. Cement Paste–Epoxy Adhesive Interactions. *Constr. Build. Mater.* **2011**, *25* (2), 411–423. https://doi.org/10.1016/j.conbuildmat.2010.02.035.
(39) Tatar, J.; Brenkus, N. R.; Subhash, G.; Taylor, C. R.; Hamilton, H. R. Characterization of Adhesive Interphase between Epoxy and Cement Paste via Raman Spectroscopy and Mercury Intrusion Porosimetry. *Cem. Concr. Compos.* **2018**, *88*, 187–199. https://doi.org/10.1016/j.cemconcomp.2018.01.012.
(40) Barde, M.; Celikbag, Y.; Via, B.; Adhikari and Maria L. Auad, S. Semi-Interpenetrating Novolac-Epoxy Thermoset Polymer Networks Derived from Plant Biomass. *J. Renew. Mater.* **2018**, *6* (7), 724–736. https://doi.org/10.32604/JRM.2018.00116.

(41) Commarieu, B.; Potier, J.; Compaore, M.; Dessureault, S.; Goodall, B. L.; Li, X.; Claverie, J. P. Ultrahigh Tg Epoxy Thermosets Based on Insertion Polynorbornenes. *Macromolecules* **2016**, *49* (3), 920–925. https://doi.org/10.1021/acs.macromol.5b02648.
(42) Lee, J.-Y.; Shim, M.-J.; Kim, S.-W. Effect of Modified Rubber Compound on the Cure Kinetics of DGEBA/MDA System by Kissinger and Isoconversional Methods. *Thermochim. Acta* **2001**, *371* (1), 45–51. https://doi.org/10.1016/S0040-6031(00)00771-1.
(43) Guzmán, D.; Ramis, X.; Fernández-Francos, X.; Serra, A. New Catalysts for Diglycidyl Ether of Bisphenol A Curing Based on Thiol–Epoxy Click Reaction. *Eur. Polym. J.* **2014**, *59*, 377–386. https://doi.org/10.1016/j.eurpolymj.2014.08.001.

Chapter 10 - Future Work and Suggestions for Experimental Progress

This chapter explores further the methods, techniques, and chemistries detailed in the previous chapters. It provides some suggestions for future work that builds upon this dissertation from my thoughts and conversations with my adviser, and all of my collaborators. Should any questions arise as a result of this chapter, please contact my advisor Dr. Beckingham at bsb0025@auburn.edu.

10.1- Summit of Statements and Conclusions

My thesis has an overall focus on multicomponent polymer systems and in this bigger context investigates the synthesis and structure-property relationships of copolymer systems and the ability of a low-field NMR spectrometer to accurately determine polymer microstructures and composition of copolymer systems. This work demonstrates the ability of low-field NMR spectrometers to produce quantitatively similar results to those produced using high-field spectrometers for a variety of polyolefins. Specifically, it demonstrates that low-field spectrometers can be utilized to in place of the more commonly used high-field spectrometers in many industrial quality control and compositional analysis experiments used to extract polyolefin microstructure and compositions. The caveat to this finding is this technique is not universally applicable and should be validated for additional applications. Secondly, this dissertation investigates the use of statistical copolymerization of thiophene and thiophene derivatives as a tool to tune and decouple important material property. It has shown that though copolymer microstructure-property relationships are very complicated, statistical copolymerization of thiophene monomers allows for the decoupling of material properties such as band gap, melting temperature, and orbital energy levels. Lastly, this dissertation investigates a potential candidate for use as a wellbore sealant. The pertinent material properties such as pre-cure mixture viscosity,

set-time, and post-cure polymer glass transition temperature as the interplay of these properties with the architecture of the selected sealant system will determine its performance in its intended use. Overall, this dissertation expands upon our understanding of these copolymer systems and benchmarks a newly available characterization technique for copolymer systems. The following sections provide further detail of these conclusive statements.

10.1.1- Analysis of Polymer Composition via Low-field NMR Spectroscopy

The drawbacks presented by the depression in sensitivity from the use of a low-field NMR spectrometer over a high-field NMR spectrometer are generally outweighed by their accessibility, versatility, and cost for routine ^{1}H NMR spectroscopy. More specifically, this dissertation demonstrates the utility of low-field NMR spectroscopy for analysis of non-novel, routine, compositional analysis of polymer systems. This is presented in **Chapters 4** and **5** for a broad range of polyolefin polymers and demonstrated that the low-field spectrometer can produce compositional results equivalent to high-field spectrometer to within two mole percent. This capability was demonstrated for a large combination of instrumental settings and sample parameters. The relevant spectrometer settings (spectral width, relaxation delay, number of data points, and number of scans) were varied and it was demonstrated that for all detectable sample concentrations, the spectrometer produced equivalent results. More importantly, this was demonstrated for mixed-microstructure polyisoprenes due to their "copolymer-like" structure with very chemically similar "comonomer" units. For a wide variety of concentrations (10, 25, and 50 mg/mL), molecular weights (see **Chapter 4**), and varied compositions (see **Chapter 4**) the low-field NMR spectrometer was able to provide results that closely matched the high-field spectrometer results.

This capability was also verified for other polymer systems including commercial triblock copolymers and polymer blends. All of the results for polystyrene/polyisoprene blends, polystyrene/polymethylmethacrylate blends, and a SIS triblock copolymer yielded results within 1 mole percent of the results from the high-field spectrometer while results for a SBS triblock copolymer fell just outside of the two mole percent regime. Overall, low-field ^{1}H NMR spectroscopy was demonstrated to be a very viable tool for analysis of polymer composition and microstructures where routine analyses are required.

10.1.2- Polythiophene Microstructure-Property Relationships

In this dissertation, a wide range of polythiophene copolymers containing 3-hexylthiophene, 3-(2'-ethylhexyl)thiophene, unsubstituted thiophene, and 3-methoxythiophene were synthesized and characterized. In **Chapter 6**, a range of 3-hexylthiophene and unsubstituted thiophene copolymers was investigated. The conclusions we were able to draw from this work show that we are able to decouple critical polymer properties via copolymerization of thiophene derivatives. This is significant as for many polymer systems, the critical material properties are interconnected, which complicates independent tuning of properties. Importantly, the narrowing of the band gap was achieved by the general depression of LUMO energy levels with decreasing 3-hexylthiophene content while the HOMO energy levels were relatively constant. While the decoupling of these aspects of polythiophenes is important, it is more important conceptually as it proves the viability of polythiophenes for decoupling other pertinent material properties; i.e. the thermal and electronic transport mechanisms.

Furthermore, as discussed in **Chapter 8**, it was shown that copolymerization of thiophene monomers via GRIM polymerization, is not random. The manner in which thiophene comonomers propagate can dictate the resulting material properties as discussed in **Chapter 2**. For even

chemically similar thiophene monomers, preferential addition of one monomer over another can occur. This is likely due to differences in concentration, stereochemistry, and electronic structure of the individual monomers. By furthering these works, semiconductive polymers with specific properties and composition can be realized to better implement into the next generation of organic electronic devices.

10.1.3- PEOD/DGEBA Crosslinked Networks

The final topic of this dissertation is the exploration of a potential candidate for wellbore sealants. The critical properties such as cure time, pre-cure viscosity, and glass-transition temperatures were characterized as the interplay of these parameters plays a large role in material performance as described in **Chapter 9**. Comonomer content, heating rate (for non-isothermal experiments), and cure temperature (for isothermal experiments) significantly affected the curing behavior of this system. These injectable sealant systems could prove to be useful for mitigation of environmental contamination by leaking wellbore systems. Our preliminary results (not shown in this thesis) with the healing of fractured cement cubes are promising and I anticipate that a technology such this one will provide an efficient and cost-effective solution to the problems presented by microfractures within wellbore systems.

10.2- GRIM Polymerization of Polythiophenes

As demonstrated in **Chapters 6-8**, the physics and chemistries of polythiophene copolymers are quite complex and much is still needed to gain a better understanding of the interplay of GRIM-synthesized polythiophene microstructures and properties. Aspects of GRIM synthesis such as solvent environment and the reactivity ratios of thiophene monomer derivatives remain largely unexplored and complicate our understanding of these highly studied polymers. This section aims

to illustrate the importance of several synthetic parameters as they pertain to GRIM polymerization.

10.2.1- 3-Position Substituent Effect on Monomer Propagation

A significant portion of this dissertation focused on the general overview of polythiophene synthesis. The underlying mechanisms that drive the nature of propagation has gone mostly unexplored for much of the literature as many groups are more focused on applications and device fabrication. This propagation chemistry is important however, as it has been repeatedly shown that small modifications to polythiophene backbones greatly affects the resulting material properties.[1–5] Many prior studies only examine final polymer structure produced from a set of reactants, neglecting the intermediates between them. For instance, as discussed in **Chapter 6**, Scheme 6.1 shows that there are many possible intermediates that can form during GRIM polymerization. What is not discussed for polythiophene copolymer chemistry is the relative reactivity between the two different comonomers as typically described by the reactivity ratios of the monomers. It is anticipated that by alteration of the 3-position substituent, not only are the resulting material properties altered, the relative reactivity of each monomer is altered.[3] To preliminarily investigate this, the dipole moments of each of the molecules were modeled as the electronic structures most certainly plays a role in the halogen dance portion of GRIM synthesis. This was done only briefly using freely available online molecular emulation resources; the results from molcalc.org are shown in **Table 10.1** and **Figure 10.1**.[6] It should be noted that these molecular models are limited to a maximum of 10 non-hydrogen molecules, therefore emulation of any dibrominated 3-alkylthiophenes beyond 3-propylthiophene was not possible. Fortunately, as the difference in dipole moments between the 3-propyl, 3-butyl, 3-pentyl, and 3-(2'-methylbutyl)thiophenes are insignificant, suggesting that these values can be extended to 3HT and 3EHT.

Table 10.1 Calculated dipole moments from molcalcs.org.[6]

Molecule	Dipole Moment (Debye)	
	Nonbrominated	Dibrominated
3-methoxythiophene	1.17	3.08
3-propylthiophene[a]	1.52	2.02
3-butylthiophene[a]	1.52	*
3-pentylthiophene[a]	1.56	*
3-(2'-methylbutyl)thiophene[a]	1.58	*
thiophene	1.23	1.56

*molcalc.org is limited to 10 non-hydrogen atoms in the model

[a] these molecules are used to emulate the negligible difference in 3-alkylthiophenes

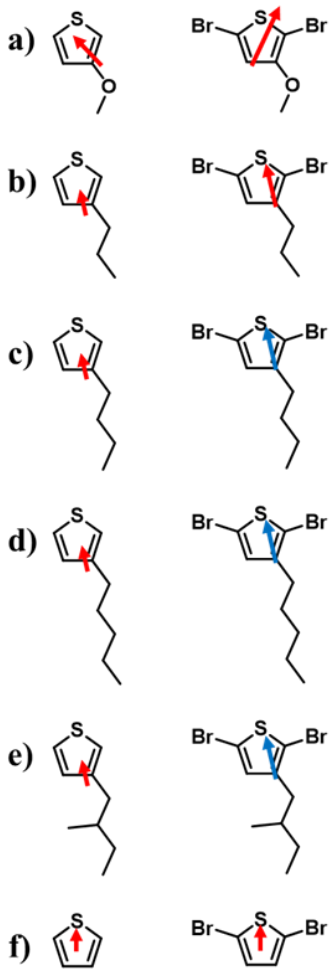

Figure 10.1 Estimated dipole moments from molcalc.org for nonbrominated and dibrominated variants of a) 3-methoxythiophene, b) 3-propylthiophene, c) 3-butylthiophene, d) 3-pentylthiophene, e) 3-(2'-methylbutyl)thiophene, and f) thiophene. Red arrows indicate prediction from website, blue arrows are approximations based on 3-propylthiophene.

As shown in **Table 10.1** and **Figure 10.1**, the dipole moment between the nonbrominated and dibrominated versions of the monomers is vastly different in each case. This suggests that the substituent group has at least some effect on the reactivity of the GRIM intermediates. It is likely that the substituents at the 3-position not only greatly affect the polymer material properties but also their respective reactivity ratios.

To probe the effect of substituent groups on propagation kinetics, compositional drift analysis of the forming polymer throughout GRIM synthesis should be performed. The tracked composition of the 74HT polymer from **Chapter 6** is shown in **Figure 8.3**. Initially the unsubstituted thiophene is added more rapidly to the growing polymer chains relative to the monomer composition. This is likely due to the accessibility of both the 2 and 5 aromatic positions as discussed in **Chapter 6**. Unfortunately, due to the ongoing global pandemic (COVID-19), collection of additional data points or subject the samples to GPC to analyze polymer molecular weight as a function of time was not performed. This work will be extended in future.

10.2.2- Solvent Environment

Since the development of the GRIM polymerization technique, research groups have followed the literature method outlined by McCullough et al.[2–4,7–16] As outlined in previous chapters, this method uses anhydrous THF as the preferred solvent and little-to-no work has been performed employing this technique with other common organic solvents such as toluene or chloroform. This is especially important for GRIM polymerization of two or more thiophene derivatives as solvent environment has been shown to affect the rate of addition of other polymer systems, as demonstrated by Beckingham et al.[17] Furthermore, THF is not necessarily the ideal solvent for every thiophene derivative, this is shown in **Chapter 6** in which the statistical copolymers with majority unsubstituted thiophenes (less than 40 mole % 3-hexylthiophene) were not soluble in

THF. While these were observed to be insoluble post-polymerization, it could be inferred that solvation is likely an issue for some of the other copolymers discussed in **Chapter 6** during synthesis. Additionally, the Soxhlet method utilized in **Chapters 6** and **7** directly depends on the solubility of the various components (Grignard salts in methanol , short chain polythiophenes in hexane, and target products in $CHCl_3$). For many of the copolymers described in **Chapters 6-8** containing unsubstituted thiophene, there was usually uncollected solids in the Soxhlet filter paper. This material is likely the result of two things: (1) higher molecular weight polymer due to enhanced chain coupling from unsubstituted thiophene and/or (2) copolymers with higher mole percent unsubstituted thiophene than the soluble fractions. Both of which would not be recovered.

Solvation during synthesis is crucial as it affects the ability of mers to add to the growing chain. This is observed in **Chapter 7** wherein the PMoT homopolymer becomes insoluble during polymerization and precipitates following sufficient chain addition. A potential solution to this issue is to heat the reaction media further to improve solubility and enhance solvation of the propagating polymer chains. However, it is an unfortunate drawback of Grignard metathesis polymerization that heating yields lower regioregularity polymers. Nearly all of the GRIM literature performs the GRIM synthesis in anhydrous THF and this is a critically overlooked aspect of this chemistry. PMoT is a prime example as the monomer appears to be soluble and behaves much like the alkyl-substituted before synthesis but then precipitates during polymerization. This is also evidenced by the statistical copolymers of 3HT and thiophene with lower 3HT content where the reaction media takes on a much a deeper red/scarlet color as opposed to the more common/expected orange. By changing the solvent environment by either using another solvent, or by using a blend of two or more solvents the resulting copolymer architecture could be altered. One potential solvent that has shown to be a good solvent for the thiophene copolymers

synthesized in this dissertation is toluene. Toluene, like THF, is a symmetrical cyclic molecule but lacks any heteroatoms such as the oxygen found in THF and as such is "nonpolar". THF has a dipole moment of 1.75 Debye while toluene's dipole moment is about 0.31 Debye. This difference in polarity should have a large impact on the propagation behavior of the comonomers while maintaining appreciable chain solubility during synthesis. Similarly, total initial monomer concentration has been shown by Iovu et al. to be directly related to the resulting chain length at each percentage of conversion and could also be used to manipulate the propagation during polymerization.[7] Overall, performing future GRIM syntheses in which the concentration of the monomers is increased significantly (2-4x) above that of the literature concentration for the initial reaction media and performing aliquotic copolymerizations similar to the method described in **Chapter 8**, of thiophenes functionalized with substituents of significantly varied electron-withdrawing behavior would both enable additional insights in to these materials synthesis.

10.2.3- Special Topic: Additive Manufacturing of π-conjugated Systems

This section is a digression from the organic syntheses discussed in the previous projects and is a result of exposure to both polythiophenes and the *Additive Manufacturing of Soft Materials Class* taught by Dr. Virginia Davis in the fall of 2018. This section contains initial insights and anticipated results based towards stereolithographically-synthesized and fabricated π-conjugated devices. Dr. Davis introduced me to the technique of stereolithographic additive manufacturing and upon seeing the advantages of this technique (high resolution and facile fabrication of complex geometries in devices), I found there was very limited literature on additive manufacturing of π-conjugated systems though some work had been done on UV photopolymerization of a polymer similar to polyaniline.[18] This work provided a potential route to simultaneously synthesize π-conjugated materials and fabricate devices through UV photopolymerizatio . This is critical as

synthesis and processing of semiconductive polymers can prove to be extremely difficult due to the interplay of monomer-synthetic strategy compatibility, polymer-solvent relationships, and number of post-polymerization processing steps can delay or prevent the realization of many semiconductive polymer systems as discussed in this dissertation.

An initial system examined was 3-bromothiophene (3BT), chlorobenzene (CB), and p-phenylenediamine (PPD) with a low-power handheld UV light (4 watts, and two wavelengths: 254 nm and 365 nm); equimolar amounts of 3BT and CB were used and 0.2 molar equivalent of PPD to 3BT+CB. Interestingly, the reaction media yielded thin films with two very distinct colors after 20 mins, shown in **Figure 10.2**. The granules of PPD are visible in the initial reaction media and are quite large. The films produced as a result of this were grainy and disintegrated upon mechanical agitation with a spatula. We next attempted to synthesize a film using 3BT and ground PPD the results of this are shown in **Figure 10.3**. In this trial the mixture was altered to consist of 1 mole percent PPD relative to 3BT. The resulting films appeared significantly more uniform but required longer cure times (~35 minutes).

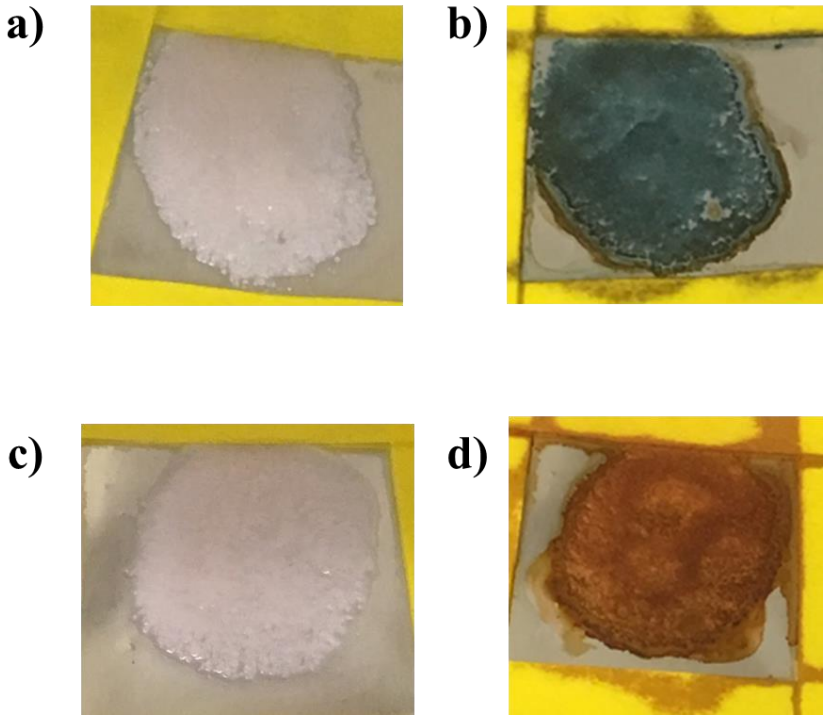

Figure 10.2 3BT+CB+PPD before and after exposure to 365 nm UV light (a&b) and 254 nm UV light (c&d) for 20 mins.

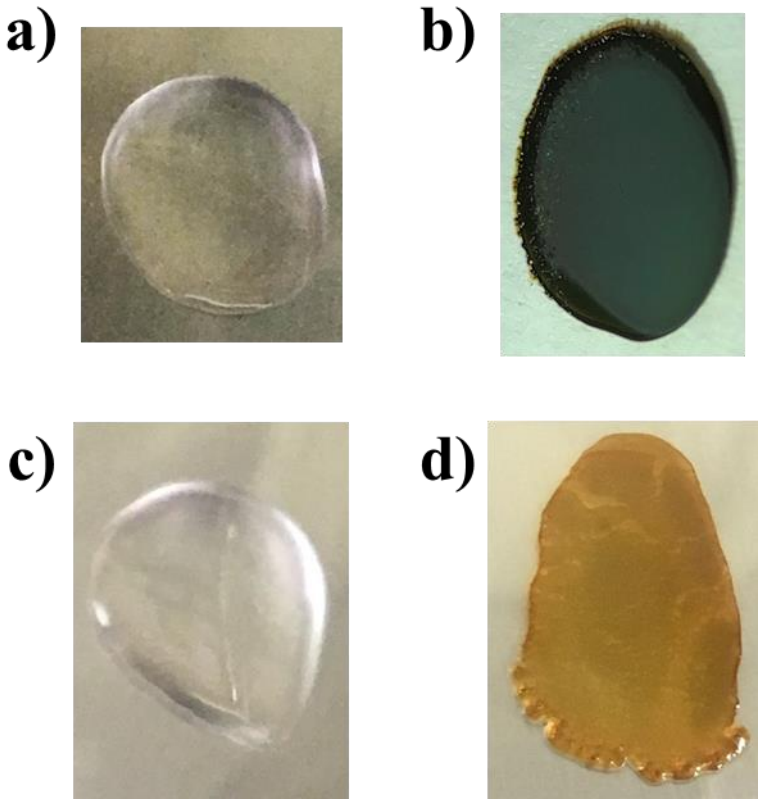

Figure 10.3 3BT+ ground PPD before and after exposure to 365 nm UV light (a&b) and 254 nm UV light (c&d) for 35 mins.

Unfortunately, these films were quite brittle, making characterization difficult and determination of the actual reaction remains elusive. One potential related reaction from the literature that follows a well-known reaction mechanism is the anti-Markarvnikov addition of secondary amines to alkynes.[19] From this a proposed scheme is shown in Scheme 10.1.

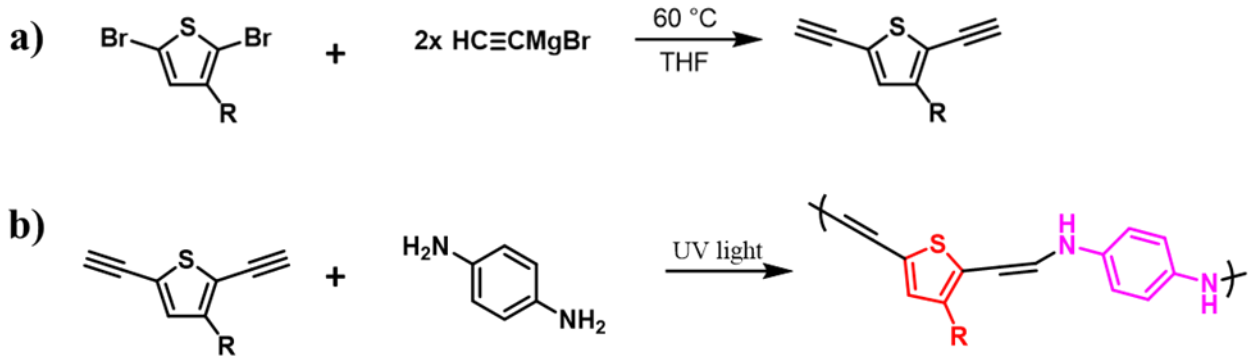

Scheme 10.1 Proposed mechanism for development of a 3D-printable π-conjugated system.

While this proposed scheme is speculative, chemistries such as this one may provide an avenue for these materials in light-based additive manufacturing. Non-halogens substituents on the 3-position of the thiophene unit should be investigated as they may interact with the ethynyl magnesium bromide. This chemistry can provide not only a synthetic route to a copolymer system that contains aspects of three of the semiconductive polymers mentioned in **Chapter 2** (polythiophene, polyacetylene, and polyaniline) and the potential for 3D-printable π-conjugated systems.

10.3- Additional Low-Field NMR Spectroscopic Experiments

As discussed in many of the previous chapters, NMR spectroscopy is utilized to characterize a wide variety of critical polymer material properties. However, all of the previously discussed work dealt strictly with product analysis; whether the intended product was an intermediate in a larger set of synthetic steps (thiophene intermediates) or the final product as in the case of the many polyolefin systems discussed in **Chapters 4** and **5**. Not directly stated in **Chapter 5** is that the methods utilized to analyze polyolefin copolymer/blend composition is not directly applicable to polythiophenes. This is due to the similarity of the available/selected protons utilized to distinguish between thiophene derivatives and the exaggerated peak broadness yielded by low-field NMR spectroscopy. This section aims to detail two projects in which low-field NMR spectroscopy can be used to analyze alternative copolymer systems to the polyolefins discussed in **Chapters 4-5** and to demonstrate the potential utility of low-field NMR spectroscopy as means to access and combine advantages of other techniques typically employed to track reactions of crosslinked and interpenetrating polymer networks.

10.3.1- Application of Low-Field NMR Spectroscopy to Polythiophene Copolymers

As discussed **Chapter 6** and **7**, polythiophenes are typically analyzed via the 3-position substituent group and/or the proton(s) located on the aromatic thiophene ring.[2,8–10,12,20–22] These signature protons are especially useful during preparation of thiophene monomers for GRIM synthesis as the ratio of the aromatic proton(s) to the side chain protons elucidates the presence of side chain substituents and in further reaction steps, the level of bromination (mono vs dibrominated). For these analyses low-field NMR spectroscopy proved extremely useful as in many cases the samples were able to be drawn straight from the reactor, placed into a tube, and analyzed which hastened the synthetic pace. The pitfall of low-field NMR spectroscopy lies in its inability to provide a facile means to characterize polythiophene copolymer compositions. Even for copolymers with high

molar content of each comonomer in **Chapter 6**, the spectrometer could not distinguish between the aromatic protons. To address this issue without completely changing the copolymer system deuterated solvents should be use in order to perform a 2-dimensional NMR spectroscopy experiment known as total-correlation spectroscopy (TOCSY). TOCSY is a NMR spectroscopy experiment in which two proton spectra are collected and plotted against one another to correlate spins through bonds. This technique is especially useful for systems, such as the thiophene copolymers, that possess overlapped/coalesced signals as it shows real signals as symmetrical signals on either side of a diagonal line and correlates signals three to four bonds away while suppressing one to two bond signals. It would be favorable before performing this experiment to determine T1 and T2 relaxation times of the sample to reduce the amount of noise and spin-echo artifacts present in the resulting 2D spectra.

Alternatively, if we wish to maintain all of the advantages of low-field NMR spectroscopy discussed in **Chapter 4** and **5**, the chemistry of our copolymers could be altered to address the peak broadness issue. This approach was not discussed in Chapter 7 (PMoT-3HT) but one advantage of the alkoxy-alkyl thiophene copolymer is the ability to use the side chain signals to analyze the polymer composition. Unfortunately, PMoT is not soluble at higher molecular weights and synthesis of a copolymer with a specific composition is difficult (**Chapter 7** PMoT-3HT copolymer had an initial 30/70 MoT/3HT monomer charge composition but had a final compositionof 10/90 MoT/3HT) likely due to solubility issues and the underlying electronic structure effects discussed in Section 10.1.1. However, longer side chains on polythiophenes typically yield a more soluble polymer. To obtain a copolymer with appreciable alkoxy and alkyl thiophene content, a thiophene with a longer alkoxy side chain substituent is necessary. Luckily, access to the necessary chemistry is readily available.[23] The synthesis of 3-ethoxythiophene (EoT)

and subsequent polymerization and copolymerization (with 3HT) via GRIM synthesis could be one avenue to investigate solubility and the ability of the low-field NMR spectrometer to analyze this system.

10.3.2- In-situ Reaction Monitoring of Interpenetrating and Crosslinked Networks

Reaction progress of crosslinked networks and interpenetrating networks are traditionally tracked either by DSC or FTIR spectroscopy for two main reasons. DSC provides a means to track a reaction in-situ and at a very controlled temperature which provides highly accurate time-resolved tracking of reaction kinetics.[24–26] The issue is that in many cases researchers want to also track the evolution of specific bonds over time, which DSC is incapable of providing. FTIR spectroscopy is typically used to address this as the bonds of interest produce distinct vibrational energies that can be tracked in the spectra.[27,28] However, to utilize FTIR to analyze these types of systems, the researcher must draw aliquots from a temperature-controlled reaction sample and place it on the ATR crystal (often at ambient conditions). While this difference in temperature is unlikely to drastically affect the reaction progress (in fact, it probably slows it down which is a good thing for analysis), this process is highly cumbersome on the researcher involved in the experiment. In this section the use of a Pulsar LFNMR spectrometer's to track the reaction progress of interpenetrating networks is examined. This technique provides a combination of the DSC and FTIR spectroscopy by providing a temperature-controlled, in-situ method that is able to track specific bond formations within a reacting system. Fortunately, this collaborative opportunity arose with Dr. Maria Auad and Nima Alizadeh.

2-Ethyl-2-(hydroxymethyl)-1,3-propanediol (TRIOL, MW=134.18 g/mol was purchased as a crosslinker from Acros Organics. Poly(tetramethylene ether) glycol (PTMG, MW=approximately 1400 g/mol) was purchased from Aldrich. Hexamethylene diisocyanate (DCH) purchased from

TCI was used as an isocyanate compound. Dibutylin dilaurate (DBTDL) and triphenylbismuth (TPB), purchased from Pfaltz & Bauer and Alfa Aesar respectively, were used as the catalyst. Ethyl acetate, purchased from Alfa Aesar, was used as solvent for the mixture of catalysts. 4A molecular sieves, purchased from Alfa Aesar, were used to remove the moisture from DCH, Styrene, TRIOL, and PTMG.

Reaction progress for PTMG +DCH and PTMG+DCH+Triol systems was tracked using an Oxford Instruments Pulsar 60 MHz NMR spectrometer. The experimental procedure was as follows: PTMG was metered into a Wilmad high-throughput class B NMR tube (8" length, and 5 mm outer diameter) placed on a scale in an Erlenmeyer flask. The sample was then subjected to an initial scan to obtain a pristine spectrum before addition of any other component. Next, DCH was added in the same manner as PTMG followed by 2 drops of each catalyst, DBTDL and TPB, each dissolved in ethyl acetate. The reaction mixture was agitated via stirring with a copper wire and manual shaking of the tube before being placed into the probe bore. The spectrometer was tuned and matched to the sample and then the experiment was started. Note that the lag time (time from addition of catalyst to start of experiment) was accounted for in both the reaction progress diagram, **Figure 10.4**, and the subsequent data analysis.

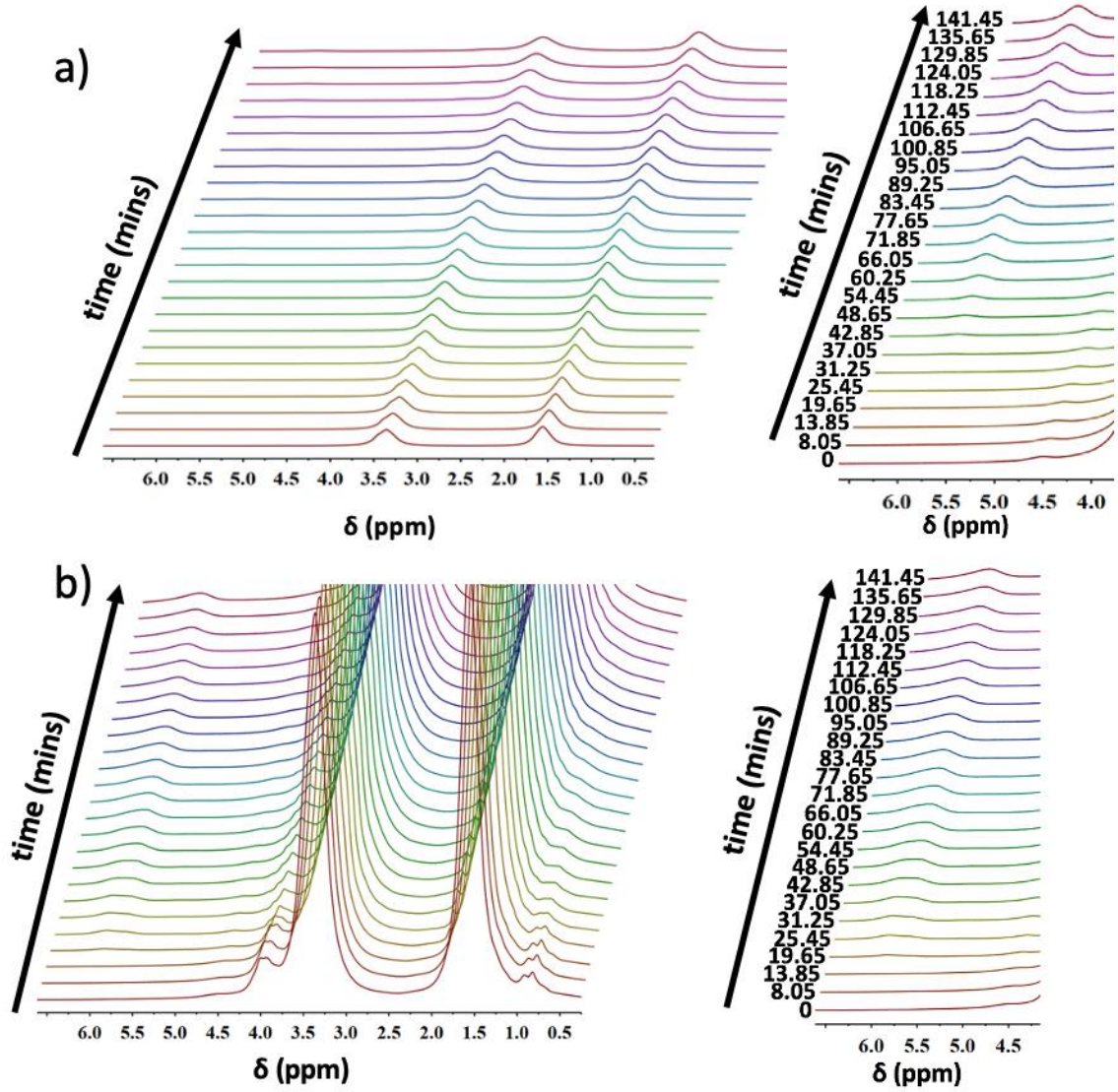

Figure 10.4 NMR spectra from in-situ reaction monitoring of a) PTMG+DCH and b) PTMG+DCH+Triol.

Tetramethylsilane (standard additive used to align most 1D ^{1}H NMR spectra) was not used here to eliminate any possible interactions with the reaction media. Instead, all spectra were shifted based on the far right peak attributed to part of the PTMG backbone for the PTMG+DCH system (1.56 ppm).[28] This peak also served as an internal calibration standard as the underlying protons associated with this peak (for both systems) are conserved; for the PTMG+DCH+Triol system, the Triol aliphatic arm also contributes to this peak so 5 additional protons were accounted for shown in **Figure 10.5**.

Unfortunately, due to the spectral overlap in the aliphatic region of the NMR spectra, Figure 10.4, the consumption of hydroxyl groups could not be tracked. However, in both cases the formation of urethane linkages could be tracked through the formation of N-H protons. By utilizing this method, we combine the advantages of the more traditional differential scanning calorimetry reaction tracking and that of the FTIR spectroscopy; in-situ/continuous reaction monitoring and bond-specific tracking. Furthermore, as discussed elsewhere, one other advantage of the Pulsar system is soft lock algorithm which eliminates the need for deuterated solvents and allows for examination of protons without any adulteration of the reaction media.[29,30] The spectrometer run settings were as follows: 64 scans at a recycle delay of 2 seconds and a spectral width of 50000 Hz.

As shown in **Figure 10.4**, the peak at 5.94 ppm grows in intensity over time due to the continuous formation of primary amine peaks as urethane linkages are formed. In the case of the PTMG+DCH system, each urethane linkage is strictly from consumption of -OH groups on the PTMG chain ends. However, for the PTMG+DCH+Triol system, this metric of conversion is complicated by the presence of additional hydroxyl groups on the arms of the Triol molecule. Conversion was

tracked as a function of peak area and number of protons responsible for each peak, shown in Equation 10.1.

$$\text{Conversion} = 100 \text{ x } \frac{A_{5.94}N_{1.56}}{A_{1.56}N_{5.94}} \quad (10.1)$$

where A_i is the peak areas at i ppm, and N_j is the number of protons associated with the peak at j ppm. Peak areas (A_i) were extracted from Gaussian fits to the peaks after spectral shifting, automatic phasing, and automatic baselining in the Mnova software. For the PTMG+DCH system, $N_{1.56}$=76.665 and $N_{5.94}$=2.0157 protons; for PTMG+DCH+Triol, $N_{1.56}$=81.70375 and $N_{5.94}$=6.04704 protons. These values are calculated for each chemistry from the reaction stoichiometry and chemical structures shown in **Figure 10.5**. For the PTMG+DCH system this analysis assumes that only one DCH molecule is present in the "repeat unit" of the network while the PTMG+DCH+Triol system has the potential for up to three DCH molecules; two amine protons and six amine protons respectively. This is important as the network is complicated by the availability of hydroxyl groups from two different mer units. The extracted conversion versus time data are shown in **Figure 10.6**.

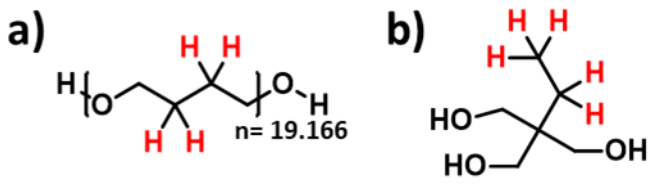

Figure 10.5 Protons used in the calculation of $N_{1.56}$ are highlighted in red for a) PTMG and b) Triol.

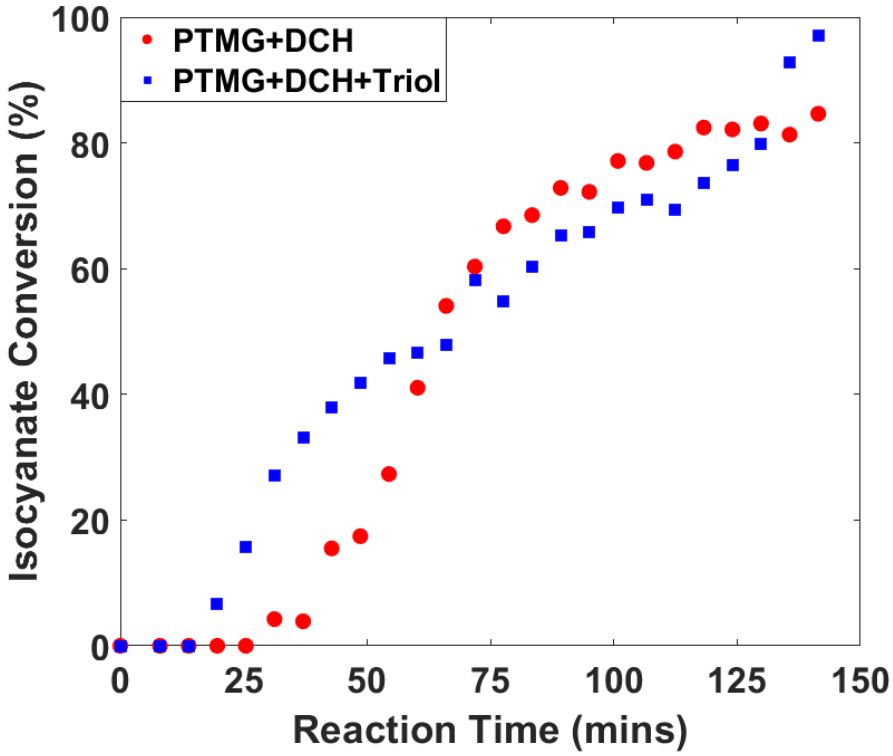

Figure 10.6 Reaction progress for both systems as a function of isocyanate conversion.

As shown in **Figure 10.6**, both systems exhibit a lag time at the beginning of the reaction. This is attributed to the low reaction rate at room temperature as the reaction media approaches the spectrometer operating temperature of 37 °C. However, the reaction can be effectively tracked over time as the DCH is incorporated within the polymeric structure and isocyanate groups are converted into primary amines within the urethane linkages. While the data points appear to be non-continuous it is important to note that the spectrometer is averaging the signal over 64 scans that are acquired over a cycle time of approximately 5 minutes and 48 seconds such that the resulting isocyanate conversion are time averaged. Additionally, conversion in each case reaches a maxima at approximately the same time as extracted from FTIR spectroscopy if the lag time is disregarded. We attribute the higher overall isocyanate conversion of the PTMG+DCH+Triol system to the higher reaction site density as compared to the PTMG+DCH system. Overall, this method provides an adequate and facile means to track both reaction progress and bond-specific formation for this particular interpenetrating network.

This technique is anticipated to be directly extendable to other similar chemistries (such as the chemistries discussed in **Chapter 9** and Section 10.4) and provide a new facile method for analysis of crosslinked polymer networks. Additionally, outfitting an NMR tube with a thermocouple to track the internal sample temperature during curing would be a facile enhancement to this methodology.

10.4- PEOD-Containing Crosslinked-Network Chemistry Alterations

The copolymers presented in **Chapter 9** presented a somewhat clear picture of microstructure-property relationships through facile synthesis and targeted characterization of specific properties. One of the advantages of chemistries such as those is that the individual components can be exchanged for others of similar structure and the same experiments repeated. This allows for rapid exploration of the relationship of microstructure and material properties. Critical properties such as crosslink density, stiffness, glass transition temperature, reaction kinetics, and many others can be altered via subtle but distinct alterations to the reagents selected.[24–26,31,32] The wide variety of attainable properties within the scope of these materials make the applicable to a very wide number of applications such as coatings, sealants, membranes, and other various crosslinked-polymer technologies. Given below in **Figure 10.7** are some variations of the structures used in **Chapter 9** that may be utilized similarly to gather additional information about structure-property relationships of these types of systems.

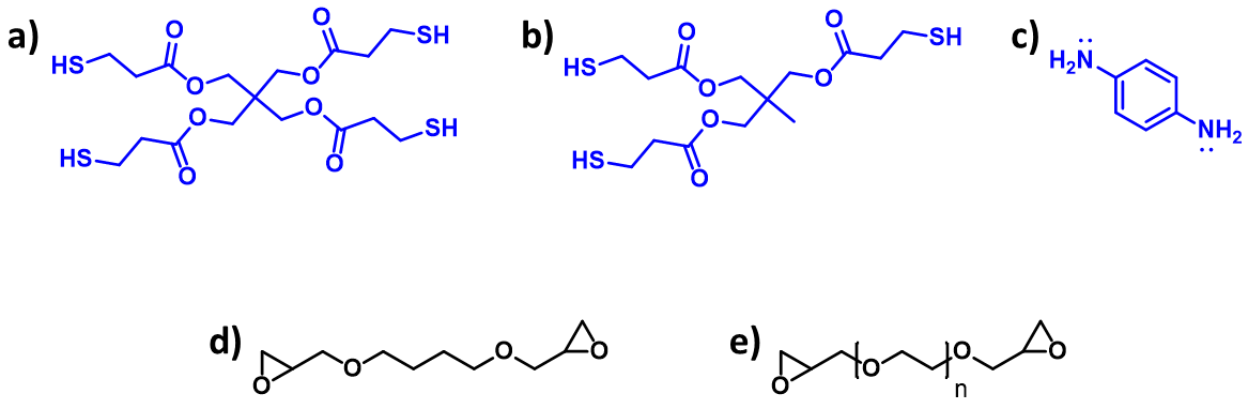

Figure 10.7 Microstructures of a) pentaerythritol tetra(3-mercaptopropionate), b) trimethylolpropane tris(3-mercaptopropianate, c) p-phenylene diamine, d) 1,4-butanediol diglycidyl ether, and e) poly(ethylene glycol) diglycidyl ether. Crosslinking agents shown in blue.

The copolymer system discussed in **Chapter 9** uses two very distinct comonomers in varying ratios to alter the resulting material properties. However, smaller changes can be made to various constituents to elicit the same types of changes observed for the PEOD/DGEBA system. The components shown above can be polymerized in a statistical manner for easily repeatable experiments and results that are directly comparable. The work for these various systems has been initiated and will continue as soon as campus operations return to normal.

10.5- Comprehensive List of Experiments Delayed by COVID-19

As the global pandemic has delayed a few of my projects, I felt it necessary to include a table in this chapter of all of the experiments yet to be performed to complete my work for the preparation of manuscripts. Shown in **Table 10.2** is the comprehensive list of experiments to be completed to finish the projects in **Chapters 4-9**.

Table 10.2 Comprehensive list of experiments affected by COVID-19.

Experiment	**Copolymer**	**Reason**
Chapter 6 Copolymers		
XRD (WAXS)[a]	95HT, 55HT, 44HT	Crystal Structure
Four-Point Probe	All	Conductivity
Scattered White Light Interferometry[b]	All	Film Thickness
Polarized Light Optical Microscopy[c]	All	Birefringent Behavior
Chapter 8 Copolymers		
NMR Spectroscopy	70/30 3EHT/3HT 70/30 3EHT/T 70/30 3HT/3MoT	Track Copolymer Composition
Gel-Permeation Chromatography	All Systems	Track Copolymer M_n

[a] Georgia Institute of Technology Materials Characterization Facility.
[b] Dr. Kyle Schulze's Lab in Mechanical Engineering at Auburn University.
[c] Dr. Virginia Davis' Lab in Chemical Engineering at Auburn University.

10.6- References

(1) Boudouris, B. W.; Ho, V.; Jimison, L. H.; Toney, M. F.; Salleo, A.; Segalman, R. A. Real-Time Observation of Poly(3-Alkylthiophene) Crystallization and Correlation with Transient Optoelectronic Properties. *Macromolecules* **2011**, *44* (17), 6653–6658. https://doi.org/10.1021/ma201316a.

(2) Minkler, M. J.; Beckingham, B. S. Statistical Copolymers of 3-Hexylthiophene and Thiophene: Impact of Thiophene Content on Optoelectronic and Thermal Properties. *Materials Today Communications* **2019**, 100547. https://doi.org/10.1016/j.mtcomm.2019.100547.

(3) Yang, Y.-L.; Lee, Y.-H.; Lee, Y.-P.; Chiang, C.-J.; Shen, C.; Wu, C.-C.; Ohta, Y.; Yokozawa, T.; Dai, C.-A. Synthesis and Characterization of Poly(3-Hexylthiophene)–Poly(3-Hexyloxythiophene) Random Copolymers with Tunable Band Gap via Grignard Metathesis Polymerization. *Polymer International* **2014**, *63* (12), 2068–2075. https://doi.org/10.1002/pi.4744.

(4) Jeffries-EL, M.; Sauvé, G.; McCullough, R. D. In-Situ End-Group Functionalization of Regioregular Poly(3-Alkylthiophene) Using the Grignard Metathesis Polymerization Method. *Adv. Mater.* **2004**, *16* (12), 1017–1019. https://doi.org/10.1002/adma.200400137.

(5) Burkhart, B.; Khlyabich, P. P.; Thompson, B. C. Influence of the Ethylhexyl Side-Chain Content on the Open-Circuit Voltage in Rr-Poly(3-Hexylthiophene- *Co* -3-(2-Ethylhexyl)Thiophene) Copolymers. *Macromolecules* **2012**, *45* (9), 3740–3748. https://doi.org/10.1021/ma300263a.

(6) Jensen, J. H.; Kromann, J. C. The Molecule Calculator: A Web Application for Fast Quantum Mechanics-Based Estimation of Molecular Properties. *J. Chem. Educ.* **2013**, *90* (8), 1093–1095. https://doi.org/10.1021/ed400164n.

(7) Iovu, M. C.; Sheina, E. E.; Gil, R. R.; McCullough, R. D. Experimental Evidence for the Quasi-"Living" Nature of the Grignard Metathesis Method for the Synthesis of Regioregular Poly(3-Alkylthiophenes). *Macromolecules* **2005**, *38* (21), 8649–8656. https://doi.org/10.1021/ma051122k.

(8) McCullough, R. D.; Lowe, R. D.; Jayaraman, M.; Anderson, D. L. Design, Synthesis, and Control of Conducting Polymer Architectures: Structurally Homogeneous Poly(3-Alkylthiophenes). *J. Org. Chem.* **1993**, *58* (4), 904–912. https://doi.org/10.1021/jo00056a024.

(9) McCullough, R. D. The Chemistry of Conducting Polythiophenes. *Advanced Materials* **1998**, *10* (2), 93–116. https://doi.org/10.1002/(SICI)1521-4095(199801)10:2<93::AID-ADMA93>3.0.CO;2-F.

(10) Minkler, M. J.; Kim, J.; Lawson, K. E.; Ali, A.; Zhao, R.; Adamczyk, A. J.; Beckingham, B. S. Solution Processible Statistical Poly(3-Methoxythiophene)-Co-Poly(3-Hexylthiophene) Copolymer. *Materials Letters* **2019**, *256*, 126563. https://doi.org/10.1016/j.matlet.2019.126563.

(11) Laiho, A.; Nguyen, H. T.; Sinno, H.; Engquist, I.; Berggren, M.; Dubois, P.; Coulembier, O.; Crispin, X. Amphiphilic Poly(3-Hexylthiophene)-Based Semiconducting Copolymers for Printing of Polyelectrolyte-Gated Organic Field-Effect Transistors. *Macromolecules* **2013**, *46* (11), 4548–4557. https://doi.org/10.1021/ma400527z.

(12) Loewe, R. S.; Ewbank, P. C.; Liu, J.; Zhai, L.; McCullough, R. D. Regioregular, Head-to-Tail Coupled Poly(3-Alkylthiophenes) Made Easy by the GRIM Method: Investigation of

the Reaction and the Origin of Regioselectivity. *Macromolecules* **2001**, *34* (13), 4324–4333. https://doi.org/10.1021/ma001677+.
(13) Zhang, Q.; Cirpan, A.; Russell, T. P.; Emrick, T. Donor−Acceptor Poly(Thiophene-Block-Perylene Diimide) Copolymers: Synthesis and Solar Cell Fabrication. *Macromolecules* **2009**, *42* (4), 1079–1082. https://doi.org/10.1021/ma801504e.
(14) Ouhib, F.; Khoukh, A.; Ledeuil, J.-B.; Martinez, H.; Desbrières, J.; Dagron-Lartigau, C. Diblock and Random Donor/Acceptor "Double Cable" Polythiophene Copolymers *via* the GRIM Method. *Macromolecules* **2008**, *41* (24), 9736–9743. https://doi.org/10.1021/ma801934g.
(15) Ouhib Farid; Dkhissi Ahmed; Iratçabal Pierre; Hiorns Roger C.; Khoukh Abdel; Desbrières Jacques; Pouchan Claude; Dagron-Lartigau Christine. Electronic Structure and Optical Properties of Poly[3-(4-octylphenoxy)Thiophene]: Experimental and Theoretical Studies. *Journal of Polymer Science Part A: Polymer Chemistry* **2008**, *46* (22), 7505–7516. https://doi.org/10.1002/pola.23056.
(16) Miyanishi, S.; Tajima, K.; Hashimoto, K. Morphological Stabilization of Polymer Photovoltaic Cells by Using Cross-Linkable Poly(3-(5-Hexenyl)Thiophene). *Macromolecules* **2009**, *42* (5), 1610–1618. https://doi.org/10.1021/ma802839a.
(17) Beckingham, B. S.; Sanoja, G. E.; Lynd, N. A. Simple and Accurate Determination of Reactivity Ratios Using a Nonterminal Model of Chain Copolymerization. *Macromolecules* **2015**, *48* (19), 6922–6930. https://doi.org/10.1021/acs.macromol.5b01631.
(18) Min, Y.-L.; Wang, T.; Zhang, Y.-G.; Chen, Y.-C. The Synthesis of Poly(p -Phenylenediamine) Microstructures without Oxidant and Their Effective Adsorption of Lead Ions. *Journal of Materials Chemistry* **2011**, *21* (18), 6683–6689. https://doi.org/10.1039/C1JM10169B.
(19) Severin, R.; Doye, S. The Catalytic Hydroamination of Alkynes. *Chem. Soc. Rev.* **2007**, *36* (9), 1407–1420. https://doi.org/10.1039/B600981F.
(20) Smith, Z. C.; Wright, Z. M.; Arnold, A. M.; Sauvé, G.; McCullough, R. D.; Sydlik, S. A. Increased Toughness and Excellent Electronic Properties in Regioregular Random Copolymers of 3-Alkylthiophenes and Thiophene. *Adv. Electron. Mater.* **2017**, *3* (1), n/a-n/a. https://doi.org/10.1002/aelm.201600316.
(21) Ho, V. Synthesis and Characterization of Poly(3-Alkylthiophene)-Containing Block Copolymers. 132.
(22) Ho, V.; Beckingham, B. S.; Ng, H. H.; Segalman, R. A. Control of Thermal and Optoelectronic Properties in Conjugated Poly(3-Alkylthiophenes). *MRS Communications* **2014**, *4* (2), 45–50. https://doi.org/10.1557/mrc.2014.9.
(23) Yao, Z.; Hu, X.; Huang, B.; Zhang, L.; Liu, L.; Zhao, Y.; Wu, H.-C. Halochromism of a Polythiophene Derivative Induced by Conformational Changes and Its Sensing Application of Carbon Dioxide. *ACS Appl. Mater. Interfaces* **2013**, *5* (12), 5783–5787. https://doi.org/10.1021/am401761n.
(24) Macan, J.; Brnardić, I.; Ivanković, M.; Mencer, H. J. DSC Study of Cure Kinetics of DGEBA-Based Epoxy Resin with Poly(Oxypropylene) Diamine. *J Therm Anal Calorim* **2005**, *81* (2), 369–373. https://doi.org/10.1007/s10973-005-0794-3.
(25) Cai, H.; Li, P.; Sui, G.; Yu, Y.; Li, G.; Yang, X.; Ryu, S. Curing Kinetics Study of Epoxy Resin/Flexible Amine Toughness Systems by Dynamic and Isothermal DSC. *Thermochimica Acta* **2008**, *473* (1), 101–105. https://doi.org/10.1016/j.tca.2008.04.012.

(26) Hardis, R.; Jessop, J. L. P.; Peters, F. E.; Kessler, M. R. Cure Kinetics Characterization and Monitoring of an Epoxy Resin Using DSC, Raman Spectroscopy, and DEA. *Composites Part A: Applied Science and Manufacturing* **2013**, *49*, 100–108. https://doi.org/10.1016/j.compositesa.2013.01.021.
(27) Pavia, D. L.; Lampman, G. M.; Kriz, G. S.; Vyvyan, J. A. *Introduction to Spectroscopy*; Cengage Learning, 2008.
(28) Cateto, C. A.; Barreiro, M. F.; Rodrigues, A. E. Monitoring of Lignin-Based Polyurethane Synthesis by FTIR-ATR. *Industrial Crops and Products* **2008**, *27* (2), 168–174. https://doi.org/10.1016/j.indcrop.2007.07.018.
(29) Chakrapani, S. B.; Minkler, M. J.; Beckingham, B. S. Low-Field 1H-NMR Spectroscopy for Compositional Analysis of Multicomponent Polymer Systems. *Analyst* **2019**, *144* (5), 1679–1686. https://doi.org/10.1039/C8AN01810C.
(30) Minkler Jr, Michael J., Jung Min Kim, Vinita V. Shinde, and Bryan S. Beckingham. "Low-Field 1H NMR Spectroscopy: Factors Impacting Signal-to-Noise Ratio and Experimental Time in the Context of Mixed Microstructure Polyisoprenes." Magnetic Resonance in Chemistry, April 7, 2020. https://doi.org/10.1002/mrc.5022.
(31) Brnardic, I.; Ivankovic, M.; Ivankovic, H.; Mencer, H. J. Isothermal and Nonisothermal Cure Kinetics of an Epoxy/Poly(Oxypropylene)Diamine/Octadecylammonium Modified Montmorillonite System. *Journal of Applied Polymer Science* **2006**, *100* (3), 1765–1771. https://doi.org/10.1002/app.23080.
(32) Liu, W.; Qiu, Q.; Wang, J.; Huo, Z.; Sun, H. Curing Kinetics and Properties of Epoxy Resin–Fluorenyl Diamine Systems. *Polymer* **2008**, *49* (20), 4399–4405. https://doi.org/10.1016/j.polymer.2008.08.004.